

Establishing the Effects of Adipose Derived Stem Cells (ADSCs) on the Tumorigenic Characteristics of Breast Cancer

Emman Thomson

Submitted to Swansea University in
fulfilment of the requirements for the
Degree of Doctor of Philosophy



Swansea University
Prifysgol Abertawe

2022

Abstract

Introduction: Breast Cancer affects approximately 55,000 women in the UK every year, with the majority (>70%) being oestrogen receptor (ER) positive. Advancements in screening, imaging and adjuvant therapies mean more women are diagnosed earlier and undergo breast-conserving surgery (BCS). There has been a resultant rise in the use of free fat transfer (FFT) to reconstruct the small to medium volume loss, utilising autologous adipose tissue. Contemporary scientific studies demonstrate that co-location of breast cancer and adipose derived stem cells (ADSCs) present in FFT, results in the conferment of a malignant advantage via cytokine release and co-located cell-to-cell interaction. As these studies predominantly utilise ADSCs isolated from healthy patients, there is a limit to how these results apply to the clinical patient group of women with breast cancer. This thesis aimed to create, for the first time, a clinically representative model by isolating ADSCs from women with breast cancer undergoing systemic treatment. Thus establishing if patient selection plays a role in the effects imparted by ADSCs upon the functional and phenotypic characteristics associated with the cancer hallmarks.

Methods: An optimised ADSC isolation protocol produced a reliable cell population for the study duration. ADSCs harvested from patients with (n=10) and without breast cancer (n=6) were isolated and fully characterised using the Dominici criteria for stem cells. Conditioned media (CM) and non-contact co-culture models were applied to examine the effect that ADSCs isolated from breast cancer patients had on the neoplastic traits of MCF-7 and T47D ER+ breast cancer cell lines when compared with their healthy counterparts. Experiments were designed to measure a range of functional and morphological endpoints, related to the cancer hallmarks. This included proliferation, changes in cellular adhesion and migration, invasion, cellular and nuclei morphology, protein expression and bioenergetics.

Results: Successfully isolated ADSCs demonstrated plastic adherence, trilineage differentiation and appropriate cell surface markers as confirmed using flow cytometry. Data showed statistically significant increases ($p < 0.05$) in proliferation and invasion only when MCF-7 cells were treated with media conditioned by ADSCs from healthy patients. Significant increases in migration and invasion, with reduction in adhesion and raised concentrations of cytokines (IL-6, VEG-F and MCP-1) was only seen when MCF-7 cells were co-cultured with ADSCs isolated from healthy patients. There was a lack of effect seen in both CM and co-culture experiments involving ADSCs isolated from cancer patients, a novel finding, as this patient group had not previously been a focus of study. Similar results were seen in the second ER+ cell line (T47D) which was used for experimental validation, with increases in proliferation, invasion, and an increase in abnormal metabolic activity when co-cultured with healthy ADSCs only.

Conclusion: Utilising a novel approach to patient selection, it has been possible to show a divergence in the behaviour of ADSCs isolated from patients with breast cancer undergoing systemic treatment, when compared with ADSCs isolated from healthy patients. This study presents a two-part cell-based model which more accurately represents the clinical population undergoing FFT. This study recommends an alternative patient group (women with cancer on systemic treatment) as the primary cell source for research examining ADSC behaviour in the breast cancer micro-environment.

Declaration and Statements

Declaration

This work has not previously been accepted in substance for any degree and is not being concurrently submitted in candidature for any degree.

Signed........ (candidate)

Date01/10/2022.....

Statement 1

This work is the result of my own independent study/investigation, except where otherwise stated. Other sources are acknowledged by footnotes giving explicit references. A bibliography is appended.

Signed........ (candidate)

Date01/10/2022.....

Statement 2

I hereby give my consent for my work, if relevant and accepted, to be available for photocopying and for inter-library loan, and for the title and summary to be made available to outside organisations.

Signed........ (candidate)

Date01/10/2022.....

Table of Contents

Abstract

Declaration

Table of Contents

Acknowledgments

Table of Figures

List of Tables

Abbreviations

Chapter One 1

Introduction

1.1 General Overview	1
1.2 Breast Anatomy	3
1.3 Breast Cancer Overview	5
1.3.1 Demographics and Incidence of Breast Cancer	7
1.3.2 Risk Factors for Breast Cancer Development	9
1.3.3 Diagnosing Breast Cancer	10
1.3.4 Treatment Overview	12
1.3.5 Surgery	13
1.3.6 Radiotherapy	15
1.3.7 Adjuvant and Neoadjuvant Treatment	15
1.3.8 Chemotherapy	15
1.3.9 Hormone Therapy	16
1.3.10 Molecular Targeted Therapy	17
1.3.11 Breast Reconstruction Post Cancer Resection	17
1.3.12 Medium to Large Volume Reconstruction	18
1.3.13 Free Fat Transfer	19
1.4 Hallmarks of Cancer	21
1.4.1 Sustained Proliferation	22
1.4.2 Evasion of Growth Suppression	23
1.4.3 Evasion of Apoptosis	24
1.4.4 Replicative Immortality	25

1.4.5 Sustained Angiogenesis	25
1.4.6 Invasion and Metastasis	27
1.5 Emerging Hallmarks and Enabling Characteristics.....	28
1.5.1 Genomic Instability	29
1.5.2 Tumour-Promoting Inflammation	31
1.5.3 Abnormal Bioenergetics.....	32
1.5.4 Evading Immune Destruction.....	33
1.6 The Tumour Microenvironment.....	35
1.6.1 Endothelial Cells and Pericytes	35
1.6.2 Fibroblasts	36
1.6.3 Mesenchymal Stem Cells and Cancer Stem Cells	36
1.7 Adipose Derived Stem Cells (ADSCs).....	38
1.7.1 ADSC Discovery and Characterisation	38
1.7.2 Scientific Laboratory Studies	41
1.7.3 Clinical Studies	44
1.7.4 Opportunities for Development.....	44
1.8 Aims and Objectives	45

Chapter Two **47**

Materials and Methods

2.1 Laboratory Consumables.....	47
2.2 Buffers, Chemicals, and Reagents	47
2.3 Cell Lines	48
2.4 Human Adipose Tissue Collection.....	48
2.5 Cell Culture	49
2.6 Cell Lines	49
2.7 Primary Cell Lines.....	50
2.7.1 Primary Cell Line Isolation	50
2.8 Cell Counting	52
2.9 Cryopreservation	53
2.9.1 Cell Lines	53
2.9.2 Primary Cell Lines.....	53

2.9.3 Initiating a Cell Line	54
2.10 Flow Cytometric Analysis.....	54
2.10.1 Compensation Matrix.....	57
2.10.2 Data Analysis.....	59
2.11 Trilineage Differentiation.....	59
2.11.1 Adipogenesis	60
2.11.2 Chondrogenesis.....	61
2.11.3 Osteogenesis.....	62
2.12 Conditioned Media Preparation	63
2.13 Non-Contact Co-Culture Preparation.....	64
2.14 MCF-7 Proliferation, Migration, Invasion and Morphology.....	66
2.14.1 Measurement of Proliferation (Conditioned Media)	66
2.14.2 Measurement of Proliferation (Co-Culture).....	68
2.14.3 Measurement of Migration (Conditioned Media).....	69
2.14.4 Measurement of Migration (Co-Culture)	70
2.14.5 Measurement of Invasion (Conditioned Media).....	71
2.14.6 Measurement of Invasion (Co-Culture).....	73
2.14.7 Measurement of Morphology (Conditioned Media).....	74
2.14.8 Measurement of Morphology (Co-Culture)	75
2.15 Human Cytokine Antibody Array Panel	76
2.15.1 ELISA.....	77
2.15.2 Measurement of ELISA (Conditioned Media and Co-Culture).....	79
2.16 Bioenergetics Analysis – Seahorse-XF	81
2.16.1 Adhesion to the Bio-Flux Plate	83
2.16.2 Bioenergetics of Co-Culture.....	84
2.17 Data Analysis.....	85
2.17.1 Proliferation.....	85
2.17.2 Migration	85
2.17.3 Invasion	86
2.17.4 Cytokine Expression Profiles	86
2.17.5 INCELL	86
2.17.6 Bioenergetics	87

Chapter Three 88

Optimisation of Adipose Derived Stem Cell (ADSC) Isolation and Assays for Evaluating MCF7 and T47D Growth and Progression

3.1 Introduction	88
3.1.1 Chapter Aims	89
3.2 Methods	91
3.2.1 Patient Selection	91
3.2.2 Sample Collection	91
3.2.3 Protocol Selection	91
3.2.4 ADSC Isolation	92
3.2.5 Tissue Culture	93
3.2.6 ADSC Characterisation	93
3.2.6.1 Flow Cytometry	93
3.2.6.2 Plastic Adherence	94
3.2.6.3 Trilineage Differentiation	94
3.2.7 Proliferation and Cell Adhesion	94
3.2.8 Invasion	95
3.2.9 Migration	95
3.2.10 Bioenergetics	95
3.2.11 Cell Morphology	96
3.2.12 ELISA	96
3.2.13 Non-Contact Co-Culture of Cell Lines with ADSCs	96
3.3 Results	97
3.3.1 Patient Cohort Used for the Duration of the Study	97
3.3.2 Optimisation of ADSC Isolation and Their Characterisation	102
3.3.2.1 Selecting the ADSC Isolation Protocol for Use in This Study	102
3.3.2.2 Challenges Arising with Protocol Two	102
3.3.2.3 Challenges Arising with Protocol Three	103
3.3.2.4 Evaluation of ADSC Isolation Using Protocol One	104
3.3.2.5 Characterising ADSCs Isolated from Protocol One	105
3.3.2.6 Determining ADSC Plastic Adherence	105
3.3.2.7 Determining ADSC Trilineage Differentiation	106
3.3.2.8 Characterising ADSC Phenotype	108

3.3.3 Media Optimisation for MCF7 and T47D Cell Culture	118
3.3.4 Optimisation for Conditioned Media and Co-Culture Studies	120
3.3.4.1 Optimisation of ADSC CM to Study the Indirect Effect	120
3.3.4.2 Optimisation of MCF-7 and T47D Cells for Proliferation.....	120
3.3.4.3 Optimisation of MCF-7 and T47D Cells for Migration	123
3.3.4.4 Optimising the Measurement of Invasion	125
3.3.4.5 Identification of the Most Relevant Cytokines Using a Panel	128
3.3.4.6 Optimising the INCELL Analyser 2000	130
3.3.4.7 Optimisation of the Seahorse XF Assay	131
3.3.4.8 Optimisation of MCF-7 and T47D Non-Contact Co-Culture ..	134
3.4 Discussion	136
3.4.1 Conclusions	141

Chapter Four 142

Evaluating the Indirect Effect of ADSC Conditioned Media from Healthy and Cancer Patients on the Neoplastic Traits of MCF7 Cells

4.1 Introduction	142
4.1.1 Chapter Aims	143
4.2 Methods	144
4.2.1 Sample Collection.....	144
4.2.2 ADSC Isolation and Characterisation	144
4.2.3 MCF-7 Cell Line.....	144
4.2.4 Tissue Culture.....	144
4.2.5 Cell Counting	144
4.2.6 Conditioned Media.....	145
4.2.7 Proliferation.....	145
4.2.8 Migration	145
4.2.9 Invasion	145
4.2.10 Morphology	146
4.2.11 Cytokine/Chemokine Expression Profiles.....	146
4.2.12 Data Analysis.....	146
4.2.12.1 Proliferation.....	146

4.2.12.2 Migration	146
4.2.12.3 Invasion	147
4.2.12.4 Morphology	147
4.2.12.5 Cytokine/Chemokine Expression Profiles	147
4.3 Results from the MCF-7 Conditioned Media Experiments.....	148
4.3.1 MCF-7 Conditioned Media Proliferation.....	148
4.3.2 MCF-7 Conditioned Media Migration	152
4.3.3 MCF-7 Conditioned Media Invasion	156
4.3.4 MCF-7 Conditioned Media Morphology	160
4.3.5 MCF-7 Conditioned Media Cytokine/Chemokine Expression Profiles.....	163
4.4 Discussion	169
4.4.1 Conclusions	174
Chapter Five	175
Using Non-Contact Co-Culture to Evaluate the Effect of Co-Locating ADSCs From Healthy and Cancer Patients on The Neoplastic Traits Of MCF-7 and T47D Cell Lines	
5.1 Introduction	175
5.1.1 Chapter Aims	176
5.2 Methods	177
5.2.1 Sample Collection.....	177
5.2.2 ADSC Isolation and Characterisation	177
5.2.3 MCF-7 Cell line	177
5.2.4 T47D Cell line	177
5.2.5 Tissue Culture.....	177
5.2.6 Cell Counting	178
5.2.7 Co-Culture Inserts.....	178
5.2.8 Proliferation.....	178
5.2.9 Migration	178
5.2.10 Invasion	179
5.2.11 Bioenergetics	179
5.2.12 Morphology	179

5.2.13 Cytokine/Chemokine Expression Profiles	179
5.2.14 Data Analysis	180
5.2.14.1 Proliferation	180
5.2.14.2 Migration	180
5.2.14.3 Invasion	180
5.2.14.4 Bioenergetics	180
5.2.14.5 Morphology	181
5.2.14.6 Cytokine/Chemokine Expression Profiles	181
5.3 Results from the MCF-7 and T47D Co-Culture Experiments	182
5.3.1 MCF-7 Co-Culture Proliferation	182
5.3.2 T47D Co-Culture Proliferation	185
5.3.3 MCF-7 Co-Culture Migration	187
5.3.4 T47D Co-Culture Migration	190
5.3.5 MCF-7 Co-Culture Invasion	192
5.3.6 T47D Co-Culture Invasion	194
5.3.7 Utilising the Seahorse XFe Real-Time Bioenergetic Analyser	196
5.3.8 MCF-7 Co-Culture Bioenergetic Analysis	196
5.3.9 T47D Co-Culture Bioenergetic Analysis	200
5.3.10 MCF-7 Co-Culture Morphology	203
5.3.11 MCF-7 Co-Culture IL-6 Expression Profile	206
5.3.12 MCF-7 Co-Culture VEG-F Expression Profile	208
5.3.13 MCF-7 Co-Culture MCP-1 Expression Profile	210
5.4 Discussion	212
5.4.1 Conclusions	221
Chapter Six	223
General Discussion	
6.1 Overview	223
6.2 Conclusions Made from ADSC Optimisation and Patient Selection ..	226
6.3 The Creation of a Clinically Relevant Cell-Based Model	228
6.4 Measuring the Effect of ADSCs Isolated from Healthy and Cancer Patients on the Neoplastic Traits of MCF-7 and T47D Cells	229
6.5 Future Work	236

6.6 Conclusion	234
Appendices	238
A.1 ADSC Isolation Protocols Two and Three	238
A.2 Cellular and Nuclei Solidarity	240
A.3 Graphical Representation: Mitochondrial Electron Transport Chain	242
A.4 Publications and Presentations	243
Bibliography	245

Acknowledgments

I can think of no better place to start than by expressing my sincerest gratitude to my primary supervisor Professor Shareen Doak. Without your constant guidance and support, this process would have been vastly more difficult and far less enjoyable. To Professor Iain Whitaker who has been such an advocate for clinical academia, thank you for empowering me to follow my research interests, and for the opportunity to work within your incredible research group. This work would not have been possible without the twenty-two patients, many of whom were undergoing difficult cancer treatment, who so graciously consented to be part of this research project. I am forever indebted to you.

Two people who deserve a special mention, because without them I would likely still be in the lab. Firstly, Dr Nick Jones, who spent countless hours with me providing expert advice, encouragement, and support, even when he didn't have to. I am an immeasurably better researcher for having had the opportunity to work with him. To my fellow doctoral candidate and good friend Tom Jovic, these last three years would have been impossible without your sense of humour and support. I have lost count of the times we kept each other (and our cells) going, thank you. To those fantastic people in the 2nd floor post-grad office who always made time (and tea) when I was most in need, thank you for always being so welcoming. To all the incredible scientists, researchers and fellow students on the 2nd and 4th floors in the ILS1 who have graciously given me your time and advice, shown me techniques, and lent me protocols, thank you for the benefit of your experience and expertise.

I feel very fortunate to have had such incredible support from my amazing family and friends, who have endured conversations about this research for the better part of five years and continued to feign interest. I appreciate always having your encouragement, I promise to stop talking about it now. To my wonderful husband Richard, who has caffeinated me during my write up, and listened to endless chapter re-writes read aloud. Thank you for your patience, love and understanding. Finally, to my incredible parents, thank you for all you have done and continue to do, and to my mother Kathryn, my inspiration, and the person to whom this work is dedicated.

List of Tables

Table	Title	Page
1.1	Summary of surgical indications for either BCS or mastectomy	14
1.2	Differences between BM-NC and ADSCs	40
2.1	MCF-7 and T47D cell line source and anatomically derived site	48
2.2	CD markers detected to determine stem-status of extracted ADSCs	56
2.3	Components of Adipogenic (top), Osteogenic (middle) and Chondrogenic (bottom) StemPro Kits	60
2.4	Ratios of fresh and conditioned media for each percentage	64
2.5	Human Cytokine Antibody Array Reagents	76
2.6	Reagents required for IL-6, MCP1 and VEGF ELISA analysis	79
2.7	Methods for calculating the respiratory parameters	83
3.1	Original ADSC isolation protocol as described by Zuk et al 2001	92
3.2	ADSC cell lines isolated from healthy patient who have never been diagnosed with breast cancer	100
3.3	ADSC cell lines isolated from patients with breast cancer	101
3.4	Positive and negative controls for each individual fluorophore demonstrating specificity of each CD cell surface marker prior to their use on the ADSC population	111
A1.1	ADSC isolation protocol number two being trialled for inclusion in the study	238
A1.2	ADSC isolation protocols number three being trialled for inclusion in the study	239

List of Figures

Figure	Title	Page
1.1	Breast cancer resectional surgery and reconstruction timeline	2
1.2	Anatomy of the breast in cross section	4
1.3	Percentage distribution of Invasive and DCIS cases by anatomical location	6
1.4	Average number of new cases of breast cancer per year with age specific incidence rates per 100,000 females (2016-2018 data)	8
1.5	Flow diagram representing the process following screening or clinical assessment of suspected new breast pathology	11
1.6	The six original cancer hallmarks	21
1.7	The emerging cancer hallmarks and enabling characteristics	29
1.8	Schematic representation of the cancer immunity cycle	34
1.9	Steps for isolating ADSCs from patient lipoaspirate	38
1.10	Diagrammatic representation illustrating key cytokines and proteins released through interactions between ADSCs and Breast cancer cell lines <i>in vivo</i> and <i>in vitro</i>	42
2.1	Image taken of the extracted ADSCs demonstrating plastic adherence seven days after isolation	52
2.2	Example of an adipose derived stem cells flow cytometry plot	56
2.3	Compensation controls: positive and negative VersaComp beads run with individual fluorophores to generate a specific compensation matrix for the chosen panel	58
2.4	The compensation matrix created in FlowJo using the VersaComp beads to create single stain compensation controls for the chosen ADSC panel	59
2.5	Image taken of extracted ADSCs differentiated into adipocytes	61
2.6	Image taken of extracted ADSCs differentiated into chondrocytes	62
2.7	Image taken of extracted ADSCs differentiated into osteocytes	63
2.8	Confocal microscopy of ADSCs in a 0.4mm transwell insert	65
2.9	ACEA Real Time Cell Analysis (RTCA) iCELLigence machine	67
2.10	Schematic representation of an EL-8 plate for use with the RTCA iCELLigence machine	67
2.11	Schematic representation of an EL-16 Plate sitting over an EL-8 plate	68
2.12	IBIDI cell culture insert used for migration assay in a standard 24 well plate	70
2.13	Schematic representation of 24 well transwell insert sitting in a 24 well plate	71
2.14	Collagen Cell Culture invasion inserts to measure MCF-7 invasion	73

2.15	Schematic overview of the steps required for a sandwich ELISA assay	81
2.16	Oxygen consumption rate (OCR) and the calculation of metabolic parameters	82
3.1	Light microscopy image taken of heterogenous cell population using Protocol 2 demonstrating near confluence after only 48 hours in culture	103
3.2	Light microscopy image taken of extracted ADSCs demonstrating plastic adherence seven days after isolation	105
3.3	Image taken of isolated ADSCs and control MSCs differentiated into adipocytes.	106
3.4	Image taken of isolated ADSCs and control MSCs differentiated into chondrocytes	107
3.5	Image taken of extracted ADSCs and control MSCs differentiated into Osteocytes	108
3.6	Fluorophore panel planning to determine potential fluorescent emission overlap	109
3.7	Schematic illustrating positive (stained) and negative (unstained) controls for each fluorophore to demonstrate fluorophore specificity prior to use on ADSCs	110
3.8	Flow cytometry for three patient cell lines at early passage (negative markers)	114
3.9	Flow cytometry for three patient cell lines at early passage (positive markers)	115
3.10	Flow cytometry for three patient cell lines at late passage (negative markers)	116
3.11	Flow cytometry for three patient cell lines at late passage (positive markers)	116
3.12	MCF-7 & T47D seeding density optimisation for measuring cellular proliferation using the iCELLigence	122
3.13	Various seeding densities for optimising the assessment of MCF-7 migration for conditioned media and co-culture experiments using an IBIDI insert	124
3.14	Various seeding densities for optimising the assessment of T47D migration for co-culture experiments using an IBIDI insert	125
3.15	Stained MCF-7 Invasion inserts at 24 and 48-hours incubation	126
3.16	Stained T47D Invasion inserts at 24 and 48-hours incubation	127
3.17	Extracted stain from invasion inserts following 24 and 48-hours incubation	127
3.18	The Human Cytokine Array panel detecting multiple cytokines in ADSC media supernatants	128
3.19	The Human Cytokine Array panel template	129
3.20	Quantified protein expression using ImageJ to evaluate spot intensity	130

3.21	Bioenergetic profiles of MCF-7 and T47D cells at various seeding densities	132
3.22	Bioenergetic profiles of MCF-7 and T47D cells at various FCCP concentrations	133
3.23	Confocal microscopy of stained ADSCs in 0.4 μ m transwell inserts following	135
4.1	CM from healthy patient ADSCs at early passage (p2), increase the rate of MCF-7 proliferation when compared with the control across all concentrations	149
4.2	CM from healthy and cancer ADSCs at late passage (p8) influence rates of MCF-7 proliferation over 48 hours	150
4.3	CM from healthy and cancer patients has no effect of real-time rate of MCF adhesion at either early (p2) or late (p8) passage	151
4.4	Rate of MCF-7 gap closure when treated with ADSC CM from a healthy patient when compared with the control (0%)	153
4.5	Rate of MCF-7 gap closure when treated with ADSC CM from a cancer patient when compared with the control (0%)	154
4.6	Analysis of gap remaining after 24 and 48 hours of treatment with ADSC CM from healthy and cancer patients at early and late passage	155
4.7	Media conditioned by healthy ADSCs increases MCF-7 invasion at late passage (p8) at all concentrations (25-100%)	157
4.8	MCF-7 cells demonstrate increased invasion at early passage (p2) when treated with healthy ADSC CM at higher concentrations (75% and 100%) when compared with the control (0%)	158
4.9	MCF-7 cells demonstrate increased invasion at late passage (p8) when treated with healthy ADSC CM at all concentrations when compared with cancer ADSC CM and the control (0%)	159
4.10	MCF-7 Cells imaged with the INCELL 2000 Analyzer (DAPI and Brightfield views)	161
4.11	MCF-7 cell measurements of both nuclei and cellular morphology demonstrate no change at increasing concentrations of ADSC CM	162
4.12	MCF-7 cells incubated with ADSC CM for 24 hours demonstrated no change in cellular eccentricity at early or late passage (p2 and p8)	163
4.13	ADSCs isolated from healthy patients secrete higher levels of IL-6 and MCP-1 when compared with ADSCs isolated from patient with breast cancer	165
4.14	Concentrations of IL-6 detected in MCF-7 media are related to percentage of ADSC CM at early and late passage	166
4.15	Concentrations of VEG-F detected in MCF-7 media are related to percentage of ADSC CM at early and late passage	167

4.16	Concentrations of MCP-1 detected in MCF-7 media are related to percentage of ADSC CM at early and late passage	168
5.1	MCF-7 cells co-cultured with ADSCs isolated from healthy patients proliferate at an increased rate when compared with ADSCs isolated from patients with cancer	183
5.2	MCF-7 cells co-cultured with ADSCs isolated from healthy patients are less adherent in cell culture compared with the control	184
5.3	T47D cells co-cultured with ADSCs isolated from healthy and cancer patients proliferate at an increased rate when compared with the control	186
5.4	T47D cells co-cultured with ADSCs isolated from healthy patients are less adherent in cell culture compared with the control	187
5.5	MCF-7 cells demonstrate increased migration when co-cultured with ADSCs isolated from healthy patients	189
5.6	MCF-7 cells co-cultured with ADSCs isolated from healthy patients demonstrate an increased rate of migration	190
5.7	There is no change in T47D migration observed when cells are co-cultured with ADSCs from either healthy or cancer patients	191
5.8	There is no change in T47D migration observed when cells are co-cultured with ADSCs from either healthy or cancer patients	192
5.9	Co-culturing MCF-7 cells with healthy ADSCs increases invasion at late passage (p8)	193
5.10	MCF-7 cells demonstrate increased invasion when co-cultured ADSCs isolated from healthy patients when compared with the control	194
5.11	Co-culturing MCF-7 cells with healthy ADSCs increases invasion at late passage (p8)	195
5.12	T47D cells demonstrate increased invasion when co-cultured ADSCs isolated from healthy patients when compared with the control	195
5.13	MCF-7 cells demonstrate increased metabolic activity when co-cultured with ADSCs from healthy and cancer patients when compared with the control	198
5.14	MCF-7 cells demonstrate increased basal and maximal glycolysis when co-cultured with ADSCs from healthy patients	199
5.15	T47D cells demonstrate increased metabolic activity when co-cultured with ADSCs from healthy patients when compared with the control	201
5.16	T47D cells demonstrate increased basal and maximal glycolysis when co-cultured with ADSCs from healthy patients	202
5.17	MCF-7 Cells imaged with the INCELL 2000 Analyzer (DAPI and Brightfield views)	204

5.18	MCF-7 cell measurements of both nuclei and cellular area demonstrate no change following co-culture with ADSCs from healthy and cancer patients	205
5.19	MCF-7 cells co-cultured with ADSCs from healthy and cancer patients demonstrated no change in cellular eccentricity at late passage (p8)	206
5.20	MCF-7s co-cultured with ADSCs isolated from healthy patients had statistically significant increases in IL-6 concentration detected in the culture media	208
5.21	MCF-7s co-cultured with ADSCs isolated from healthy patients had statistically significant increases in VEG-F concentration detected in the culture media	210
5.22	MCF-7s co-cultured with ADSCs isolated from healthy patients had statistically significant increases in MCP-1 concentration detected in the culture media	211
A2.1	MCF-7 cell measurements of both nuclei and cellular solidarity demonstrate no change at increasing concentrations of ADSC CM	240
A2.2	MCF-7 cell measurements of both nuclei and cellular solidarity demonstrate no change following co-culture with ADSCs from healthy and cancer patients	241
A3.1	Graphical representation of the mitochondrial electron transport chain	242

Abbreviations

β	Beta
Δ	Delta
$\Delta CI/\Delta T$	Change in Cell Index/Change in Time
cm	Centimetre
IU	International Units
g	Gravity
nl	Nanolitre
μl	Microlitre
μg	Microgram
μm	Micrometre
M	Mole
mg	Milligram
ml	Millilitre
mM	Millimole
mpH	milli-pH unit
mV	Millivolt
N	Number of equivalents of solute dissolved in 1L of solution
ng	Nanogram
pmole	Picomole
AD	Anno Domini
ADM	Acellular Dermal Matrix
ADSC	Adipose Derived Stem Cell
ANOVA	Analysis of Variance
APC	Antigen Presenting Cell
AR	Androgen Receptor
ASPRS	American Society of Plastic and Reconstructive Surgeons
ASPS	American Society of Plastic Surgeons
ATCC	American Type Culture Collection
ATP	Adenosine Triphosphate
BAPRAS	British Association of Plastic, Reconstructive and Aesthetic Surgeons
BCL-2	B-Cell Lymphoma 2

BCS	Breast-Conserving Surgery
BM-NC	Bone Marrow Derived Nucleated Cell
BRCA	Breast Cancer gene
BSA	Bovine Serum Albumin
CAF	Cancer Associated Fibroblast
CCL2	Chemokine (C-C motif) Ligand 2
CCR2	C-C Chemokine Receptor Type 2
CD	Cluster of Differentiation
c-GMP	Cyclic Guanosine Monophosphate
CI	Cell Index
CM	Conditioned Media
CO₂	Carbon Dioxide
CRUK	Cancer Research UK
CSC	Cancer Stem Cell
CT	Computed (axial) Tomography
CTx	Chemotherapy
DAPI	4',6-diamidino-2-phenylindole
DC	Dendritic Cell
DCIS	Ductal Carcinoma <i>in Situ</i>
DFS	Disease Free Survival
DIEP	Deep Inferior Epigastric Perforator
DM	Diabetes Mellitus
DMEM	Dulbecco's Modified Eagle's Medium
DMSO	Dimethyl Sulphoxide
DNA	Deoxyribonucleic Acid
EC	Endothelial Cell
ECAR	Extracellular Acidification Rate
ECM	Extracellular Matrix
EDTA	Ethylenediaminetetraacetic acid
EGFR	Epidermal Growth Factor Receptor
ELISA	Enzyme Linked Immunosorbent Assay
EMT	Epithelial to Mesenchymal Transition
ER	Oestrogen Receptor
ERK	Extracellular Signal-Regulated Kinases
FACS	Fluorescence Activated Cell Sorting

FBS	Foetal Bovine Serum
FCCP	Carbonyl cyanide-p-trifluoromethoxyphenylhydrazone
FFG	Free Fat Graft
FFT	Free Fat Transfer
FGF	Fibroblastic Growth Factor
GCO	Global Cancer Observatory
GLUT	Glucose Transporter
GMP	Good Manufacturing Practice
Gy	Gray (unit)
H₂SO₄	Sulphuric Acid
HCL	Hydrochloric Acid
HER2	Human Epidermal Growth Factor Receptor 2
HIV	Human Immunodeficiency Viruses
HRP	Horseradish Peroxidase
HRT	Hormone Replacement Therapy
HUVEC	Human Umbilical Vein Endothelial Cells
IARC	International Agency for Research on Cancer
ICAM-1	Intercellular Adhesion Molecule-1
IFATS	International Federation for Adipose Therapeutics and Science
IL-6	Interleukin-6
IL-8	Interleukin-8
ILS	Institute of Life Science
ISCT	International Society for Cellular Therapy
JAK2	Janus Kinase 2
JLA	James Lind Alliance
KHCO₃	Potassium Bicarbonate
LD	Latissimus Dorsi
MAP Kinase	Mitogen Activated Protein Kinase
MCF-7	Michigan Cancer Foundation - patient 7 (Breast cancer cell line)
MCP-1	Monocyte Chemoattractant Protein 1
MDT	Multi Disciplinary Team
MEM	Minimum Essential Media
MHC	Major Histocompatibility Complex
miRNA	Micro-RNA
MMP	Matrix Metalloproteases

MRI	Magnetic Resonance Imaging
MSC	Mesenchymal Stem Cell
NAC	Nipple Areolar Complex
NH₄Cl	Ammonium Chloride
NHS	National Health Service
NSABP	National Surgical Adjuvant Breast and Bowel Project
NST	No Specific Type
Ob-R	Leptin Receptor
OCP	Oral Contraceptive Pill
OCR	Oxygen Consumption Rate
OXPHOS	Oxidative Phosphorylation
P/S	Penicillin/Streptomycin
PARP	Poly-ADP-Ribose Polymerase
PBS	Phosphate Buffered Saline
PDGF	Platelet Derived Growth Factor
PFA	Paraformaldehyde
pH	Potential of Hydrogen
pHPL	Pooled Human Platelet Lysate
PLA	Processed Lipoaspirate
PR	Progesterone Receptor
QC	Quality Control
qRT-PCR	Quantitative Real Time Polymerase Chain Reaction
RANTES	Regulated on Activation, Normal T cell Expressed and Secreted
RB	Retinoblastoma Protein
RBC	Red Blood Cell
RNA	Ribonucleic Acid
RNS	Reactive Nitrogen Species
ROS	Reactive Oxygen Species
rpm	Revolutions Per Minute
RTCA	Real Time Cell Analysis
RTx	Radiotherapy
SBUHB	Swansea Bay University Health Board
SDF-1	Stromal cell Derived Factor 1
SEM	Standard Error of the Mean
SEM	Scanning Electron Microscope

SERD	Selective Oestrogen Receptor Degraders
SERM	Selective Oestrogen Receptor Modulator
SGAP	Superior Gluteal Artery Perforator
SLNB	Sentinel Lymph Node Biopsy
SLUG	Zinc Finger Protein SNAI2
SNAIL	Zinc Finger Protein SNAI1
STAT3	Signal Transducer and Activator of Transcription 3
SVF	Stromal Vascular Fraction
T47D	ER+ PR+ HER2- breast cancer cell line
TAM	Tumour Associated Macrophage
TCR	T Cell Receptor
TDLU	Terminal Duct Lobular Units
TGF-β	Transforming Growth Factor- β
TMB	Tetramethylbenzidine
TNBC	Triple Negative Breast Cancers
TNF-α	Tumour Necrosis Factor α
TNM	Tumour, Nodes, Metastases
TOMS	Theatre Operation Management System
TP53	Tumour Protein p53
TRAM	Transverse Rectus Abdominus Myocutaneous
TTC	Time To Cure
TWIST	Twist-Related Protein
UK	United Kingdom
US	United States
USA	United States of America
UV	Ultraviolet
VEGF-A	Vascular Endothelial Growth Factor-A
WHO	World Health Organisation
ZEB	Zinc Finger E Box-binding Homeobox

Chapter One

Introduction

1.1 General overview

In data recently released by the World Health Organisations (WHO) International Agency for Research on Cancer (IARC) and Global Cancer Observatory (GCO), the incidence of breast cancer is rising, and is now the most commonly diagnosed malignancy world-wide with an estimated 2.3 million cases reported annually (Gu *et al.*, 2021; Sung *et al.*, 2021). In the UK there are around 55,000 new cases per year, with surgery continuing to prove an essential cornerstone of treatment (Jeevan *et al.*, 2014; Sung *et al.*, 2021). With the evolution of radiological imaging, staging and neoadjuvant therapies, more women are being diagnosed at an earlier stage, resulting in reduced mortality and the need for less radical resectional surgery (Forman *et al.*, 2014; Carioli *et al.*, 2017). As emphasised in each of the four national mastectomy and breast reconstruction audits, breast reconstruction forms an essential part of the patient's journey, and should be carefully considered at an early stage (Jeevan *et al.*, 2011, 2014). The positive impact on patient health and wellbeing resulting from early discussions regarding suitable reconstruction options is well documented and is intrinsically linked to the patient journey (Jeevan *et al.*, 2011; Somogyi *et al.*, 2015; Mokhatri-Hesari and Montazeri, 2020). It is essential to understand therefore what surgical options are available to patients, the timing of surgery, and impact that any treatment might have on long term outcomes including recurrence.

The development of breast cancer surgery has evolved significantly since early advocacy of clear operative margins by Galen [120-200 AD] in response to the 'crab-like' projections noted to extend from the primary tumour (Figure 1.1) (Combella *et al.*, 2016). Halstead's radical mastectomy, despite being first described in the late 1800s, remained the gold standard of resectional breast cancer surgery well into the 1970s, until trials conducted in the US and Europe were able to show comparable outcomes using breast-conserving surgery (BCS) techniques (Hermann *et al.*, 1985; Fisher *et al.*, 2002; Cotlar, Dubose

and Rose, 2003; Asgeirsson *et al.*, 2005; Baum, 2013; Gu *et al.*, 2021). Post-surgery, the resulting defect must be assessed to determine the most appropriate reconstruction option to restore the breast mound, in the context of the available options and with consideration of any further adjuvant treatment that may be required (e.g., chemotherapy or radiotherapy).

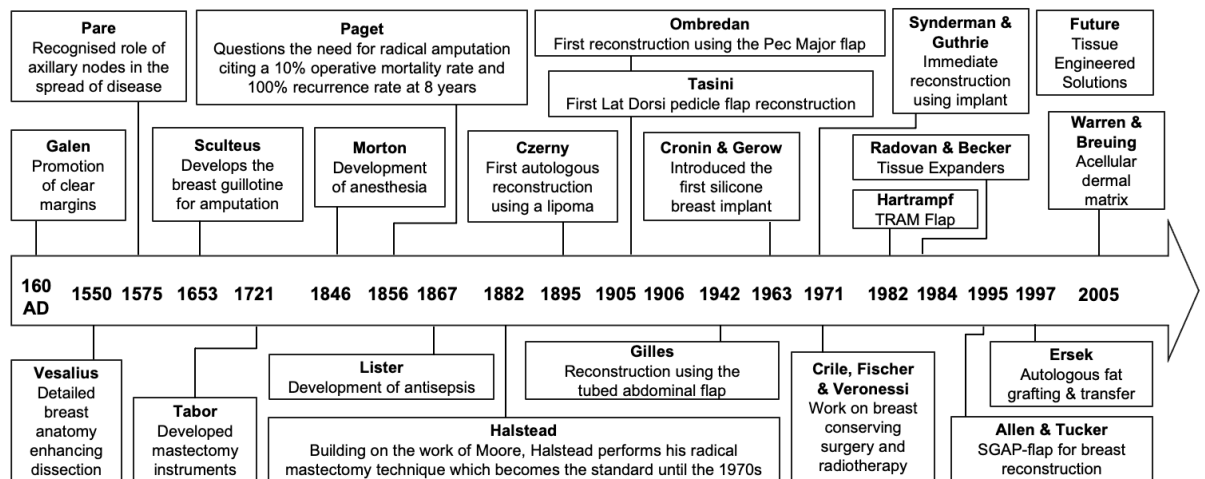


Figure 1.1: Breast cancer resectional surgery and reconstruction timeline

Timeline representing the surgical developments in breast cancer recognition, resection and reconstruction over the last 2000 years (Combella *et al.*, 2016). Reproduced with permission.

While the gold standard autologous option for large volume defects remains free tissue transfer, the contour deformity resulting from BCS requires an alternative approach to produce a reliable reconstruction option for women who have different volume requirements. Balancing the advantages of autologous reconstruction with minimal donor site morbidity, free fat transfer (FFT) or lipofilling for these small to medium volume defects post-BCS has become significantly more common place since the mid 2000s (Losken *et al.*, 2011; Biazús *et al.*, 2015; Maione *et al.*, 2015). The relative ease of the technique, coupled with the option to offer patients the procedure as a local anaesthetic day case, means that it is significantly more accessible, with patients able to have the procedure done outside traditional tertiary microsurgical centres.

Controversies regarding safety however have prompted questions regarding the suitability of this technique in the context of BCS and the potential microenvironment of breast cancer. Within the adipose tissue harvested for transfer are a mesenchymal stem cell (MSC) population termed adipose derived stem cells (ADSCs) which were initially characterised in 2001 (Zuk *et al.*, 2001). While thought to have a range of applications from regenerative therapy to tissue engineering, questions were raised regarding their potential interaction with breast cancer and co-location in the breast following BCS (Jotzu *et al.*, 2011; Riggio, Bordoni and Nava, 2013; Wei *et al.*, 2015; Wu *et al.*, 2019). While there are a number of *in vivo* and *in vitro* studies that demonstrate the pro-tumorigenic effects of ADSCs on a number of breast cancer cell lines, the clinical studies fail to reflect this in early reviews of small group patient outcomes (Bertolini, Petit and Kolonin, 2015; Schweizer *et al.*, 2015; Kronowitz *et al.*, 2016; Wu *et al.*, 2019; T. Li *et al.*, 2020).

The absence of clear clinical guidance on the use of this technique in patients, demonstrates a lack of consensus between scientific and clinical studies, which must be better understood to provide a more detailed explanation to patients. Limitations with regards to clinical applicability of cell line based models to study the effect of ADSCs interaction with breast cancer are accepted. In much of the scientific work already published, there is a clear disparity between primary cell line sources, and the clinical patient group undergoing reconstruction. It is important to address this when approaching experimental design ensuring the clinical cohort is appropriately represented and the effects of ADSCs on the hallmarks of breast cancer are better elucidated.

1.2 Breast Anatomy

The female mammary glands (breasts) are paired apocrine glands located on the anterior chest wall between the second and sixth rib, overlying the pectoralis major and minor muscles (Hicks and Lester, 2016) (Figure 1.2). Comprised of glandular breast tissue and lobules connected by ducts to openings within the nipple areolar complex (NAC), the breast is adherent to the fascia overlying the chest wall and supported by a network of suspensory

ligaments (of Cooper) (Rehnke *et al.*, 2018). The ductal system within the breast is lined internally by luminal epithelium and an outer myoepithelial layer which terminates in distally located terminal duct lobular units (TDLUs) (Gudjonsson *et al.*, 2005). The tissue composition and volume of the breast changes over time in response to menarche, pregnancy, lactation, menopause, and ageing, all of which must be considered in the context of disease development. The synergistic actions of numerous hormones including oestrogen and progesterone drives the highly dynamic and specialised glandular tissue to change and develop. Ductal morphogenesis is initially driven during menarche by oestrogen, with progesterone later playing a role in ductal branching (Yang, Wang and Jiao, 2017).

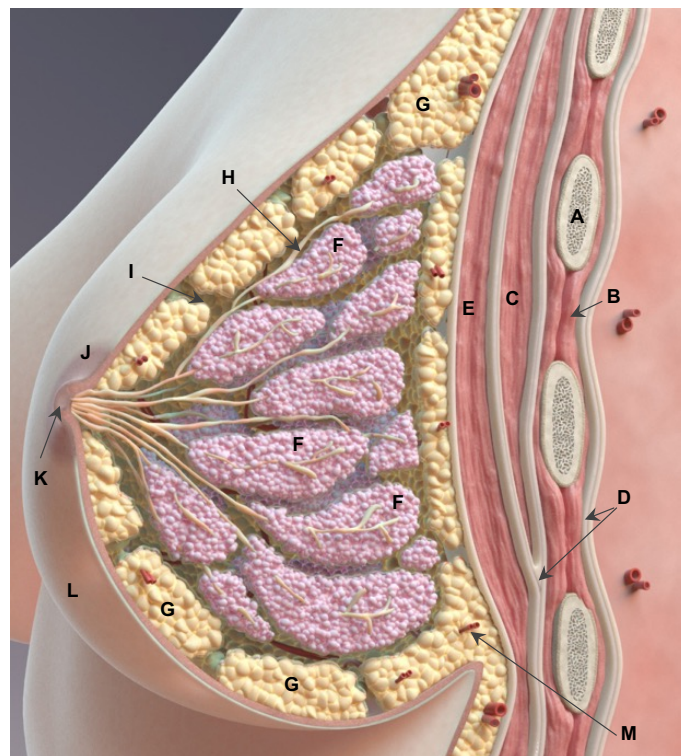


Figure 1.2: Anatomy of the breast in cross section

3D cross section of the left breast demonstrating some of the key anatomical features. (A) Cross section of the rib. (B) Intercostal muscles. (C) Pectoralis minor muscle. (D) Fascia. (E) Pectoralis major muscle. (F) Breast lobules. (G) Glandular / adipose tissue. (H) Ducts. (I) Suspensory ligaments (of Cooper) (J) Nipple areolar complex (NAC). (K) Nipple. (L) Skin. (M) Vessels supplying the breast parenchyma. Important structures not shown are the lymphatic ducts and lymph nodes which are primarily located in the axilla. (Open access image adapted from <https://www.turbosquid.com/3d-models/breast-cross-section-3d-model-1237788>).

1.3 Breast Cancer Overview

Breast cancer is the most common cancer diagnosed worldwide and is the leading cancer cause of mortality in women (Akram *et al.*, 2017), with one in five women (approximately 20%) projected to get disease recurrence, related to their original tumour stage and grade, as such it presents a complex clinical challenge (Mayor, 2012; Pan *et al.*, 2017). As previously described (Section 1.1), there are approximately 55,000 new cases diagnosed in the UK each year, with the majority (estimated 70%) found to be ER+ (Caul and Broggio, 2019; Public Health Scotland, 2020; Public Health Wales, 2021; Sung *et al.*, 2021). Most breast cancers diagnosed are invasive or no special type (NST) having previously being labelled invasive ductal carcinoma, with approximately 15% of new diagnosis being ductal carcinoma *in situ* (DCIS) (Caul and Broggio, 2019; Public Health Scotland, 2020; Public Health Wales, 2021). The anatomical location for each varies, and when confined to a single anatomical region, invasive breast cancer is most commonly found in the upper outer quadrant. Similarly, the vast majority of DCIS diagnosed is found within the ducts lined with luminal epithelium (Figure 1.3).

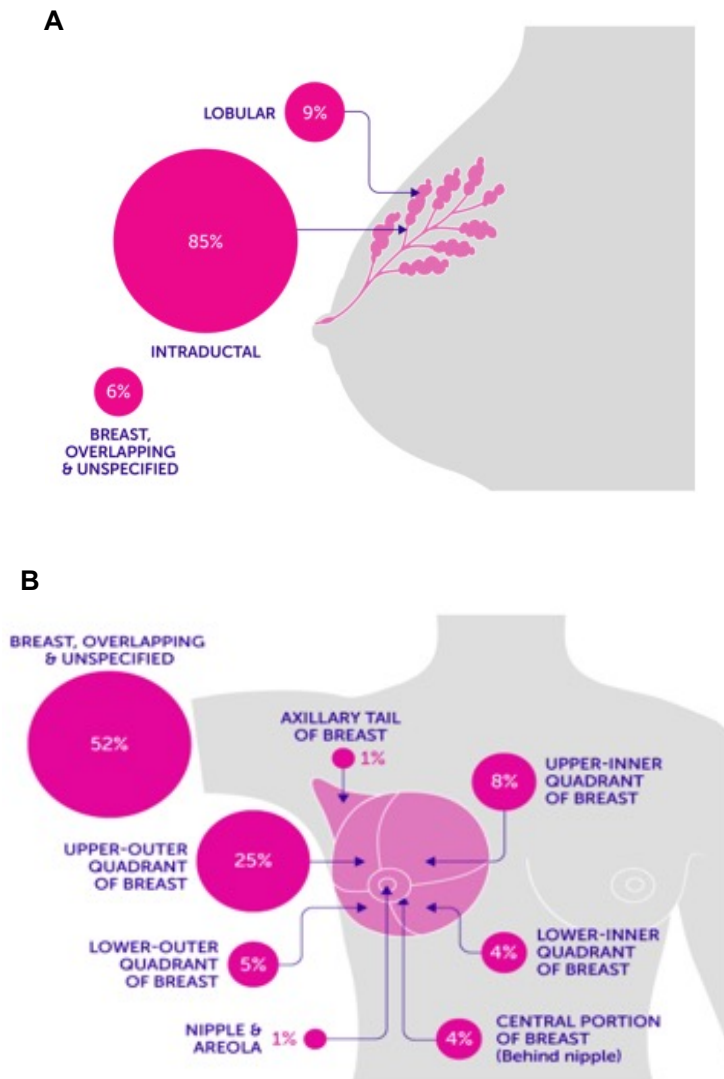


Figure 1.3: Percentage distribution of Invasive and DCIS cases by anatomical location

Percentage distribution for DCIS (A) and Invasive breast cancer (B) by anatomical location. (A) The overwhelming majority of DCIS cancers are found in the ductal system (85%), with very few found in the lobular structures. (B) The majority of invasive cancers (52%) are either overlapping or unspecified anatomically. For those confined to a single anatomical region, the majority are found in the upper outer quadrant (25%). Sourced with permission (Cancer Research UK, https://www.cancerresearchuk.org/sites/default/files/cstreamnode/inc_anatomicalsite_breast.pdf, https://www.cancerresearchuk.org/sites/default/files/cstreamnode/inc_anatomicalsite_breastinsitu_0.pdf Accessed November 2021).

Breast tumours originate from cellular hyperproliferation and progression to neoplastic disease following stimulation and pro-tumorigenic signalling, with cues from the microenvironment playing a vital role (Sun *et al.*, 2017). The mechanisms outlining the initiation, development and progression of cancer

are discussed in detail (Section 1.4) and the understanding of breast cancer biology has evolved significantly over the last two decades beyond the clinical metrics and pathological markers (Prat *et al.*, 2015). Five intrinsic molecular subtypes of breast cancer have been identified as; Luminal A and B, HER2 enriched, Claudin-low and Basal-like (Prat *et al.*, 2015; Mesa-Eguiagaray *et al.*, 2020). These subtypes reflect the diverse biology of breast cancer and are important clinically as they have been shown to be associated with varied treatment responses and survival outcomes (Gabos *et al.*, 2010; Voduc *et al.*, 2010; Millar *et al.*, 2011). The majority of initial pathological assessment aims to identify the hormone or receptor status (ER, PR, HER2) following biopsy as there is significant evidence that oestrogen plays an important role in the stimulation and progression of the majority of breast cancers (>70% are ER+), and receptor status is a key feature in treatment selection (Fragomeni, Sciallis and Jeruss, 2018).

For those patients with triple negative breast cancer (TNBC), there is an absence of all hormones and HER2 receptors on pathological examination. Accounting for approximately 18% of all invasive breast cancer diagnosis, they include NST along with other variants such as carcinoma with medullary features and carcinoma with apocrine features, adenoid cystic carcinoma, secretory carcinoma and metaplastic carcinoma (Tan *et al.*, 2020). The lack of detectable receptor, resistance to endocrine therapy and difficulty managing this complex cancer sub-type is illustrated in the high rate of metastatic progression, propensity to relapse and poor clinical outcome (Yin *et al.*, 2020). However, as a result of screening programmes, self-examination and the development of more advanced surgical techniques and (neo)adjuvant treatment, mortality is declining (Carioli *et al.*, 2017). Despite this considerable progress, the complex heterogeneity of the disease can make it a challenge to diagnose, treat and manage with clarity regarding long term prognosis.

1.3.1 Demographics and Incidence of Breast Cancer

As the most common cancer diagnosed worldwide, and with a life time risk of 1 in 7 for women, breast cancer incidence is increasing and accounts for around 15% of all new cancers in the UK annually (Sung *et al.*, 2021). Cancer

Research UK (CRUK) estimate there are 55,920 new cases of breast cancer each year and approximately 11,547 deaths, representing a reduction in mortality of around 38% since the early 1970s (Carioli *et al.*, 2017). The incidence of breast cancer is related strongly to age, with the highest rates of cancer in women aged over 75, peaking in the over 90s (Figure 1.4). Although there are around 300 cases per year diagnosed in men, this accounts for less than one percent (0.6%) of total cases (Caul and Broggio, 2019; Sung *et al.*, 2021).

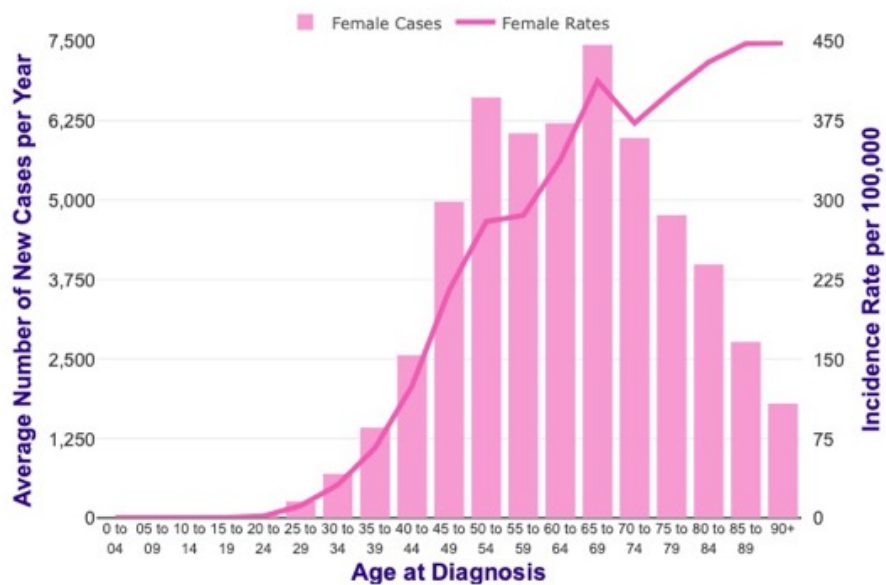


Figure 1.4: Average number of new cases of breast cancer per year with age specific incidence rates per 100,000 females (2016-2018 data)

Graph demonstrating the increased incidence of female breast cancer with age. The brief plateau after the age of 50 is the result of screening program intervention, which may also account for the plateau noted at age 70 when the programme ends as breast cancer diagnosis has been brought forward. After which the incidence then continues to rise. Sourced with permission (Cancer Research UK, <https://www.cancerresearchuk.org/health-professional/cancer-statistics/statistics-by-cancer-type/breastcancer/incidence-invasive#heading-One> Accessed November 2021).

Studies examining variability in stage of diagnosis and survival have identified some key disparities within groups that present an opportunity to reduce mortality. Lower socioeconomic status and advancing age is associated with reduced relative cancer survival and more advanced stage of disease at diagnosis (Rutherford *et al.*, 2013, 2015). While some features, which relate to

survival are independent of these factors e.g., cancer sub-type, anatomical location, patient risk factors, it is essential that preventable causes of mortality are addressed.

1.3.2 Risk Factors for Breast Cancer Development and Their Management

Risk factors for developing breast cancer are varied and include both intrinsic factors which are often out of patients control and extrinsic factors which individually or in combination can influence the development of breast cancer. Intrinsic risks include genetic mutations such as *BRCA* or *TP53* which are associated with the development of various breast cancer sub-types (Holm *et al.*, 2017). Also increasing age, early menarche or late menopause, high baseline hormone levels, positive family history and the development of benign breast disease can all contribute to the development of malignant breast tumours (Dossus and Benusiglio, 2015; Sun *et al.*, 2017). Extrinsic or lifestyle factors can include the use of hormone replacement therapy (HRT) or the oral contraceptive pill (OCP), sedentary lifestyle, excessive use of alcohol and obesity (Dossus and Benusiglio, 2015; Hao *et al.*, 2021; Jiang, Xie and Chen, 2021). Anything which increases the risk of developing the disease is technically termed a 'risk factor', however it is important to clarify that not all people with risk factors for breast cancer will go on to develop it, and some patients with relatively few or no risk factors at all may be diagnosed with the disease. Understanding key risks is essential for stratifying women in resource limited healthcare settings, and the recent ENVISION consensus reinforces these opportunities if risk-stratification models are used in conjunction with resource planning and effective stakeholder engagement (Pashayan *et al.*, 2020).

Targeted monitoring, patient education and preventative interventions reduce the likelihood of breast cancer development, or bring forward the stage of diagnosis which potentially improves patient outcomes (Evans *et al.*, 2016). First established in 1988, the national breast cancer screening programme offers routine three-yearly appointments to women between the ages of 50 and 70, and the government estimate that there is a breast cancer detection rate

of around 30% (Massat *et al.*, 2016; Public Health England, 2016). Alongside the screening programme there are patient information documents available to explain the process and answer any initial queries, as informed consent remains an essential part of engagement (Public Health England, 2018). In addition to picking up *de novo* cancers, it has been demonstrated that women participating in these screening programmes can also experience over investigation of benign disease or false positives, undue worry and additional procedures with associated morbidity (Gøtzsche and Jørgensen, 2013). Recently the results of the UK Age trial were published which examined the impact of lowering the age of screening commencement to 40. Findings demonstrated that although the absolute risk reduction remained constant, there was a relative risk reduction in cancer mortality and that reviewing the age screening limit may have value (Duffy *et al.*, 2020). The ongoing AgeX trial which is also examining extending the screening age range to 47-73 is not expected to report until sometime in 2026 (Moser *et al.*, 2011).

1.3.3 Diagnosing Breast Cancer

Breast cancer is generally diagnosed following routine breast cancer screening, patient self-examination resulting in referral to acute breast clinics, or rarely in routine histological examination of tissue excised for other reasons (e.g., breast reduction surgery). The gold-standard assessment (Figure 1.5) is triple-assessment and involves clinical examination, needle biopsy and appropriate imaging which can be ultrasound, mammography or MRI followed by discussion at a specialist breast multi-disciplinary team (MDT) meeting (Public Health England, 2016).

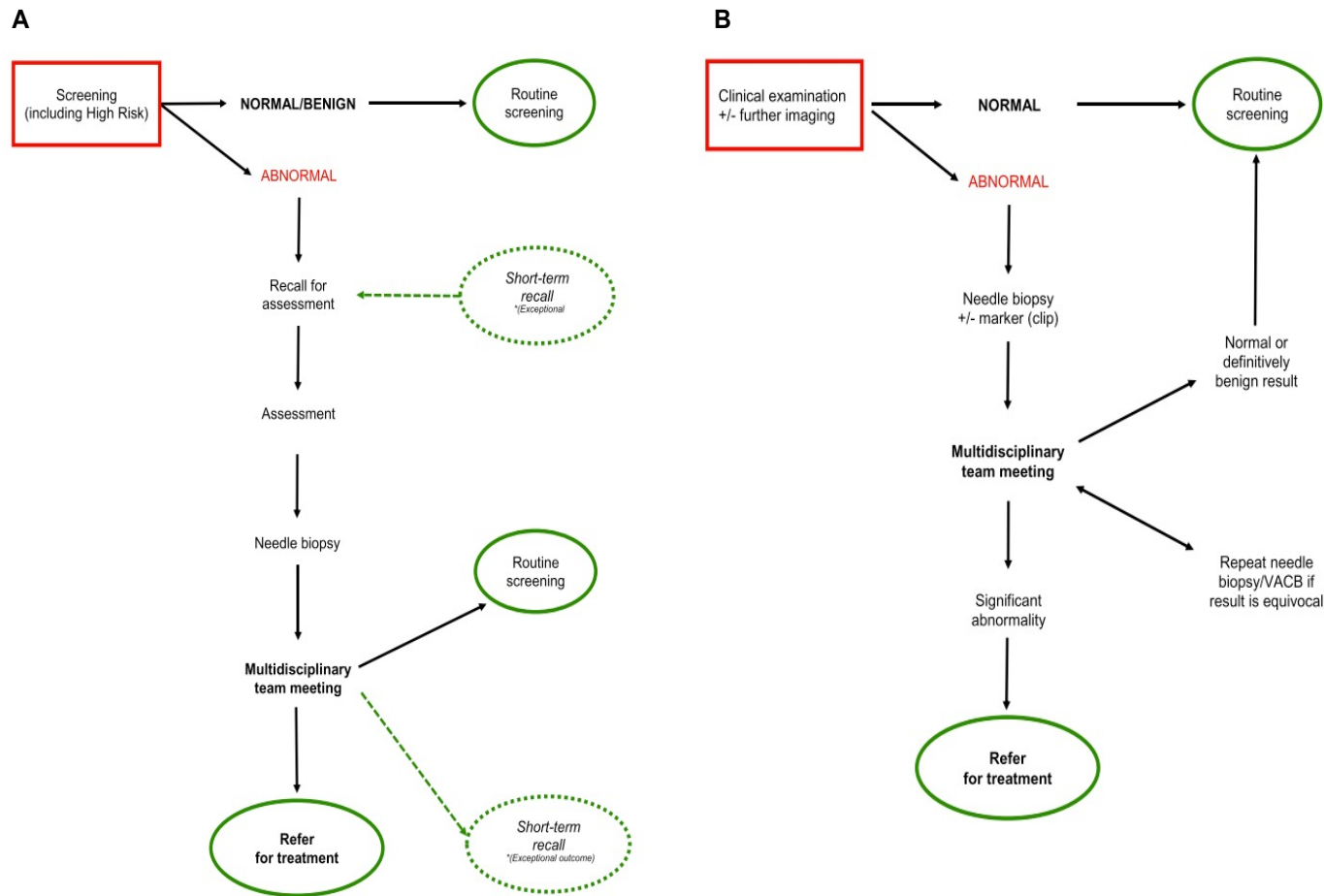


Figure 1.5: Flow diagram representing the process following screening or clinical assessment of suspected new breast pathology

Flow diagrams detailing patient pathways following detection of pathology as part of (A) routine breast screening or (B) after self-examination. Each pathway includes the gold standard triple assessment which involves examination by a qualified medical professional, imaging and histological assessment following biopsy. Followed by discussion at the breast MDT. Open access images taken from the clinical guidance for breast screening number 49 (Public Health England, 2016)

The treatment of breast cancer is largely dictated by the Tumour-Node-Metastasis (TNM) staging at diagnosis. Following the histopathological confirmation which provides information on the tumour (T) stage, additional investigations are required to establish nodal status and the presence of metastatic deposits. Regional lymph node basins are imaged and either biopsied or surgically sampled to ascertain the presence of lymphatic spread, which provides the nodal status. Computed (axial) tomography (CT) or magnetic resonance imaging (MRI) scans of the head, chest, abdomen, and pelvis provides additional information regarding tumour extent (volume) and the presence of metastatic deposits in distant organs or within the skeleton. The 8th edition of the TNM staging manual was published in 2018 and has resulted in a stage change for approximately one third of patients with breast cancer, and compared with previous guidance, attempts to expand beyond the anatomical extent of the disease to enable a more patient focused classification to be applied (Cserni *et al.*, 2018; Plichta *et al.*, 2020). Anatomical staging should only be used where biomarker tests are not routinely available, as the ER, PR and HER2 status is widely recognised as an important part of the clinical prognostic staging of patients with breast cancer.

1.3.4 Treatment Overview

As illustrated by the four national mastectomy and breast reconstruction audits, the primary aim of breast cancer treatment is to remove or ablate the tumour to reduce the risk of premature death (Jeevan *et al.*, 2011). The treatment decisions should be made in conjunction with the patient following a specialist MDT discussion to establish the most appropriate option for managing the disease, based on the tumour stage, nodal status, and presence of metastatic spread. The treatment for most breast cancers will involve some type of surgical treatment, often with adjuvant therapy to enhance the primary treatment, prolong disease free survival or extend life. Breast mound reconstruction has also been highlighted as a crucial part of the patient journey, and a plan for simultaneous or delayed reconstruction should be discussed with the patient, prior to commencing primary resectional surgery (Jeevan *et al.*, 2011, 2014).

1.3.5 Surgery for Breast Cancer

Surgery remains the mainstay of primary treatment for women diagnosed with breast cancer (Tomlins and Parker, 2016). The choice of surgical procedure depends on several factors including whether the cancer is invasive or *in situ* (DCIS), the size of the primary tumour and position in the breast, and whether clear margins can be achieved with the surgical procedure of choice. The radical mastectomy described and popularised by William Halsted in the 1880s, involved removing the breast and overlying skin, pectoralis muscles and fascia in addition to resecting the axillary lymph nodes, and became the gold standard for resectional breast cancer surgery until the 1970s (Losken and Jurkiewicz, 2002; Cotlar, Dubose and Rose, 2003). This *en bloc* resection, routinely termed 'The cancer operation' due to its adoption by other surgical disciplines, followed the principle of centrifugal tumour spread into adjacent anatomical structures that must be controlled with radical tissue resection (DeVita and Rosenberg, 2012).

Although modified versions of his original operation were described which left behind more anatomical structures such as the pectoralis muscles, surgery that conserved the breast mound raised concerns regarding rates of recurrence. The national surgical adjuvant breast and bowel project (NSABP) which was commenced in 1971, initiated a randomised clinical trial with the aim of resolving the controversy surrounding the surgical management of breast cancer. The published findings demonstrated that over a 25 year follow up period, there was no statistically significant difference in survival when comparing Halsted's radical mastectomy with less extensive resections (Fisher *et al.*, 2002). Similarly in a second trial (B-06), the concept of breast-conserving surgery (BCS) was evaluated with and without adjuvant radiotherapy for early stage (I and II) breast cancers for tumours less than 4 cm in diameter, with survival comparable to total mastectomy (Fisher *et al.*, 2002). BCS offered surgeons the opportunity to effectively treat breast cancer with significantly reduced morbidity for patients. Lumpectomies or quadrantectomies are now routinely used in patients found to have early stage disease, often combined with additional treatment (Public Health England, 2016). The choice of surgical approach depends on several factors (Table 1.1)

and must follow appropriate discussion by a specialist MDT and the patient. Regardless of the choice, it is essential to ensure that oncological clearance is achieved.

Table 1.1: Summary of surgical indications for either BCS or mastectomy

Indications for BCS	Indications for Mastectomy
Patient preference	Patient preference
Tumours <4cm within an average sized breast	Tumours >4cm diameter suitable for surgery
Multi-focal tumours confined to one quadrant	Multi-focal tumours in more than one quadrant
Tumours >4cm combined with additional oncoplastic procedures	Failed BCS which includes positive margins and local recurrence
No patient contraindications to radiotherapy	Recurrent breast cancer
Following neo-adjuvant therapy to reduce tumour size prior to resection	Central breast cancer or inability to get clear margins with good cosmesis

Key indications for choosing either BCS or mastectomy as the surgical modality for the treatment of breast cancer. Either surgical option can be combined with axillary surgery, radiotherapy, chemotherapy, or hormone therapy as required. Taken from open access guidelines (Public Health England, 2016).

Axillary surgery is also important as part of disease management, forming an essential element of the TNM staging criteria and helping to inform the choice of adjuvant therapy (Magnoni *et al.*, 2020). There should be consideration of axillary surgery in all patients who present with invasive breast cancer to ascertain the presence of disease in the primary breast lymph node basin, need for additional treatment and provide important staging information (McDonald *et al.*, 2016). For patients with early breast cancer and clear axillary nodal basins on clinical exam, sentinel lymph node biopsy (SLNB) is an alternative option to provide a similar level of information with reduced morbidity (Krag *et al.*, 2010; Gatzemeier and Bruce Mann, 2013).

1.3.6 Radiotherapy Treatment for Breast Cancer

The use of external beam or targeted radiation as an adjunct to treat patients with breast cancer, often in conjunction with surgery and hormone therapy, has evolved significantly since it was first described in the early 1900s (Ekmektzoglou *et al.*, 2009; DeVita and Rosenberg, 2012). The use of a more tightly controlled beam aims to deliver targeted radiation to destroy cancer cells and prolonging disease free survival, which involves the delivery of a standard dose of around 40 – 50 Gy in smaller fractions, to reduce toxicity (Liu *et al.*, 2020). Conventional fractionated or the more targeted hypofractionated radiotherapy does have drawback for patients, as the surrounding tissue often absorbs some of the energy resulting in skin and lung toxicity, lymphoedema, restriction in shoulder movement and delayed cardiac toxicity (Gu *et al.*, 2021). Serial follow up scans with either CT, MRI, or ultrasound can be used to monitor remnant breast tissue, the contralateral breast and axilla in addition to the common sites of metastatic spread to monitor the response to treatment.

1.3.7 Adjuvant and Neoadjuvant Treatment for Breast Cancer

The use of systemic therapy and its timing in relation to surgery, either before (neoadjuvant) or after (adjuvant), is well described and has become a routine part of the treatment for breast cancer with the aim to increase disease free survival (DFS). As our understanding of novel biomarkers and molecular drug targets develops, the effect these drugs have has improved, enabling clinicians to select tailored therapy for individual tumour characteristics, alone or in combination (Shien and Iwata, 2020). Broadly classified into chemotherapy, hormone therapy or molecular targeted therapy, treatment choices are guided by the MDT, tumour specific hormone receptors, treatment combinations required, and cost (Shien and Iwata, 2020).

1.3.8 Chemotherapy for Breast Cancer

The use of chemotherapy pre-operatively was introduced initially in the 1970s as a neoadjuvant treatment, designed to reduce the tumour bulk, treat micro metastatic disease and enable surgical resections to take place (Asselain *et al.*, 2018). It is now frequently used in early stage or locally advanced breast cancer to down-stage disease and facilitate the option of BCS (Fisusi and

Akala, 2019). Cytotoxic chemotherapy targets rapidly dividing cancer cells and is often delivered intravenously across successive weeks in cycles prior to surgery. There are numerous drug combinations described in the literature, e.g., mitoxantrone, methotrexate, and mitomycin-C (MMM) or cyclophosphamide, methotrexate, and 5-fluorouracil (CMF) which have been trialled and their efficacy compared (Gazet *et al.*, 2001; Taucher *et al.*, 2008). If patients have positive nodal disease, a high-grade tumour diagnosed histologically post resection, or do not have hormone receptor positive cancer, chemotherapy is a useful adjunct to achieve disease control. For those patients with metastatic disease at a distant site, chemotherapy is an option for palliative treatment to improve disease control by targeting the distant cancer cells with the aim to stabilise the disease and slow the progression (Maughan, Lutterbie and Ham, 2010; McDonald *et al.*, 2016). As chemotherapy targets rapidly dividing cells, healthy cells can also be affected by this systemic treatment, which can result in side effects such as nausea, diarrhoea and weight loss, and hair loss. Similarly, bone marrow suppression can leave patients vulnerable to infection and prone to bleeding, easy bruising, and severe fatigue, all of which can be challenging for patients to manage (Robiolle *et al.*, 2015; Schmidt *et al.*, 2015; Browall *et al.*, 2018).

1.3.9 Hormone Therapy for Breast Cancer

Breast cancers are heterogeneous in their clinical course, histopathological appearance, response to treatment and time to recurrence, which is reflected by the diverse molecular classifications of breast cancer by sub-type (Voduc *et al.*, 2010; Dai *et al.*, 2016). The contemporary management of breast cancer, driven by a greater understanding of the cancer hallmarks and genetic expression of cancer sub-types has resulted in a range of targeted therapies which interact with cell expressed hormone receptors (ER+ and PR+) (Fragomeni, Sciallis and Jeruss, 2018). Selective oestrogen receptor modulator (SERM) Tamoxifen and aromatase inhibitors Letrozole and Exemestane are generally used to treat ER+ breast cancer patients for a period of five years (Patel and Bihani, 2018). While Letrozole and Exemestane are used exclusively in post-menopausal women, the drugs all exhibit anti-oestrogen effects and have shown to reduce the incidence of recurrence in

women with ER+ breast cancer (Maughan, Lutterbie and Ham, 2010). Recurrent ER+ breast cancer drugs such as Fulvestrant are selective oestrogen receptor degraders (SERDs) and have been shown to slow down or suspend the progression of metastatic disease for a period of time (Foulds, 2018; Pernas *et al.*, 2018).

1.3.10 Molecular Targeted Therapy for Breast Cancer

Unlike drugs that modulate hormone receptors, targeted cancer drugs focus on specific cellular elements or pathways to influence the cells behaviour. HER2 protein receptors on the cancer cell surface can be targeted with a monoclonal antibody therapy such as Trastuzumab (Herceptin), which induces an immune response affecting the overexpression of HER2, and has demonstrated improved patient outcomes (Fragomeni, Sciallis and Jeruss, 2018). They can also be combined with other drugs such as chemotherapy to address early stage HER2+ breast cancers which did not respond as expected to radiotherapy, or in combination with aromatase inhibitors for disease which has metastasised (Cook *et al.*, 2021). Drug resistance does present a specific challenge in these cancer subtypes, and trials are focusing on additional downstream receptor expression and the inhibition of CDK4/6 in patients with HER2 positive breast cancer (Goel *et al.*, 2016; Pernas *et al.*, 2018).

1.3.11 Breast Reconstruction Post Cancer Resection

The importance of breast reconstruction following surgery for women with breast cancer is well recognised, with successive national mastectomy and breast reconstruction audits reinforcing the essential element it plays in the holistic care of patients (Jeevan *et al.*, 2011). As part of the routine discussions at the earliest stages of diagnosis and management, options for reconstruction should be clearly identified and explained to allow patients to choose an option that is right for them. This theme of holistic care and patient prioritisation has become a more central part of the clinical journey and treatment of breast cancer. In conjunction with the James Lind Alliance (JLA) priority setting partnership, 10 essential questions have been identified by surgeons in Canada, highlighting the importance of patient centred research priorities in post breast cancer reconstruction (Zhong *et al.*, 2021). The impact on patient

psychology cannot be underestimated, with studies demonstrating that patient experience is not necessarily correlated with size of primary resection (Grujic *et al.*, 2021). Patients who choose to undergo reconstruction, whether immediate or delayed, demonstrate higher levels of wellbeing and satisfaction with reduced psychological distress (Jeevan *et al.*, 2014). As more patients are diagnosed at an earlier stage, and the advancements in detection, non-surgical treatment and monitoring continue, more women are having less radical surgical procedures (Asselain *et al.*, 2018; Sun *et al.*, 2021). An increase in BCS with potentially closer surgical margins, highlights the importance of putting reconstruction in the context of potential recurrence to ensure the procedures offered are robustly evaluated for safety.

1.3.12 Medium to Large Volume Reconstruction

As previously described in Section 1.1 (Figure 1.1), breast reconstruction techniques have evolved significantly over the last 110 years (Combella *et al.*, 2016). Approximately 40% of patients with breast cancer go on to have a mastectomy resulting in a significant skin and soft tissue deficit, often in conjunction with adjuvant or neoadjuvant treatment (Jeevan *et al.*, 2011). Reconstruction must not only address the volume loss on the mastectomy side but consider patient priorities such as desire to achieve symmetry with the contralateral breast. The timing of procedures must also be carefully planned as radiotherapy has been shown to increase the complication rate of surgery, so clinicians must be mindful to counsel their patients accordingly (Kronowitz, 2012). Staged procedures enable patients to complete their emergent treatment prior to undergoing the reconstruction, with key considerations including volume required, missing structures, and physical activity which may limit the use of some autologous options.

The use of prosthesis for breast reconstruction with a silicone implant, with or without acellular dermal matrix (ADM) is seen more commonly in younger patients undergoing bilateral procedures where the skin envelope is preserved (skin-sparing mastectomy) (Panchal and Matros, 2017). While offering a shorter operative time with no donor site morbidity, some studies quote a complication rate of around 34%, with higher rates noted in patients

undergoing or having undergone radiotherapy (Kalstrup *et al.*, 2021). Autologous options include pedicled flaps, which remain attached to their primary blood supply e.g., latissimus dorsi (LD), or free tissue transfer, which are disconnected from their primary blood supply and re-vascularised in their new location e.g., deep inferior epigastric perforator artery (DIEP) flap (Blondeel and Christiaens, 2002; Nano *et al.*, 2004; Sturtz *et al.*, 2005; Masia *et al.*, 2015). Seen as the gold standard for autologous reconstruction, they can be lengthy operations that require specialist equipment and skilled microsurgeons to perform, in addition to trained staff to monitor the flaps post operatively (Tamai, 2009). There is also the donor site morbidity to consider, including functional shoulder impairment following LD, or significant abdominal scar and associated wound healing complications in patients undergoing DIEP reconstruction (Grotting, Beckenstein and Arkoulakis, 2003; Grünherz *et al.*, 2020). While a range of well evidenced options exist for large volume reconstruction, the small volume deficits created by BCS present an altogether more complex reconstructive challenge for surgeons aiming to restore the breast mound.

1.3.13 Free Fat Transfer for Small to Medium Volume Defects

Free fat transfer (FFT) or lipofilling involves the harvesting and processing of subcutaneous fat (adipose tissue) from one anatomical location (e.g., abdomen or thighs), to increase volume at a second anatomical site (e.g., breast or face). The use of adipose tissue as an autologous filler was initially described by Neuber in 1893, however it was not popularised again until the 1980s following published works by Coleman who strongly advocated for this technique (Neuber, 1893; Mojallal and Foyatier, 2004). In 1987 the American Society of Plastic and Reconstructive Surgeons (ASPRS) *ad hoc* committee on new procedures reviewed the technique in the context of breast cancer. Transferred fat which does not pick up a new blood supply necroses and calcifies, raising concerns that the use of FFT in the breast region would impede the detection of breast cancer, which led to an outright ban on the technique (ASPRS, 1987). Despite refinements in the 1990s to reduce the rate of resorption, it was not until a further review by the American Society of Plastic Surgeons (ASPS) in 2007 regarding the safety and efficacy of the technique

that the decision regarding its considered use within the breast was reversed (Gutowski *et al.*, 2009). Concerns regarding breast cancer detection in the previously lipofilled breast were addressed following papers demonstrating the efficacy of modern imaging techniques to delineate between cancer and benign fat necrosis (Veber *et al.*, 2011; Costantini *et al.*, 2013; Noor *et al.*, 2016). This technique was subsequently adopted back into the surgical repertoire of surgeons worldwide who felt the primary safety concerns had been robustly addressed.

Free fat transfer to the breast therefore offered patients an autologous option for small to medium volume defects, which could be performed as local anaesthetic day case procedure with minimal down time (Singla, 2016). Expected rates of resorption are quoted between 10 and 50%, however most patients find sufficient volume is achieved with one or two procedures (Fitoussi *et al.*, 2009; Losken *et al.*, 2011). Although complications can include localised infections, fat necrosis or volume resorption, the procedure is generally well tolerated with additional evidence suggesting patients undergoing FFT post radiotherapy report a noticeable improvement in skin quality and pliability (Losken *et al.*, 2011; Sarfati *et al.*, 2011; Debald *et al.*, 2017). FFT was now viewed as a suitable reconstructive option with few downsides which was supported by a recent taskforce review. As expected, following its publication, the frequency of FFT use increased. Simultaneously in 2001 and 2002 initial papers were published characterising a group of unique progenitor cells present in adipose tissue (ADSCs) which held substantial regenerative potential (Zuk *et al.*, 2001, 2002). Regardless of developments in technique and imaging technologies, surgical regulatory bodies including the ASPS and British Association of Plastic, Reconstructive and Aesthetic Surgeons (BAPRAS) accepted that with limited understanding of the basic science surrounding ADSCs, formal guidelines were difficult to establish, and further research was needed to understand how they might influence long term safety (Gutowski *et al.*, 2009; Fatah *et al.*, 2012).

1.4 Hallmarks of Cancer

The six well described biological capabilities acquired in the evolution of neoplastic disease are considered the original ‘hallmarks’ of cancer. The multistep process of pathogenesis involves a complex interplay between distinctly separate but intrinsically linked capabilities which facilitate the growth, progression and metastasis of cancer (Hanahan and Weinberg, 2000). In the 20 years since their initial description, a broader understanding of the mechanisms that drive this process have seen the introduction of four additional hallmarks which alongside the effect of the tumour microenvironment, expand our understanding of this intricate process (Hanahan and Weinberg, 2011). The initial six hallmarks set out to establish a framework to better to understand the fundamental alternations in cellular physiology and regulatory mechanisms that collectively define the pathogenesis of malignancy (Hanahan and Weinberg, 2000). This concept addressed the core commonalities across hundreds of cancers and tumour subtypes with innumerable genomic variations to identify the six essential abnormalities in cellular physiology which result in the growth and progression of cancer (Figure 1.6).

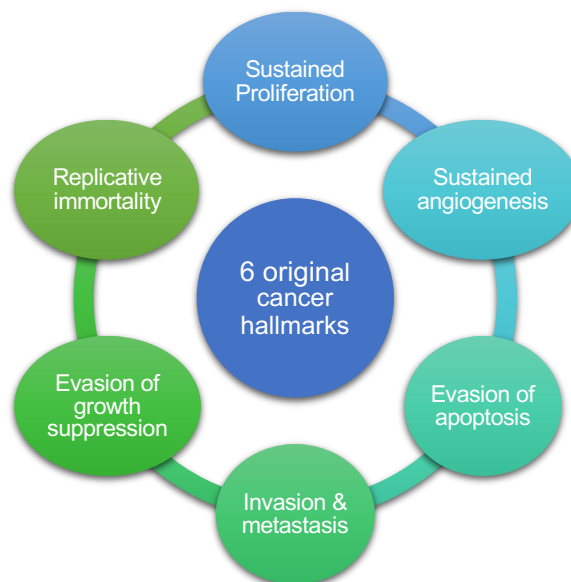


Figure 1.6: The six original cancer hallmarks

Diagrammatic representation of the six original cancer hallmarks described by Hanahan and Weinberg encompassing the common properties acquired by the majority of cancer cells which facilitates the development into cancer (Hanahan and Weinberg, 2000).

1.4.1 Sustained Proliferation

The lack of reliance on exogenous growth stimulation and unchecked cellular proliferation resistant to growth suppressor signals is a key characteristic seen across tumour cells, common in breast cancer (Dai *et al.*, 2016). Unlike normal healthy cells which rely on the external mitogenic growth signals to determine the point of transition into a state of growth, tumour cells seemingly disregard these external cues, and rather rely on internal signals produced by various oncogenes (Hanahan and Weinberg, 2000). The ability to circumvent normal cellular homeostasis is a fundamental trait of cancer cell development and since its initial description 20 years ago, our understanding of the mitogenic signalling between cancer cells has expanded and is now better understood (Hynes and MacDonald, 2009; Lemmon and Schlessinger, 2010; Trenker and Jura, 2020). Abnormalities in receptor protein expression at the tumour cell surface have the potential to increase the responsiveness of the cell to relatively low levels of growth factor ligand, or result in abnormal ligand-independent function (Hanahan and Weinberg, 2011). Mechanisms for sustaining unimpeded growth have been suggested which include the autocrine stimulation of proliferation through the production of growth factor ligands which bind to the associated receptors on the cancer cells (Cheng *et al.*, 2005, 2008). Furthermore, in the wider tumour stroma, the induction of paracrine growth factors, extracellular matrix (ECM) components and proteolytic enzymes from normal cells (e.g. fibroblasts) which support dysregulated proliferation, has been described (Bhowmick, Neilson and Moses, 2004; Tripathi, Billet and Bhowmick, 2012).

Studies focused on breast neoplasia have demonstrated the response of the leptin receptor Ob-R on ER+ MCF-7 breast cancer resulting in STAT3 and p42/p44 (MAP)-kinase activations and increased proliferation when exposed to the hormone leptin produced by healthy white adipocytes (Dieudonne *et al.*, 2002). The complex influence of growth factor receptors is further illustrated when examining genomic mutations in breast cancer which result in abnormal activation of signalling pathways usually triggered by activated receptors (Foulds, 2018; Moses *et al.*, 2018). Naturally occurring mutations in ER receptor genes such as *ESR1* have been linked with the clinical development

of oestrogen independent breast cancer proliferation and resistance to the selective oestrogen receptor modulator, Tamoxifen (Harrod *et al.*, 2017). The additional resistance to the usual negative feedback loops responsible for managing cellular homeostasis, also has a role to play and may contribute to the acquired resistance to breast cancer treatments which target mitogenic signalling (Hanahan and Weinberg, 2011; Fiorillo *et al.*, 2018). The development of endocrine therapy resistance in ER+ breast cancer is an important example as the loss of the oestrogen induced negative feedback loop is associated with a poor prognostic outcome for patients (Xiao *et al.*, 2018). Rather than being triggered by a single process, the numerous components of dysregulated cell function, abnormal signalling, receptor expression and gene mutations contribute to the uncontrolled proliferation and disruption of feedback loops which drive breast cancer growth and progression.

1.4.2 Evasion of Growth Suppression

As a complex multi-step process, success relies on the ability to continue to proliferate and propagate whilst evading the numerous mechanisms designed to suppress atypical cellular growth. While numerous tumour suppressors exist, the two most often implicated in the evasion of growth suppression by cancer are *TP53* and retinoblastoma (*RB*) (Hanahan and Weinberg, 2000, 2011). *TP53* is a critical tumour suppressor gene and the cellular p53 protein acts as a checkpoint in response to DNA damage (Schon and Tischkowitz, 2018). Mutations in *TP53* have been found in 30% of breast carcinomas and are associated with a high penetrance of breast cancer, with a cumulative incidence of 85% by 60 years of age in patient cohorts (Bertheau *et al.*, 2013; Mai *et al.*, 2016). Understanding how these mutations affect cell function is an essential part of clinical classification and development of therapeutic agents. TNBC are generally understood to have a poor clinical outcome when compared with their ER+, (progesterone receptor) PR+, (human epidermal growth factor receptor 2) HER2+ counterparts (Prat *et al.*, 2015; Yin *et al.*, 2020). In studies examining TNBC and association with Poly-ADP-Ribose Polymerase (PARP) proteins found that over 80% express mutant p53, which as part of a wider stratification, may be useful to guide dual therapy treatment

with PARP inhibitors and cytotoxic treatment (Xiao *et al.*, 2020). *RB* similarly plays a key role in proliferation as a cell cycle gate keeper, loss of which allows dysregulated cell cycle firing. ER+ breast cancer often retains *RB* function, and is underpinned by hyperactivity in the D-type cyclins, cyclin-dependent kinase 4 (CDK4) and CDK6 axis (Pernas *et al.*, 2018). This preservation of function is important as the intact axis makes an attractive therapeutic target, demonstrated by the range of CDK4/6 inhibitors that have been developed (e.g. Ribociclib) used to treat locally advanced ER+ breast cancer (Hortobagyi *et al.*, 2016). The loss of expression of the *RB* protein (pRB) is often associated with TNBC, reducing their responsiveness to CDK4/6 inhibitors, further illustrating the key role *RB* plays in the progression of neoplastic disease and resistance to growth suppression (Johnson *et al.*, 2016; Pernas *et al.*, 2018).

1.4.3 Evasion of Apoptosis

Cell death by apoptosis is a programmed response to various triggers including DNA damage, telomere shortening and abnormal oncogene expression which serves as a mechanism to prevent the development of neoplastic disease (Evan and Littlewood, 1998; Węsierska-Gądek *et al.*, 2007; Tompkins and Thorburn, 2019; Yang *et al.*, 2021). Not only is an impairment in apoptosis critical in the development of neoplastic autonomy, but also in the developed resistance to treatment with cytotoxic therapies (Adams and Cory, 2007). The complex processes which control apoptosis are balanced between upstream triggers and downstream effectors, executed by intracellular cysteine proteases (caspases) (Singh, Letai and Sarosiek, 2019). Apoptosis can be triggered by an intrinsic intracellular 'stress' response or by an extrinsic response to 'death-receptor' ligands which bind to the cell surface and trigger cellular destruction (Adams and Cory, 2007). The careful balance is controlled by pro- and anti-apoptotic regulatory *BCL-2* and associated proteins (Bax and Bak) which respond to apoptotic signals (Adams and Cory, 2007; Carneiro and S. El-Deiry, 2020). In breast cancer patients, *BCL-2* expression has been highlighted as a potential predictive factor for chemosensitivity (Yang *et al.*, 2013), with bioinformatic studies examining abnormalities within this protein as potential therapeutic targets for future breast cancer treatment (Køinig *et al.*, 2019). Abnormalities in cellular function and sensors have been theorised to

contribute to abnormal apoptotic signals and responses which develop as breast cancer cells evolve strategies to circumvent cell death, including the loss of cell cycle arrest enforcer *TP53* (Evan and Littlewood, 1998; Evan, Lowe and Cepero, 2004; Goldar *et al.*, 2015; Yang *et al.*, 2021). Approximately 30% of ER+ breast carcinomas contain *TP53* mutations which is believed to be linked to both the molecular subtype and as a likely indicator for chemotherapy response in ER+ tumour types (Bertheau *et al.*, 2013).

1.4.4 Replicative Immortality

The ability of cancer cells to indefinitely replicate is an essential part of the pathogenic nature of this neoplastic disease. The resistance to senescence and crisis which normally triggers cell death, results in an immortalised cell population which seemingly possess limitless replicability (Hanahan and Weinberg, 2000, 2011). Essential to this process is the upregulation of the enzyme telomerase, which is responsible for mediating cancer cell immortality through repeated telomere extension (Rhyu, 1995; Guterres and Villanueva, 2020), a process which in contrast is silenced in most adult somatic cells. In studies examining pre-malignant breast lesions and established breast cancer, abnormalities in telomere length were seen early in the acquisition of malignant transformation, and differentiated cancers from pre-neoplastic lesions (Raynaud *et al.*, 2010; Yuan, Larsson and Xu, 2019). Therapeutic targeting of telomere maintenance is one of a number of approaches in the development of novel therapeutics for treating patients with breast cancer (Yaswen *et al.*, 2015).

1.4.5 Sustained Angiogenesis

Angiogenesis describes a process through which new blood vessels are derived from pre-existing vasculature in response to pro-angiogenic signalling. Tumour angiogenesis is essential for the continued growth of cancer which requires the rapid delivery of nutrients and oxygen, alongside the ability to eliminate carbon dioxide and metabolic by-products whilst providing access for the haematogenous spread of malignant cells. As cancer cell proliferation increases, the rate of apoptosis diminishes and hyperplastic growth results in a tumour size which is critical in relation to its existing blood supply. Rather

than succumb to the resultant sequelae of hypoperfusion, growth restriction and necrosis, the 'angiogenic switch' stimulates the transition of normally quiescent vasculature to become activated and create new vessels to support sustained tumour growth (Hanahan and Folkman, 1996; Baeriswyl and Christofori, 2009). As a discrete component of the multistage development of cancer, the angiogenic switch occurs when the balance of pro- and anti-angiogenic factors tips in favour of proangiogenic activities supporting vascularisation and tumour growth (Tonini, Rossi and Claudio, 2003; Baeriswyl and Christofori, 2009). Of the plethora of pro-angiogenic growth factors that have been described, vascular endothelial growth factor-A (VEGF-A) is a prototypic factor and a major driver of both physiological and pathogenic angiogenesis and can be upregulated by both hypoxia and oncogene signalling (Dvorak *et al.*, 1995; Baeriswyl and Christofori, 2009; Ferrara, 2009).

Studies specifically examining the links between proangiogenic factors as markers of breast cancer tumour burden, have demonstrated raised levels of VEGF-A and intercellular adhesion molecule-1 (ICAM-1) in patients with advanced nodal disease, with VEGF-A additionally being raised in patients with distant metastasis (Rykala *et al.*, 2011). ER+ breast cancer cell lines utilised for study further illustrate that the progression of tumours closely depends on the continued pro-angiogenic signalling, driving neoplastic transformation (Comşa, Cîmpean and Raica, 2015). Once activated, neo-angiogenesis often results in fragile, aberrant and poorly organised vasculature, with erratic blood flow and abnormal endothelial cell (EC) signalling and function, which results in leaking and micro-haemorrhaging (Hanahan and Weinberg, 2011; Asprițoiu *et al.*, 2021). This is often seen clinically on imaging of breast cancer with radiopaque contrast bleeding from the convoluted tumour vasculature. Rather than being a phenomena associated only with advanced cancer, induction of angiogenesis occurs early in the development of neoplastic disease, often contributing to the pre-malignant phase of tumour progression, highlighting its importance as a key cancer hallmark (Hanahan and Folkman, 1996; Hanahan and Weinberg, 2011).

1.4.6 Invasion and Metastasis

Cancer invasion leading to metastasis is often the final clinical phase, overcoming the biological and physical barriers resulting in end-stage disseminated disease, and significantly limiting treatment options available. Based on global statistics, approximately 20% of breast cancer patients will go on to develop metastatic disease, however only 6% have evidence of disease deposition at distant anatomical sites (lymph nodes, lung, bone, liver) at the time of diagnosis (Fridrichova and Zmetakova, 2019). Building on the 'seed' and 'soil' model proposed by Paget in 1889, the concept of cross talk between the breast tumour cells and the microenvironment still holds true (Fidler, 2003). The invasion-metastasis cascade describes interlinked processes which define a range of changes in; cell-cell adhesion, invasion through the basement membrane into nearby lympho-vasculature, leading to transport and extravasation of breast cancer cells resulting in distant micro and macro metastasis, and disseminated disease (Hanahan and Weinberg, 2000, 2011; Talmadge and Fidler, 2010). Tumour associated macrophages (TAMs) at the tumour peripheries can additionally release enzymes such as matrix metalloproteases (MMPs) and cysteine cathepsin proteases which support local invasion through surrounding structures (Boire *et al.*, 2005; Kessenbrock, Plaks and Werb, 2010; Macklin *et al.*, 2020).

Malignant invasion requires upregulation of the genes and transcription factors (e.g., *SNAIL*, *ZEB1/2*, *TWIST* and *SLUG*), which facilitate the epithelial-to-mesenchymal transition (EMT) of cancer cells by repressing E-cadherin and other regulators of cell-to-cell adhesion, thereby increasing motility (Hajra, Chen and Fearon, 2002; Berx and van Roy, 2009; Fridrichova and Zmetakova, 2019). The function of E-cadherin is altered in most epithelial tumours as part of their transition to invasive disease, with the functional impairment responsible for active signalling which support tumour cell invasion and migration (Cavallaro and Christofori, 2004). However there are exceptions, as seen in certain types of inflammatory breast cancer which demonstrates elevated levels of E-cadherin regardless of molecular profile or histological subtype (Berox and van Roy, 2009). However, the majority of breast cancer subtypes demonstrate enhanced migration, increased invasion and

development of metastasis when E-cadherin is downregulated (Berx *et al.*, 1995; Hajra, Chen and Fearon, 2002). In numerous tumour types, the 'cadherin switch' occurs with the loss of E-cadherin resulting in the gain of mesenchymal cadherins (e.g., N-cadherin) which interact with fibroblastic growth factors (FGFs) inducing invasion and migration (Hajra, Chen and Fearon, 2002; Cavallaro and Christofori, 2004; Berx and van Roy, 2009). Pro-inflammatory cytokines such as interleukin-6 (IL-6) have been shown to play an essential role in oncogenesis and induction of EMT, increasing migration and invasive potential (Li *et al.*, 2009; Weng *et al.*, 2019). Clinical studies have correlated high serum levels of IL-6 in patients with breast cancer, which reflected more advanced tumour stage and poorer prognosis (Ma *et al.*, 2017). The significant role played by cytokines such as IL-6 and their influence over key oncogenes have made them a target for immunotherapy (Weng *et al.*, 2019).

1.5 Emerging Hallmarks and Enabling Characteristics

In the 20 years since their original description, researchers have contributed significantly to the understanding of the complexity of cancer and the processes by which the original hallmarks were acquired. Building on this foundation (Figure 1.6), a deeper understanding of dysregulated tumour bioenergetics and the ability of cancer cells to evade immune destruction has seen these features added to the list of cancer hallmarks (Figure 1.7) (Hanahan and Weinberg, 2011). The acquired genomic instability which drives genetic abnormalities and inflammation, altering signalling pathways further demonstrate the importance of these enabling characteristics and their influence over disease progression (Moses *et al.*, 2018).

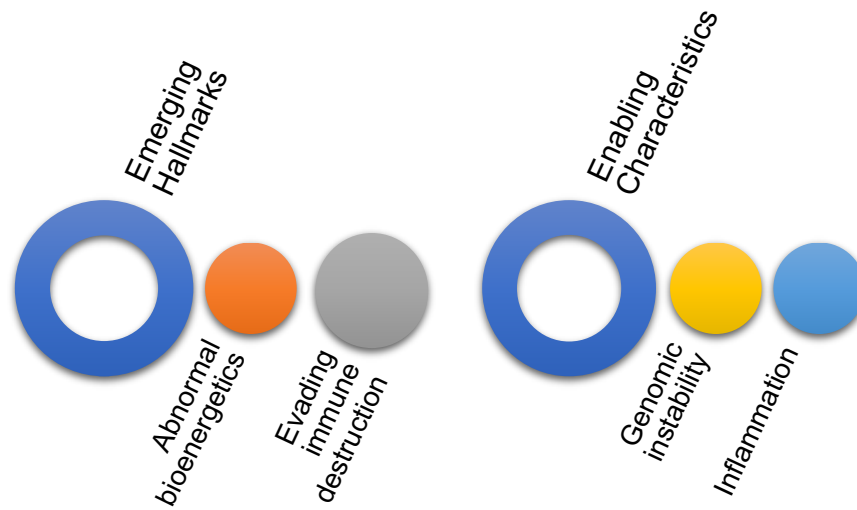


Figure 1.7: The emerging cancer hallmarks and enabling characteristics

Research in the 20 years since the original six hallmarks were described have highlighted the importance of additional factors in the understanding of this complex disease. The abnormal metabolic pathways and ability to modulate the immune response are intrinsically linked to growth, progression and establishment of metastatic deposits at distant sites (Hanahan and Weinberg, 2011).

1.5.1 Genomic Instability

Biological heterogeneity is found in both primary cancers and distant metastasis which reflects the selective process stemming from the rapid evolution and diverse phenotype of successful clonal tumour growth (Fidler, 2003). As with many clonal populations of malignant cells there is an inherent genetic and phenotypic instability, with studies demonstrating metastatic cells are intrinsically less stable than their benign counterparts (Talmadge and Fidler, 2010; Valles *et al.*, 2020). The acquisition of the cancer hallmarks which facilitate the progression of abnormal cells through neoplastic transformation, relies in part on successful genomic mutations which facilitate sustained malignant change. The disruption of the normal systems responsible for DNA and genome surveillance and maintenance (e.g., nucleotide-excision repair, base-excision repair and homologous recombination end joining) result in an accumulation of mutations which can accelerate malignant transformation (Hoeijmakers, 2001; Jackson and Bartek, 2009). Chromosomal instability is seen in most sporadic solid tumours which may in part be due to the fusion of critically short telomeres in *de novo* cancers (Jackson and Bartek, 2009). As

cancer progresses, intertumoral hypoxia and necrosis can accelerate the metastatic phenotype secondary to genetic instability, with studies demonstrating upregulation of the *MET* protooncogene inducing cell motility (Pennacchietti *et al.*, 2003). The central nature of the tumour suppressors p53 and *RB* in the surveillance and regulation of the cell cycle and have been previously discussed (Section 1.4.2) (Sherr and McCormick, 2002). Mutations in *TP53* are associated with uncontrolled proliferation of abnormal cells with an increase in genomic instability and rate of mutations (Dai *et al.*, 2016). Breast cancer with *TP53* and associated PR mutations have been found to be associated with the worst clinical outcomes and prognosis for patients (Olivier *et al.*, 2006).

Rather than solely being influenced by abnormalities in oncogenes or tumour suppressor genes responsible for essential maintenance of homeostatic function, studies examining the influence of epigenetic mechanisms (e.g., micro-RNA expression, histone modification and DNA methylation) have contributed significantly to the understanding of regulatory pathways influenced by critical gene expression (Berdasco and Esteller, 2010; Fridrichova and Zmetakova, 2019). When comparing micro-RNAs in human cancers to those in healthy cells, clear differences in expression are found (Martin *et al.*, 2014; Fridrichova and Zmetakova, 2019). Accepting there are a wide range of cancer-associated micro-RNAs which can have dual function, research has shown that they play a key role in the metastatic spread in breast cancer (Serpico, Molino and Di Cosimo, 2014). Down regulation of miR-34c has been found in breast cancer cells which initiate cell renewal, migration and EMT as a consequence of target gene *NOTCH4* expression (Fridrichova and Zmetakova, 2019). Modelling the complex and multi-step genetic alterations that must sequentially occur to drive the evolving cancer phenotype has been essential to interrogate the effect of various gene mutations on the development of cancer (Moses *et al.*, 2018). Although the influence of genomic alterations vary widely between cancer types, the developing research landscape is helping to broaden the understanding of genomic instability as an enabling characteristic in hallmark acquisition (Hanahan and Weinberg, 2011).

1.5.2 Tumour-Promoting Inflammation

The inflammatory nature of cancer and the surrounding microenvironment plays a critical role in its development (Rous and Kidd, 1941; Balkwill and Mantovani, 2001) with infectious diseases and chronic inflammation estimated to account for up to 25% of cancer cases (Hussain and Harris, 2007). The link between inflammation and cancer was initially observed by Virchow who noted the presence of leukocytes within malignant tumours (Grivennikov, Greten and Karin, 2010). During injury or infection, part of the natural response to the ensuing inflammation is the multifaceted cellular and signalling pathways which drives normal healing. Migration of leukocytes (e.g., neutrophils and monocytes) have a significant role in the response to inflammation and recruitment of essential cells to provide an optimised environment to facilitate restoration of tissue integrity. The multi-step process involves the release and regulation of a number of chemotactic cytokines (including TNF- α and TGF- β 1) which influence the balance of inflammation and repair (Coussens and Werb, 2002). Whilst normally tightly regulated, disruption in this process coupled to chronic inflammation can facilitate the development of cancer (Coussens and Werb, 2002; Murata, 2018). Chronic inflammation results in the accumulation of reactive oxygen and nitrogen species (ROS and RNS) which specifically contributes to DNA damage and an accumulation of mutations, that in turn underpin carcinogenesis (Murata, 2018).

Pro-inflammatory signals resulting in the co-optation of macrophages by cancer cells (TAM), referred to in the literature as tumour-associated M2 polarisation has been shown to facilitate EMT and drive metastatic progression. (Solinas *et al.*, 2009; Suarez-Carmona *et al.*, 2017; Coletta *et al.*, 2021). The recruitment of these macrophages has been hypothesised as contributing towards up to 50% of the total tumour mass (Hembruff *et al.*, 2010; Qian *et al.*, 2011). In addition to their assimilation into the tumour, leukocytes have been shown to secrete numerous growth factors (e.g., VEG-F, TGF- β , PDGF) which are particularly important in the propagation and progression of high grade breast cancer (Leek *et al.*, 1996). The secretion of acute pro-inflammatory chemokines including MCP-1 (CCL2), RANTES and IL-8 by cells

within the tumour microenvironment further amplify the pro-metastatic activities observed within tumour stroma, including morphological changes, angiogenesis and increased tumour migration and invasion (Soria *et al.*, 2008; Hembruff *et al.*, 2010; Liubomirski *et al.*, 2019). The CCL2/CCR2 inflammatory signalling pathway has been shown play a vital role in the regulation of TAM recruitment into the tumour microenvironment, with studies correlating high levels of CCL2 (MCP-1) with advanced breast cancer invasion and decreased patient survival (Valković *et al.*, 1998; Soria *et al.*, 2008). As with the other features, understanding the key drivers in the development and perpetuation of cancer poses an opportunity for the utilisation of anti-inflammatory agents and their role in cancer treatment and prevention (Coussens and Werb, 2002).

1.5.3 Abnormal Bioenergetics

In the presence of oxygen, normal cells consume glucose as a central macronutrient for utilisation through mitochondrial oxidative phosphorylation (OXPHOS). Research in the 1920s demonstrated that even in an oxygen rich environment, tumour cells undertook aerobic glycolysis, and preferentially metabolised glucose into lactate, a process which was subsequently termed the 'Warburg effect' (Warburg, Wind and Negelein, 1927b). The shift of ATP production from OXPHOS to aerobic glycolysis provides energy more rapidly, however it is significantly less efficient and requires a markedly increased rate of glucose uptake to support rapid tumour growth (Potter, Newport and Morten, 2016; Sancho, Barneda and Heeschen, 2016). Metabolic dysfunction has been observed in a number of neoplastic subtypes including breast cancer, which found an over-expression of glucose transporters (e.g. GLUT) and associated metabolic enzymes within tumour cells, which facilitated the rapid transport and consumption of this essential energy source (Shin and Koo, 2021). This metabolic reprogramming was further elucidated as the technology to examine mitochondrial function in greater detail has been developed.

Warburg originally postulated that the propensity towards excessive lactate production was related to abnormal mitochondrial behaviour, however a number of studies have since demonstrated that functional mitochondria have been found across a range of tumour types (Martin *et al.*, 1998; Guppy *et al.*,

2002; Moreno-Sánchez *et al.*, 2007; Ju *et al.*, 2014). It has been suggested that there may be multiple sub-populations within tumours which create metabolic flexibility related to tumour size or environment, with symbiotic relationships between cells that preferentially utilise lactate as their primary energy source (Feron, 2009; Kennedy and Dewhirst, 2010; Jose, Bellance and Rossignol, 2011). Some researchers postulate that gene regulation can activate or suppress OXPHOS within cancer cells, essentially switching metabolic pathways during tumorigenesis in response to key environmental cues demonstrating the complexity of the bioenergetic profile of cancer (Funes *et al.*, 2007; Moiseeva *et al.*, 2009; Smolková *et al.*, 2011). Although the metabolic mechanisms of cancer are not entirely understood, the ability to reprogramme their bioenergetic processes makes this an important emerging hallmark that must be considered in the wider context of the development of neoplastic disease.

1.5.4 Evading Immune Destruction

The interaction of neoplastic disease with the immune system is of significant research interest and is intrinsically linked with the development of novel immunotherapy for the treatment of cancer (Pardoll, 2012; Durrechou *et al.*, 2020; Petitprez *et al.*, 2020). The accumulation of abnormal cells containing sporadic genetic mutations can lead to the presentation of peptides bound to major histocompatibility class I (MHC I) receptors on the cancer cell surface, which can be recognised by CD8⁺ T cells (Cerottini, Liénard and Romero, 1996). The development of cancer in the immunocompromised patient (e.g., solid organ transplant, HIV, pharmacological) has been described and often thought to be associated with suppression of the host immune system and viral infections (Strauss and Thomas, 2010; Lucar, Keith Reeves and Jost, 2019; Greuter *et al.*, 2020; Takeda *et al.*, 2021). For the immunocompetent patient, a response requires the immune system to be activated and enabled as illustrated by the cancer immunity cycle (Figure 1.8). The capture and release of neoantigens resulting from oncogenesis by antigen presenting cells (APC) e.g., dendritic cells (DCs), enables the initiation of the effector T cell response against the cancer specific antigen (Gardner and Ruffell, 2016). The activated effector T cells infiltrate the tumour bed by binding to the MHC I receptor,

resulting in cell death and the release of additional antigens which can amplify and continue to drive the immune response (Chen and Mellman, 2013).

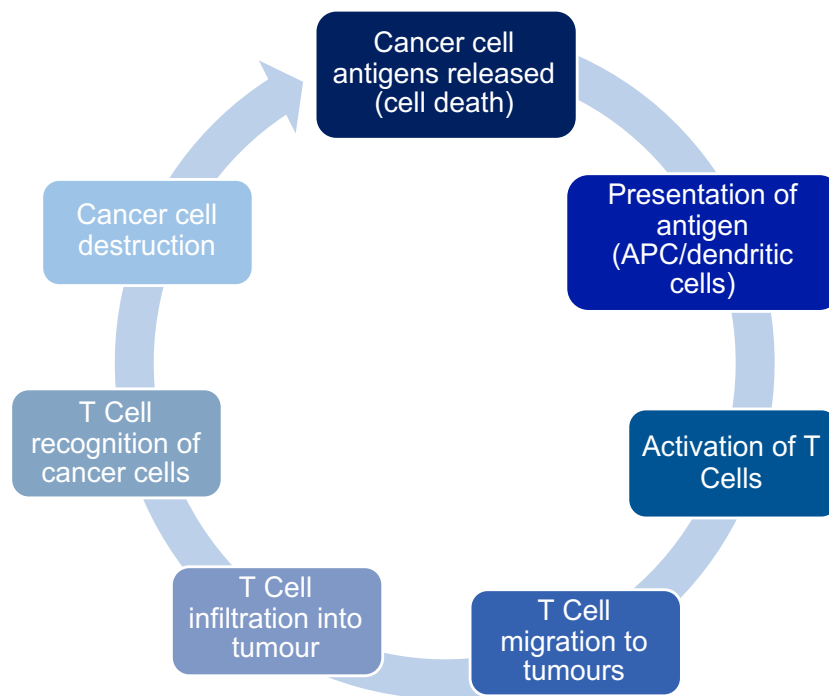


Figure 1.8: Schematic representation of the cancer immunity cycle

The immune response to cancer is a multi-step process which is triggered when APCs/DCs present antigens to specialised T cells, resulting in activation and migration to the tumour site. After the T cell receptor (TCR) binds to the conjugate antigen on the cancer cell surface, tumour cell death occurs which results in the additional release of antigens, amplifying the immune response. Image created from text descriptors (Chen and Mellman, 2013).

While there are a number of APCs within the body, DCs predominate as the central regulator of the adaptive immune response and are largely responsible for triggering cytotoxic T cells and regulating the balance between immunity and tumour antigen tolerance (Gardner and Ruffell, 2016; Fu and Jiang, 2018). The activation of these specialised immune cells can occur as part of the adaptive response, however numerous negative regulators have been described in both the tumour microenvironment (immunostat function) and lymphoid organs (checkpoints) which may explain the failure of the immune system to protect patients from the development of cancer (Pardoll, 2012; Mullard, 2013; Fu and Jiang, 2018; Petitprez *et al.*, 2020). The complex relationship between neoplastic disease and the immune system is not fully

understood, as with many of the hallmarks described modulation of the adaptive response to cancer may occur to reduce the impact of the immune response on its development or allow the tumour to evade detection entirely. Current research examining key immune pathways with the objective of improving understanding and identifying novel anti-cancer therapies illustrate the importance of this emerging hallmark.

1.6 The Tumour Microenvironment

No longer a disease centred on a core of abnormally proliferating malignant cells, the heterogeneity and structural complexity of cancer requires a broader understanding of the fundamentally disordered behaviour within the surrounding cellular milieu. The wider implications of the tumour microenvironment and its effect on cancer development and progression is now an essential part of understanding how this complex disease initiates, progresses and perpetuates. There are numerous processes that occur and coincide to support the sustained proliferation of abnormal cells which must be considered. The stromal compartments of tumours contains much of the cellular heterogeneity found within cancers and remain an important focus (Hanahan and Weinberg, 2011).

1.6.1 Endothelial Cells and Pericytes

Comprising an essential component of the cellular lining of blood vessels, endothelial cells are metabolically active and play an important role in normal tissue homeostasis and regulation (Aird, 2008). In cancer, they play a central role in establishing blood supply, triggering the 'angiogenic switch' (Section 1.4.5) which is key to the continued vascularisation of malignant tumours, a critical step in their propagation and growth (Maishi and Hida, 2017). Unlike their normal counterparts, tumour associated epithelial cells respond to growth factors secreted by tumours, exhibit altered phenotypes, chromosomal abnormalities and demonstrate an increased resistance to anti-cancer treatments (Streubel *et al.*, 2004; Akino *et al.*, 2009; Akiyama *et al.*, 2012; Hida and Maishi, 2018). As mural cells associated with normal blood vessels, pericytes are important in the development, regulation and structural stability of blood vessels, supporting quiescent epithelial cells through paracrine

signalling (Hanahan and Weinberg, 2011; Attwell *et al.*, 2016). Although their role in the development of tumour vasculature is still to be fully established, studies have demonstrated that pericyte abnormalities may play a role in PDGF signalling pathways and contribute to vascular irregularities and an increased risk of haemorrhage (Abramsson, Lindblom and Betsholtz, 2003; An *et al.*, 2019).

1.6.2 Fibroblasts

Cancer associated fibroblasts (CAF) are another significant contributor to the tumour microenvironment and surrounding tumour stroma, and is one of the predominant cell types found in breast cancer (Kalluri and Zeisberg, 2006). As a perpetually activated fibroblast, they are responsible for the production of essential components of the ECM, proteolytic enzymes and growth factors (Bhowmick, Neilson and Moses, 2004; Kalluri and Zeisberg, 2006; Nurmik *et al.*, 2020). While tumour cells are known to release a number of pro-angiogenic cytokines, fibroblasts and associated inflammatory cells are one of the principle sources of VEG-F within the tumour microenvironment (Fukumura *et al.*, 1998). *In vivo* studies examining CAF sub-populations in more detail have established that quantifying gene expression as a proxy for cell number has potential as a predictor for breast cancer dissemination and indicator for the development of metastatic disease (Bartoschek *et al.*, 2018). Published studies have suggested that fibroblasts found within distant metastasis promote the proliferation and progression in a comparable way as CAF within the main tumour (Kalluri and Zeisberg, 2006; Hao, Baker and Dijke, 2019). While significantly contributing to the tumour stroma, there are numerous novel sub-sets within the CAF population, presenting the potential for targeted therapy which may increase tamoxifen sensitivity (CD63+ population) in certain breast cancers (Gao *et al.*, 2020).

1.6.3 Mesenchymal Stem Cells and Cancer Stem Cells

Inflammatory cues play a role in the initial attraction and recruitment of leukocytes and associated cells which have been shown to amplify pro-tumorigenic activity (Coussens and Werb, 2002; Grivennikov, Greten and Karin, 2010). As a significant constituent of tumours, leukocytes play a varied

role in the immune response to chronic inflammation producing numerous cytokines and growth factors that sustain the tumour and surrounding microenvironment and attract mesenchymal stem cells (MSC) (Solinas *et al.*, 2009; Iqbal, Chong and Tan, 2013; Murata, 2018). The influence of stem cells within the tumour or surrounding stroma must therefore be examined as MSCs within cancer adjacent tissues have been shown to migrate to sites of injury and inflammation (Kidd *et al.*, 2009; Atiya *et al.*, 2020). Once co-located within the tumour microenvironment, MSCs such as ADSCs have been reported to support angiogenesis, suppress the immune response, differentiate into essential ECM components and promote tumour growth and metastasis (Spaeth *et al.*, 2009; Suzuki *et al.*, 2011; Xu *et al.*, 2012; Guan and Chen, 2013). Numerous ADSC secreted factors including monocyte chemoattractant protein-1 (MCP-1 or CCL2), IL-6 and VEG-F have been shown to enhance breast cancer progression and support a shift to a more aggressive phenotype (Muehlberg *et al.*, 2009; Kucerova *et al.*, 2011; Zimmerlin *et al.*, 2011; Teufelsbauer *et al.*, 2019). ADSCs within the surrounding breast parenchyma similarly respond to inflammatory cancer signals, with numerous *in vitro* and *in vivo* studies demonstrating pro-tumorigenic effects of ADSCs on breast cancer growth and progression (Schweizer *et al.*, 2015; Wu *et al.*, 2019).

Within tumours there are a recognised group of cancer stem cells (CSCs) that possess the ability to self-renew and contribute to the varied cell types within tumours in addition to driving treatment resistance and recurrence (Reya *et al.*, 2001; Barbato *et al.*, 2019; Walcher *et al.*, 2020). Similar to adult MSCs, these cells have been described as sitting atop a hierarchy of more differentiated cells with the potential to account for drug resistance and sustained treatment resilience within the tumour (Liu *et al.*, 2006; Bajaj, Diaz and Reya, 2020). Accepting there are likely to be variations between tumour types with these unique cell populations, there are an increasing number of cancers reported to contain CSC subpopulations (Hanahan and Weinberg, 2011). As discussed previously (Section 1.5.2), the environmental cues of chronic inflammation can have a significant impact on CSCs within tumours, driving DNA damage which can result in the development of cancer with aggressive clinical features (Murata, 2018).

1.7 Adipose Derived Stem Cells (ADSCs), Discovery, Opportunity, and Safety Concerns

1.7.1 ADSC Discovery and Characterisation

First discovered in 2001, adipose derived stem cells (ADSCs) were successfully isolated following mechanical and enzymatic extraction from adult lipoaspirate, and fully characterised with the use of flow cytometry, protein analysis and multi-lineage differentiation (Figure 1.9) (Zuk *et al.*, 2001, 2002). Found in abundance in peripheral adipose tissue, their relative high concentration per ml of fat extracted and ease of harvest in comparison to other sources of MSCs, meant they understandably attracted significant scientific interest (Fraser *et al.*, 2006; Banyard *et al.*, 2015; Bowen, 2015; Li *et al.*, 2015). Since their initial discovery, ADSCs have been utilised for a range of clinical and scientific applications including regenerative medicine and tissue engineering, wound healing and as a model for drug delivery (Josiah *et al.*, 2010; Liu *et al.*, 2010; Cherubino *et al.*, 2011; Naderi *et al.*, 2017; T. Li *et al.*, 2020).

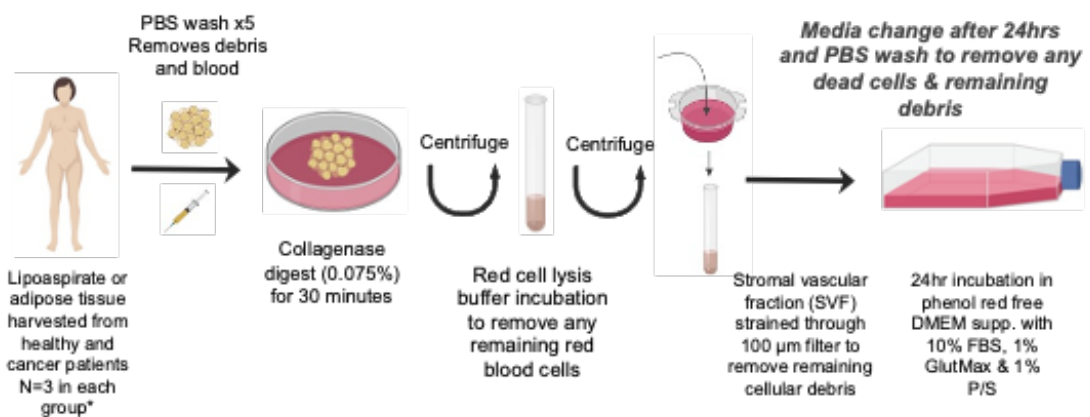


Figure 1.9: Steps for isolating ADSCs from patient lipoaspirate

Illustrative steps as described by Zuk *et al.* detailing the steps used to isolate ADSCs from lipoaspirate. The samples were taken from healthy volunteers and characterised using flow cytometry, protein expression analysis (Western blot and PCR) and multi-lineage differentiation (Zuk *et al.*, 2001). Image reproduced with permission.

Following the initial ADSC isolation protocol published in 2001, numerous amendments, alternative techniques and a variety of culture conditions have since been described (Bunnell, Flaat, *et al.*, 2008; Trojahn Kølle *et al.*, 2013; Domenis *et al.*, 2015; Bellei *et al.*, 2017). Similarly with regards to characterisation, various parameters were suggested including preferential plastic adherence over other components of the stromal vascular fraction (SVF), phenotypic identification using flow cytometry and confirmation of MSC potential through differentiation (Dominici *et al.*, 2006). There are numerous studies describing additional phenotypic cell surface markers purported to ensure the cell population isolated are indeed ADSCs (Schäffler and Büchler, 2007; Vater, Kasten and Stiehler, 2011; Trojahn Kølle *et al.*, 2013). A position statement from the International Federation for Adipose Therapeutics and Science (IFATS) and the International Society for Cellular Therapy (ISCT) presented a paper for the scientific community working with ADSCs with the aim to facilitate reproducible standards (Bourin *et al.*, 2013). The similarities between ADSCs and comparable MSC sources such as bone marrow derived nucleated cells (BM-NC) were noted and influenced the choice of recommended phenotypic markers to differentiate the cells from one another (Table 1.2). Importantly, ADSCs should be negative for haematopoietic markers CD45 and CD11b, and positive for stromal markers including CD73, CD90 and CD13.

Table 1.2: Differences between BM-NC and ADSCs

	BM-NC	ADSC	MSC
CD34	±	±	--
CD45	++	--	--
CD13	++	++	++
CD73	±	++	++
CD90	±	++	++
CD105	±	++	++
CD10	±	++	±
CD36		+	--
CD106		±	+

Phenotypical cell surface markers present in varying quantities within ADSC, BM-NC populations, with core MSC phenotypic markers suggested. ++ = >70%, + = >30-70%, ± = >2-30%, -- = <2% table created and adapted from paper text (Bourin *et al.*, 2013).

A hallmark of ADSCs is their multilineage potential which remains a crucial part of characterisation. Trilineage differentiation down the adipogenic, osteogenic and chondrogenic lineages has emerged as a standardised benchmark to establish this key feature of MSC behaviour (Schäffler and Büchler, 2007; Li *et al.*, 2015; Hajmoussa and Harmsen, 2017; Wang *et al.*, 2021). With preferential plastic adherence, essential CD markers for ascertaining phenotype and recommended trilineage pathways, the minimum criteria for characterising ADSCs were therefore established (Dominici *et al.*, 2006). As the knowledge regarding this MSC population expanded, the properties that once made ADSCs so desirable were now central to questions being raised regarding their potential interaction within the cancer microenvironment, and it was widely acknowledged that more information was needed regarding their potential interaction with breast cancer (Fatah *et al.*, 2012; Combella *et al.*, 2016).

1.7.2 Scientific Laboratory Studies Examining ADSCs and Breast Cancer Interaction

The subsequent increase in both *in vivo* and *in vitro* studies to examine the influence of ADSCs on numerous breast cancer cell lines illustrated some concerning behavioural characteristics. ADSC's ability to hone to sites of inflammation and tissue injury were established, lending to their potential interaction within the tumour microenvironment (Schlosser *et al.*, 2012; Bachmann *et al.*, 2020). As previously illustrated (Figure 1.6), published findings have suggested that ADSCs confer a malignant advantage to breast cancer cells via the release of cytokines into the surrounding stroma and through direct cell-to-cell interaction, affecting their phenotype, morphology, and rate of proliferation (Figure 1.10) (Prantl *et al.*, 2010; Manzotti *et al.*, 2011; Cho *et al.*, 2012; Song *et al.*, 2015; Wu *et al.*, 2019). The complexity of the tumour microenvironment and interaction of ADSCs with the cancer stroma led authors to suggest varied fates for these progenitor cells including differentiation into cancer associated fibroblasts (CAF) or as support for neoangiogenesis (Li *et al.*, 2009; Donnenberg *et al.*, 2010; Dirat *et al.*, 2011; Orecchioni *et al.*, 2013).

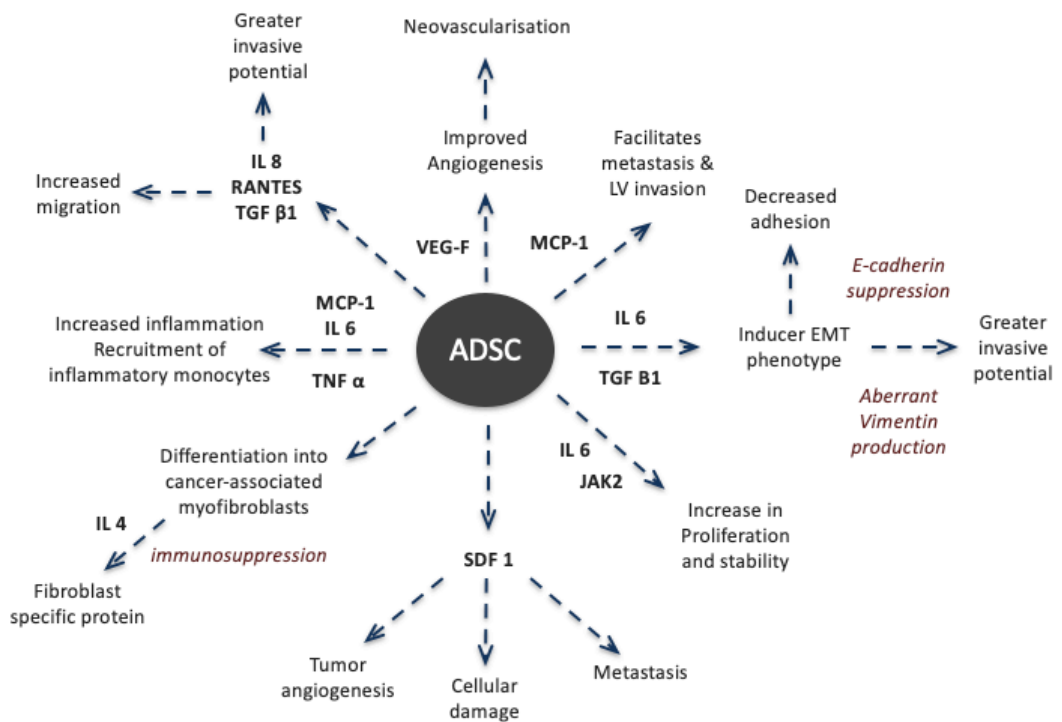


Figure 1.10: Diagrammatic representation illustrating key cytokines and proteins released through interactions between ADSCs and Breast cancer cell lines *in vivo* and *in vitro*.

Summary of numerous scientific peer-reviewed papers in a single diagram focusing on key cancer hallmarks. Each dotted arrow represents an interaction with a breast cancer cell line, the resultant cytokine / protein excretion and demonstrated or inferred effect on the breast cancer hallmarks (Muehlberg *et al.*, 2009; Xu *et al.*, 2012; Wei *et al.*, 2015; Gallo *et al.*, 2018; Wu *et al.*, 2019; L. Li *et al.*, 2020).

Accepting there are limitations of the cell culture and cell line models, a broad range of cancer lines have been examined indirectly and more directly, through various 2D and 3D models to better delineate the effects of ADSCs on the hallmarks of breast cancer (Section 1.4) (Yu *et al.*, 2008; Weigand *et al.*, 2016; Angeloni *et al.*, 2017; Teufelsbauer *et al.*, 2019). Correlation of clinical breast cancer diagnosis with chosen cell lines for research was highlighted in clinically focused papers, with ER+ luminal A cell lines such as MCF-7 and T47D frequently chosen as an ideal experimental model (Holliday and Speirs, 2011; Jiang *et al.*, 2016; Yu *et al.*, 2017). MCF-7 was the most common cell line of choice, providing an ideal model to assess the progression from a relatively indolent cancer to phenotypically invasive and metastatic disease and representative of the clinical problem being interrogated as over 70% of

new breast cancer diagnosed is ER+ (Li *et al.*, 2009; Gourdon *et al.*, 2012; Lin, Wang and Zhao, 2013; Lee, Jung and Koo, 2015; Wu *et al.*, 2019). ADSC cell source was also vital, as in many papers lipoaspirate was harvested from young healthy women undergoing elective cosmetic surgery as the primary cell source for experimentation, which contrasts significantly with the patient population undergoing reconstruction (Zuk *et al.*, 2001; Barbarestani *et al.*, 2006; Gourdon *et al.*, 2012; Teufelsbauer *et al.*, 2019). Whilst healthy ADSCs have an obvious advantage over those isolated from animal sources, numerous factors have been shown to affect the function of ADSCs including age, co-morbidities, anatomical location and medications used to treat breast cancer, which is not reflected in models utilising ADSCs from healthy patients (Engels *et al.*, 2013; Pike *et al.*, 2015; Liu *et al.*, 2017; Varghese *et al.*, 2017). This is illustrated in work done to examine ADSCs isolated from older patients and those exposed to increasing doses of tamoxifen which demonstrate reduced trilineage differentiation potential and impaired response to external stimulation which would potentially have a bearing on their behaviour in co-culture (Pike *et al.*, 2015; Liu *et al.*, 2017). It is therefore difficult to draw conclusions from studies that utilise primary ADSC lines from patients that do not accurately represent the patient group undergoing breast reconstruction, which have the potential to respond differently in culture.

Accepting there may be a difference in behaviour of ADSCs isolated from different patient groups (with and without breast cancer) and from different anatomical locations (cancer adjacent and distant anatomical site), the focus of many studies broadened to more closely mimic the breast microenvironment (Hanson, Kim and Hematti, 2013; Yuan *et al.*, 2015; Schmid *et al.*, 2018). Studies have shown that ADSCs isolated from both breast and abdominal sites are phenotypically comparable, however evidence suggests anatomical location can influence morphology, with visceral ADSCs demonstrating more epithelial like structure rather than the typical fibroblast like morphology seen in subcutaneous ADSCs (Hanson, Kim and Hematti, 2013; Yuan *et al.*, 2015). Interestingly, subcutaneous ADSCs exhibited an increased tropism toward breast cancer cells compared to those isolated from visceral adipose tissue, with differences noted in rates of EMT induction and cytokine secretion

between both ADSC populations when co-cultured with various breast cancer cell lines (Yuan *et al.*, 2015). Considering anatomical location for ADSC harvest is increasingly important when planning cell models to mimic the post-BCS breast microenvironment as the cell population needs to reflect the anatomical location most likely to be used for reconstruction. It is therefore essential to correlate the laboratory and clinical studies to ascertain if the theorised pro-tumorigenic effects are detectable in the patient population.

1.7.3 Clinical Studies Examining the Use of FFT

Clinical studies comparatively have not demonstrated a statistically significant increase in rate of breast cancer recurrence in women who have undergone FFT compared with patients who had either an autologous (free) flap or no reconstruction (Maione *et al.*, 2015; Masia *et al.*, 2015; Batista *et al.*, 2016; Silva-Vergara *et al.*, 2016). There are numerous possibilities why this may be the case, with sample size, duration of study, patient factors and ADSC location all representing potential areas for focus. Many of the clinical studies are small, single centre or single region with limited sample size as the technique was not widely used prior to 2007. Follow up time is also crucial, with evidence to demonstrate time to cure (TTC) models for breast cancer at almost 12 years, with some patients experiencing recurrence as late as 20 years later (Gabos *et al.*, 2010; Mayor, 2012; Pan *et al.*, 2017; Boussari *et al.*, 2018). Comparatively, many of the clinical studies did not follow the patients up specifically for recurrence beyond 36 months, and in many cases the time was substantially shorter (Chirappapha *et al.*, 2015; Batista *et al.*, 2016; Moltó García, González Alonso and Villaverde Doménech, 2016).

1.7.4 Opportunities for Development

While robust longitudinal clinical studies are essential, there are potential opportunities to address the gaps within the cell culture models. The use of clinically comparable cancer lines and more diverse ADSC harvest locations for modelling are an opportunity for refinement. Breast reconstruction generally follows the completion of surgery, (neo)adjuvant treatment, and hormone therapy. It is well documented in the literature that patient factors such as obesity, diabetes mellitus and a variety of medications, including

Tamoxifen, can impact the function of ADSCs including their viability, altered cytokine release and impaired production of extracellular matrix (ECM) (Nagawa *et al.*, 2007; Pike *et al.*, 2015; Silva *et al.*, 2015; Varghese *et al.*, 2017). As described previously (Section 1.3) ER+ breast cancers account for more than >70% of new diagnosis resulting in the use of either Tamoxifen or Letrozole, unless contraindicated for five years following their initial diagnosis and treatment (Rosenberg, Barker and Anderson, 2015; Tomlins and Parker, 2016). Given the potential systemic effects of breast cancer treatment on the function and behaviour of ADSCs likely to be utilised for reconstruction, patient groups identified as primary cell line sources for breast cancer cell culture models requires further investigation.

1.8 Thesis Aims and Objectives

The aim of this thesis is to create a clinically representative model to more accurately study the effects of ADSCs on the hallmarks of ER+ breast cancer. The unique focus of this work is the specific selection of ADSCs isolated from women with ER+ breast cancer, commenced on either Tamoxifen or Letrozole, undergoing FFT as part of their breast reconstruction (hereafter known as cancer ADSCs). This contrasts with the current scientific literature in which the use of ADSCs isolated from healthy patients predominates, from which concerns regarding their pro-tumorigenic effects have been raised. Therefore, ADSCs isolated from healthy women who have never had cancer (of any kind), undergoing FFT or liposuction as part of a cosmetic procedure (hereafter known as healthy ADSCs) will be used as a comparator. By examining ADSCs taken from these two distinct patient populations it is possible to compare their effects on the neoplastic traits of the MCF-7 cell line to establish if there are any differences in their pro-tumorigenic effects which may be attributable to the difference in patient selection.

It is hypothesised that ADSCs isolated from patients on systemic hormone therapy do not produce the pro-tumorigenic effects seen with ADSCs isolated from healthy patients. It is theorised that the systemic therapy affects their ability to promote the neoplastic characteristics required to support breast cancer growth and progression and will be determined by comparing the

effects of healthy and cancer ADSCs on the hallmark of ER+ breast cancer.

This will be evaluated by addressing three objectives:

1. To establish and optimise an ADSC isolation protocol capable of reliably and repeatedly isolating ADSCs from human lipoaspirate, which can be fully characterised for use in subsequent experiments.
2. To compare the effects of healthy and cancer ADSCs on the neoplastic traits of the MCF-7 cell line using conditioned media
3. To compare the effects of healthy and cancer ADSCs on the neoplastic traits of the MCF-7 cell line using non-contact co-culture and validation of key measures with an additional breast cancer cell line (T47D).

Chapter Two

Materials and Methods

2.1 Laboratory Consumables

Plastic consumables, cell culture flasks and multi-well plates for tissue culture were purchased from Greiner Bio-One GmbH (UK) unless otherwise stated. All co-culture plastic consumables and transwell inserts were purchased from Corning (USA). The RTCA iCELLigence multi-well plates and transwell inserts were purchased from ACEA Bioscience (UK) until September 2020 at which point the company merged with Agilent. These consumables subsequently, along with the 24 well plates and cartridges for the Seahorse assay were ordered from Agilent (UK). Migration inserts were purchased from IBIDI (Germany) with the collagen invasion inserts, 0.2 μm filter and 100 μm nylon mesh all purchased from Merck Millipore (Germany). Chambered borosilicate cover-glass systems used for confocal microscopy were purchased from ThermoFisher Scientific (Massachusetts, USA). Countess™ slides and Trypan blue for use with the automated cell counter were purchased from Life Technologies (UK).

2.2 Buffers, Chemicals, and Reagents

All cell culture media and supplementation including phenol red free Dulbecco's Modified Eagle's Medium (DMEM), Foetal Bovine Serum (FBS), Glutamine and Penicillin/Streptomycin (pen/strep) were all purchased from Gibco, Life Technologies (UK). All Seahorse XF media and supplements, including L-glutamine, Glucose and Pyruvate and the plate calibrant were purchased from Agilent (UK). The oxidative phosphorylation inhibitors oligomycin, antimycin A and rotenone, along with the ionophore carbonyl cyanide-p-trifluoromethoxyphenylhydrazone (FCCP) were all purchased from Sigma-Aldrich (UK).

Flow cytometry antibodies for confirming isolation optimisation and monitoring stem cell phenotype and characterisation were; CD13 (anti-human antibody) Brilliant Violet 421™, CD44 (anti-mouse/human antibody) Brilliant Violet

605™, APC anti-human CD73™ (Ecto-5'nucleotidase) antibody, Alexa Fluor® 647 anti-human CD90 (Thy1) antibody, Alexa Fluor® 488 anti-human CD105 antibody, PE/Dazzle™ 594 anti-human CD11b Antibody, PE anti-human CD31 antibody, Brilliant Violet 785™ anti-human CD45 antibody and PE anti-human CD106 Antibody were all purchased from BioLegend (San Diego, USA). VersaComp antibody capture beads used for flow cytometry optimisation and production of a compensation matrix were purchased from Beckman Coulter life sciences (US). Reagents for the human cytokine array panel, and the development and detection of ELISAs for IL-6, MCP-1 and VEG-F were purchased from R&D systems (Minneapolis, USA).

2.3 Cell Lines

Authenticated oestrogen receptor positive (ER+) breast cancer cell lines MCF-7 and T47D cells were obtained from ATCC.

Table 2.1: MCF-7 and T47D cell line source and anatomically derived site.

Cell line	Derived From	Source
MCF-7	mammary gland; derived from metastatic site: pleural effusion	ATCC
T47D	mammary gland; derived from metastatic site: pleural effusion	ATCC

Each of the two immortalised breast cancer lines used in the study are derived from metastatic pleural effusions and were sourced from ATCC.

2.4 Human Adipose Tissue Collection

En bloc fat or lipoaspirate was collected from patients at either Morriston Hospital (Heol Maes Eglwys, Swansea, SA6 6NL, Wales) or Singleton Hospital (Sketty Lane, Swansea, SA2 8QA, Wales) undergoing elective surgical procedures. The tissue collected was otherwise bound for incineration (waste). Patients recruited were in one of two groups of interest (those with breast cancer and those with no history of any cancer). All samples were collected with informed written consent on the morning of their procedure and ethics

approval was obtained from the Wales Research Ethics Committee (12/WA/0029; IRAS 99202). The sample was collected by the operating surgeon under sterile conditions and the *en bloc* fat or lipoaspirate was placed into a sterile container before being placed into a clear protective bag, pre-coded with the patient's unique identifier and placed into an opaque tissue carrier and taken directly to the second-floor labs at the Institute of Life Science 1 (ILS 1) for immediate processing. Samples were collected from two patient groups, those with ER+ positive cancer currently on systemic therapy (n=10) and those that had never had cancer and were not on any systemic treatment (n=6) as described in Section 3.3.1.

2.5 Cell Culture

All cell culture was carried out under sterile conditions in a ScanLaf Mars Class II hood (Denmark), which was thoroughly wiped down with 70% Ethanol beforehand. Any additional items being introduced into the hood were sprayed down with 70% ethanol. Separate ScanLaf Mars Class II hoods were used for cell line and primary cell work to minimise contamination.

2.6 Cell Lines

Authenticated breast cancer MCF-7 and T47D cells were obtained from ATCC and cultured in sterile and endotoxin free phenol red free DMEM (Gibco, Life Technologies, UK) supplemented with 10% Foetal Bovine Serum (FBS, Gibco, Life Technologies, UK) and 2mM GlutaMAX (ThermoFisher Scientific, UK) (Gibco, Life Technologies, UK) hereafter referred to as cell line media, was warmed to 37°C for a minimum of 30 minutes prior to use. Initially for both the MCF-7 cells and T47D, the primary vial supplied by ATCC was removed from the liquid nitrogen store and thawed in the 37°C water bath before being added to a small tissue culture flask (25 cm², Greiner Bio-One GmbH) along with 10 ml of the cell line media.

Cells were passaged when 80% confluent using 2.5mls of Trypsin-EDTA (0.05%, Gibco, Life Technologies, UK) which was pre-warmed at 37°C in the water bath for 30 minutes. Once visual confirmation using a light microscope

(Zeiss, Axiovert 40C) that cells had detached from the tissue culture flask, the Trypsin-EDTA was neutralised with equal parts warmed cell line media. They were then pipetted into a 50 ml skirted falcon tube (Greiner Bio-One GmbH) and centrifuged for five minutes at 300g in a benchtop centrifuge (Eppendorf, Centrifuge 5804 R, Eppendorf AG). MCF 7 or T47D cells were then seeded at densities between $1-3 \times 10^5$ into a single 75 cm² tissue culture flask (Greiner Bio-One GmbH) with 10 mls of cell line media (Gibco, Life Technologies, UK) and cultured in a humidified Memmert CO₂ incubator ICO (Mettler GmbH, Germany) at 37°C and 5% CO₂ in air (unless otherwise stated) until 80% confluent.

2.7 Primary Cell Lines

ADSC populations were extracted and isolated from either *en bloc* adipose tissue or lipoaspirates obtained from both healthy and cancer patients recruited from Morriston or Singleton Hospital and cultured in phenol red free DMEM media supplemented with 10% FBS, 2 mM GlutaMAX (ThermoFisher Scientific, UK) and 100 U/ml Penicillin, 100 µg/ml Streptomycin (pen/strep), (Gibco, Life Technologies, UK) hereafter referred to as ADSC media. All cell lines were cultured in a 175 cm² tissue culture flask (Greiner Bio-One GmbH) with 25 mls of ADSC media (Gibco, Life Technologies, UK) maintained in a humidified Memmert CO₂ incubator ICO (Mettler GmbH, Germany) at 37°C and 5% CO₂ in air. ADSCs were not permitted to become more than 70% confluent to prevent differentiation into mature adipocytes, at which point they were passaged using trypsin as described previously and re-seeded into a 175 cm² tissue culture flask (Greiner Bio-One GmbH) with 25 mls of ADSC media.

2.7.1 Primary Cell Line Isolation

En bloc whole fat or lipoaspirate was collected intra-operatively as previously described. Once in the ScanLaf Mars Class II hood (Denmark), which was thoroughly wiped down with 70% Ethanol, the sample was processed. *En bloc* fat was minced with two sterile 10 blade disposable scalpels (Swann Morton, Sheffield UK) on a 10 cm² petri dish until emulsified, equating it to lipoaspirate, at which point both samples were then processed identically. The sample was

then extensively washed with Phosphate Buffered Saline (PBS) (Gibco, Life Technologies, UK), by placing the lipoaspirate into a 50 ml skirted falcon tube (Greiner Bio-One GmbH) with an equal volume of PBS (between 5 and 10 mls). The tube was then inverted several times before being centrifuged at 500g for two minutes in a benchtop centrifuge (Eppendorf, Centrifuge 5804 R, Eppendorf AG), and this washing procedure was carried out a total of five times.

Following this, the lipoaspirate was transferred to a 10 cm² petri dish and the extracellular matrix (ECM) was digested with 0.075% Collagenase (Sigma, UK) prepared in ADSC media in a humidified Memmert CO₂ incubator ICO (Mettler-Toledo GmbH, Germany) at 37°C and 5% CO₂ in air for 30 minutes. The enzyme activity was neutralised with an equal volume of ADSC media, before the contents of the petri dish was transferred to a 50 ml falcon tube and centrifuged at 1200g for 10 minutes. The supernatant was discarded, and the pellet was re-suspended in red cell lysis buffer (155 mM Ammonium Chloride (NH₄Cl, Sigma, UK), 10 mM Potassium Bicarbonate (KHCO₃, Sigma, UK) and 0.1 mM Ethylenediaminetetraacetic acid (EDTA, Sigma, UK), prepared to pH 7.3 in 1 L ddH₂O and sterile filtered using 0.2 µm filter (Millex-HA, Merck Millipore, Germany)) for 10 minutes at room temperature. The samples were then centrifuged once more at 1200g for 10 minutes at which point the supernatant was discarded, and the stromal vascular fraction (SVF) was collected.

The SVF was filtered through a 100 µm nylon mesh (Merck Millipore, Germany) to remove any cellular debris and the cells were placed in a 175 cm² tissue culture flask with 25mls of ADSC media overnight in a humidified Memmert CO₂ incubator ICO at 37°C and 5% CO₂ in air. After 24 hours, the ADSCs had adhered to the flask and were extensively washed with PBS (three times with 20 mls each time) to remove any non-adherent cells and debris. ADSCs were not permitted to become more than 70% confluent to prevent differentiation into mature adipocytes, at which point they were passaged using

trypsin as described previously and re-seeded into a 175 cm² tissue culture flask with 25 mls of ADSC media see Figure 2.1.

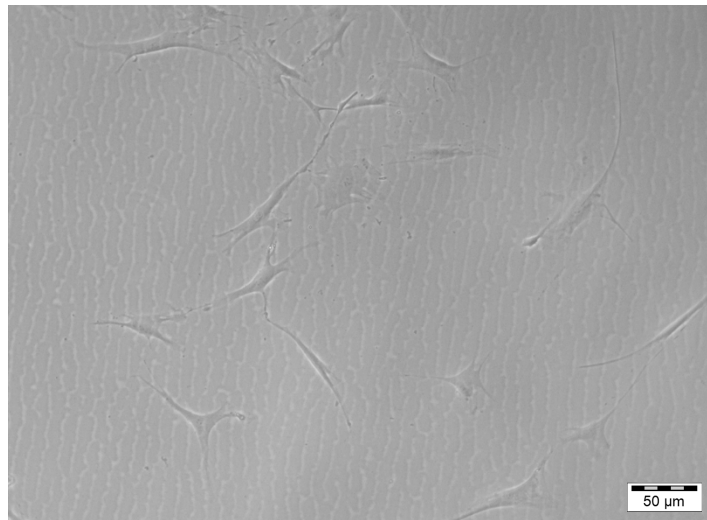


Figure 2.1: Image taken of the extracted ADSCs demonstrating plastic adherence seven days after isolation.

Cells extracted and isolated from patient adipose tissue demonstrated plastic adherence – image taken x10 magnification on a standard light microscope (Zeiss Axiovert 40C, Germany).

2.8 Cell Counting

Cell counting and viability were calculated using the Countess™ automated cell counter (Life Technologies, UK). Cells were trypsanised and resuspended in between 1 and 3 mls of cell specific media (volume based on anticipated cell number). Equal volumes (10 μl) of cell suspension and 0.4% Trypan blue (Life Technologies, UK) were added to a 1.5 ml microcentrifuge tube (Greiner Bio-One GmbH). Once mixed, 10 μl of stained cells were then added into one well of a cell counter slide (Life Technologies, UK) which was inserted into the Countess™ automated cell counter (Life Technologies, UK). The display was focused and then the density determined via the equivalent counting of four 1 mm x 1 mm squares on a standard haemocytometer. The total live cell count (via trypan blue exclusion) was used for downstream experimentation inclusive of applicable dilution factor.

2.9 Cryopreservation

2.9.1 Cell Lines

Once the cells had been passaged for 21 days, multiple 75 cm² tissue culture flasks with 10mls of complete media were seeded to enable expansion of the cell line and a stock to be created. Once each flask had achieved 80% confluence, they were all trypsinised and counted as previously described and resuspended in a 9:1 solution of FBS : DMSO (Sigma-Aldrich, UK) creating a final cell density of between 2 and 3 x10⁶ cells per ml. Under sterile conditions, they were then pipetted into pre-labelled cryovials (Sigma-Aldrich, UK) and placed into a room temperature Nalgene Mr. Frosty™ Freezing Container (ThermoFisher Scientific, UK) containing isopropanol (Sigma-Aldrich, UK) and placed immediately into the -80°C Freezer. These were then transferred to the Liquid Nitrogen Dewar (ThermoFisher Scientific, UK) three to seven days later for long term storage and to act as a stock for the duration of the project.

2.9.2 Primary Cell Lines

Given the difficulty in procuring large numbers of primary cells lines and their temperamental nature, where possible, between passage 2 (p2) and passage 5 (p5), cells remaining after reseeding 175 cm² tissue culture flasks were then pipetted into a 50ml skirted falcon tube and centrifuged for five minutes at 300g in a benchtop centrifuge. The media was discarded, and they were resuspended in a 9:1 solution of FBS: DMSO at between 1-2 x10⁶ cells per ml. Under sterile conditions, they were then pipetted into pre-labelled cryovials (Sigma-Aldrich, UK) and placed into a room temperature Nalgene Mr. Frosty™ Freezing Container containing isopropanol and placed immediately into the -80°C freezer. These were then transferred to the Liquid Nitrogen Dewar three to seven days later for long term storage and to act as a stock for the duration of the project.

2.9.3 Initiating a Cell Line

Initiating a cell line involved the removal of one cryovial (Sigma-Aldrich, UK) of the required cell line from liquid nitrogen stores and thawing it in the water bath at 37°C (for 2-3 minutes until the last ice crystals started to dissolve). This was then added to 9 mls of warmed cell line media in a 50 ml skirted falcon tube and placed in a benchtop centrifuge for five minutes at 300g to remove the DMSO (Sigma-Aldrich, UK). The pellet was resuspended in 10 mls of fresh warmed cell line media before being added to a 75 cm² tissue culture flask for incubation in a humidified Memmert CO₂ incubator ICO at 37°C and 5% CO₂ in air. Cells were passaged at 70% confluence and re-seeded as previously described. All cells were cultured for a minimum of 21 days before use in any experiments to reduce the impact of the effects of liquid nitrogen on the cells influencing their characteristics during experiments.

2.10 Flow Cytometric Analysis

Flow cytometry was utilised to monitor the ADSC populations and ensure the presence of progenitor cell phenotypes at early and late passage, confirming the cell population remained as ADSCs rather than differentiated adipocytes. Cells were washed twice with PBS before harvesting using trypsin-EDTA (0.05%, Gibco, Life Technologies, UK) for five minutes at 37°C. An equal volume of ADSC media was used to neutralise the trypsin and the contents of the flask were added to a 50 ml skirted falcon tube. The cells were centrifuged at 500g for five minutes to pellet the cells and the pellet was re-suspended in fresh ADSC media before counting via the Countess™ Cell Counter. To each flow cytometry tube, 1x10⁵ cells were added, and the tubes were centrifuged at 515g for seven minutes at 4°C. The supernatant was discarded, and the cell pellet was re-suspended in 100 µl of flow cytometry buffer (PBS, 0.2% Bovine Serum Albumin (BSA, Sigma, UK) and 0.05% sodium azide (NaN₃, Sigma, UK).

The appropriate antibody (5 µl for all except CD73 for which 4 µl was added; see Table 2.2) was added to each tube, vortexed and incubated for 30 minutes, on ice, in the dark. Following this, the cells were centrifuged at 515g

for 7 minutes at 4°C. The supernatant was discarded, and the cell pellet was re-suspended in 3 ml of FACS buffer, before being vortexed and centrifuged as before. The supernatant was discarded, and the cell pellet was re-suspended in 200 µl of FACS buffer and vortexed. The cells were immediately run on the flow cytometer (Novocyte, ACEA Biosciences, USA). This was done with each primary ADSC cell line isolated from a patient at early and late passage (p2 and p8), and for each patient three tubes were run (no stain, positive stains, negative stains).

Initially using the no stain sample, appropriate photomultiplier tube (PMT) voltages were set for both side scatter (SSC) as a measure of cellular granularity, and forward scatter (FSC) as a measure of cell size. Once these parameters were established, they were set for each of the nine fluorophore channels listed below (Table 2.2). The voltages were maintained and used for all future ADSC experiments. For each tube run, typically 10,000 events were acquired of the cell population of interest (ADSCs) for gating, with data inclusive of percentage of events shown on the graph (Figure 2.2). From this the presence or absence of each CD marker was observed, allowing for determination of cell line markers.

Table 2.2: CD markers detected to determine stem-status of extracted ADSCs.

CD Marker	Fluorophore	Excitation-Emission (nm)	Detection Channel (Novocyte)	Isotype	Clone
CD11b	PE-Dazzle 594	566-610	BL3	Mouse IgG1	ICRF44
CD13	Brilliant Violet 421	405-421	VL1	Mouse IgG1	WM15
CD31	PE-Cy7	565-780	BL5	Mouse IgG1	WM59
CD44	Brilliant Violet 605	405-603	VL4	Rat IgG2b	IM7
CD45	Brilliant Violet 785	405-785	VL6	Mouse IgG1	HI30
CD73	APC-Cy7	755-755	RL2	Mouse IgG1	AD2
CD90	AlexaFluor 647	633-668	RL1	Mouse IgG1	5E10
CD105	AlexaFluor 488	488-519	BL1	Mouse IgG1	43A3
CD106	PE	570-578	BL2	Mouse IgG1	STA

Antibodies raised against specific CD makers were obtained conjugated to specific fluorophores to prevent overlap of the emission spectra. All antibodies were obtained from Biologend, USA.

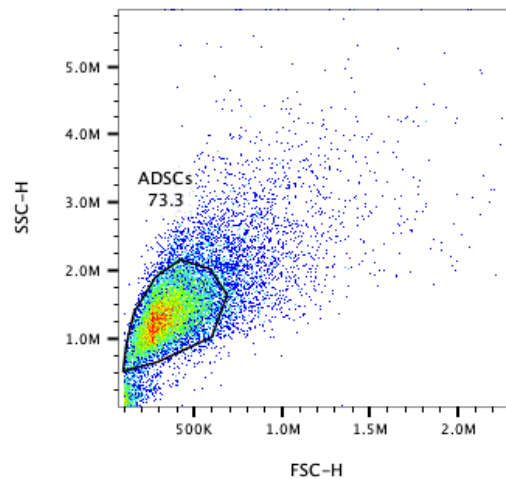


Figure 2.2: Example of an adipose derived stem cells flow cytometry plot.

Example of an ADSC cell population acquired on the Novocyte 3000 flow cytometer. The cells were gated using the multi-sided gates (shown in black) according to side scatter (SSC) and forward scatter (FSC) parameters. Percentage of total events acquired noted on plot.

2.10.1 Compensation Matrix

Potential spectral overlap upon emission of two or more fluorophores within the same tube require compensation to adjust for this. VersaComp antibody Capture beads were purchased from Beckman Coulter (IN, USA) in a kit to create the compensation matrix (Figure 2.4). One bottle in the kit contained positive beads, which capture conjugates in single colour stains, and one contained negative beads, which provides a profile similar to unstained cells across the different emission / excitation spectrum (Figure 2.3). Following the manufacturer's instruction, the bottles were removed from 4°C, vortexed and inverted 10 times before one drop of each positive and negative beads was added to a FACS tube. They were treated like cells and the protocol was followed as previously described in this section.

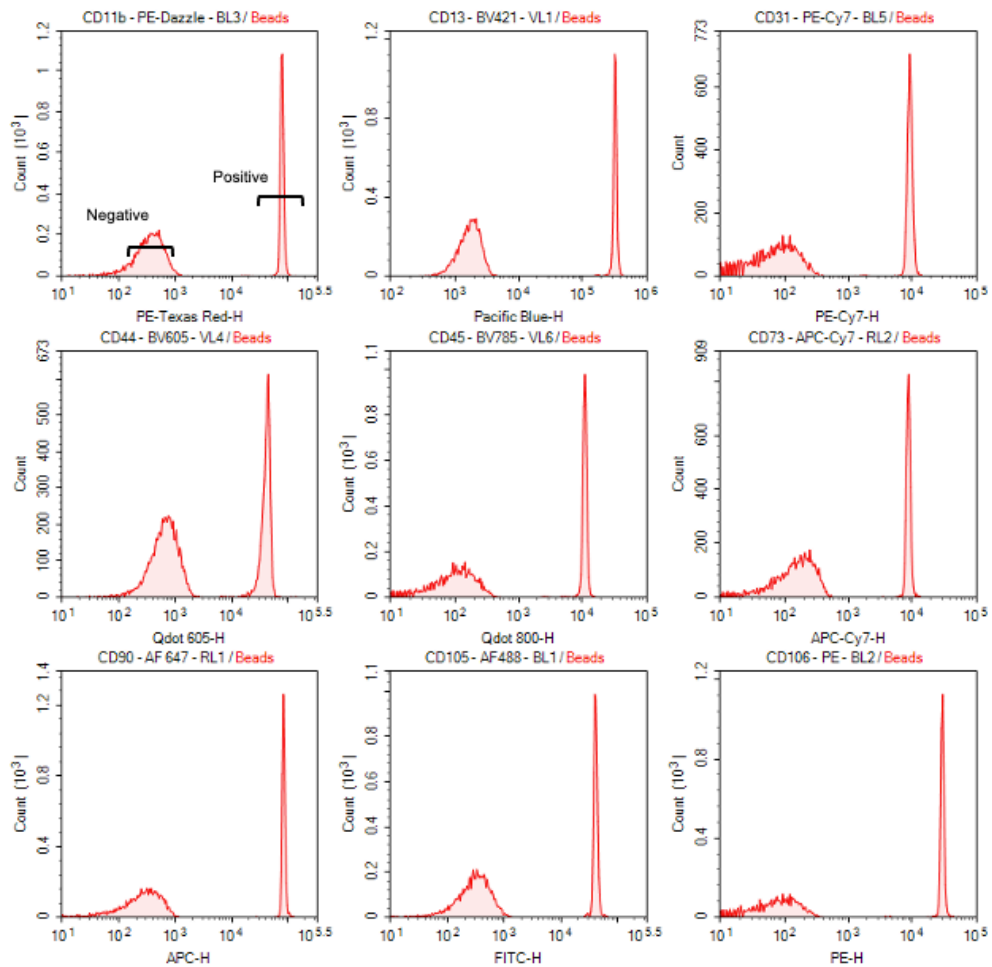


Figure 2.3: Compensation controls: positive and negative VersaComp beads run with individual fluorophores to generate a specific compensation matrix for the chosen panel.

Fluorescence profiles for each fluorophore demonstrating the positive peaks and negative controls created using the VersaComp beads. The graphs were created using FlowJo version 1.3 (Oregon, USA) and were collated into a single compensation matrix to ensure reliable results when running multicoloured flow cytometry panels.

Events were labelled and gated as described in Section 2.10 and applied to the positive and negative events. By utilising the initial single stains and compensation controls, a compensation matrix was generated using FlowJo version 1.3 (Oregon, USA) and the protocol was saved. This compensation matrix was then applied to all flow cytometry data collected prior to any data analysis.

Show All	BL1-H :: FITC-H	BL2-H :: PE-H	BL3-H :: PE-Tex...	BL5-H :: PE-Cy...	RL1-H :: APC-H	RL2-H :: APC-C...	VL1-H :: Pacific ...	VL4-H :: Qdot 60...
<input checked="" type="checkbox"/> BL1-H :: FITC-H	100	8.5895	4.4933	0.0071	0	0	0.1122	0.0774
<input checked="" type="checkbox"/> BL2-H :: PE-H	3.4081	100	114.2172	0.1886	0.0394	0	0.1711	24.4114
<input checked="" type="checkbox"/> BL3-H :: PE-Texas Red-H	0.13	2.6031	100	0.474	0.0587	0	0.0504	19.9182
<input checked="" type="checkbox"/> BL5-H :: PE-Cy7-H	0.6025	1.7818	1.7142	100	0.0208	20.5666	0.5543	0.3272
<input checked="" type="checkbox"/> RL1-H :: APC-H	0.0047	0.0011	0	0.007	100	4.0959	0.0689	0.0109
<input checked="" type="checkbox"/> RL2-H :: APC-Cy7-H	0.0673	0.0228	0.0334	0.2598	7.3815	100	1.0036	0.0189
<input checked="" type="checkbox"/> VL1-H :: Pacific Blue-H	0.0002	0.0009	0.0009	0	0.0016	0	100	0.1449
<input checked="" type="checkbox"/> VL4-H :: Qdot 605-H	0.0021	0.0592	3.8197	0.0189	0.0397	0.0044	13.9912	100
<input checked="" type="checkbox"/> VL6-H :: Qdot 800-H	0.046	0.0263	0.0631	1.5889	0.1098	12.8308	87.7243	0.5593

Figure 2.4: The compensation matrix created in FlowJo to correct for fluorescence spillover emissions for the chosen ADSC panel.

Produced in FlowJo using the data generated in Figure 2.3. The checkboxes on the left show which parameters are being used in the display, with the numbers representing the spill values between the two parameters. The colour coding represents a heatmap, with darker colours applied to higher spills, which is used to identify compensation problems. The individual files created running single stains with the beads enabled the creation of a compensation file that was then added each time the panel was run to account for the fluorescence spillover emissions.

2.10.2 Data Analysis

All data was initially generated using the Novocytte Flow Cytometer (Agilent, UK) and NovoExpress Software. All data analysis post acquisition was performed using FlowJo version 1.3 (Oregon, USA). The gated populations (ADSCs) were used to exclude any debris or dead cells and individual histograms were generated for the specific fluorophores of interest.

2.11 Trilineage Differentiation

To prove that the ADSC cells have retained multi-lineage capacity the cells must be induced to differentiate into three separate cell types. In the present study, the ADSCs were induced to differentiate into adipocytes, osteocytes and chondrocytes using the StemPro™ differentiation kits (Product codes 10154093, 10771764 and 10216663 Gibco, Life Technologies, UK). The details of each kit are provided below in Table 2.3 and were used to evaluate the trilineage capability of the cells isolated from the adipose tissue collected from patients. As a positive control, mesenchymal stem cells (MSC) were differentiated alongside the ADSCs to prove that the differentiation had occurred.

Table 2.3: Components of Adipogenic (top), Osteogenic (middle) and Chondrogenic (bottom) StemPro Kits.

Adipogenesis Differentiation Media	Concentration	Volume
StemPro Adipocyte Differentiation Basal Medium	1x	90 ml
StemPro Adipocyte Supplement	1x	10 ml
Gentamicin Reagent (10 mg/ml)	5 µg/ml	50 µl

Chondrogenesis Differentiation Media	Concentration	Volume
StemPro Osteocyte/Chondrocyte Differentiation Basal Medium	1x	90 ml
StemPro Chondrogenesis Supplement	1x	10 ml
Gentamicin Reagent (10 mg/ml)	5 µg/ml	50 µl

Chondrogenesis Differentiation Media	Concentration	Volume
StemPro Osteocyte / Chondrocyte Differentiation Basal Medium	1x	90 ml
StemPro Chondrogenesis Supplement	1x	10 ml
Gentamicin Reagent (10 mg/ml)	5 µg/ml	50 µl

Differentiation media as detailed in the StemPro differentiation kits used for adipocyte, chondrogenic and cartilage differentiation of MSCs. Each kit is supplied with the basal medium, supplementation, and antibiotic, along with culture and staining instructions.

2.11.1 Adipogenesis

ADSCs were harvested and seeded in 6 well plates at a density of 1×10^4 cells/ml in ADSC media and were incubated at 37°C, 5% CO₂ for four days. The cells were washed with PBS and the media was replaced with pre-warmed Complete Adipogenesis Differentiation Medium (StemPro Adipocyte Differentiation Basal Medium (90 ml), StemPro Adipocyte Supplement (10 ml) and Gentamicin Reagent (5 µg/ml)), and the cultures were supplemented every three to four days. Following the differentiation period, the media was removed from the cells, rinsed once with PBS and the cells were fixed with 4% paraformaldehyde solution (ThermoFisher Scientific, USA) for 30 minutes.

Following this, the wells were rinsed twice with PBS and once with 60% isopropanol (ThermoFisher Scientific, USA). To show the presence of lipids, the cells were stained with Oil Red O (Sigma, UK): A stock solution of 0.5% Oil Red O was prepared in 100% isopropanol, this was diluted 3:2 with distilled water and filtered through filter paper (Whatman No1, Sigma, UK). The diluted working solution was added to the cells for 30 minutes at room temperature. The wells were washed several times with distilled water to remove any residual stain and imaged using a light microscope (Zeiss, Axiovert 40C) and images were captured for analysis (Figure 2.5).

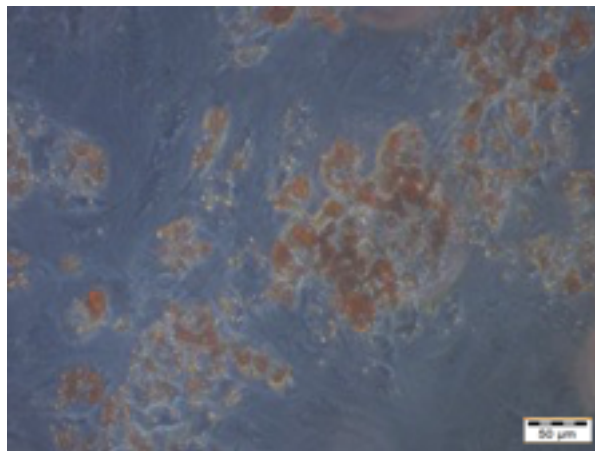


Figure 2.5: Image taken of extracted ADSCs differentiated into adipocytes. Adipose tissue stained with Oil Red O to demonstrate the presence of lipids after 4 days of culture in adipogenic media. Image taken x10 magnification on a standard light microscope (Zeiss Axiovert 40C, Germany).

2.11.2 Chondrogenesis

ADSCs were harvested and a cell suspension of 1×10^7 cells/ml was prepared. Micromass cultures were generated by adding 1 ml of the prepared cell suspension to a 1.5 ml microcentrifuge tube and pelleting. The cells were gently dislodged from the bottom of the tube using a pipette tip, allowing the pellet to float in the media. The pellets were incubated for two days before the warm chondrogenesis media (StemPro osteocyte/chondrocyte differentiation basal medium (90 ml), StemPro chondrogenesis supplement (90 ml) and gentamicin Reagent (5 $\mu\text{g/ml}$)), was added to the tubes and the cells were incubated at 37°C, 5% CO₂. The cultures were supplemented every two to three days. After 14 days of incubation, the cells were transferred to a 6 well

plate and Alcian Blue staining was carried out to show the production of proteoglycans by chondrocytes. The media was removed from the culture plate; the cells were rinsed once with PBS and fixed with 4% paraformaldehyde solution for 30 minutes. The wells were then rinsed twice with PBS and the cells were stained with 1% Alcian Blue solution prepared with 0.1N HCl for 30 minutes. The wells were then rinsed three times with 0.1N HCl followed by three washes with distilled water to neutralise the acidity. The cells were visualised under the light microscope and images were captured for analysis (see Figure 2.6).



Figure 2.6: Image taken of extracted ADSCs differentiated into chondrocytes. The cultured pellets were stained with Alcian Blue to demonstrate the presence of proteoglycans by chondrocytes after 14 days of culture in chondrogenic media. Image taken x10 magnification on a standard light microscope (Zeiss Axiovert 40C, Germany).

2.11.3 Osteogenesis

ADSCs were harvested and a cell suspension of 5×10^3 cells/ml was prepared and seeded into a 6 well plate. The cells were incubated at 37°C , 5% CO_2 for four days and following this, the media was replaced with pre-warmed complete osteogenesis differentiation media (StemPro osteocyte/chondrocyte differentiation basal medium (90 ml), StemPro chondrogenesis supplement (90 ml) and gentamicin reagent (5 $\mu\text{g}/\text{ml}$)). The cultured cells were supplemented every three to four days for 21 days. The media was removed from the wells; the cells were rinsed with PBS and fixed with 4% paraformaldehyde solution for 30 minutes. The wells were then rinsed twice

with distilled water and the cells were stained with 2% Alizarin Red S staining solution (pH 4.2 prepared in distilled water) for 2-3 minutes. The cells were then rinsed three times with distilled water, visualised under the light microscope and images were captured for analysis. Red stain indicates the presence of calcific deposition by cells of an osteogenic lineage (Figure 2.7).

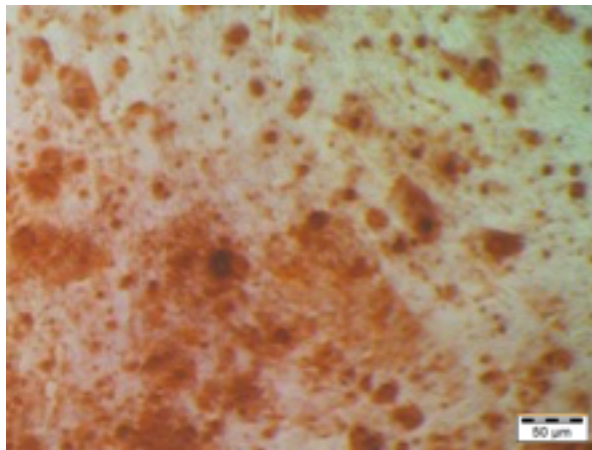


Figure 2.7: Image taken of extracted ADSCs differentiated into osteocytes. The cultured cells were stained with Alizarin Red S to demonstrate the presence of calcific deposition by cells of an osteogenic lineage after 21 days of culture in osteogenic media. Image taken x10 magnification on a standard light microscope (Zeiss Axiovert 40C, Germany).

2.12 Conditioned Media Preparation

ADSCs were cultured in ADSC media at 37°C, 5% CO₂ until passage 2 and 8 (p2 and p8) in a T175 flask until 60% confluent, the medium was then replaced with fresh ADSC media, and the cells were incubated for 24 hours to condition the media. ADSC conditioned media (ADSC-CM) was then harvested, centrifuged at 300g for five minutes and filtered through a 0.2 μm syringe filter to remove contaminating cells and debris. This was then combined with fresh ADSC media to create different concentrations (0, 25, 50, 75, 100%) for use to treat the MCF-7 cells (Table 2.4).

Table 2.4: Ratios of fresh and conditioned media for each percentage.

Conditioned Media %	Ratio of Media Types
0	0% Conditioned Media / 100% Fresh ADSC Media
25	25% Conditioned Media / 75% Fresh ADSC Media
50	50% Conditioned Media / 50% Fresh ADSC Media
75	75% Conditioned Media / 25% Fresh ADSC Media
100	100% Conditioned Media / 0% Fresh ADSC Media

Concentrations of fresh and conditioned media making up each of the different ratios for use in the conditioned media experiments.

2.13 Non-Contact Co-Culture Preparation

Co-culturing the ADSCs and MCF-7 cells together using a non-contact model enables their effect on one another to be examined whilst keeping the cell populations separate for individual assessment. To create a comparable co-culture model across the various plate sizes, cells were optimised using a 6-well plate and standardised by calculating cells per cm^2 to ensure comparability. For all experiments, regardless of plate size, 0.4 μm transwell co-culture inserts (6 and 24 well Corning™, USA and EL-16 plates from ACEA and Bioscience, UK) were used to allow free movement of soluble proteins without migration and contact between the cells. Following optimisation, 4×10^4 ADSCs in a 0.4 μm transwell insert for a 6 well plate translated to 19,047.61 cell/ cm^2 which was applied to the various sizes of inserts ensuring no more than 70% confluence of ADSCs in co-culture, therefore minimising the risk of their differentiation (Figure 2.8).

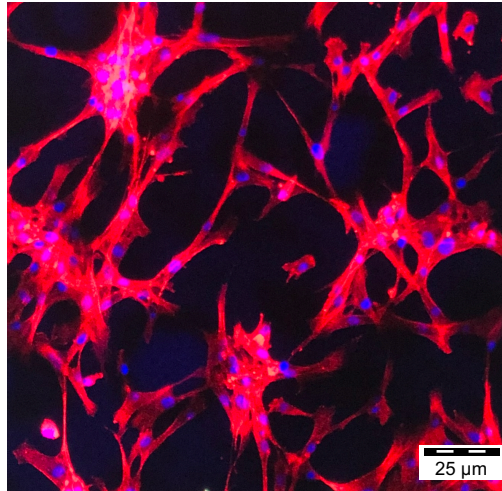


Figure 2.8: Confocal microscopy of ADSCs in a 0.4mm transwell insert. ADSCs 4×10^4 in 0.4 μm Corning™ co-culture insert, fixed with 4% PFA and stained with DAPI (4',6-diamidino-2-phenylindole blue-fluorescent DNA stain that exhibits ~20-fold enhancement of fluorescence upon binding to AT regions of dsDNA.) and Phalloidin 633 (high-affinity F-actin probe conjugated to a bright, photostable, far-red fluorescent Alexa Fluor™ 633 dye) on a Confocal Microscope at high resolution (1024 x 1024).

The addition of a second breast cancer cell line (T47D) was done for validation of results, to enable comparison between ADSCs taken from two distinct patient populations (healthy and cancer patients) and two oestrogen receptor positive (ER+) breast cancers. This helped to determine if the effects being observed were unique to one specific cancer cell line or if the differences were likely to translate to other ER+ cell lines. For each experiment, ADSCs taken from healthy and cancer patients were cultured in a T175 flask until 60% confluent at passage 8 (p8) and trypsinised as described previously before being counted using the Countess™ cell counter and seeded at 19,047.61 cell/cm² into the appropriate 0.4 μm mesh insert. They were covered with fresh ADSC media over both the bottom well and transwell insert for 24 hours at 37°C, 5% CO₂ prior to the experiment. The cancer cell lines (MCF-7 or T47D) were seeded at the densities previously stated in the bottom of the wells as described for the conditioned media experiments and incubated at 37°C, 5% CO₂ to ensure they had adhered to the plate. Where T47D seeding densities differ to those for MCF-7 cells, these are stated.

2.14 The Measurement of MCF-7 Proliferation, Migration, Invasion and Morphology

2.14.1 Measurement of Proliferation in Response to Conditioned Media

In order to determine whether differing concentrations of ADSC-CM had an effect on the adhesion and proliferation of MCF 7 cells, their proliferation was measured using a real time cellular impedance assay. The functional unit on the inferior aspect of the EL-8 microtiter plate is a gold micro electrode with a positive and negative terminal enabling an electrical current to be passed through an electrically conductive solution (standard or conditioned culture media). The impedance of this impulse increased as more cells adhere to the uncoated plastic well (electrode-solution interface), delaying the current (22 mV) and providing a real time measurement of adhesion (first two hours) and proliferation measured over a defined period of time. Importantly, neither the applied electrical potential nor the gold microelectrode surfaces have any effect on the cell behaviour or health.

The RTCA iCELLigence instrument was placed in the incubator for two hours prior to the start of the experiment in order for it to equilibrate to the humid environment (Figure 2.9). To each well of the EL-8 plate (Figure 2.10), 150 μ l of complete conditioned medium was added, this was placed into the cradle pocket of the iCELLigence instrument, and the lid was securely closed. A cell suspension of 5×10^5 cells/ml of MCF-7 cells was prepared in varying concentrations of ADSC-CM (0, 25, 50, 75 and 100%). The experimental profile was set up on the connected iPad and following the equilibration of the media in the EL-8 plate (approximately 30 minutes), the play button was pressed on the iPad, initiating the background sweep. Immediately following the background sweep, the EL-8 plate was removed from the cradle and the MCF-7 cells (350 μ l) from the prepared cell suspensions were added to the appropriate wells. The plates were then returned to the iCELLigence instrument, and the experiment resumed by pressing the play button. Readings were taken every minute for the first two hours, then every hour for 48 hours.



Figure 2.9: ACEA Real Time Cell Analysis (RTCA) iCELLigence machine. Image from the ACEA website (ACEA Bioscience, UK, now part of Agilent, UK) showing the RTCA iCELLigence analyser used to measure cell adhesion, index and proliferation using a microtiter well plate to measure electrical impedance between a positive and negative terminal.

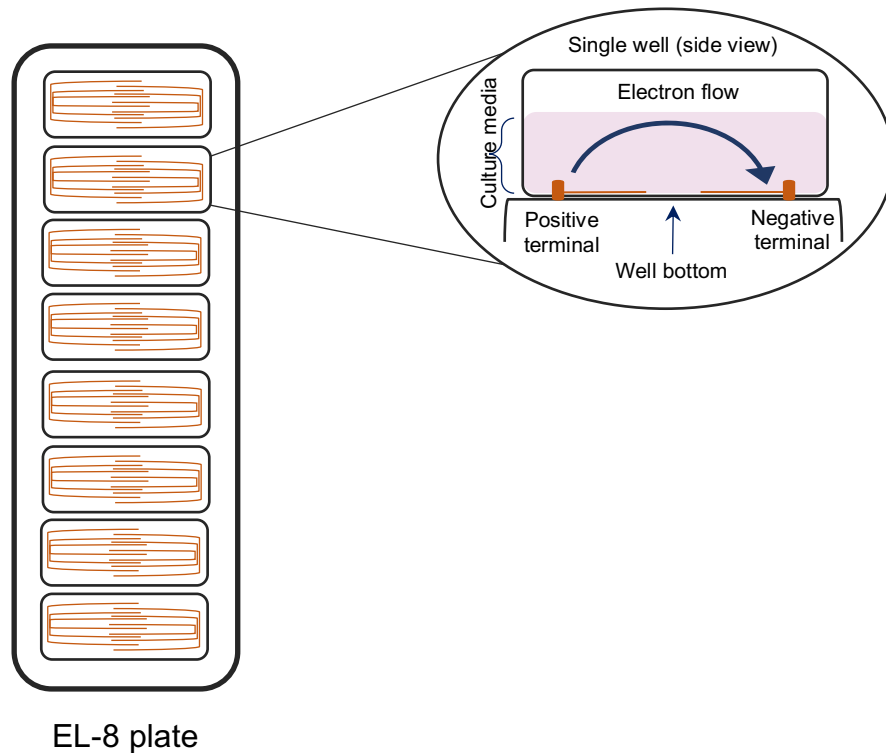


Figure 2.10: Schematic representation of an EL-8 plate for use with the RTCA iCELLigence machine.

Schematic representation of EL-8 plate demonstrating each individual well covered by gold microelectrodes used for measuring impedance of a 22 mV electric potential. The RTCA iCELLigence machine holds two of these plates giving a total of 16 wells per patient for testing with differing concentrations of conditioned media plus wells for control.

2.14.2 Measurement of Proliferation in Response to Co-Culture

To determine whether ER+ breast cancer (MCF-7 and T47D) proliferated differently when co-cultured with ADSCs isolated from patients with and without breast cancer, EL-16 transwell inserts were used to create non-contact co-culture models and enable measurement of the breast cancer proliferation using a real time cellular impedance assay. Prior to the experiment commencing, 95 μl of a 1.08×10^4 cells/ml cell suspension of ADSCs was seeded into each of the 16 wells on the EL-16 plate where two transwell inserts sit within one EL-8 plate well (Figure 2.11). They were incubated for 24 hours at 37°C, 5% CO₂ to allow the cells to adhere.

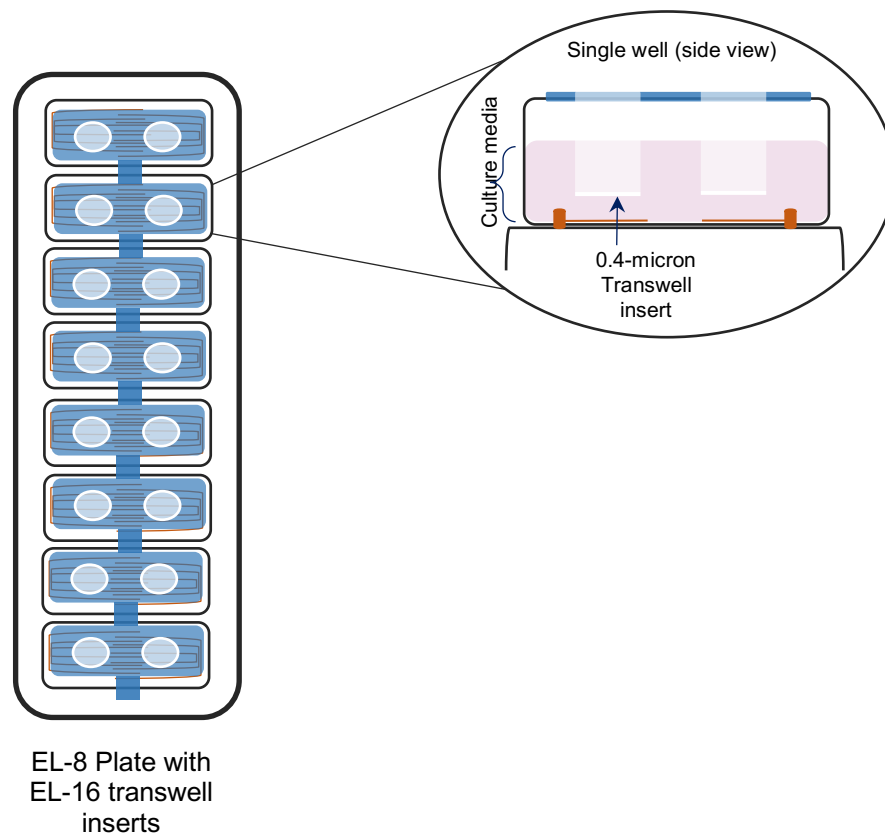


Figure 2.11: Schematic representation of an EL-16 Plate sitting over an EL-8 plate.

Schematic representation of EL-16 transwell insert plate sitting over an EL-8 plate demonstrating the non-contact co-culture model to enable the effects of ADSCs from healthy and cancer patients on the proliferation of MCF-7 and T47D breast cancer to be examined.

The protocol on the machine was kept consistent throughout the study for both CM and co-culture experiments. On the day of the experiment, 150 μl of warmed cell line media was added to each well of the EL-8 plate. This was placed into the cradle pocket of the iCELLigence instrument, and the lid was securely closed. A cell suspension of 5×10^5 cells/ml of MCF-7 cells and 7×10^5 cell/ml of T47D cells were prepared in warmed cell line media. After the experimental set up was confirmed and the background sweep was completed, the EL-8 plate was removed from the cradle and 350 μl from the prepared cell suspensions of MCF-7 and T47D were added to the appropriate wells. Using sterile tweezers, the EL-16 plate was carefully removed from the ADSC media and placed into the EL-8 plate (Figure 2.11). The plates were then returned to the iCELLigence instrument, and the experiment resumed by pressing the play button. Readings were taken every minute for the first two hours, then every hour for 48 hours.

2.14.3 Measurement of Migration in Response to Conditioned Media

To determine if the differing concentrations of ADSC-CM had an impact on MCF-7 migration an assay was performed creating a gap within the cells and measuring the time taken to close using serial photographs. This differed from a standard scratch assay as a silicone cell culture insert (IBIDI, Germany) was used to create a uniform gap and prevent cellular damage which would have been caused had the tip of a pipette been used. A cell suspension of 4×10^5 cells/ml of MCF-7 cells was prepared in cell line media and 70 μl was added to each section of the cell culture insert in addition to this, 300 μl of cell suspension was added to the well around the outside of the insert (Figure 2.12). The plate was incubated for 24 hours at 37°C , 5% CO_2 to allow the cells to adhere to the surface of the plate. The cell line media was removed from the plates and discarded, and the insert was removed from the well using sterile tweezers. The cells were washed with PBS to remove any remaining media and the media was replaced with varying dilutions of ADSC-CM (0, 25, 50, 75 and 100%). The plate was returned to the incubator and the cells were monitored for 48 hours and the closure of the $500\mu\text{m}$ gap was observed using serial photographs on a standard light microscope (Zeiss Axiovert 40C, Germany) with a camera (Canon EOS 77D SLR, Japan).

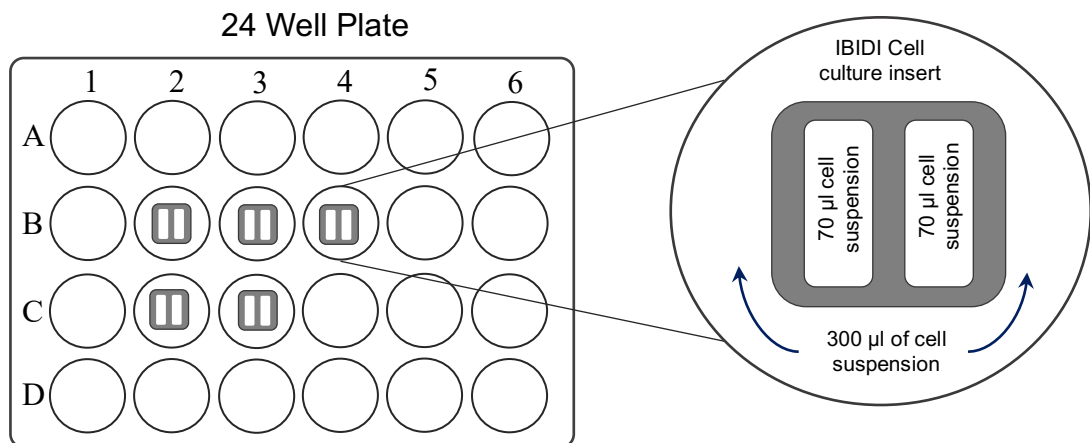


Figure 2.12: IBIDI cell culture insert used for migration assay in a standard 24 well plate.

Schematic representation of a 24 well plate containing IBIDI cell culture inserts used to create a uniform gap in the cells. A different well was used for each of the concentrations of conditioned media (0, 25, 50, 75 and 100%), with 70 µl added to each well and 300 µl added to the space around the insert filling up the well. The MCF-7 cells were incubated for 24 hours at 37°C, 5% CO₂ before the insert was removed with sterile tweezers, the well was washed with PBS and 750 µl of conditioned media was added. Over the next 48 hours serial photographs were taken to monitor the closure of the standardised 500 µm gap.

2.14.4 Measurement of Migration in Response to Co-culture

In order to determine whether ER+ breast cancer (MCF-7 and T47D) migrated at a different rate when co-cultured with ADSCs isolated from patients with and without breast cancer, a non-contact co-culture model was used. The same migration assay was performed creating a gap within the cells and measuring the time taken to close using serial photographs as done with conditioned media. However a 24 well transwell insert seeded with ADSCs was suspended in the well for the duration of the experiment. A cell suspension of 4×10^5 cells/ml of MCF-7 cells and 7×10^5 cells/ml of T47D were prepared in cell line media, and as with the conditioned media protocol, seeded in triplicate around an IBIDI cell culture insert (Figure 2.12). The plate was incubated for 24 hours at 37°C, 5% CO₂ to allow the cells to adhere to the surface of the plate before the insert was removed 24 hours later with sterile tweezers. At the same time the ADSCs at passage 8 (p8) which had been grown in a T175 flask to 60% confluence were trypsinised and resuspended in warmed ADSC media. 300 µl

of the ADSC cell suspension (1.9×10^4 cells/ml) was seeded into 24 well transwell inserts (Corning® USA) suspended in a well containing 1 ml of warmed ADSC media. 24 hours after both the ADSCs and breast cancer cell lines were seeded, the insert was transferred across and suspended over the migration assay (Figure 2.13). Over the next 48 hours, serial photographs were taken at the same time points as in the conditioned media experiment for the next 48 hours. Prior to each photograph being taken, the plate was taken back into the tissue culture hood, and using sterile tweezers, the insert was moved temporarily into an empty well containing only ADSC media to ensure the photo of the gap was unobscured.

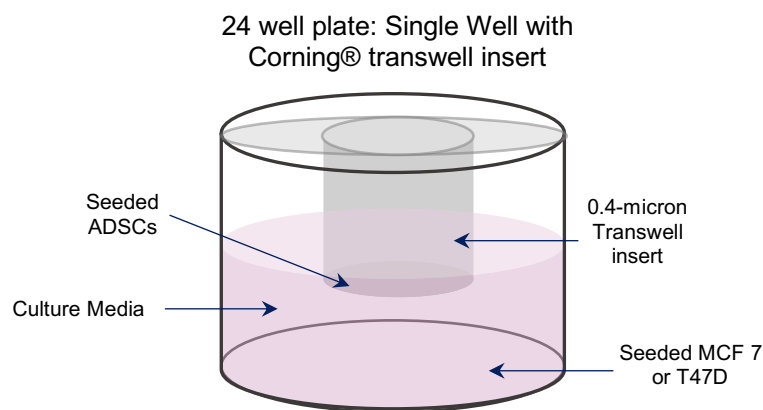


Figure 2.13: Schematic representation of 24 well transwell insert sitting in a 24 well plate.

This diagram shows how 24 hours after ADSCs were seeded into 24 well transwell inserts and MCF-7 or T47D were seeded around the IBIDI migration inserts, the migration inserts were removed and the transwell insert was positioned over the top of the well. Photographs were taken at regular intervals over the next 48 hours and the gap closure was measured.

2.14.5 Measurement of Invasion in Response to Conditioned Media

Acting as a mechanical barrier to the spread of malignant cells, basement membrane integrity degradation sees the transition from *in situ* carcinoma to fully fledged malignance worthy of TNM grading. The extra-cellular matrix (ECM) is composed of three-dimensional macromolecules such as collagen and glycoproteins which form essential parts of this important anatomical barrier. The 24 well collagen invasion assay (Merck Millipore, Germany) uses a type-1 purified chicken collagen as a structural matrix to provide a

quantification of invasion which as a result of processing is comparable to humans.

MCF-7 cells were grown to confluency in T75 tissue culture flasks and subsequently serum starved for 24 hours prior to harvesting. Prior to their use, the invasion inserts were removed from the fridge (4°C) and brought to room temperature for a minimum of 30 minutes, after which the collagen layer of the collagen invasion assay insert was rehydrated by adding 300 µl of pre-warmed serum free media (SFM) for 15-30 minutes at room temperature. A cell suspension of 1×10^6 cells/ml was prepared in SFM and 250 µl of this was added to the interior of the collagen insert following rehydration. Varying concentrations of ADSC-CM (0, 25, 50, 75 and 100%) were added to the bottom of the well to a final volume of 500 µl and this was incubated at 37°C, 5% CO₂ for 24 hours (Figure 2.14).

Following this incubation, the media in the interior of the insert was carefully removed by pipetting and the invasion chamber was placed into a well containing 400 µl of cell stain provided in the kit. This was incubated for 20 minutes at room temperature, then insert was then washed by dipping in water several times to remove the unbound cell stain. While the insert was still moist, a cotton-tipped swab was used to remove any non-invading cells from the interior of the insert, this was then repeated with a second cotton-tipped swab. The insert was then placed into an empty well and allowed to air dry overnight at room temperature.

Once dry, images of the inserts were taken using the tissue culture camera (Canon EOS 77D SLR) and microscope (Zeiss, Axiovert 40C). The insert was then placed into a well containing 200 µl of extraction buffer to remove the stain from the collagen insert. This was incubated for 15 minutes at room temperature, after which 100 µl was transferred to a 96 well plate along with extraction buffer alone as a control. The absorbance was measured at 560 nm using a microplate reader (POLARstar Omega, BMG Labtech, Germany).

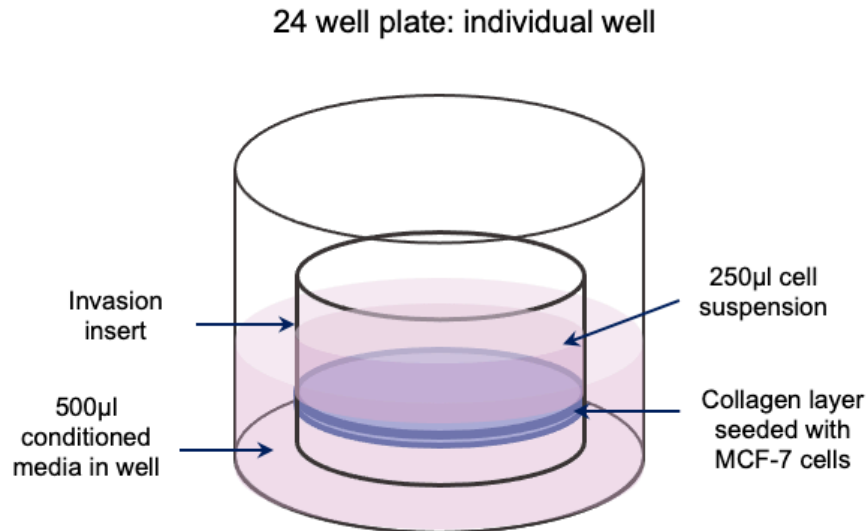


Figure 2.14: Collagen Cell Culture invasion inserts to measure MCF-7 invasion. Schematic representation of a single well of a 24 well plate with an individual Collagen Cell Culture Insert. This assay provided a qualitative measure (photographs taken at x4 and x10 magnification on a standard light microscope with a camera) and qualitative measure (stain extraction and plate reader at 560nm).

2.14.6 Measurement of Invasion in Response to Co-Culture

Changes in invasive potential were examined to determine whether ER+ breast cancer (MCF-7 and T47D) cell lines behaved differently when co-cultured with ADSCs isolated from patients with and without breast cancer. A non-contact co-culture model was used to evaluate this. The same 24 well collagen invasion assay was used for the experiment and both cell lines were grown to confluency in T75 tissue culture flasks and subsequently serum starved for 24 hours prior to harvesting. The ADSCs were concomitantly grown in a T175 flask to 60% confluence at p8 and were trypsinised and resuspended in warmed ADSC media, counted using the Countess™ cell counter and resuspended at a density of $(4.83 \times 10^4 \text{ per ml})$. For each patient, three wells on a 24 well plate were used for each cancer cell line with 500 µl of the cell suspension pipetted into each. They were incubated at 37°C, 5% CO₂ for 24 hours to allow them to adhere.

The following day, as with the conditioned media experiments, prior to their use, the invasion inserts were removed from the fridge (4°C) and brought to room temperature for a minimum of 30 minutes, after which the collagen layer

of the collagen invasion assay insert was rehydrated by adding 300 μ l of pre-warmed SFM for 15-30 minutes at room temperature. Following this, 250 μ l of media was removed, and the insert was gently transferred over to a well containing ADSCs. A cell suspension of 1×10^6 cells/ml for both MCF-7 and T47D cells were prepared in SFM and 250 μ l of the cell line being observed was added to the interior of the collagen insert following rehydration. There is a gap underneath each collagen membrane which ensures that there is no contact between the cell populations. For each plate, there was a collagen insert with either MCF-7s or T47D cells cultured independently, to ensure that each plate had an internal control. The cells were incubated at 37°C, 5% CO₂ for 24 hours to allow them to adhere before the media in the inserts was carefully removed and insert stained as previously described in the conditioned media experiments. With photographs taken of each insert after staining, prior to the stain extraction and reading of the absorbance at 560 nm using a microplate reader.

2.14.7 Measurement of Cell Morphology in Response to Conditioned Media

There are numerous reasons cancer cells experience morphological change, as cancer migrates and becomes more invasive there is a shift in cell-cell contact and overall morphology. Using the INCELL 2000 (GE, Boston USA) enables the examination of the morphology of MCF-7 cells and their response to the varying concentrations of ADSC-CM. MCF-7 cells were seeded at a density of 1×10^5 cells/ml in 6 well plates in MCF-7 media and allowed to adhere for 24 hours. The media was then removed; the cells were washed with PBS to remove any residual media and replaced with varying concentrations of ADSC-CM (0, 20, 50, 75 and 100%). The cells were then incubated at 37°C, 5% CO₂ for 4 or 24 hours before being harvested and fixed in 4% paraformaldehyde (PFA). The media was removed and put into sterile labelled microcentrifuge tubes for ELISA analysis at a later date. The samples were stored in the -20°C freezer. Following fixation, cells were stained with Hoechst stain (Sigma, UK) for 30 minutes at room temperature, in the dark. The cells were then washed twice with PBS before 2 mls of PBS was added to prevent the cells from drying out. The plate is read on the INCELL Analyser 2000 which

took a series of 300 photographs (fields of view) using a high-performance CCD camera from each well for analysis.

2.14.8 Measurement of Cell Morphology in Response to Co-Culture

Morphological changes to the cell or nucleus were measured as detailed above using the INCELL Analyser 2000 after staining, washing, and fixing the cells with 4% paraformaldehyde. As with the conditioned media experiments, MCF-7 cells were seeded at a density of 1×10^5 cells/ml in 6 well plates in MCF-7 media and allowed to adhere for 24 hours. The ADSCs had been cultured in a T175 flask to 60% confluence at p8 and were trypsinised and resuspended in warmed ADSC media, counted using the Countess™ cell counter and resuspended at a density of 4×10^4 per ml. Following this, 500 μ l of this cell suspension was seeded into a 6 well transwell insert with 500 mls of fresh warmed media in the insert and 2 mls below in the empty well. Both the MCF-7 cells and ADSCs were incubated (in separate incubators) for 24 hours at 37°C, 5% CO₂. After 24 hours the media on both the cells was replaced with warmed cell specific media and the transwell insert containing the ADSCs was placed in the well containing the MCF-7s. The cells were then incubated at 37°C, 5% CO₂ for 4 or 24 hours before being harvested and fixed before being stained and imaged using the following parameters which were standardised for each of the 2D photographs:

- Objective; Nikon 20X/0.45,
- Plan Fluor
- ELW
- Corr Collar 0-2.0
- CFI/60
- 0.030 DAPI Exposure
- 2.00 AF offset

The media was removed and put into sterile labelled microcentrifuge tube for ELISA analysis at a later date.

2.15 Human Cytokine Antibody Array Panel

The behaviour and progression of breast cancer is complex and multifactorial and results from the disruption of normal signalling pathways which cells rely on to respond appropriately to the extracellular environment. Extracellular signalling is an essential part of this process and examining the production of certain key proteins is important to understand how this abnormal signalling might be contributing to the development, progression, and metastasis of the breast cancer. Prior to the selection of three discrete cytokines, chemokines and acute phase proteins to measure in the media, a broader panel array was purchased (R&D systems, Minneapolis, USA) and undertaken to establish whether levels of the proteins of interest were in fact detectable at discernible levels to warrant measurement. Reagents required for the human cytokine antibody array (Table 2.5) were prepared immediately before use.

Table 2.5: Human Cytokine Antibody Array Reagents.

Buffer	Supplied As	Action
Blocking Buffer	1x Working Concentration	None
Wash Buffer 1	20x Concentration	Dilute 20-fold with distilled water
Wash Buffer 2	20x Concentration	Dilute 20-fold with distilled water
Biotin-Conjugated Anti-Cytokines	2000x Concentration	Centrifuge vial to ensure contents are at the bottom, reconstitute by adding 2 ml of 1x Blocking Buffer
HRP-Conjugated Streptavidin	1000x Concentration	Mix contents and briefly centrifuge before use. Dilute 1000-fold with 1x Blocking Buffer
Detection Buffers C and D	1x Working Concentration	None

Reagents required for the human cytokine antibody array that were prepared immediately before use.

The cytokine antibody array membrane was placed print side up in the provided 8-well tray and was blocked in 2 ml of blocking buffer for 30 minutes at room temperature. Following this, the blocking buffer was removed, and 1 ml of undiluted sample was added to the membrane, which was then incubated overnight at 4°C. The sample was then removed, and the membrane washed as follows: 10 ml of wash buffer 1 for 45 minutes at room temperature, 3 x 5 minutes with 2 ml wash buffer 1 and 3 x 5 minutes with 2 ml wash buffer 2. The prepared 1x Biotin-Conjugated Anti-Cytokine (1 ml) was added to the membrane and incubated for 2 hours at room temperature. The membrane was then washed 3 x 5 minutes with 2 ml wash buffer 1 and 3 x 5 minutes with 2 ml wash buffer 2. The prepared 1x HRP-Conjugated Streptavidin (2 ml) was applied to the membrane and incubated for 2 hours at room temperature. The wash steps were repeated, and the membranes were blotted dry using tissue paper before being transferred to the plastic sheet provided in the kit. The working detection reagent was prepared by adding 1:1 ratio of buffers C and D into a fresh tube, this was then added to the membrane and incubated for two minutes at room temperature. The second plastic sheet was applied to the top of the membrane and was imaged using the ChemiDoc (Bio-Rad, UK). ImageJ software was used to measure the intensity of each spot, following by subtracting the background and normalising to the positive controls.

2.15.1 Measurement of Enzyme-Linked Immunosorbent Assay (ELISA)

Interleukin-6 (IL-6) is a pleiotropic pro-inflammatory cytokine and anti-inflammatory myokine and its over-expression has been effectively demonstrated in a number of tumour microenvironments, with high levels linked to dysregulation in cancer. The promotion of tumorigenesis and key cancer hallmarks involve avoidance of apoptosis, upregulated proliferation and EMT induction resulting in more invasive disease with higher metastatic potential. Monocyte chemoattractant protein-1 (MCP-1) is a potent monocyte attracting chemokine, greatly contributing to the recruitment of blood monocytes into sites of increased inflammation such as the tumour macroenvironment. While MCP-1 production was initially thought to be part of the host defence against cancer, increasingly, *in vivo* and *in vitro* studies are demonstrating that it may play a significant role in amplifying the interplay

between tumour cells and macrophages which promotes the progression of cancer. Vascular endothelial growth factor (VEG-F) is a heparin binding dimeric protein with a number of functions including stimulation of endothelial cells to degrade ECM, migrate, proliferate and induced the formation of tubules. Playing a role in vascular permeability and neoangiogenesis, high levels in breast cancer patients has been linked to advanced differentiation, lymph node metastasis and higher clinical stage. Following the analysis of the cytokine antibody array, the three proteins of interest were identifiable and individual kits were acquired (R&D systems, Minneapolis, USA) to examine the specific cytokines or chemokines using a sandwich ELISA as per the manufacturer's instructions (Figure 2.12). Three proteins were analysed using the following ELISA protocol: IL-6, MCP-1 and VEG-F. For all experiments wash buffer (0.05% Tween 20 (Sigma, UK) in PBS) and reagent diluent (1% BSA in PBS) were used, all other antibodies are described in Table 2.6.

Table 2.6: Reagents required for IL-6, MCP-1 and VEG-F ELISA analysis.

Protein	Capture Antibody	Standards	Detection Antibody	Streptavidin-HRP
IL-6	Reconstitute in 0.5 ml PBS (120 µg). Working concentration: 2 µg/ml	Reconstitute with 0.5 ml dH ₂ O (90 ng). Working concentration: 600 pg/ml	Reconstitute with 1 ml Reagent Diluent (3 µg). Working Concentration: 50 ng/ml	Dilute 40-fold with Reagent Diluent
MCP-1	Reconstitute in 0.5 ml PBS (60 µg). Working concentration: 1 µg/ml	Reconstitute with 0.5 ml Reagent Diluent (70 ng). Working concentration: 1000 pg/ml	Reconstitute with 1 ml Reagent Diluent (6 µg). Working Concentration: 100 ng/ml	Dilute 40-fold with Reagent Diluent
VEG-F	Reconstitute in 0.5 ml PBS (60 µg). Working concentration: 1 µg/ml	Reconstitute with 0.5 ml Reagent Diluent (60 ng). Working concentration: 2000 pg/ml	Reconstitute with 1 ml Reagent Diluent (6 µg). Working Concentration: 100 ng/ml	Dilute 40-fold with Reagent Diluent

Antibodies and reagents required for ELISA analysis of the chosen proteins, detailing the dilution, and working concentration for each protein of interest.

2.15.2 Measurement of Enzyme-Linked Immunosorbent Assay (ELISA) in Response to Conditioned Media and Co-Culture with ADSCs

After establishing their presence in baseline media, the measurements of the three specific proteins that had been identified (IL-6, VEG-F and MCP-1), from the cell free culture media was performed using the sandwich ELISA technique as described in the manufacturer's instructions (R&D Systems, Bio-Techne, Minneapolis, USA). Media was harvested from MCF-7 cells at 4 hours and 24 hours after the addition of different concentrations of conditioned media (0, 25, 50, 70 and 100%) and after the commencement of co-culture with ADSCs. Media was removed and pipetted into sterile, labelled microcentrifuge tubes and put into the -20°C freezer for analysis together at a later stage.

To a clean, half-area 96 well plate, 50 µl of diluted capture antibody of interest (IL-6, MCP-1 or VEG-F) was added to each well and incubated overnight at 4°C. The capture antibody excess was then removed the following day, and remaining protein binding sites were blocked by adding 150 µl of blocking buffer to each well and incubating for one hour at room temperature with gentle agitation. The wells were then washed four times with 200 µl of wash buffer (0.05% Tween 20 (Sigma-Aldrich, UK) in PBS). The standards were removed from the freezer and allowed to defrost on ice before 50 µl of sample were added to the appropriate well along with standards to generate the appropriate standard curve. The plate was then covered and incubated overnight at 4°C. Following this incubation, the standards and samples were removed from the wells and the wash steps were repeated as stated above.

The diluted detection antibody (50 µl) was added to each well and incubated for two hours at room temperature with gentle agitation, followed by removal of the detection antibody and a repeat of the wash steps. At this point 50 µl of the diluted streptavidin-horseradish peroxidase (HRP) was added to each well and incubated for 20 minutes at room temperature whilst covered with gentle agitation. The streptavidin-HRP was then removed, and the wash steps were repeated for a final five times. The substrate solution was prepared by adding 50 µl of a 1:1 mixture of substrate buffer A and B (hydrogen peroxide and tetramethylbenzidine (TMB)), to each well and incubated at room temperature, in the dark, until the blue colour develops (Figure 2.15), the standards were used for observation. Once the standards showed a stepwise reduction in colour, 50 µl of 1M Sulphuric acid (H₂SO₄) was added to each well to prevent any further colour development, turning the solution yellow. The plate was read at 450 nm using a plate reader and final protein concentration calculated in relation to the standard curve.

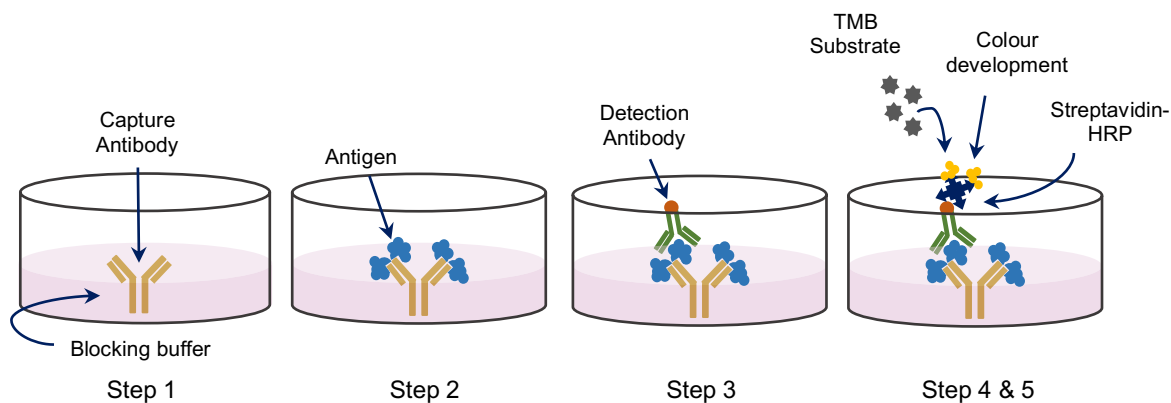


Figure 2.15: Schematic overview of the steps required for a sandwich ELISA assay.

Step 1: Capture antibody binds to the plate, with the blocking buffer eliminating any alternative binding sites. Step 2: Addition of sample to the well and protein of interest (antigen) binding to the capture antibody site. Step 3: Addition of biotin labelled detection antibody. Step 4 & 5: Addition of conjugated Streptavidin-HRP which binds to the detection antibody. Addition of TMB substrate results in the development of blue colour which is stopped by the addition of Sulphuric Acid. The plate can then be read at 450nm.

2.16 Bioenergetics Analysis – Seahorse-XF

During tumorigenesis, cellular metabolism is often skewed towards glycolysis, a phenomenon known as the “Warburg Effect”. Understanding cellular energetics is central to the understanding of how cancer behaves and progresses. In order to examine the various metabolic parameters of MCF-7 and T47D cells after co-culture with ADSCs, extracellular flux analysis was carried out using a Seahorse XFe24 analyser (Seahorse Bioscience, USA). The two energy producing metabolic pathways, glycolysis and oxidative phosphorylation (OXPHOS) are directly correlated to the extracellular acidification rate (ECAR; mpH/min) and oxygen consumption rate (OCR; pmole/min) respectively. Both ECAR and OCR measurement was performed using an adherent cell monolayer within a transient micro chamber. The real-time measurement of dissolved oxygen and pH change accompanied by a series of either metabolic enhancing or reducing injections over time, enabled the calculation of these metabolic parameters.

Cartridge sensor hydration was performed 24 hours prior to the assay being conducted by adding 1 mL of XF calibrant solution to each well of an XF

cartridge and placed in an oven at 37°C in a sealed plastic bag to prevent excessive evaporation. Each calibration plate contains miniature pH and oxygen sensors that are linked to a fibre optic waveguide. The excitation signal is read as a fluorescent signal that is transmitted to a photodetector, allowing the dual measurement of ECAR and OCR in a single experiment. Non-mitochondrial respiration can be calculated following all three injections and determining the difference between the final measurement to give the proton leak and non-mitochondrial respiration. Removing the non-mitochondrial respiration enables the basal respiration to be calculated which then facilitates the calculation of the ATP linked production. Maximum respiration is the change detected following the FCCP injection and before the Rotenone/Antimycin-A injection, after which the spare respiratory capacity can be calculated (see Figure 2.16 and Table 2.7).

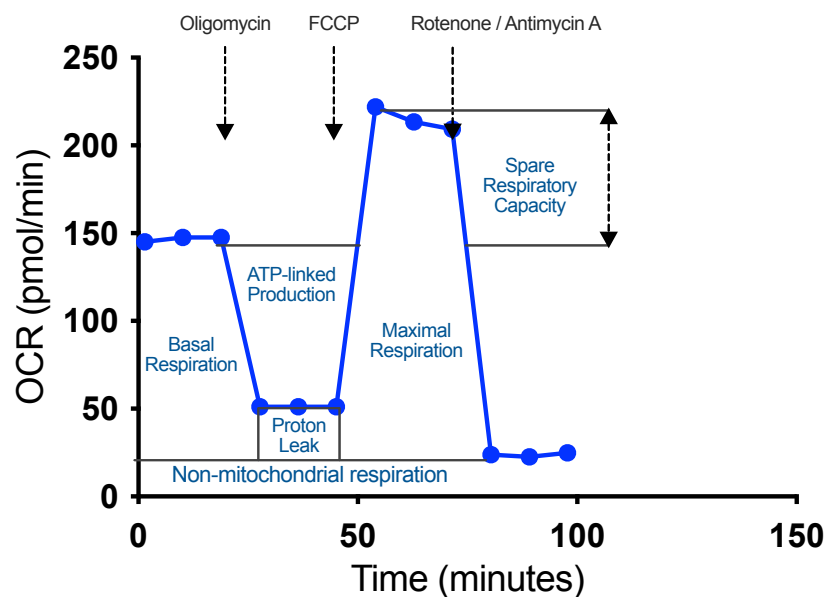


Figure 2.16: Oxygen consumption rate (OCR) and the calculation of metabolic parameters.

The calculation of mitochondrial oxidative parameters using OCR (pmoles/min), measured by the Seahorse XF analyser to determine non-mitochondrial respiration and proton leak, basal and maximal respiration, ATP-linked production, and spare respiratory capacity after timed injections of Oligomycin, FCCP and Rotenone/Antimycin-A.

Table 2.7: Methods for calculating the respiratory parameters

Respiratory Parameter	Calculation Method
Non-mitochondrial respiration	Measurement following the Rotenone/Antimycin A injection
Proton leak	The difference between the final three data points following the oligomycin injection and the end of the three injections
Basal Respiration	Initial measurements prior to the first injection minus the non-mitochondrial respiration
ATP-linked Production	Basal respiration minus proton leak
Maximal Respiration	Difference between the FCCP injection and the end of the Rotenone/Antimycin-A injection
Spare Respiratory Capacity	Maximal respiration minus the Basal Respiration

Calculation of the parameters using the data generated from the Seahorse XF analyser following the XF24e assay. Calculated using the OCR data which is performed in triplicate and averaged.

2.16.1 Adhesion to the Bio-Flux Plate

MCF-7 and T47D Cancer cell lines were co-cultured (non-contact) for 24 hours using a transwell system in a 6 well plate as previously described (Section 2.13) with ADSCs suspended in a transwell insert above the cancer cell lines which were at the bottom of the 6 well plate. To enable the cells to be examined within a short time frame post separation from co-culture, the base of the XFe24 bioflux plate (Seahorse Bioscience, Copenhagen, Denmark) used for bioenergetics analysis, was coated with Cell-Tak (Corning, Massachusetts, USA). Cell-Tak is a polyphenolic protein secreted by *Mytilus edulis* and was used at 3.5 $\mu\text{g}/\text{cm}^2$ per well to attach them to the bottom of the wells. 0.1 M of sodium bicarbonate (Life Technologies) was added to the Cell-Tak in the bottom of each well and left to sit in a tissue culture hood for 20 minutes. The liquid was then carefully removed, and each individual well was washed with endotoxin free, sterile water (Sigma, UK) and left in the tissue culture hood for 60 minutes to air dry. The plate could either be used immediately or stored at 4°C for seven days. Prior to use, the XFe24 bioflux plate with Cell-Tak coating was placed in the oven at 37°C for at least 30 minutes.

On the day of the assay, cells were trypsinised and resuspended in warmed XF phenol red free pH adjusted Assay/Base Media (Seahorse Bioscience, Copenhagen, Denmark) which was supplemented with 1 mM pyruvate, 5 mM glucose and 1 mM L-glutamine. Cells were seeded into a XFe24 bioflux plate (Seahorse Bioscience, Copenhagen, Denmark) in 150 µl of the media and centrifuged for 1 minute at 200g with 0 acceleration and 1 break, to encourage the cells to stick down to the bottom of the well. After a visual confirmation that the cells were present, the cells were incubated at 37°C for 30 minutes before a total of 525 µl media was in each well before being returned to the oven for 20 minutes while the protocol was set up on the machine. The three injections were prepared (Oligomycin, FCCP and Rotenone/Antimycin-A) and 75 µl of each injection was put into the appropriate port in the XF cartridge. The cartridge was loaded into the Seahorse and when ready, the bioflux plate with the MCF-7 and T47D cells was loaded in place of the utility plate for completion of the assay.

2.16.2 Bioenergetics of Co-Culture

MCF-7 and T47D cells were cultured to confluence in a T75 flask prior to the experiment, trypsinised and resuspended in warmed cell line media and seeded at a density of 1×10^5 cells/ml into the bottom of a 6 well plate. The ADSCs had been cultured in a T175 flask to 60% confluence at p8 and were trypsinised and resuspended in warmed ADSC media, counted using the Countess™ cell counter and resuspended at a density of 4×10^4 per ml into a 6 well transwell insert. Both the cancer cell lines and ADSCs seeded in the inserts were put in their respective incubators 37°C, 5% CO₂ for 24 hours to allow them to adhere. After this, the plates were removed from the incubator, and in the tissue culture hood, with sterile tweezers, the transwell insert was moved across into the well containing either MCF-7 or T47D cells. They were then returned to the incubator at 37°C, 5% CO₂ for 24 hours prior to the commencement of the Seahorse assay.

2.17 Data Analysis

Statistical data analysis was performed using GraphPad Prism version 9.1.0 (216) and unless otherwise stated are represented as the mean +/- standard error. Analysis of variance (ANOVA) was used to compare two or more group means with one variable (one-way ANOVA) with either Bonferroni or Tukey's post hoc analysis unless otherwise stated. For multiple comparisons a two-way ANOVA or three-way ANOVA was used. All experiments have replicate sample sizes of at least $n=3$ and significant values were taken as $p < 0.05$ graphically denoted as * $p \leq 0.05$, ** $p \leq 0.01$, *** $p \leq 0.001$.

2.17.1 Proliferation

Statistical analysis was performed using GraphPad Prism version 9.1.0, after exporting the file into RTCA Data Analysis Software 1.0 (ACEA Bioscience, UK). A two-way ANOVA was used to compare proliferation of each group (healthy and cancer) with each other and against a control (0%). All experiments were repeated in triplicate across both patient groups (conditioned media: $n=6$ healthy, $n=10$ cancer and co-culture $n=6$ healthy and $n=6$ cancer). Significant values were taken as $p < 0.05$ graphically denoted as * $p \leq 0.05$, ** $p \leq 0.01$, *** $p \leq 0.001$, **** $p \leq 0.0001$. Adhesion was calculated as the change in cell index divided by the change in time ($\Delta CI/\Delta T$) and a two-way ANOVA with multiple comparison tests was applied.

2.17.2 Migration

Images captured on a light microscope (Zeiss, Axiovert 40C) at x10 magnification were assessed visually initially before the gap was measured using ImageJ to quantify the gap remaining from the original 500 micron starting point as described previously (Section 2.14.3). Statistical analysis was performed using GraphPad Prism version 9.1.0, after exporting the file into RTCA Data Analysis Software 1.0 (ACEA Bioscience, UK). A two-way ANOVA was used to compare different concentrations of conditioned media against the control (0%) across both patient groups (healthy and cancer). All experiments were repeated in triplicate across all concentrations of conditioned media at both p2 and p8, and co-culture at p8.

2.17.3 Invasion

Data quantified using extracted stain as previously described in Chapter Two (Section 2.14.5). Statistical analysis was performed using GraphPad Prism version 9.1.0 after exporting the data from the plate reader into MS Excel. A two-way ANOVA was used to compare the effects of ADSCs isolated from healthy and cancer patients on MCF-7 and T47D invasion. Data shown is from technical replicates (n=3) across both patient groups (conditioned media: n=6 healthy, n=10 cancer and co-culture n=6 healthy and n=6 cancer) and data is expressed as the mean \pm SEM.

2.17.4 Cytokine Expression Profiles

Statistical analysis was performed using GraphPad Prism version 9.1.0 after exporting the data from the plate reader into MS excel. A two-way ANOVA was used to compare the concentrations of different detected proteins in the media against the control (0%). Data shown is from technical replicates (n=3) across both patient groups (conditioned media: n=6 healthy, n=10 cancer and co-culture n=6 healthy and n=6 cancer) and data is expressed as the mean \pm SEM. Significant values were taken as $p < 0.05$ graphically denoted as * $p \leq 0.05$, ** $p \leq 0.01$, *** $p \leq 0.001$ and **** $p \leq 0.0001$.

2.17.5 INCELL

Images captured using the INCELL analyser 2000 were processed using the open source CellProfiler™ image analysis software version 3.1.5 (USA). The algorithm enabled the 300 individual images from each well to be sequentially loaded into the software, creating a pipeline to measure cell area, eccentricity, perimeter and solidarity. Data generated was initially exported into MS Excel before statistical analysis was performed using GraphPad Prism version 9.1.0. A two-way ANOVA was used, with co-culture data from technical replicates (n=3) at p8 across separate experiments with patients taken from two patient groups (healthy n=6 and cancer n=6) and data is expressed as the mean \pm SEM.

2.17.6 Bioenergetics

Metabolic analysis of MCF-7 and T47D cells was carried out using the Seahorse Extracellular Flux Analyzer XFe24 (Seahorse Bioscience) as described in the methods (Section 2.16). Following 24 hours of non-contact co-culture with ADSCs isolated from healthy and cancer patients, MCF-7 or T47D cells were seeded onto a Cell-Tak plate and the two energy producing metabolic pathways, which are directly correlated to the extracellular acidification rate (ECAR; mpH/min) and oxygen consumption rate (OCR; pmole/min), were measured during the experiment through the use of the three injections (Oligomycin, FCCP and Rotenone/Antimycin-A). Statistical analysis was performed using GraphPad Prism version 9.1.0 and data shown is from technical replicates (n=3) at one time point (p8) across separate experiments with patients taken from two patient groups (healthy n=6 and cancer n=6) with data expressed as the mean \pm SEM.

Chapter Three

Optimisation of Adipose Derived Stem Cell (ADSC) Isolation and Assays for Evaluating MCF-7 and T47D Growth and Progression

3.1 Introduction

As illustrated in Section 1.4, there are numerous mechanisms by which ADSCs have been purported to influence the breast microenvironment, and the hallmarks of cancer (Li *et al.*, 2009; Devarajan *et al.*, 2012; Fujisaki *et al.*, 2015). The use of ADSC enriched FFT following BCS, has the potential to interact with residual microscopic cancer post-resection, impacting patient outcomes including, disease free survival, recurrence, and cancer behaviour (Xu *et al.*, 2012; Schmid *et al.*, 2018; Wu *et al.*, 2019). As discussed in Chapter One, while much of the scientific research has focused on breast cancer interaction with healthy ADSCs, evidence is emerging that factors including systemic therapies, can affect their behaviour (Razmkhah *et al.*, 2010; Fujisaki *et al.*, 2015; Pike *et al.*, 2015; Varghese *et al.*, 2017; Teufelsbauer *et al.*, 2019; Wu *et al.*, 2019). As such, the potential difference in the effects of ADSCs isolated from patients with breast cancer when compared with their healthy counterparts is of specific interest in this study (Li *et al.*, 2009; Xie *et al.*, 2012; Ziegler *et al.*, 2014; Wu *et al.*, 2019).

A range of experimental models aimed at mimicking elements of the breast microenvironment have been described to examine the effect of ADSCs on breast cancer hallmarks, including conditioned media and co-culture (Fujisaki *et al.*, 2015; Wei *et al.*, 2015; Koellensperger *et al.*, 2017; Schmid *et al.*, 2018; Wu *et al.*, 2019). Whilst the limitations of cell-based models are generally understood, their use is essential in developing our understanding of the interaction between ADSCs and ER+ breast cancer. As outlined in Section 1.7.2 the MCF-7 cell line is widely studied and given its ER+ receptor status is an ideal cell line for study. Regardless of the experimental model selected, a robustly isolated and characterised ADSC population is required to ensure experimental reliability and results analysis. As highlighted in Section 1.7, since their discovery in 2001, ADSCs have been utilised by scientific and

clinical researchers, due to their ease of harvest and broad clinical application. As the first published protocol detailing their successful isolation and characterisation, the methodology described by Zuk *et al.*, 2001 is routinely cited by other authors. A general lack of consensus however, has resulted in numerous papers that discuss refinements of ADSC isolation, suggesting theirs is a more reliable technique for producing a predictable cell population (Locke, Windsor and Dunbar, 2009; Bourin *et al.*, 2013; Busser *et al.*, 2014; Iyyanki *et al.*, 2015; Chen *et al.*, 2016). As their use in clinical trials developed, protocols reflect scalability requirements and GMP regulations (Schäffler and Büchler, 2007; Trojahn Kølle *et al.*, 2013). Newer techniques vary digest times, harvesting methods and utilise additional media components. These changes could influence the suitability of the isolated ADSC population and their interaction with any cell lines being studied. It is therefore essential to ensure that the population isolated is of an adipose progenitor cell type, prior to the commencement of any experiments.

3.1.1 Chapter Aims

The aim of this chapter is to trial and select a reliable ADSC isolation protocol, which can be used in the creation of a clinically representative model to more accurately study the effects of ADSCs on the hallmarks of ER+ breast cancer. This ensures that ADSCs can be reliably isolated from two patient groups (healthy and cancer) for use in the conditioned media (Chapter Four) and co-culture (Chapter Five) experiments. Prior to expanding the number of patients included in the study, each of the hallmark assays must be optimised with both the ER+ breast cancer cell lines (MCF-7 and T47D). This ensures appropriate consideration is given to the primary cell lines collected from patients.

This will be achieved by meeting the objectives below:

1. Identify an appropriate and reliable ADSC isolation protocol
2. Characterise the ADSCs isolated by the chosen protocol based on the Dominici Criteria
3. Establish a reliable method for identifying and selecting patients for sample collection

4. Optimise MCF-7 and T47D assays (key assays) to evaluate the chosen hallmarks of cancer as previously described in Chapter One for conditioned media and co-culture studies:
 - a. Invasion
 - b. Migration
 - c. Proliferation
 - d. Morphology
 - e. ELISA
 - f. Bioenergetics

3.2 Methods

3.2.1 Patient Selection

In this study ADSCs were taken from two distinct patient groups as detailed in Section 1.8.

1. Female patients who had never had cancer and were on no systemic treatment and were otherwise fit and well. This was defined as the healthy group
2. Female patients who had a diagnosis of an ER+ breast cancer and were currently taking systemic therapy in the form of an oestrogen receptor antagonist (Tamoxifen or Letrozole depending on menopause status). This was defined as the cancer group.

Patient samples were collected across the full duration of the study with 22 patients enrolled in total (ADSC001 – ADSC022). Four primary cell lines were collected and used for protocol selection and eventual optimisation, two primary cell lines were unfortunately lost to infection and 16 primary cell lines were included in the final results (10 cancer and 6 healthy). There was an inability to collect samples during the COVID-19 pandemic as all elective surgery in the trust was suspended as we resumed frontline NHS duties on an emergency rota which meant approximately seven months away from research.

3.2.2 Sample Collection

Samples were collected as described in Chapter Two (Section 2.4) and transferred to the laboratory for isolation. They were collected from the two patient groups, those with ER+ positive cancer currently on systemic therapy (n=10) and those that had never had cancer and were not on any systemic treatment (n=6) as described in Section 3.2.1.

3.2.3 Protocol Selection

As illustrated in Section 1.7.1, there are numerous ADSC isolation techniques described since the original protocol was published (Table 3.1) (Zuk *et al.*, 2001, 2002). To determine the most appropriate protocol for use in this study, three were identified following a review of the literature examining commonly

referenced protocols, in addition to the one taken forward (Table 3.1), protocols two and three are outlined in Appendix One.

Tables 3.1: Original ADSC isolation protocol as described by Zuk *et al* 2001.

Protocol	One
Paper	Zuk et al 2001 Multilineage Cells from Human Adipose Tissue: Implications for Cell-Based Therapies (Zuk <i>et al.</i> , 2001)
Materials	All Materials Sigma (St Louis, MO) Tissue Culture reagents Life Technologies (New York, NY), FBS (Hyclone, Logan, UT)
Cell lines	Adipose tissue taken during elective procedures, lipoaspirate, Human
Harvest	Done under local anaesthetic (with saline and adrenaline infused to prevent bleeding and prevent contamination by peripheral RBCs). Hollow blunt tipped cannula with gentle suction (approx. 300cc).
Isolation and Culture	<p>Do as much as possible on ice</p> <ol style="list-style-type: none"> 1. Lipoaspirate is extensively washed (5 times) with equal amount of PBS 2. Digest the ECM with 0.075% collagenase at 37°C for 30 minutes 3. Neutralise enzyme activity with Dulbecco's modified Eagle's medium (DMEM) with 10% FBS (equal volume) 4. Centrifuge at 1200g for 10 minutes to get high density pellet 5. Re-suspend pellet in 160mM NH₄Cl and incubate at room temperature for 10 minutes to lyse the remaining RBCs 6. Centrifuge at 1200g for 10 minutes to get pellet 7. Collect SVF 8. Filter through 100-µm nylon mesh to remove cellular debris 9. Put cells into control medium [DMEM, 10%FBS, 100 U/ml Penicillin, 100 µg/ml Streptomycin (pen/strep)] and incubate overnight 10. Following incubation wash plates extensively to remove residual non-adherent blood cells. 11. This is termed processed lipoaspirate (PLA) 12. Maintain cells at sub-confluence levels (80%) to prevent spontaneous differentiation to adipocytes

Protocol one is well established and recurrently cited in the literature, upon which many papers are based. This was the first published protocol that successfully isolated ADSCs and was ultimately the protocol that was used in this study.

3.2.4 ADSC Isolation

ADSCs were isolated as described in Chapter Two (Section 2.10). For each primary cell line isolated from a patient, cells were cryopreserved as described in Section 2.9.2 of the methods chapter at various passages to ensure redundancy in case of infection or cell line loss during the duration of the study.

3.2.5 Tissue Culture

While three protocols were trialled initially, primary cell lines were ultimately isolated as described in Section 2.7. The primary cell lines isolated were not permitted to become more than 70% confluent to prevent differentiation prior to evaluation. The MCF-7 and T47D breast cancer cells were cultured in phenol red free DMEM supplemented with 10% FBS and 2mM GlutaMAX. Cell lines were all grown to 80% confluence before being passaged as described in the methods (Section 2.6) and they were cultured for 14 days prior to any use in experimentation once removed from liquid nitrogen.

3.2.6 Adipose Derived Stem Cell (ADSC) Characterisation

With a variety of stem cell sources, isolation techniques and protocols for culture and characterisation, it is essential to have a minimum criteria for determining a cell as a multipotent MSC to enable research comparison. In 2006 The Mesenchymal and Tissue Stem Cell Committee of the International Society for Cellular Therapy proposed a minimum criteria to define an MSC which identifies three key points (Dominici *et al.*, 2006).

1. In standard tissue culture conditions, MSC should maintain plastic adherence
2. MSC must express CD105, CD90 and CD73 and should be negative for a combination of markers which include CD34, CD45, CD11b, CD79 α etc.
3. MSCs must have trilineage potential and have the ability to differentiate into adipocytes, chondroblasts and osteoblasts in vitro.

While the panel of cell surface markers used to phenotypically characterise ADSCs has evolved since 2002 as our understanding of the cell population has developed, these three criteria have been shown to be a reliable benchmark for standardising the definition of an MSC and better enable comparison between studies.

3.2.6.1 Flow Cytometry

To characterise the primary cell populations isolated, a flow cytometry panel was devised based on the published minimum criteria for ADSC

characterisation and identification in SVF and in culture (Bourin et al., 2013). The panel chosen, as detailed in Section 2.10, comprised of five positive and four negative CD markers, and ensured primary cells could be quantified and monitored. Flow cytometry was used on newly isolated and resuscitated ADSCs as described in Chapter Two, to ensure the consistent presence of cell surface markers. This was done at early and late passage to ensure the cells remained consistent throughout.

3.2.6.2 Plastic Adherence

As one of the defined criteria used to determine if isolated cells from the adipose tissue are MSCs, primary cells isolated were cultured in T175 tissue culture flasks with 25 mls of culture media as described in Section 2.7. Plastic adherence was evaluated as cells adherent after a wash with PBS or media change following seven days of standard culture conditions at 37°C, 5% CO₂. Adherence was assessed using a light microscope (Zeiss, Axiovert 40C) at x4 and x10 magnification to determine if a comparable number of cells were still adherent to the bottom of the tissue culture flask before and after a PBS wash or media change.

3.2.6.3 Trilineage Differentiation

As outlined in Section 2.11, one of the three essential criteria required for MSC characterisation is to demonstrate multilineage potential in culture (Zuk *et al.*, 2001, 2002). The primary cells isolated using the selected protocol (Table 3.1) were induced to differentiate into adipocytes, osteoblasts and chondroblasts using the StemPro differentiation kits purchased from Gibco as described in Section 2.11. As a positive control, mesenchymal stem cells (MSC) which were kindly gifted, were differentiated alongside the ADSCs to prove that the differentiation had occurred.

3.2.7 Proliferation and Cell Adhesion

MCF-7 and T47D proliferation was measured in real time using the automated and continuous ACEA Biosciences iCELLigence system as described previously (Section 2.14.1). In addition to offering the ability to measure real time proliferation and maximum cell index, the iCELLigence system enables

the measurement of cellular adhesion. Using the iCELLigence impedance values obtained within the first two hours after cell seeding enabled the cellular adhesion rate to be calculated. Cell adhesion is then defined as the change in cell index divided by the change in time ($\Delta CI/\Delta T$).

3.2.8 Invasion

MCF-7 and T47D invasion was measured as previously described (Section 2.14.5) using the widely available colorimetric collagen cell invasion assay from Merck Millipore. This enabled a quantifiable, standardised measurement of invasion with a collagen membrane acting as a suitable substrate for human basement membrane. By only allowing invasive cells to migrate through the insert, thus providing a reliable comparative quantitative measure of MCF-7 and T47D lines' invasive potential and change from baseline.

3.2.9 Migration

To ensure accuracy and standardisation along with preventing cellular damage as caused by traditional scratch assays, migration was assessed as described in Section 2.14.3 using the IBIDI inserts. A standardised 500 μm gap was created, prior to the commencement of the experiment to determine whether conditioned media or non-contact co-culture increased the rate of migration of MCF-7 and T47D cells over 48 hours.

3.2.10 Bioenergetics

As previously described in Section 2.16, as the cell lines were run immediately following 24 hours of co-culture; Cell Tak was used to attach the MCF-7 and T47D cells to the bottom of the XFe24 bioflux plate (Seahorse Bioscience, Copenhagen, Denmark) used for the bioenergetic analysis as described in Section 2.16.1. As each plate had an internal control and as the cell number was defined and the plate was coated with Cell Tak, there was no need for a BCA assay as protein concentration was comparable across all wells of each cell type. The calculation of the oxygen consumption rate and metabolic parameters were performed as outlined in Table 2.7.

3.2.11 Cell Morphology

As described in Section 2.14.7, cells that had previously been fixed in 4% PFA were stained and imaged on the INCELL Analyser 2000. Cells were only stained if they were being run within 60 minutes on the analyser to prevent any decay in the stain. The 300 individual photographs taken from each well were then used to evaluate Nuclear Area, Cellular Perimeter, Cell Solidarity, Cellular Eccentricity and Form Factor with CellProfiler™ image analysis software version 3.1.5 (USA) as previously described in Section 2.17.2.

3.2.12 ELISA

The analysis of chosen cytokines and chemokines in the media at a 4 and 24hour time point were undertaken as described previously in the Methods (Section 2.15.1) as per the manufacturer's instructions for IL-6, VEG-F and MCP-1 (Duosets; R&D systems).

3.2.13 Non-Contact Co-Culture of Cell Lines with ADSCs

Each experiment was optimised to allow non-contact co-culture of MCF-7 or T47D cells with ADSCs from patients in two groups. As there were a variety of different well sizes across the various assays, to ensure comparability, ADSCs were optimised per cm² using a 6 well plate and 6 well co-culture insert before being scaled to a 24 well plate, 24 well insert, and EL-16 insert. Following optimisation, 4×10^4 ADSCs in a 0.4 μm transwell insert for a 6 well plate translated to 19,047.61 cell/cm². This was scaled and applied to the various sizes of inserts ensuring no more than 70% confluence of ADSCs in co-culture for the duration of the experiment. This therefore minimised the risk of their differentiation as described in Section 2.13, to ensure they maintained their MSC phenotype.

3.3 Results

Reliable ADSC isolation from the two distinct patient groups (healthy and cancer) is an essential part of this study, and by ensuring the repeatable and reliable isolation of MSCs ensures that the two patient populations can be effectively compared. This facilitates an evaluation of the impact that patient selection might have on the ADSCs isolated, and their indirect and co-located effect on two clinically representative ER+ breast cancer cell lines (MCF-7 and T47D). Optimising the isolation and characterisation of ADSCs is the first part of this study and supports the further optimisation of both the conditioned media and co-culture studies undertaken to establish their indirect and co-located effect on the hallmarks of cancer. These cell-models are well described in the literature as useful adjuncts to approximate the breast microenvironment and the effects ADSCs might have on the neoplastic traits of cancer. The healthy ADSCs therefore reflect the cell line most commonly used in lab-based research, and cancer ADSCs representing patients undergoing reconstruction. Therefore, with the clinical picture in mind, the choice of two different patient populations provides an opportunity for a more direct comparison between the lab studies and the clinical findings.

3.3.1 Patient Cohort Used for the Duration of the Study

Patient recruitment as part of this study was commenced in 2015 with initial primary cell lines being used for isolation and assay optimisation and to establish the scope of access likely for the duration of the research project informing anticipated sample sizes. It was hoped that as a member of a clinical team, that collecting patient samples would be relatively straightforward, however it quickly became apparent that there were a number of challenges that would need to be addressed and adapted to during the research period. Whilst collecting samples from ER+ breast cancer patients currently undergoing long term hormone therapy (Tamoxifen or Letrozole) was more straightforward, collecting samples from patients that were healthy became more challenging. During the five years that samples were being collected, pressures on beds and services resulted in fewer elective cosmetic breast procedures being performed, with more of these patients being cancelled to make way for emergent cancer and trauma operating. On average, these

patients can sit on the waiting list in excess of 24 months and often choose alternative routes for their procedures. Additionally, the last year of sample collection was hindered significantly by the COVID-19 pandemic when the research had to be suspended along with sample collection for seven months as frontline clinical duties resumed. On return to the research environment, pre-pandemic bed pressures were amplified, and no further sample collection was possible as restrictions were increased and access to clinical research samples changed. At this point, only six healthy samples had been collected in comparison to the 10 cancer patient samples that were collected; thus, an n=6 in both groups was employed to allow for direct comparability in the co-culture experiments (Section 2.14).

For each of the patient samples, a range of information was collected including age at time of surgery, pathological cancer diagnosis if applicable which included ductal carcinoma *in situ* (DCIS), ductal carcinoma and invasive ductal carcinoma. Where available, the histological subtype including ER, PR and HER2 status was recorded along with hormone treatment and any adjunctive chemotherapy (CTx) and radiotherapy (RTx). Lifestyle factors were also included such as key comorbidities (e.g., diabetes mellitus (DM)), smoking status and number of pregnancies. The two groups were broadly comparable in age, with regards to the conditioned media experiments in Chapter Four, the mean age in the healthy group (n=6) was calculated at 48 years (range 39-61 years) and for the cancer group (n=10) was 54 (range 37-67 years) for all cancer types. For the co-culture experiments detailed in Chapter Five, the average age in the cancer group (n=6) was slightly higher at 56, with the same age range of 37-67 years. The age standardised incidence rate (globally) is 47.8 years old (Sung *et al.*, 2021) for all breast cancer types. 60% of the patients (n=6) in the cancer group had mastectomies compared with 33% (n=2) in the healthy group which was part of risk management as they were BRCA positive patients having risk reducing surgeries (Tables 3.2 and 3.3).

Of the six cell lines (ADSC001-004 and ADSC006 and ADSC007) that were not included in the main study, ADSC001 - 003 were used to optimise the isolation protocols and characterisation. Primary cell line ADSC004 was used

for some additional flow cytometry optimisation after the refinement of the panel and compensation matrix. They were all grown to p12 before being destroyed. ADSC006 and ADSC007 were unfortunately lost due to an incubator infection.

Table 3.2: ADSC cell lines isolated from healthy patient who have never been diagnosed with breast cancer.

Research Identifier	Sample Type	Age at operation	Diagnosis	Primary / Recurrence	ER status	PR status	HER2 status	BRAC status	Nodes	Side	Mastectomy	RTx	CTx	Hormone	Cardiac co-morbidities	DM	Smoker	Alcohol	Pregnancies
ADSC005	Lipoaspirate	41	BRAC 1 - risk reducing mastectomy	Risk reducing				+	-	Bilateral	Yes	n/a	No	No	No	No	Yes	Occasional	0
ADSC011	Lipoaspirate	39	BRAC 1 - risk reducing mastectomy	Risk reducing				+	-	Bilateral	Yes	Yes	Yes	No	No	No	No	Occasional	0
ADSC012	Lipoaspirate	42	Lipofilling for contour defect	Cosmetic							No	n/a	No	No	No	No	No	Occasional	2
ADSC020	en bloc	57	Cholystectomy	healthy							No	n/a	No	No	No	No	No	Occasional	2
ADSC021	en bloc	51	Cholystectomy	healthy							No	n/a	No	No	Yes	No	Yes	Occasional	0
ADSC022	en bloc	61	Cholystectomy	healthy							No	n/a	No	No	No	No	No	Occasional	2

Each patient gave informed consent for the collection of an intra-operative sample to be taken from tissue destined for clinical waste. During the consent process, additional information was collected in conjunction with the patient. All patients included in the study had never been diagnosed with cancer or treated for cancer in their lifetime. All six patients were included in the conditioned media experiments and in the co-culture experiments.

Table 3.3: ADSC cell lines isolated from patients with breast cancer.

Research Identifier	Sample Type	Age at operation	Diagnosis	Primary / Recurrence	ER status	PR status	HER2 status	BRAC status	Nodes	Side	Mastectomy	RTx	CTx	Hormone	Cardiac co-morbidities	DM	Smoker	Alcohol	Pregnancies
ADSC008	en bloc	64	Grade 3 invasive ductal ca	Primary	+	+	-	-	+	Left	Yes	Yes	Yes	Tamoxifen	No	No	No	Occasional	1
ADSC009	en bloc	67	Grade 2 infiltrative ca	Primary	+	+	-	-	-	Right	Yes	No	Yes	Tamoxifen	No	No	No	Occasional	3
ADSC010	en bloc	38	Grade 3 invasive ductal ca	Primary	+	+	+	-	+	Right	Yes	Yes	Yes	Tamoxifen	No	No	No	Occasional	3
ADSC013	Lipoaspirate	59	DCIS	Primary	+	-	-	-	-	Left	Yes	No	No	Tamoxifen	No	No	No	Occasional	2
ADSC014	Lipoaspirate	61	Grade 2 infiltrative ca	Primary	+	+	-	-	-	Left	Yes	Yes	Yes	Letrozole	No	No	Yes	Occasional	2
ADSC015	Lipoaspirate	48	Grade 1 infiltrative ca	Primary	+	-	-	-	-	Right	No	No	No	Tamoxifen	No	No	No	Occasional	2
ADSC016	Lipoaspirate	42	DCIS	Primary	+	-	-	-	-	Right	No	No	No	Tamoxifen	No	No	No	Occasional	1
ADSC017	en Bloc	61	Grade 2 infiltrative ca	Primary	+	+	-	-	-	Right	Yes	No	Yes	Letrozole	No	No	Yes	Occasional	0
ADSC018	Lipoaspirate	67	DCIS	Recurrence	+	-	-	-	-	Left	No	Yes	No	Letrozole	Yes	No	No	Occasional	0
ADSC019	Lipoaspirate	37	Grade 2 ductal carcinoma	Primary	+	+	-	-	-	Right	No	Yes	No	Letrozole	No	No	Yes	Occasional	1

Each patient gave informed consent for the collection of an intra-operative sample to be taken from tissue destined for clinical waste. During the consent process, additional information was collected in conjunction with the patient and review of histology. All patients included in the study had completed their acute treatment for breast cancer and were undergoing reconstructive surgery. They had all been taking an oestrogen receptor antagonist / aromatase inhibitor (Tamoxifen or Letrozole for at least 12 months). All 10 patients were included in the conditioned media experiments, and patients ADSC008-10 and ADSC017-9 (n=6) were included in the co-culture experiments.

3.3.2 Optimisation of ADSC Isolation and Their Characterisation

3.3.2.1 Selecting the ADSC Isolation Protocol for Use in This Study

Patient samples ADSC001 - ADSC003 were used to trial each of the isolation techniques (see Appendix 1), with the protocol detailed in Table 3.1 ultimately being taken forward. The media and additives were purchased in advance of the sample collections and complete media for each protocol was made up as described in each of the protocols outlined in Section 3.2.3. Cell populations were cultured following isolation from each of the three protocols; with issues arising with certain aspects of protocol two and protocol three that made them difficult to replicate and ultimately lead to them not being taken forward in the study.

3.3.2.2 Challenges Arising with Protocol Two

For the duration of the study an Eppendorf 5210R benchtop centrifuge was used and during step 8, 10 and 14 required a spin of 2000 xg (395 g lower than protocol one and three). After each spin, although the pellet appeared to be formed, it disrupted very easily when pipetting off the supernatant. Multiple additional spins were required to produce a reliable pellet and it became very time consuming. This likely also contributed to the significant quantity of cellular debris that was observed during the cell count using the Countess™ Cell Counter which demonstrated very low viability rates at each attempt with this technique. The debris made it very challenging to visualise the cells after Trypan blue staining and there was a very heterogenous cell population observed using the light microscope after isolation which made culture difficult (Figure 3.1). It was clear there were multiple cell types present and after 48 hours in culture in a 6 well plate (approximately 600 mg of lipoaspirate was used), the cells were entirely confluent, indicating it was unlikely that they were predominantly ADSCs.

This was the only protocol that coated the tissue culture plates with lysine, which appeared rather counterintuitive as one of the key elements of the Dominici criteria is plastic adherence in standard tissue culture. While it may not have been an essential component of long-term culture, it appears to have

significantly impacted the number of cell types that adhered to the plate initially, potentially causing the culture of multiple cell types and rapid confluence over such a short space of time. All of the protocols found in the literature stress the importance of keeping the primary cell lines below 80% confluence to prevent differentiation of the ADSCs, while this is unlikely to happen instantly, spontaneous differentiation at confluence is a recognised issue when working with this cell type (Zuk *et al.*, 2001, 2002). The cell population was visually heterogenous and due to the early confluence and need for lysine coating on the plate, this method was not taken forward for further evaluation.

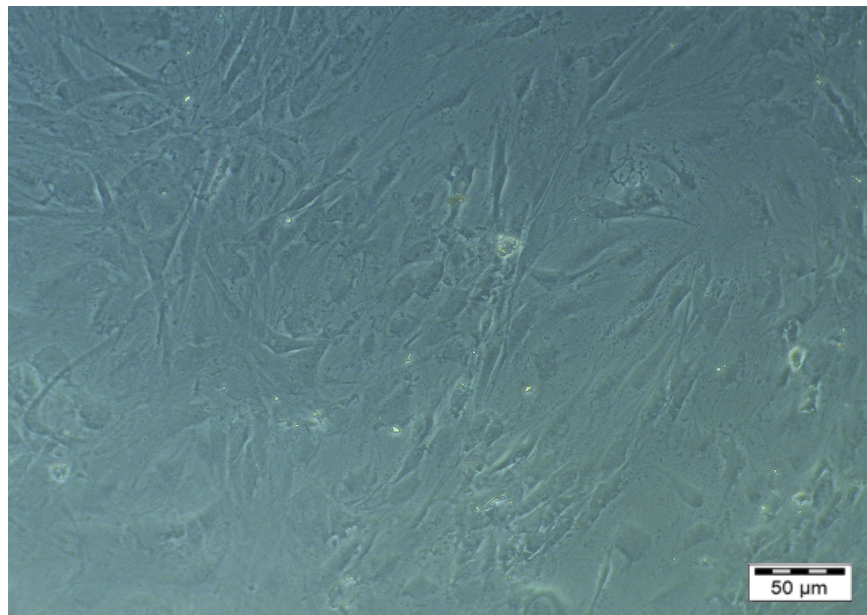


Figure 3.1: Light microscopy image taken of a heterogenous cell population isolated using protocol two

Primary cells isolated from human adipose tissue after trialling protocol two demonstrated near confluence after only 48 hours in tissue culture. This likely represents a mixed cellular picture (adipocytes, ADSCs, fibroblasts etc.) and not true ADSCs – image taken at x10 magnification on a standard light microscope (Zeiss Axiovert 40C, Germany).

3.3.2.3 Challenges Arising with Protocol Three

In this paper the authors key focus in using this isolation protocol was to produce a comparable technique for ADSCs isolation that would be suitable for use in clinical trials. They substituted FBS for pooled human platelet lysate

(pHPL) in half of their study to facilitate current good manufacturing practices (GMP) and move away from FBS as a media growth supplement. The variability in batch production and animal origin is highlighted as an issue for reliable and standardised protocols for *ex vivo* expansion and use of ADSCs. As such the protocol which used pHPL was assessed to replicate their prepared protocol. Pooled human platelet lysate is a costly consumable, and it is hardly surprising, therefore, that this protocol was the most expensive of the three. To order 100 mls of Heparin-free pHPL cost £351 (Sigma Aldrich, UK), which is 6.88 times more when compared with the same quantity of FBS which can be purchased from the same supplier at a cost of £51. The collagenase contact time was almost double that of the other two protocols (45-60 minutes vs. 30 minutes) and given the potential degradation to cells because of prolonged contact, this was identified as a potential issue. While the advantages of using a protocol that eliminated FBS were clear for the purposes of clinical trials, the quantity of pHPL that would be required for the duration of the study proved to be prohibitively expensive and this protocol was deemed unsuitable.

3.3.2.4 Evaluation of ADSC Isolation Using Protocol One

Recognising the need for an alternative human MSC source to those derived from bone marrow, this paper described a simple way of isolating multipotent cells from adipose tissue. This protocol was the most consistent and repeatable, with ADSCs isolated on the first attempt, proven after characterisation (Section 3.3.2.5). The range of new and amended protocols in the literature certainly raised the question regarding the ongoing suitability of this technique for isolating ADSCs and whether it had now been surpassed as our understanding of this cell population had developed. With so many more recent iterations published, it was initially expected that one of the more modern protocols, designed with clinical trials or higher cell yield in mind would prove to be more suitable. However, in this case, the original protocol described in the literature proved to be the most reliable and replicable. Therefore, the cells isolated from this protocol only, were the ones taken forward to determine if they met the criteria stated in the aims and for use in the rest of the study.

3.3.2.5 Characterising ADSCs Isolated from Protocol One

The variety of ADSC extraction protocols evaluated in this study and available in the literature demonstrate the range of techniques purported to successfully isolate ADSCs. However, without establishing that the cell population in question meets the minimum criteria for an MSC (Section 3.2.6), they cannot be reliably defined as adipose derived stem cells. It is therefore an essential step in the characterisation to establish that the cells isolated using protocol one (Table 3.1) meets these three criteria and are therefore suitable for use in this study.

3.3.2.6 Determining ADSC Plastic Adherence

Cells isolated using the chosen ADSC isolation protocol (Table 3.1) were seeded directly into a 175 cm² tissue culture flask (Greiner Bio-One GmbH) with 25 mls of ADSC media as described (Gibco, Life Technologies, UK) and were cultured overnight in a humidified CO₂ incubator ICO (Memmert GmbH, Germany) at 37°C and 5% CO₂ in air. After 24 hours, the ADSCs had adhered to the flask and were extensively washed with PBS (three times with 20 mls each time) to remove any non-adherent cells and debris. The adherent ADSCs were confirmed with a light microscope at x4 and x10 magnification (see Figure 3.2) at day seven as the cells were plastically adherent without the addition of a plate coating and cells required trypsinisation in order to facilitate passage.

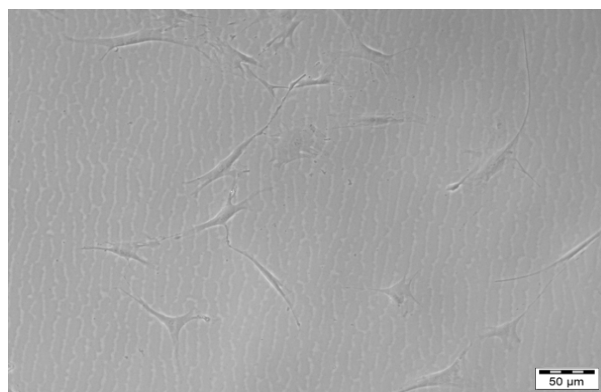


Figure 3.2: Light microscopy image taken of extracted ADSCs demonstrating plastic adherence seven days after isolation.

Cells extracted and isolated from patient adipose tissue demonstrated plastic adherence – image taken x10 magnification on a standard light microscope (Zeiss Axiovert 40C, Germany).

3.3.2.7 Determining ADSC Trilineage Differentiation

As described in Section 3.2.6, and in keeping with the minimum criteria proposed to define an MSC, multipotent differentiation potential of the isolated cell population was assessed using trilineage differentiation kits, alongside an MSC control which was used to validate the results. ADSCs and MSC controls were cultured as described in the StemPro kits (Table 2.3) to differentiate the known and proposed MSC population into three tissue types to establish trilineage potential. To determine if under the right conditions ADSCs would differentiate into adipocytes, ADSCs isolated from patients were cultured with the supplemented media as directed using the StemPro kit (Table 2.3) for four days in standard culture conditions at 37°C and 5% CO₂. Following four days of culture the cells were fixed with 4% formaldehyde and stained with Oil Red O, with the visual confirmation of red staining indicating the presence of lipids and a successful differentiation down an adipose lineage. This positive result demonstrated that the primary cells isolated using the chosen protocol (Table 3.1) were able to differentiate into adipocytes (Figure 3.3).

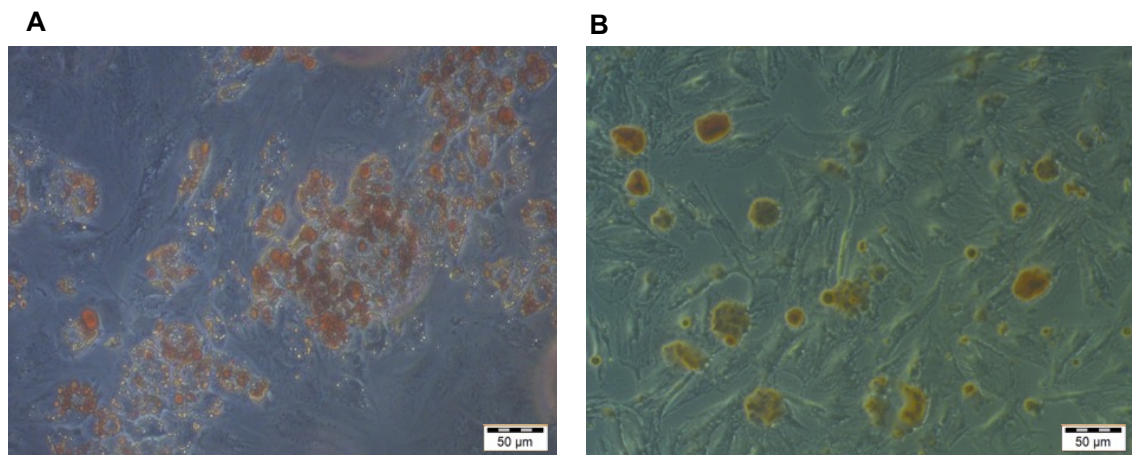


Figure 3.3: Image taken of isolated ADSCs and control MSCs differentiated into adipocytes.

Adipose tissue stained with Oil Red O to demonstrate the presence of lipids and differentiation of ADSCs into adipocytes after 4 days of culture in adipogenic media. (A) Differentiated ADSCs. (B) Differentiated MSC control. Images taken x10 magnification on a standard light microscope (Zeiss Axiovert 40C, Germany).

Similarly, primary cells isolated by the chosen protocol were simultaneously cultured with the StemPro kit described in Table 2.3 to determine if under the

appropriate culture conditions, isolated cells would differentiate into chondrocytes. After 14 days of tissue culture under standard conditions, the cells were fixed with 4% formaldehyde solution and stained with 1% Alcian Blue solution prepared with 0.1 N HCl and rinsed. The cells were visualised under the light microscope and images were captured for analysis (Figure 3.4). Blue staining indicated the synthesis of proteoglycans by chondrocytes and a positive result, demonstrating that the cell population isolated were able to differentiate into chondrocytes.

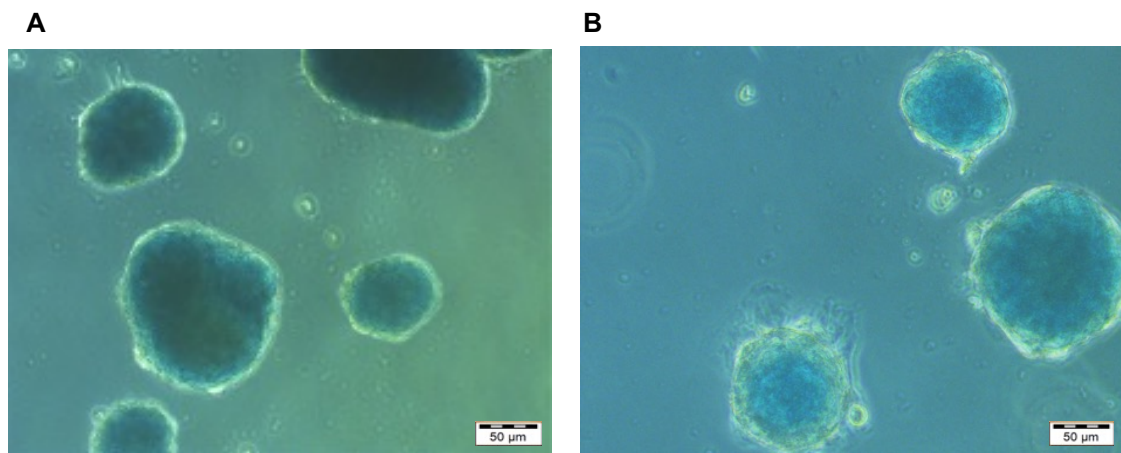


Figure 3.4: Image taken of isolated ADSCs and control MSCs differentiated into chondrocytes.

The cultured pellets were stained with Alcian Blue to demonstrate the presence of proteoglycans by chondrocytes after 14 days of culture in chondrogenic media. (A) Differentiated ADSCs. (B) MSC control image. Both images showing they are positively stained for chondrocytes. Image taken x10 magnification on a standard light microscope (Zeiss Axiovert 40C, Germany).

The longest of the three cultures was the use of the StemPro osteogenic kit (Table 2.7) to establish if after three weeks, primary cells isolated by the chosen protocol would differentiate and create calcified deposits indicating successful differentiation down the osteogenic lineage. Following the 21-day culture period under standard conditions as previously described, the cells were fixed with 4% formaldehyde solution prior to staining. Successfully differentiated ADSCs and MSCs were visualised as dark red deposits following staining with 2% Alizarin Red S solution (pH 4.2), which indicated the presence

of calcified deposition by cells of an osteogenic lineage. Cells were visualised under the light microscope and images were captured for analysis (Figure 3.5).

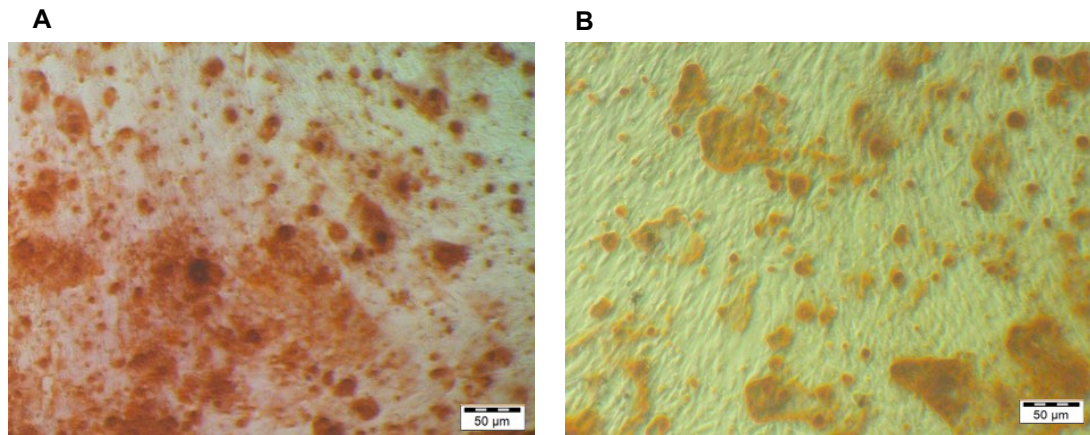


Figure 3.5: Image taken of extracted ADSCs and control MSCs differentiated into Osteocytes.

Following an extended 21-day culture in osteogenic media, areas which stained red following Alizarin Red S stain application were positive for the presence of calcific deposition by cells of an osteogenic lineage. Positive result with cultured ADSCs image A, and a positive MSC control B is demonstrated. Image taken x10 magnification on a standard light microscope (Zeiss Axiovert 40C, Germany).

The primary cell population isolated using the chosen protocol demonstrated trilineage differentiation potential alongside the control MSC under various culture conditions. In addition to being plasticly adherent under standard culture conditions, the trilineage potential demonstrated the isolated cell population had MSC potential. Further characterisation was therefore undertaken to characterise the cells using flow cytometry to determine phenotypic surface markers.

3.3.2.8 Phenotype Characterisation of the Isolated ADSC Population

Immunophenotyping of primary cells by flow cytometry, utilises the targets found on the cell surface, providing a high throughput, non-mutagenic, and reproducible method for characterisation of a primary cell population (Riordon and Boheler, 2018). To ascertain if the cell population isolated were phenotypical of ADSCs as defined in the literature (see Section 2.10) a panel of nine fluorophores to detect the presence or absence of cell surface markers (CD markers) was created. Of these markers, five were expected to be

expressed by the cells (hereafter known as the positive markers) and four were expected not to be expressed by the cells (hereafter known as the negative markers) as detailed in Table 2.2. It was essential to demonstrate that the cells were positive for the ADSC progenitor surface markers that had been described in the literature previously. Similarly it was key to ensure the absence of markers associated with other cell types such as leukocytes (CD45), endothelial cells or platelets (CD31), macrophages and granulocytes (CD11b) or lymphocytes, dendritic cells or bone marrow fibroblasts (CD106). Each antibody with its associated emission fluorescence was initially mapped out on the BioLegend Aurora Spectra Analyser (Figure 3.6) to ensure that the emissions did not significantly overlap. The planning tool was configured for the ACEA NovoCyte 3000, which is the machine that was used for the duration of the study.

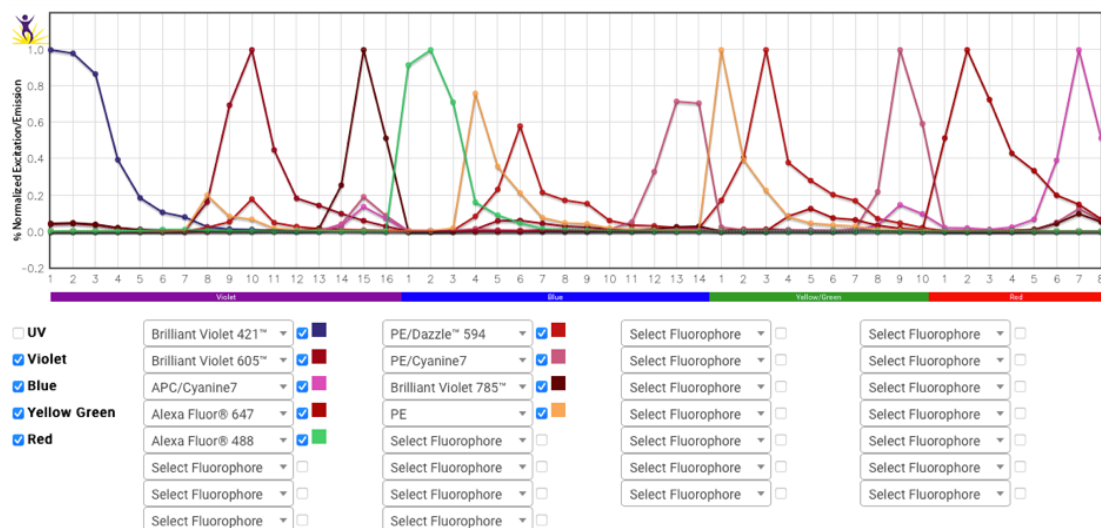


Figure 3.6: Fluorophore panel planning to determine potential fluorescent emission overlap.

Fluorophore planning tool used to determine the likely overlap in detectable emission of each fluorophore for specific ADSC CD markers when using the Novocyte flow cytometer. Minimising the overlap reduces the fluorescent spillover emissions. All antibodies were obtained from Biolegend, USA.

To ensure that the antibodies were specific for the CD markers of interest, positive and negative controls were run through the NovoCyte flow cytometer with each fluorophore in a single tube (Figure 3.7), including a positive and negative control (Table 3.4). Cells were stained and prepared as previously described in the methods (Section 2.10) prior to being analysed.

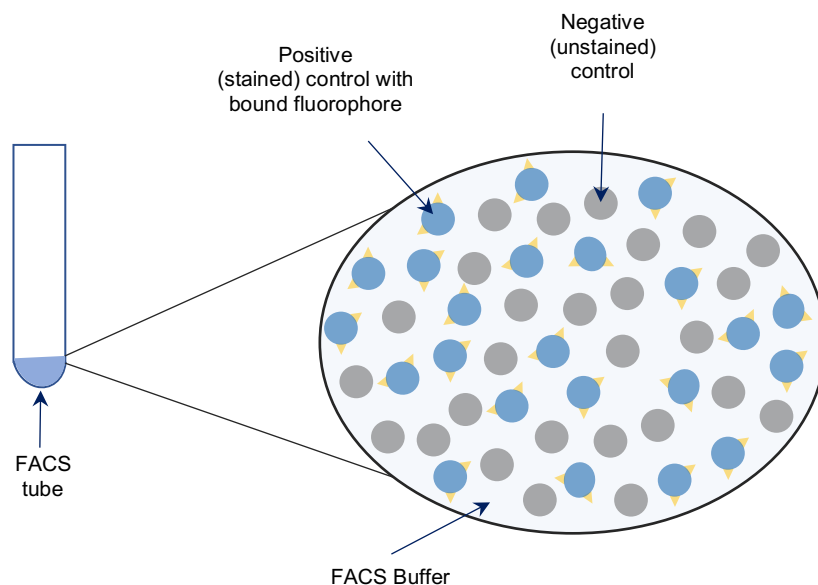
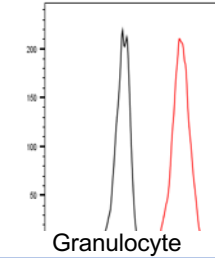
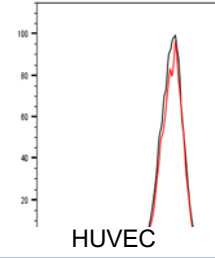
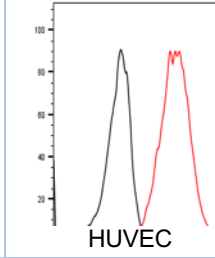
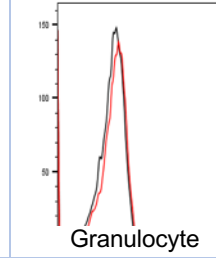
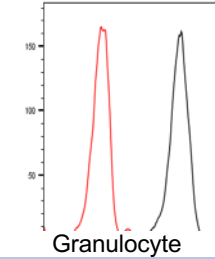
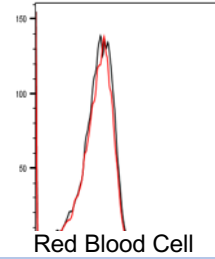
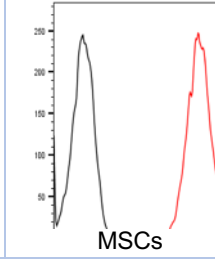
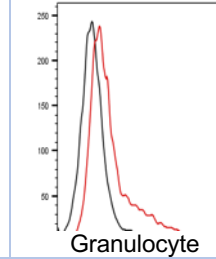
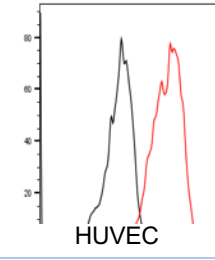
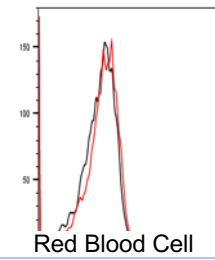
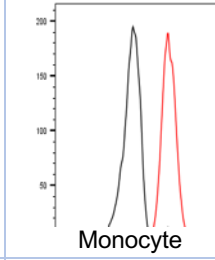
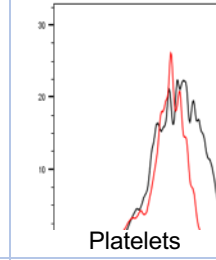
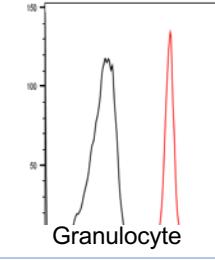
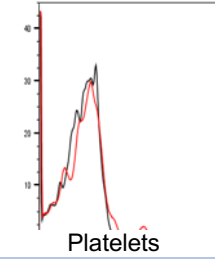
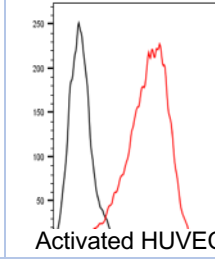
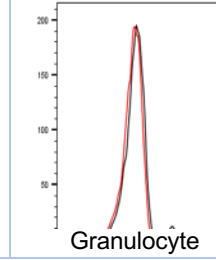
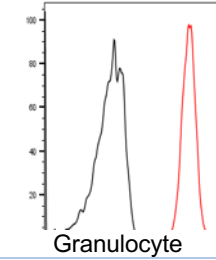
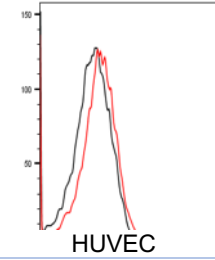


Figure 3.7: Schematic illustrating positive (stained) and negative (unstained) controls for each fluorophore to demonstrate fluorophore specificity prior to use on ADSCs.

The specificity of each fluorophore was validated by running single stained tubes with a known positive and negative control, e.g., CD45 (Brilliant Violet 785) in a tube with Granulocytes (positive control) and HUVEC cells (negative control) to establish that a positive or negative peak reflected the presence or absence of the cell surface CD marker.

Table 3.4: Positive and negative controls for each individual fluorophores demonstrating specificity of each CD cell surface marker prior to their use on the ADSC population.

Marker	Positive Control	Negative Control	Marker	Positive Control	Negative Control
CD11b			CD73		
CD13			CD90		
CD31			CD105		
CD44			CD106		
CD45					

Each fluorophore specificity was validated by running single stained tubes with a positive and negative control, for each fluorophore. The black histogram represents the 'no stain' (negative) population and the red histogram represents the stained (positive) population. The generation of these positive and negative peaks demonstrates the specificity of each of the chosen fluorophores for that CD marker and their detection on the Novocyte. The histograms were created using FlowJo version 1.3 (Oregon, USA).

The size of the CD marker panel presented some challenges with regards to fluorescence spillover emissions, as the fluorophores did not entirely adhere to the tight range of emissions detected by the instrument. In a multi-colour flow cytometry panel such as this, in addition to each channel detecting the primary fluorescence of the fluorophore in question, it will also detect the secondary fluorescence contributed to each channel by the other fluorophores (Nguyen *et al.*, 2013). To account for this overlap, single stain controls using compensation beads are run in individual tubes to determine the amount of secondary fluorescence generated and allow the creation of a compensation matrix (Byrd *et al.*, 2015). This allows the FlowJo software to be scaled ahead of time and ensure that the spillover emissions can be corrected and removed from the display to facilitate accurate interpretation of the data.

VersaComp antibody capture beads were purchased from Beckman Coulter (IN, USA) in a kit to create the compensation matrix (Figure 2.3). There are two bottles in the kit, one contains positive beads, capturing conjugates in single colour stains, and once contains negative beads, which provides a fluorescence similar to unstained cells across the different emission / excitation spectrum (Figure 2.4). Following the manufacturer's instructions, the bottles were removed from 4°C, vortexed and inverted a number of times before one drop of each positive and negative beads was added to a flow tube. At which point they were treated like cells and the protocol was followed as previously described (see Section 2.10).

For each patient, ADSCs were evaluated using flow cytometry at early (p2) and late (p8) passage to ensure they phenotypically remained MSCs and were suitable for continued use. To minimise potential issues with fluorescent overlap, three tubes were run for every patient, consisting of a no stain tube, positive CD markers tube, and negative CD markers tube (Figure 3.8-3.11). Additionally, the compensation matrix (Figure 2.4) was applied to each panel to account for fluorescent spillover emissions. As previously described, (Section 2.10) the unstained population was used to gate the cell population of interest (Figure 2.2) which was then applied to the nine fluorophore channels. The lasers in the flow cytometer illuminate the stained cell

population producing a FSC and SSC, and almost simultaneously exciting the fluorophores resulting in a fluorescence emission which is detected and processed by the Novocyte flow cytometer. The no stain cell population generates a black histogram that was used to ascertain if the subsequent stained cells were positive, i.e., expressed the CD cell surface marker; or were negative, i.e., did not express the cell surface marker. The presence of a CD marker on the ADSCs resulted in a positive emission detected in that channel and the generation of a red histogram that was distinctly separate from the no stain population (Figure 3.8 and 3.9). This enabled optical assessment of whether the cell surface marker was present which was important for characterisation, but also monitoring throughout the study. If a CD marker was not present on the ADSCs, then the fluorescent stain in the tube would remain unbound to the cell and there was no detected fluorescence in that channel. This would result in the red and black histograms overlapping each other. It was therefore possible to demonstrate that the positive and negative CD markers were present post cell isolation and maintained through tissue culture, with ADSC specific markers present at both early (p2) and late passage (p8). This confirmed that ADSCs had been successfully isolated and that they maintained their MSC phenotype at the time points of interest and were therefore suitable for use in the study.

The primary cells isolated using protocol number one (Table 3.1) (Zuk *et al.*, 2001) had therefore met the minimum criteria outlined in Section 3.2.6 in order to be classified as ADSCs (Dominici *et al.*, 2006), demonstrating plastic adherence in standard tissue culture conditions (Figure 3.2), trilineage differentiation (Figures 3.3-3.5) and expression of specific ADSC phenotypic cell surface markers which were maintained during extended tissue culture (Figures 3.8-3.11). This confirmation established that the primary cells were able to be characterised as ADSCs and could be predictably maintained in an MSC state without differentiating into adipocytes at the time points of interest in this study (p2 and p8). It was therefore possible to optimise the next part of the study and examine the impact that ADSCs taken from both healthy patients and patients with breast cancer, have on the hallmarks of ER+ breast cancer in both conditioned media and non-contact co-culture models.

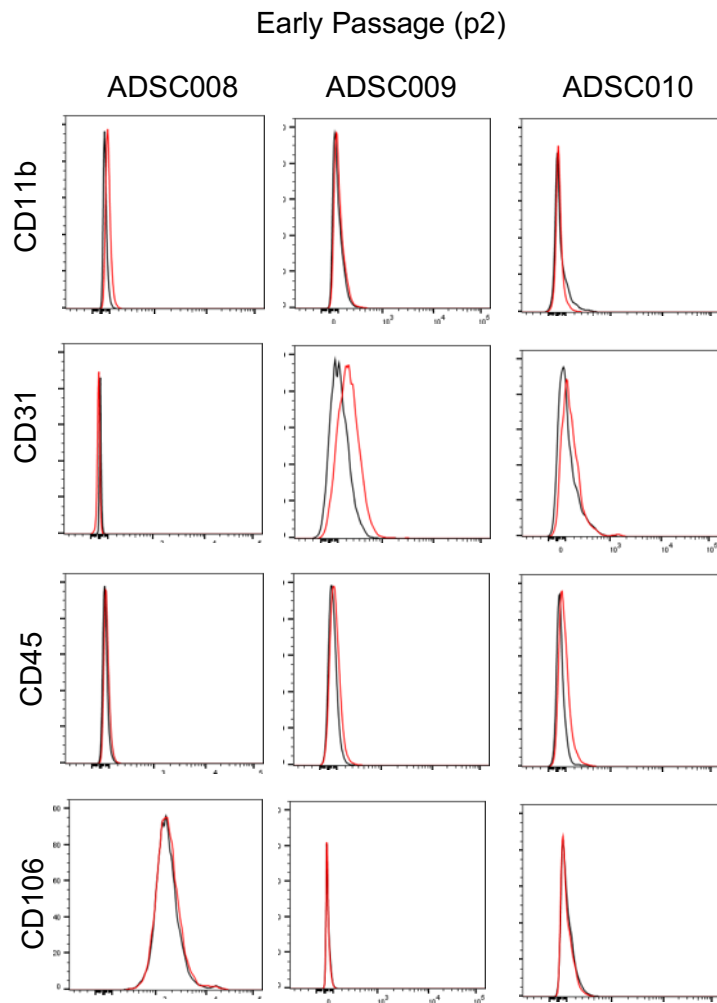


Figure 3.8: Flow cytometry for three patient cell lines at early passage (negative markers).

Flow data for patients ADSC008, 009 and 010 at early passage (p2) obtained using the ACEA NovoCyte 3000 and the graphs were produced on FlowJo (replicates n=3). The black histogram denotes the no stain population, and the red histogram denoted the cells incubated with the fluorophores that are not expected to be seen if the cell population is characteristic of ADSCs. The overlap between these two histograms demonstrated that CD 11b, 31, 45 and 106 are not present on these cells and it is therefore possible to say this cell population is negative for these markers.

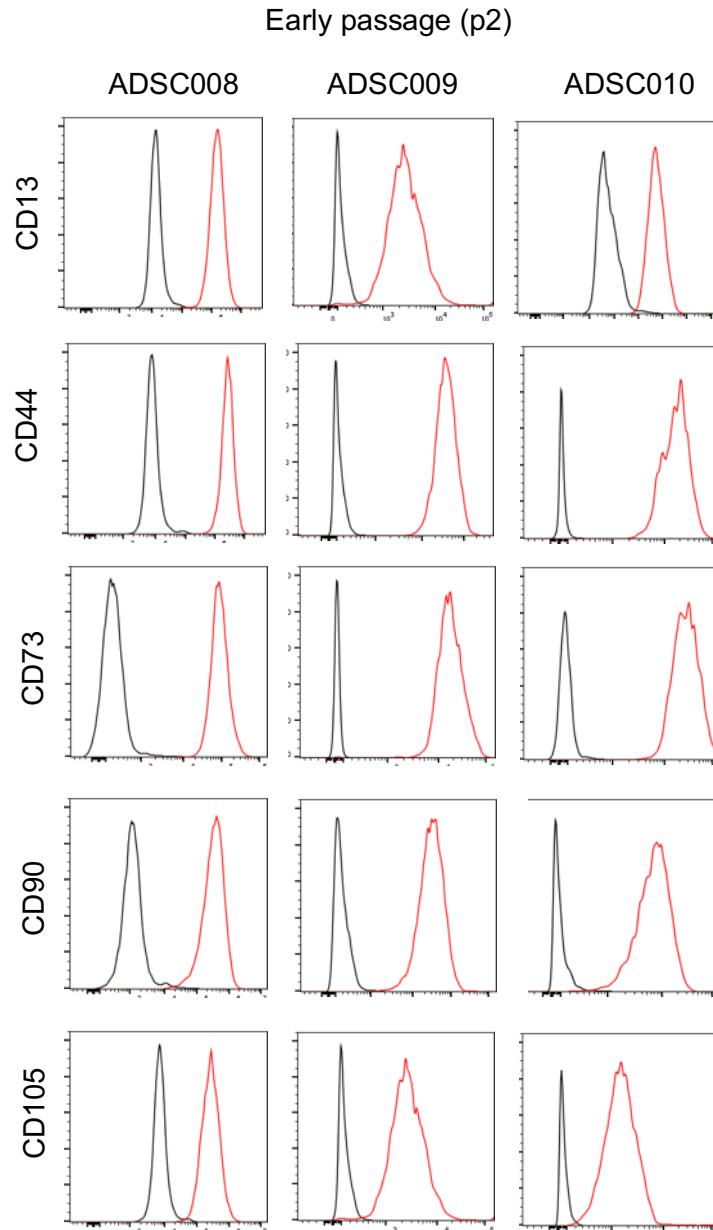


Figure 3.9: Flow cytometry for three patient cell lines at early passage (positive markers).

Flow data for patients ADSC008, 009 and 010 at early passage (p2) obtained using the ACEA NovoCyte 3000 and the graphs were produced on FlowJo (replicates n=3). The black histogram denotes the no stain population, and the red histogram denoted the cells incubated with the fluorophores that are expected to be seen if the cell population is characteristic of ADSCs. The distinct separation between these two histograms demonstrated that CD 13, 44, 73, 90 and 105 are all present on these cells and it is therefore possible to say these cell populations are positive for these markers.

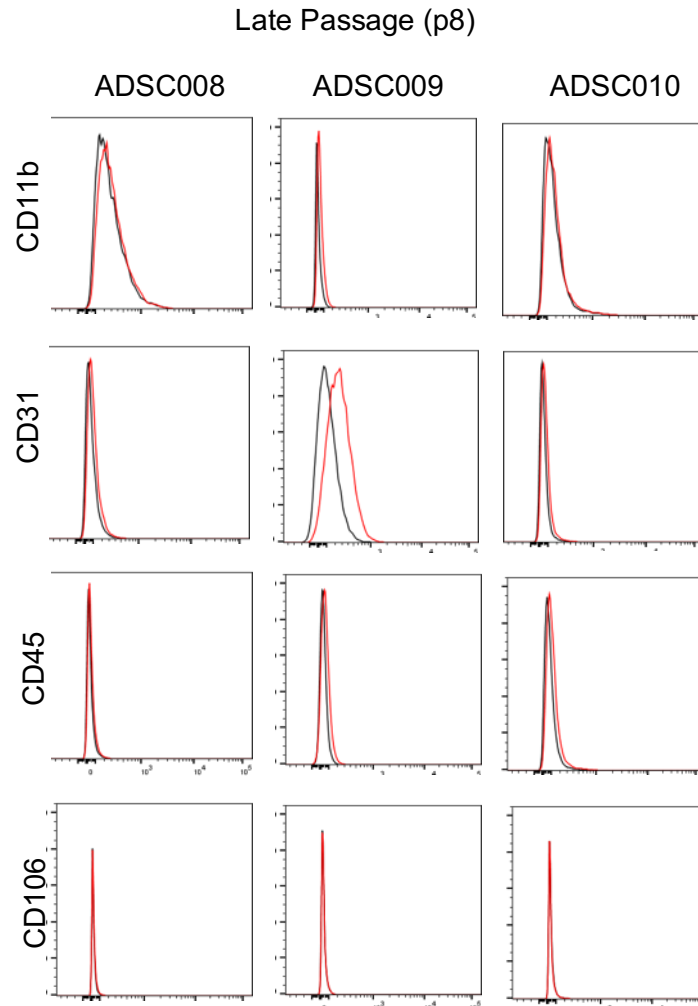


Figure 3.10: Flow cytometry for three patient cell lines at late passage (negative markers).

Flow data for patients ADSC008, 009 and 010 at late passage (p8) obtained using the ACEA NovoCyte 3000 and the graphs were produced on FlowJo (replicates n=3). As in previous figures, the black histogram denotes the no stain population, and the red histogram denoted the cells incubated with the fluorophores that are not expected to be seen if the cell population is characteristic of ADSCs. The overlap between these two histograms demonstrated that CD 11b, 31, 45 and 106 are not present on these cells and it is therefore possible to say this cell population remains negative for these markers.

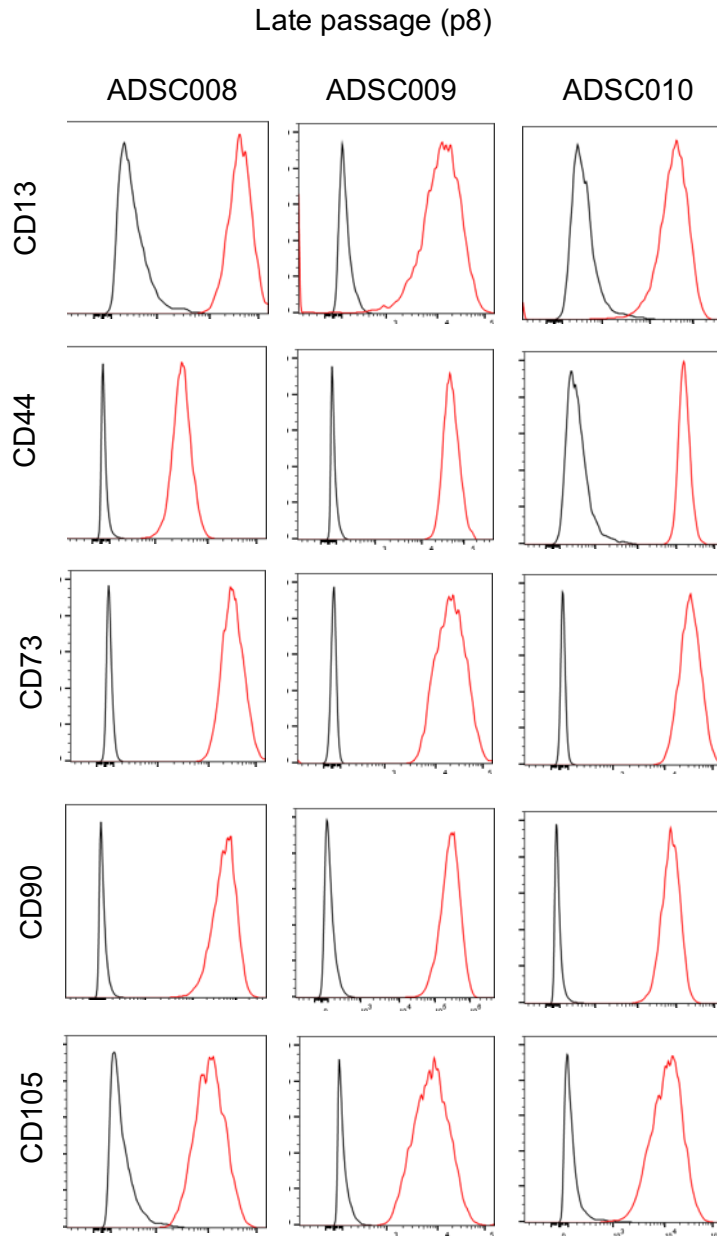


Figure 3.11: Flow cytometry for three patient cell lines at late passage (positive markers).

Flow data for patients ADSC008, 009 and 010 at late passage (p8) obtained using the ACEA NovoCyte 3000 and the graphs were produced on FlowJo (replicates n=3). The black histogram denotes the no stain population, and the red histogram denoted the cells incubated with the fluorophores that are expected to be seen if the cell population is characteristic of ADSCs. The distinct separation between these two histograms demonstrated that CD 13, 44, 73, 90 and 105 are all present on these cells and it is therefore possible to say these cell populations are positive for these markers.

3.3.3 Optimising ADSC Media Suitability for MCF-7 and T47D Cell Culture

Prior to optimising the conditioned media and co-culture experiments it was essential to ensure that the media chosen to culture the isolated ADSCs did not independently influence the behaviour of the breast cancer cell lines. The complete culture medium from the chosen ADSC isolation protocol (Table 3.1) was comprised of phenol red containing DMEM (supplemented with 2mM GlutaMAX), 10% FBS and pen/strep (Zuk *et al.*, 2001). As this was the media being used to culture the isolated ADSCs, it was therefore important to ensure it was comparable to the media used to culture the breast cancer cell lines (MCF-7 and T47D). This was principally to guarantee, in addition to successful cell culture, that any effects seen during the conditioned media (Chapter Four) and co-culture experiments (Chapter Five) were not attributable to changes in media constituents. By ensuring the ADSC, MCF-7 and T47D cells were cultured in media that was comparable, meant that any effects observed could be reliably attributed to the cells themselves. Crucially, specific components within the media needed to be scrutinised to ensure there were no unnecessary effects on cellular behaviour that could influence the data generated.

The only difference in media composition is the use of antibiotics, which were added to the media used only for ADSC culture. There is significant literature on the importance of good cell culture practice and asepsis when undertaking tissue culture. The use of antibiotics in cell line tissue culture risks masking sub-clinical infections which can have significant impact on the findings of end-point experiments (Coecke *et al.*, 2005; Nims and Price, 2017). To mitigate this, MCF-7 and T47D cell lines were grown in media free from any antibiotic/antimycotic solutions and particular attention was paid to tissue culture technique alongside regular media sterility tests and laboratory wide, mandated mycoplasma testing every two months (primary and cell line media). The cell lines and primary cells were kept in separate incubators and different tissue culture hoods within the lab. Pen/strep was only used for ADSCs as these were coming from patients and they could not be screened to the same exacting standard a cell line could when purchased from a reputable company.

All tissue culture flasks were optically assessed at x4 and x10 magnification using a light microscope at every media change for any obvious contamination.

Phenol red as a media component has been discussed in the literature since the 1980s, with studies demonstrating structural similarities between phenol red and some nonsteroidal oestrogens (Berthois, Katzenellenbogen and Katzenellenbogen, 1986). As there was the potential for this additive to influence both the MCF-7 and T47D cell lines, it was removed, and phenol red free DMEM (Gibco, Life Technologies, UK) was therefore sourced. The media was supplied without any amino acids, so 2mM GlutaMAX (Gibco, Life Technologies, UK) was added to ensure the composition was comparable to the phenol red containing media used in the original ADSC isolation protocol, and 100 U/ml penicillin, 100 µg/ml streptomycin (pen/strep) (Gibco, Life Technologies, UK) was added only to the ADSC media, as described by protocol one (Zuk *et al.*, 2001).

While there are a number of published protocols and various media compositions for culturing MCF-7 and T47D cell lines, containing a variety of supplements and additives, the European Collection of Authenticated Cell Cultures (ECACC) recommends a comparable media to that used to culture ADSCs with DMEM free of phenol red, supplemented with 10% FBS and 2mM GlutaMAX recommended for any study with an interest in the activity of the oestrogen receptors (Cooper, 2012; Abaan *et al.*, 2013). Both cell lines (MCF-7 and T47D) grew well in the ADSC media, minus the pen/strep, for the duration of the study, and this standardisation of the media, prior to commencement of the next stage meant that the same media could be used throughout. This ensured that any changes observed during the conditioned media (Chapter Four) or co-culture experiments (Chapter Five), would be independent of the base media in which the cells were cultured.

3.3.4 Optimisation to Support Conditioned Media and Co-Culture Studies

3.3.4.1 Optimisation of ADSC Conditioned Media to Study the Indirect Effect of ADSCs On the Hallmarks of Breast Cancer (MCF-7)

To determine the indirect effect of ADSCs from different patient groups (healthy and cancer) on the neoplastic traits of MCF-7 cells, the media needed to be conditioned. ADSCs at early and late passage (p2 and p8) were cultured in standard conditions until approximately 70% confluent, at which point the media was changed and left to condition for 24 hours prior to its use in the experiments (Chapter Four). Rather than apply a binary quantity of conditioned media (e.g., 0% or 100%) as seen in previous studies, the decision was made to ascertain if there was a dose dependent effect on MCF-7 invasion, migration, proliferation, protein expression or morphology, when treated with conditioned media in various concentrations. A ratio of conditioned to fresh media was created to enable any dose dependant patterns to be established. The conditioned media removed from the ADSCs after 24 hours was mixed with fresh, warmed ADSC media to create concentrations of 0% (fresh ADSC media, no conditioned media) up to 100% (0% fresh media, 100% conditioned media) (Table 2.4).

3.3.4.2 Optimisation of MCF-7 and T47D Seeding Densities for The Proliferation Assay

Prior to the commencement of conditioned media (Chapter Four) and co-culture experiments (Chapter Five), optimum seeding density for proliferation was determined. MCF-7 and T47D cells were seeded into EL-8 plates as previously described in methods (Section 2.14.1) at varying densities ranging from 2.5×10^4 to 1×10^6 before being placed into the RTCA iCELLigence instrument (ACEA Bioscience, UK now part of Agilent, UK). The instrument was set up to take a reading every minute for the first two hours, then every hour for 48 hours and the experiment was repeated in triplicate. Data was analysed using the RTCA Data Analysis Software 1.0 (ACEA Bioscience, UK) to determine proliferation over 48 hours and the maximum cell index. From this analysis, it was determined that MCF-7 cells were optimally seeded at a density of 5×10^5 per ml and T47D cells were optimally seeded at a density of

7×10^5 per ml (Figure 3.12), as cells at these densities remained in the log phase of growth with comparable cell index values. Cell Index (CI) is derived as a relative change in measured electrical impedance to represent cell status and is marginally a monotonical function of cell number. A change in cell status, such as cell morphology, cell adhesion or cell viability, will lead to a change in CI and it is therefore an important additional measurement that was calculated alongside proliferation.

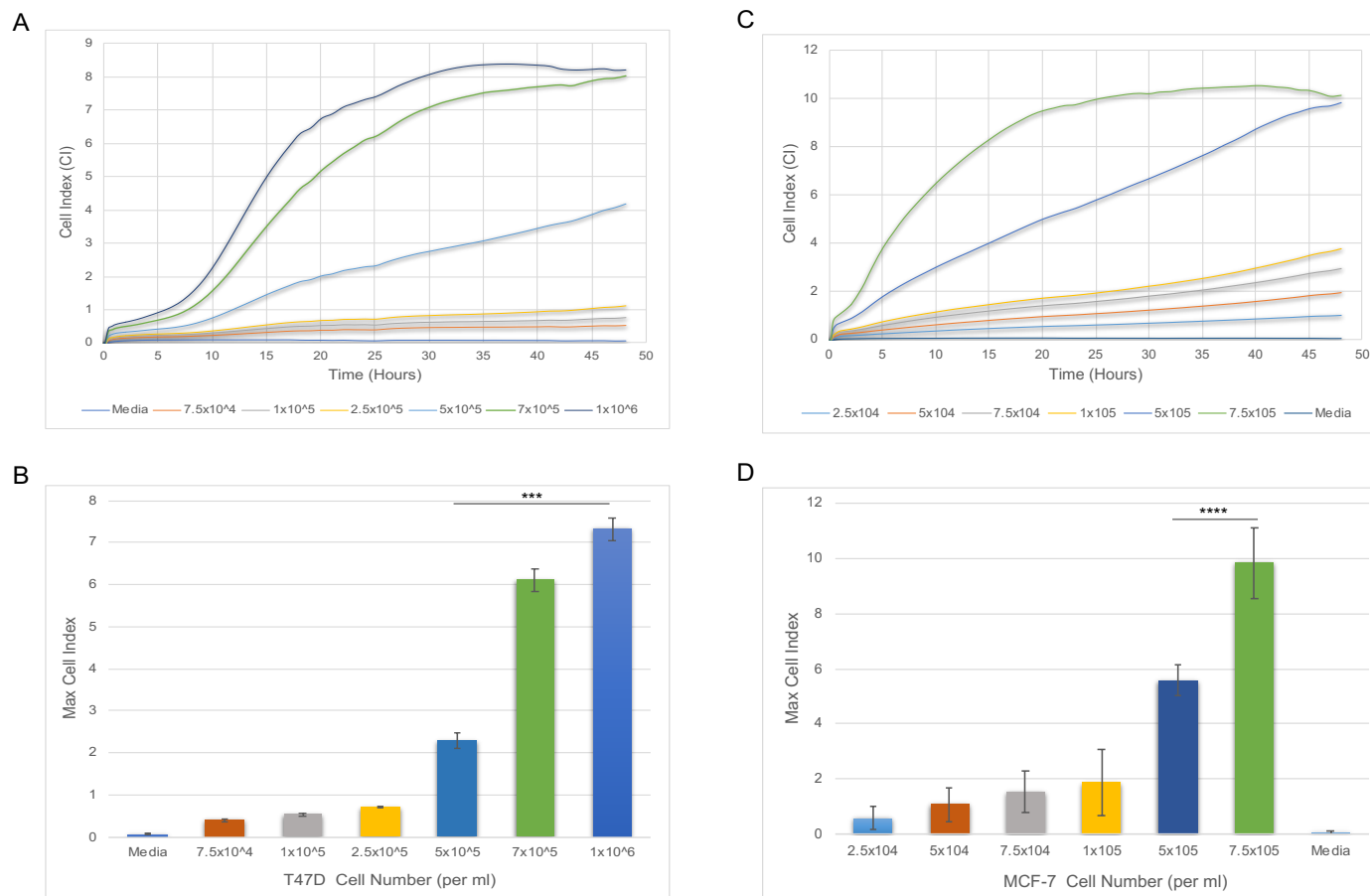


Figure 3.12: MCF-7 & T47D seeding density optimisation for measuring cellular proliferation using the iCELLigence.

A. & C. Average proliferation of three EL-8 plates seeded at different densities with MCF-7 (C) and T47D (A) cells as part of assay optimisation. The RTCA iCELLigence analyser measuring proliferation, cell adhesion, and maximum cell index over 48 hours. (C) A seeding density of 5x10⁵ cells per ml was chosen for MCF-7. (A) A seeding density of 7x10⁵ was chosen for T47D cells. (B and D) Maximum Cell Index (CI) at 24 hours for MCF-7 cells (D) and T47D cells (B). This can be used as a monotonical function of cell number, demonstrating at higher seeding density, more cells adhere to the bottom of the well. Data is from three replicates and one-way ANOVA was used to compare maximum cell index across the varying seeing densities. Significant values were taken as ** p ≤ 0.01, *** p ≤ 0.001, **** p ≤ 0.0001

3.3.4.3 Optimising MCF-7 and T47D Seeding Density to Measure the Changes in Migration

Prior to evaluating the impact of conditioned media (Chapter Four) and non-contact co-culture (Chapter Five) on the migration of MCF-7 and T47D (co-culture only), seeding densities were optimised to ensure a standardised assay enabling reliable comparison between the control and treated wells. To evaluate this, varying densities of MCF-7 and T47D cells ranging from 2×10^5 to 7×10^5 were seeded around each section of the cell culture insert (IBIDI, Germany) as described previously in the methods (Section 2.14.3). Cells were seeded around the insert for 24 hours at 37°C , 5% CO_2 to allow the cells to adhere to the surface of the plate before the inserts were removed using sterile tweezers and the gap analysed at x4 and x10 magnification on a standard light microscope (Zeiss Axiovert 40C, Germany) with a Canon camera. The wells were examined for a clear barrier following the removal of the insert without excessive gaps and the experiments were repeated in triplicate (Figures 3.13 and 3.14).

As demonstrated in Figure 3.15, Image A and B demonstrate a sparsity of MCF-7 cells and an inconsistency in the gap created making them unpredictable and unsuitable for use. Image C demonstrates that at this density, there is a clearly defined gap with a straight edge all the way down, comparable with images D and E. Therefore, for migration experiments involving MCF-7 cells, a seeding density of 4×10^5 cells / ml was used as this provided an adequate cell density to create a predictable gap. Examining the T47D cell gap in Figure 3.16, images A-D demonstrate sparsity of cells and an inconsistency in the gap created at these seeding densities. Image E demonstrates that at this density, there is a clearly defined gap, with a straight edge all the way down and as such, for migration experiments involving T47D a cell density of 7×10^5 cells / ml was used to create the initial 500-micron gap.

MCF-7

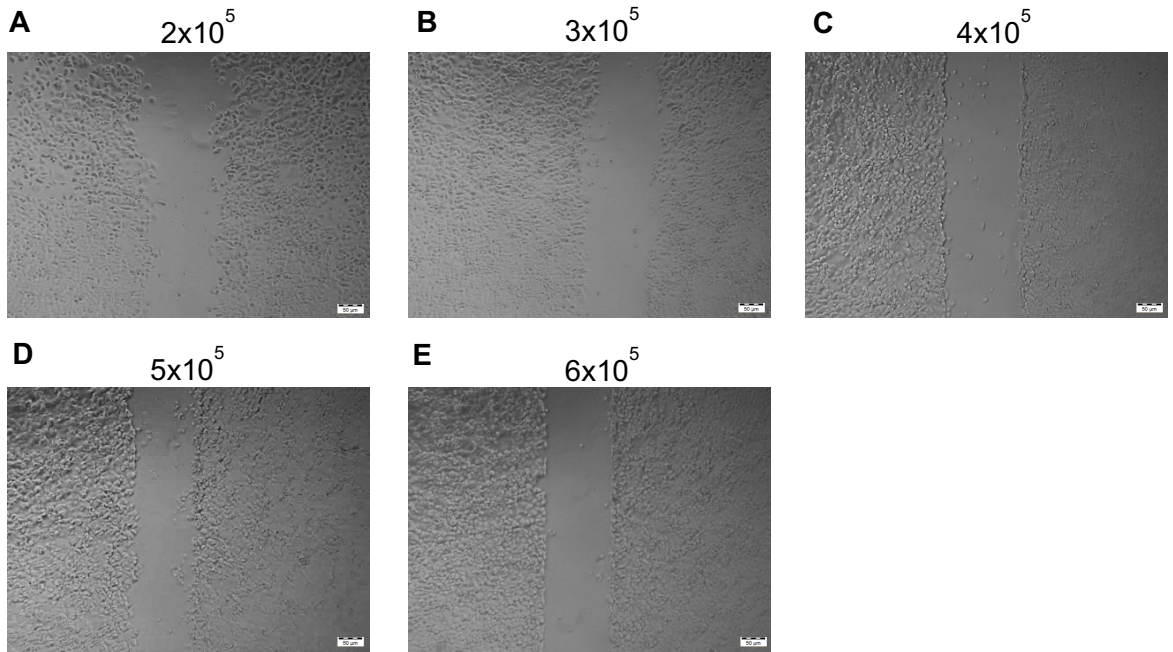


Figure 3.13: Various seeding densities for optimising the assessment of MCF-7 migration for conditioned media and co-culture experiments using an IBIDI insert.

MCF-7 cells seeded at various densities (noted above each image) representing cells/ml (A) 2×10^5 (B) 3×10^5 (C) 4×10^5 (D) 5×10^5 (E) 6×10^5 . Each of the images demonstrates the gap created with a different seeding density after 24 hours. Cells were incubated with the insert for 24 hours before they were removed with sterile tweezers and imaged, at which point the quality of the gap and seeding density was assessed. Images taken at x4 magnification with a standard light microscope and a Canon camera of the 500-micron gap created by the insert and the experiment was repeated in triplicate. The aim was the creation of a well-defined gap that would enable a standardised measurement of gap closure and migration over 48 hours.

T47D

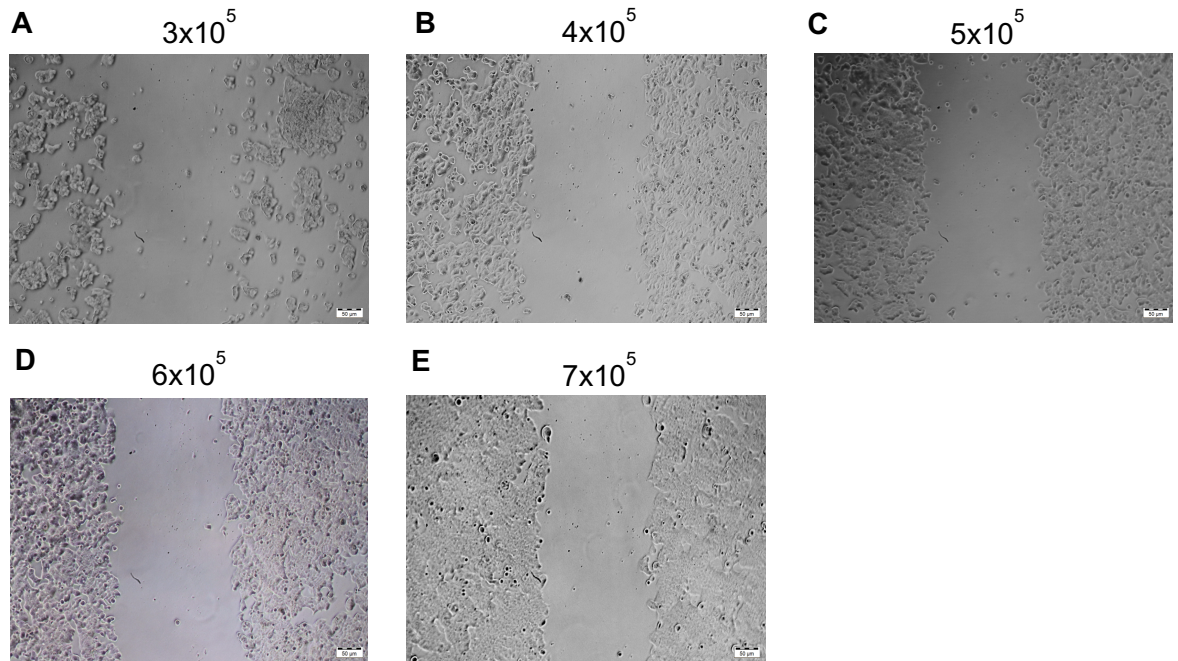


Figure 3.14: Various seeding densities for optimising the assessment of T47D migration for co-culture experiments using an IBIDI insert.

T47D cells seeded at various densities (noted above each image) representing cells/ml (A) 3×10^5 (B) 4×10^5 (C) 5×10^5 (D) 6×10^5 (E) 7×10^5 . Each of the images demonstrates the gap created with a different seeding density after 24 hours. Cells were incubated with the insert for 24 hours at standard culture conditions before they were removed with sterile tweezers and photographed. Images taken at x4 magnification with a standard light microscope and a Canon camera of the 500-micron gap created by the insert. The experiment was repeated in triplicate and the gap created was assessed for clarity and seeding density.

3.3.4.4 Optimising the Measurement of Invasion

Prior to the commencement of conditioned media (Chapter Four) and co-culture experiments (Chapter Five), the 24 well Collagen Invasion Assay (Merck Millipore, Germany) was optimised to determine the incubation time required for the MCF-7 and T47D cells to invade through the collagen membrane. As previously described in the methods (Section 2.14.5) cells were serum starved for 24 hours prior to being used in the experiment. To ascertain the length of time needed to assess MCF-7 and T47D invasion in response to conditioned media or co-culture with ADSCs, the bottom of the well beneath the inserts was covered with complete media. The cells were then incubated in the invasion insert for either 24 or 48 hours allowing the cell lines to invade

before being assessed. Following these two time points, the non-invading cells were removed as previously described and remaining cells were stained and imaged using the benchtop light microscope at x4 and x10 magnification (Figures 3.15 and 3.16). The stain was extracted and quantified for both cell lines (MCF-7 and T47D) using the microplate reader (POLARstar Omega, BMG Labtech, Germany) at 560nm. There was no significant difference in absorbance or invasion between the 24 and 48 hour incubation periods and therefore 24 hours was chosen for the study (Figure 3.17). The experiment was repeated in triplicate.

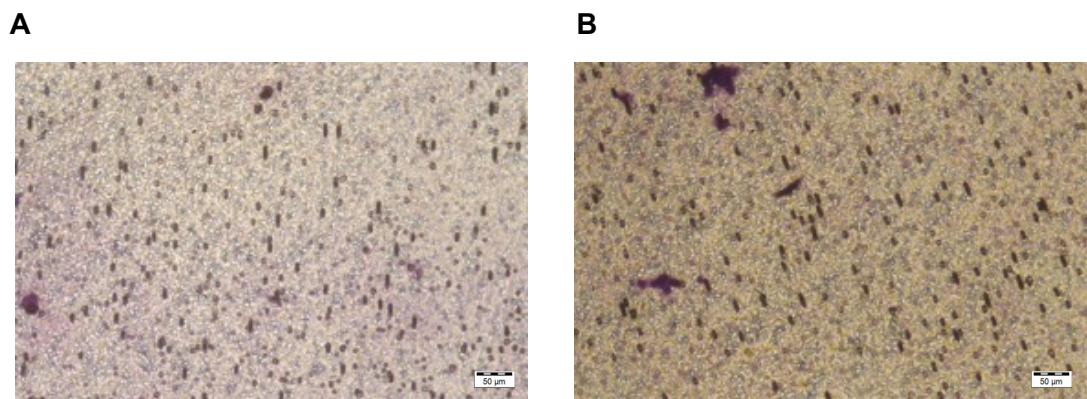


Figure 3.15: Stained MCF-7 Invasion inserts at 24 and 48 hours incubation. (A) MCF-7 cells at 24 hours and (B) MCF-7 48 hours of incubation. Images taken at x10 magnification with a standard light microscope and a Canon Camera of the inserts after staining. Experiment repeated in triplicate. There is no significant optical difference in invasion when comparing the durations, subsequently, the stain is extracted as previously described in Section 2.14.5 and read on the plate reader at 560nm to quantify invasion.

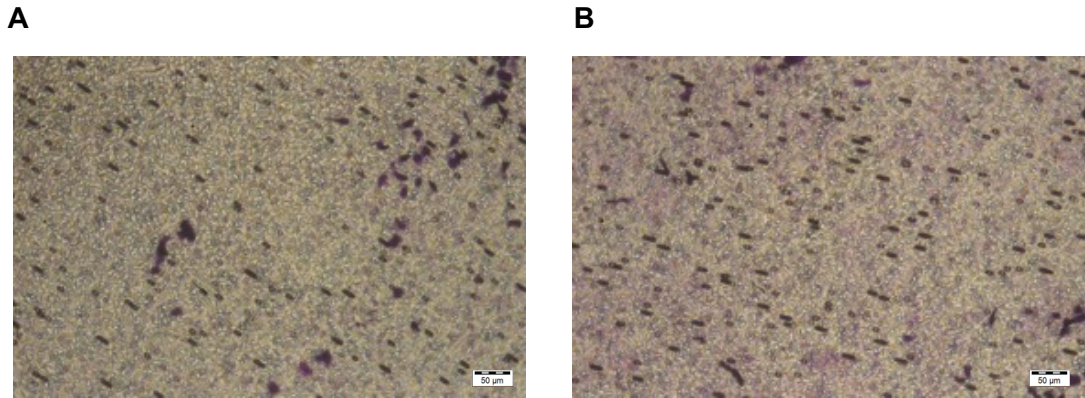


Figure 3.16: Stained T47D Invasion inserts at 24 and 48 hours incubation. (A) T47D cells at 24 hours and (B) T47D cells at 48 hours incubation. Images taken at x10 magnification with a standard light microscope and a Canon Camera of the inserts after staining. There is no significant optical difference in invasion when comparing the durations, subsequently, the stain is extracted as previously described in Section 2.14.5 and read on the plate reader at 560 nm to quantify invasion.

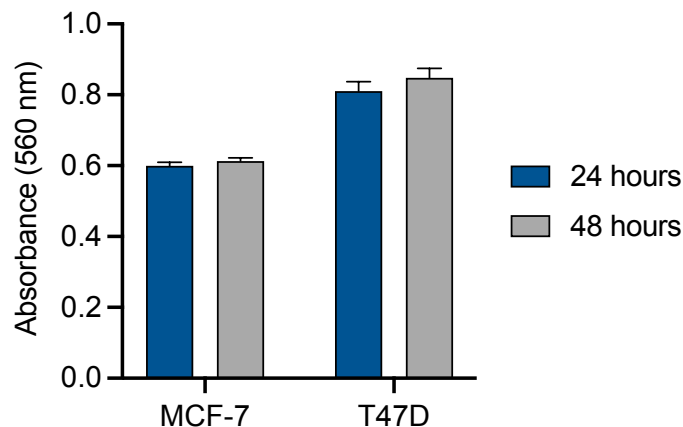


Figure 3.17: Extracted stain from invasion inserts following 24 and 48 hours incubation.

Invasion observed as measured by quantifying stain extraction from the collagen membrane following either 24 or 48 hours incubated at 37°C, 5% CO₂. Unbound stain is removed before the bound stain is extracted and read in a 96 well plate on the plate reader at 560nm. Analysis was performed in GraphPad (Prism 9) with data from three replicates and a paired t-test was used to compare absorbance at 560 nm at 24 and 48 hours. There is no statistically significant difference in invasion, for either MCF-7 or T47D between the two time points, and 24 hours was therefore selected as the timepoint for the study.

3.3.4.5 Identification of the Most Relevant Cytokines Using a Panel

Prior to determining which ELISAs would be used, a cytokine antibody array (R&D Systems, Bio-Techne, Minneapolis, USA) was purchased and trialled with media from two patient cell lines (one healthy and one cancer), to determine which proteins that were excreted into the ADSC media, were detectable and may influence the MCF-7 cell line. ADSC009 (cancer patient) and ADSC011 (healthy patient) were cultured in standard conditions in a T175 flask at 37°C, 5% CO₂ for a minimum of seven days and were not allowed to become more than 70% confluent. Media was left to condition for 24 hours following a media change, after which 5 ml of media was removed, prior to protein analysis at early passage (p2). As previously described in the methods (Section 2.15), after the membrane was prepared and ready, the second plastic sheet was applied to the top of the membrane and was imaged using the ChemiDoc (Bio-Rad, UK). ImageJ software was used to measure the intensity of each spot, followed by subtracting the background and normalising to the positive controls (Figure 3.18). The template supplied with the human cytokine array panel subsequently enabled the various proteins to be identified (Figure 3.19).

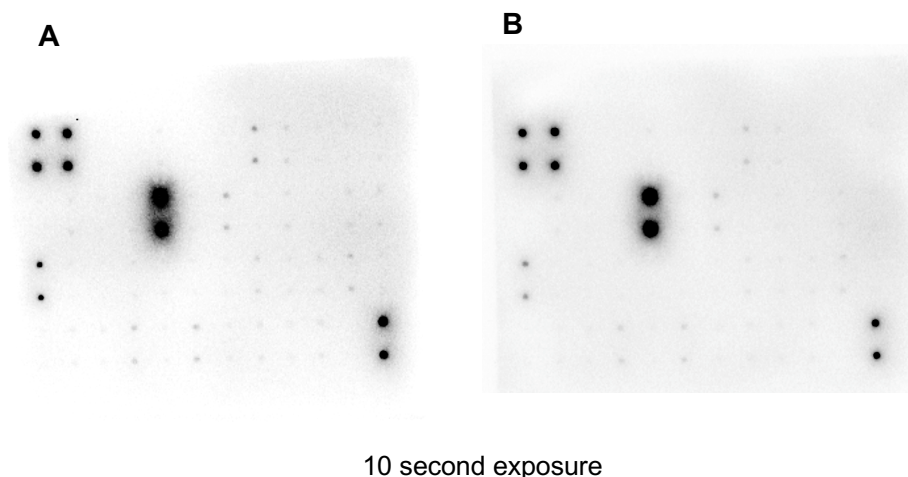


Figure 3.18: The Human Cytokine Array panel detecting multiple cytokines in ADSC media supernatants.

For each patient, 1000 µL of cell culture supernatant taken from ADSC009 (A) and ADSC011 (B) and was run on each array, data shown above from multiple exposures and represent media taken from two cell lines after 24 hours of incubation. ImageJ software was used to measure the intensity of each spot, following by subtracting the background and normalising to the positive controls.

	A	B	C	D	E	F	G	H	I	J	K	L
1	Pos	Pos	Neg	Neg	ENA-78	GCSF	GM-CSF	GRO	GRO- α	I-309	IL-1 α	IL-1 β
2	Pos	Pos	Neg	Neg	ENA-78	GCSF	GM-CSF	GRO	GRO- α	I-309	IL-1 α	IL-1 β
3	IL-2	IL-3	IL-4	IL-5	IL-6	IL-7	IL-8	IL-10	IL-12	IL-13	IL-15	IFN- γ
4	IL-2	IL-3	IL-4	IL-5	IL-6	IL-7	IL-8	IL-10	IL-12	IL-13	IL-15	IFN- γ
5	MCP-1	MCP-2	MCP-3	MCSF	MDC	MIG	MIP-1 δ	RANTES	SCF	SDF-1	TARC	TGF- β 1
6	MCP-1	MCP-2	MCP-3	MCSF	MDC	MIG	MIP-1 δ	RANTES	SCF	SDF-1	TARC	TGF- β 1
7	TNF- α	TNF- β	EGF	EGF-I	Angiotensin	Oncostatin M	Thrombopoietin	VEG-F	PDGF BB	Leptin	Neg	Pos
8	TNF- α	TNF- β	EGF	EGF-I	Angiotensin	Oncostatin M	Thrombopoietin	VEG-F	PDGF BB	Leptin	Neg	Pos

Figure 3.19: The Human Cytokine Array panel template.

The template map supplied with the human cytokine array panel to facilitate identification of proteins of interest by testing 42 proteins simultaneously. These plate maps correlate with the ChemiDoc image (Figure 3.19).

As demonstrated in Figure 3.20, there were numerous cytokines detected in the ADSC media. While high concentrations of the clinically specific proteins, IL-6 and MCP-1 made them ideal choices, it was important to select a third that further represented the spectrum of hallmark measures. IL-6 has been widely identified as an inducer of EMT (Section 1.4.6) and MCP-1 has been linked to increased rates of lymphovascular invasion and metastasis (Section 1.5.2). Unlike TARC and GRO, VEG-F could be used to interrogate neoangiogenesis which is an essential feature of tumour growth and progression and clinically relevant in breast cancer (Section 1.4.5). Importantly there were comparable quantities of VEG-F produced by ADSCs isolated from women with and without breast cancer. Individual ELISA kits were then purchased from R&D for each protein of interest (IL-6, VEG-F and MCP-1) and used as outlines in the methods (Section 2.15.1) to evaluate protein expression at two time points (4 hours and 24 hours) after either the application of conditioned media on MCF-7 cells or the commencement of non-contact co-culture. At 4 and 24 hours the early conditioned media and co-culture effect could be evaluated before significant protein degradation occurred.

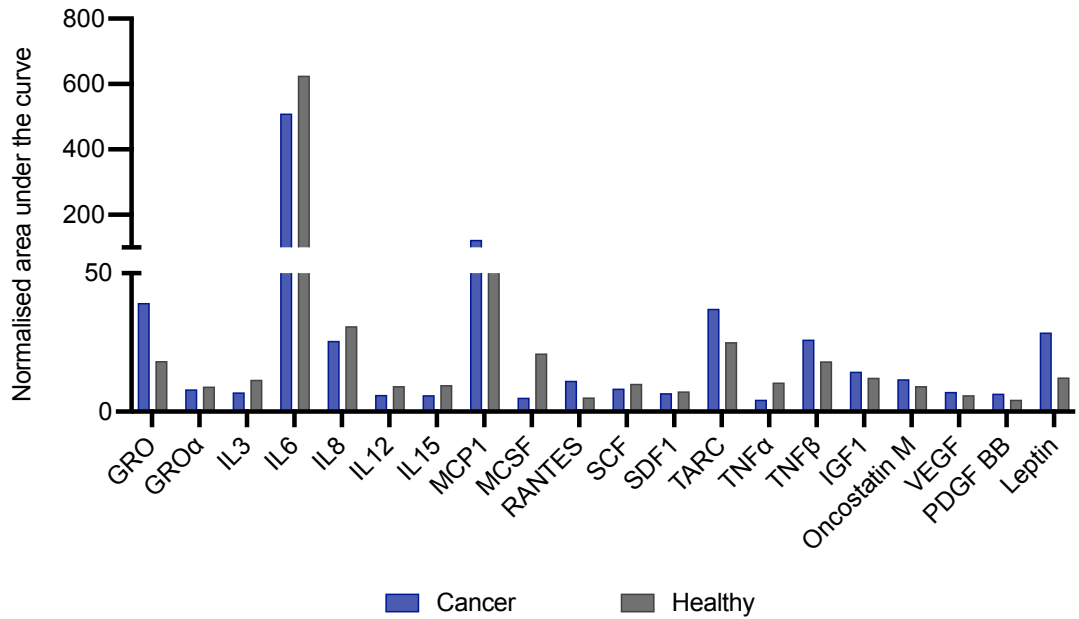


Figure 3.20: Quantified protein expression using ImageJ to evaluate spot intensity.

For each patient, pixel density was averaged between the duplicate spots which represented each protein. The background average was subtracted, and signal comparisons were made to determine relative change in protein levels in between each sample, normalised to the positive controls. The kit allowed for a single panel of 42 cytokines to be run for each patient, as such, no statistical tests could be performed on this data.

3.3.4.6 Optimising the INCELL Analyser 2000 to Capture MCF-7 DAPI and Brightfield Images for Analysis

A protocol for the INCELL analyser 2000 (GE Healthcare, Boston, USA) was obtained from the manufacturer as described in the methods (Section 2.14.7). The lack of standardised set up meant that the image capture settings on the machine needed to be optimised along with the Cell Profiler pipeline to effectively handle the images that were captured. Hoechst was used to stain the cells, which were imaged by the INCELL analyser 2000. After trialling a number of settings, including number of photos per well, offset and image settings using the machine, the following parameters were standardised for each of the 2D photographs:

- Objective; Nikon 20X/0.45,
- Plan Fluor
- ELW

- Corr Collar 0-2.0
- CFI/60
- 0.030 DAPI Exposure
- 2.00 AF offset

This final configuration for each plate was used to standardise the images captured using the INCELL analyser 2000 were processed using the open source CellProfiler™ image analysis software version 3.1.5 (USA). Plates containing MCF-7 cells treated with either conditioned media or in non-contact co-culture for 24 hours had a number of images taken from the central portion of each well. Three hundred individual images were taken, and these were sequentially loaded into the software, creating a pipeline to successfully measure cell area, eccentricity, perimeter, and solidity which was then analysed in Microsoft Excel.

3.3.4.7 Optimisation of Seahorse XF Assay for the Measurement of MCF-7 and T47D OCR and ECAR

Realtime glycolytic activity is measured by the Seahorse XF machine as the rate of extracellular acidification (ECAR), which is proportional to the rate of glycolysis, while mitochondrial respiration is determined by quantifying the rate at which the cells consume oxygen (OCR). This simultaneous measurement of metabolic parameters is an advantageous feature of this real-time assay. Prior to FCCP optimisation, the ideal seeding density was first established, so an artificially high concentration of FCCP was used at 2.0mM to enable optimal MCF-7 and T47D seeding to be evaluated. For both cell lines, a seeding density of 2×10^4 was selected after running the assay, as there were no negative values and the OCR starting point for both cell lines were within the normal range (approximately 150pmol/min) as shown in Figure 3.21. The other seeding densities had a much higher starting point which was not ideal for this assay and had the potential to skew the results.

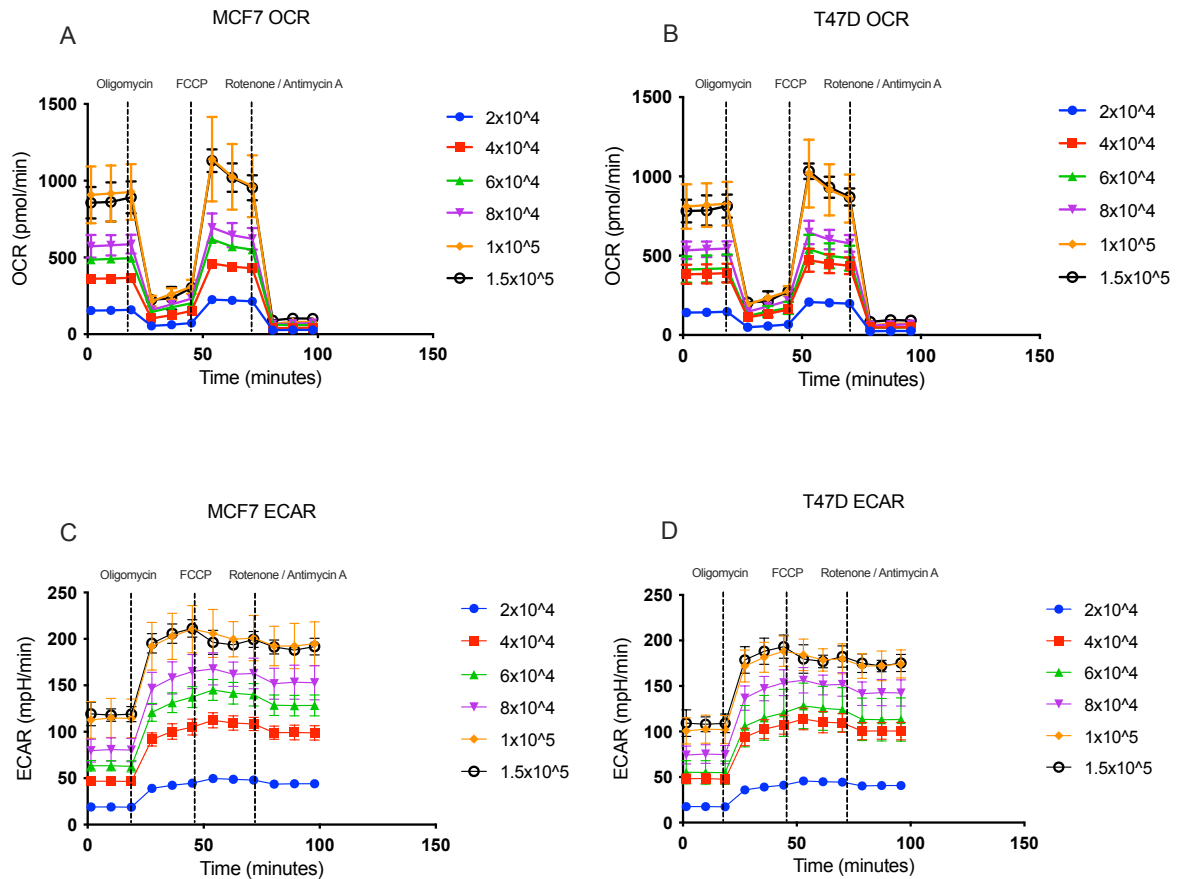


Figure 3.21: Bioenergetic profiles of MCF-7 and T47D cells at various seeding densities.

Combined metabolic profiles of the (A and C) MCF-7 and (B and D) T47D cell lines with timed injections of Oligomycin (2 mM), FCCP (2 mM) and Rotenone / Antimycin-A (2 mM) showing both (A and B) the oxygen consumption rate (OCR) and (C and D) the extracellular acidification rate (ECAR). Data shown is from three separate experiments and data is expressed as the mean \pm SEM.

Once the MCF-7 and T47D seeding densities were determined, FCCP concentration could be established by repeating the assay with a range of concentrations (0.5, 1.0, 1.5, 2.0, 2.5, 3.0 mM) to determine a reliable and repeatable measure of maximum respiration rate (Figure 3.22).

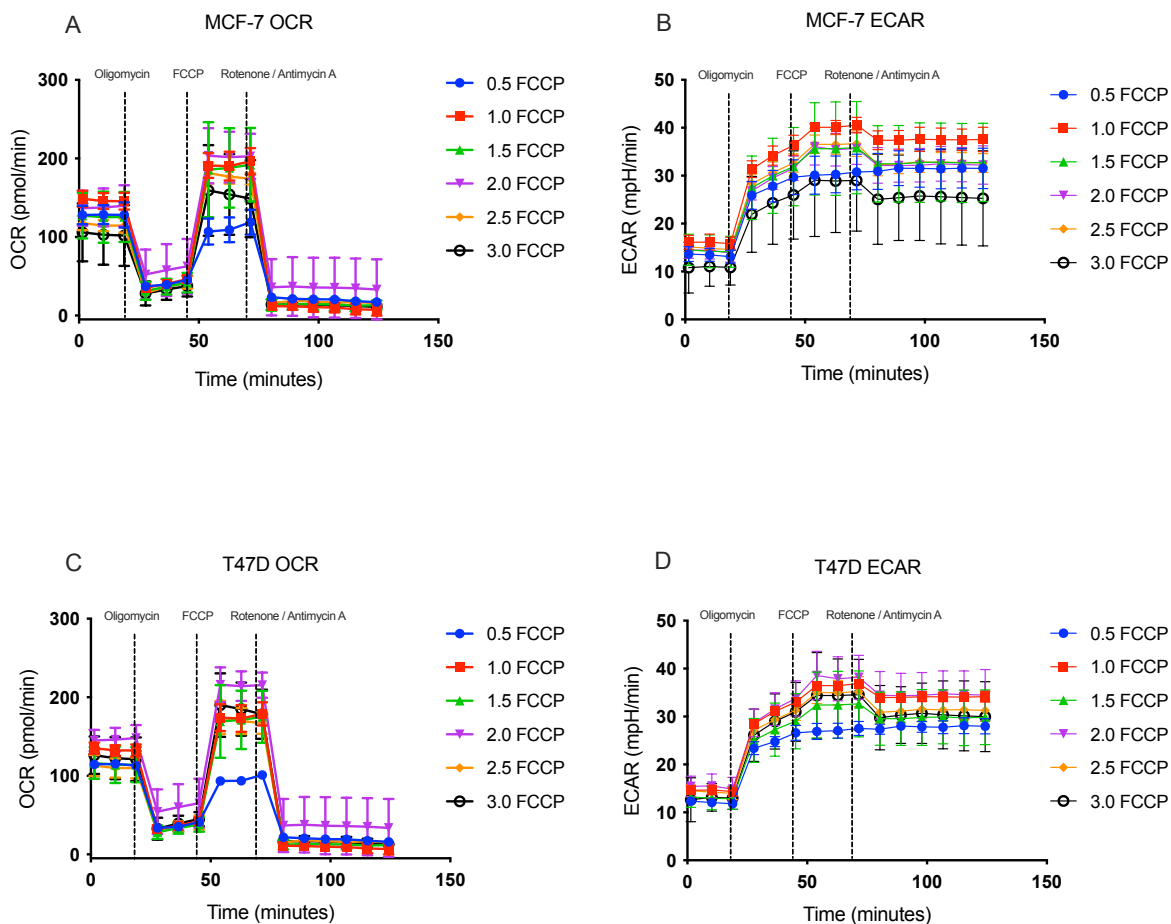


Figure 3.22: Bioenergetic profiles of MCF-7 and T47D cells at various FCCP concentrations.

Combined metabolic profiles of the (A and B) MCF-7 and (C and D) T47D cell lines with timed injections of Oligomycin (2 mM), FCCP (varying mM concentrations) and Rotenone / Antimycin-A (2 mM) showing both the (A and C) oxygen consumption rate (OCR) and the (B and D) extracellular acidification rate (ECR). Data shown is from three separate experiments and data is expressed as the mean \pm SEM.

The data for each of the concentrations was evaluated in GraphPad Prism version 9.1.0 (216) after exporting the WAVE file from the Seahorse XFe24 machine (Seahorse Bioscience, Copenhagen, Denmark). An FCCP concentration of 1.5 mM was chosen as although optically comparable to a concentration of 1.0, on a number of replicates for both cell lines, negative values were noted at the end of the assay and as this was a key issue previously, a higher concentration was chosen to ensure that issue could be predictably avoided. Following optimisation of seeding density and FCCP concentration the assay could be run and using the results, the respiratory and

metabolic parameters could be calculated using the data generated by the Seahorse XFe analyser.

3.3.4.8 Optimisation of Assays for the Assessment of MCF-7 and T47D in Non-Contact Co-Culture

Each of the assays to evaluate the hallmarks of cancer being studied were initially optimised to evaluate the indirect effect (conditioned media) of ADSCs on the hallmark traits of the MCF-7 cell line. As described in the methods (Section 2.13), a transwell, non-contact, co-culture system was chosen to examine the effect of ADSCs from two patient populations (healthy and cancer) on the neoplastic traits of MCF-7 and T47D. To replicate the assays completed with the conditioned media, the ADSCs and ER+ cell lines needed to be kept separate, so that the MCF-7 and T47D cells could be evaluated. There are numerous studies in the literature describing the use of non-contact co-culture with ADSCs, utilising 0.4µm transwell co-culture inserts (Wei *et al.*, 2010; Hanson, Kim and Hematti, 2013; Strassburg *et al.*, 2016; Preisner *et al.*, 2018a). Ensuring free movement of soluble proteins while preventing migration and cell contact, 6 and 24 well (Corning™, USA) and EL-16 inserts (ACEA and Bioscience, UK) were used to allow the effect of co-locating ADSCs on the MCF-7 and T47D cells to be observed.

As previously described in Section 3.3.2.1 literature describing ADSC culture outlines the need to maintain confluence at below 80% to prevent differentiation and loss of the mesenchymal potential of the cell (Zuk *et al.*, 2002; Banie *et al.*, 2008; Palumbo *et al.*, 2015). To simplify co-culture optimisation across the different assays and plate sizes, ADSCs were optimised to a 6-well insert. Once the ideal seeding density was identified, it could then be scaled for the different well and insert sizes by seeding ADSCs per cm² based on the optimised 6-well plate. This ensured that the assays could be easily compared to one another, as ADSCs were standardised across each of the experiments. A range of seeding densities in the literature have been described with a number of studies utilising seeding per cm², per plate or per ml (Razavi *et al.*, 2013; Lee, Park and Roh, 2015; Wang *et al.*, 2018; Wu *et al.*, 2019). The optimal seeding density needed to ensure that sufficient

ADSCs were seeded for an effective experiment, whilst ensuring no more than a 70% confluence after 72 hours of standard tissue culture as this was the maximum duration of any of the assays. After each of the 6 well transwell inserts were seeded (range 0.5×10^4 – 1×10^5), they were placed in a new well on the corresponding companion plate which contained 2 mls of warmed fresh ADSC media. The plates were then incubated for 72 hours before the supernatant was removed, along with the membranes which were stained and mounted on glass slides as described in the methods (Section 2.13). The membranes were then imaged on the Confocal Microscope to evaluate the seeding densities and confluence after 72 hours, the experiment was repeated in triplicate across five different seeding densities (Figure 3.23).

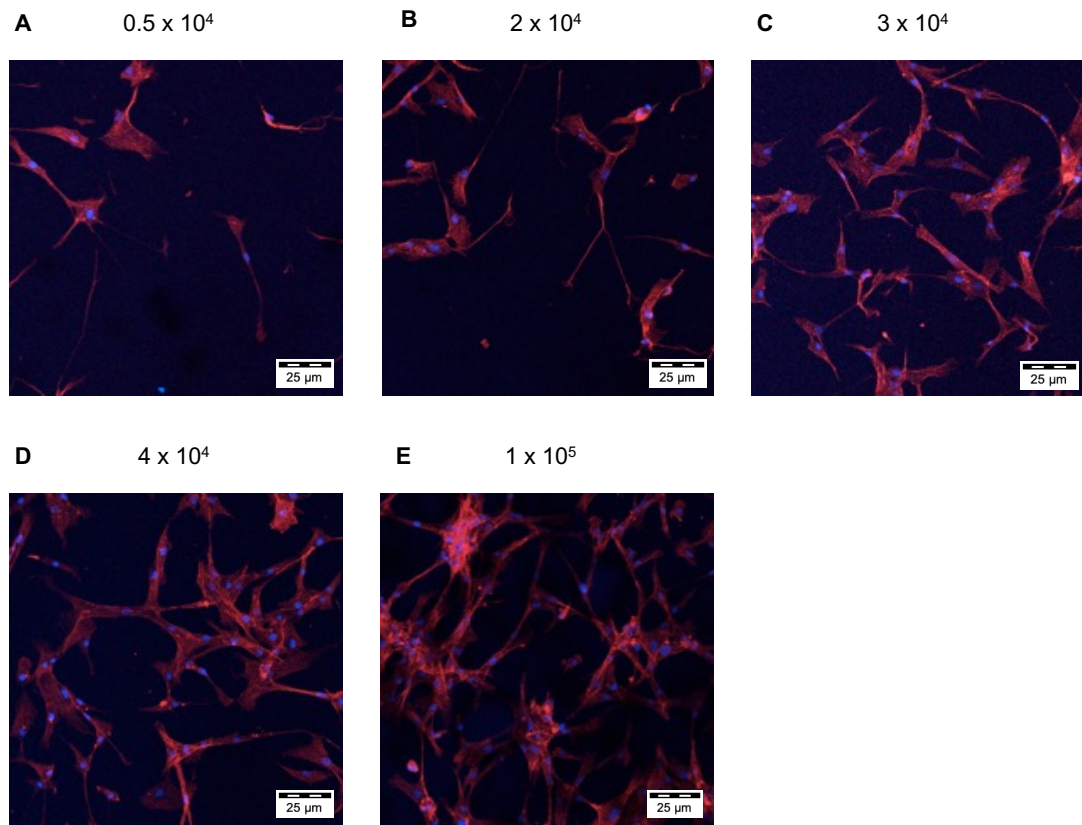


Figure 3.23: Confocal microscopy of stained ADSCs in 0.4µm transwell inserts. ADSCs at various seeding densities denoting total number of cells cultured for 72 hours. A - C demonstrate inserts that remain less than 50% confluent, which reduces differentiation risk alongside potentially minimising cellular interaction. Insert E is density populated and at risk of differentiating. Insert D demonstrating the optimised balance. All ADSCs were seeded in a 0.4µm Corning™ co-culture insert, fixed with 4% PFA and stained with DAPI (nucleus) and Phalloidin 633 (Actin) on a Confocal Microscope at high resolution (1024x1024). The experiment was repeated in triplicate.

Image acquisition parameters were optimised to enable the stained co-culture inserts to be successfully imaged, and the stained ADSCs were evaluated for confluence within the insert. The aim was to find a balance between too few cells as to artificially minimise the effects of the ADSCs on the cancer cell lines. This is best illustrated in in Figure 3.23 images A, B and C, which show sparsely populated inserts at seeding densities between 0.5 and 3×10^4 . It was also important to avoid excessive ADSC crowding as might result in areas of confluence approaching 80% or more. As numerous papers have illustrated and as has been previously discussed (Section 2.13), ADSCs which are allowed to achieve confluence may begin to differentiate and result in signalling changes. This is best represented as shown in Figure 3.23 image E. A seeding density of 4×10^4 was therefore selected following optical assessment of each of the three replicates across all seeding densities (Figure 3.23 Image D), as the confluence was adequate and unlikely to represent >80%. Additionally, it appeared to provide a sufficient number of cells to establish whether their presence resulted in an effect within a non-contact co-culture setting. This is also in line with published co-culture studies that use comparable seeding densities, which was additionally validating for the choice of this seeding density.

3.4 Discussion

The clinical need for understanding the interaction between ADSCs and breast cancer is well established, as we expand screening programs and develop (neo)adjuvant treatments resulting in an increasingly conservative surgical approach driving forward the need for small volume autologous reconstruction (Fujisaki *et al.*, 2015; Combellack *et al.*, 2016; Groen *et al.*, 2016; Wu *et al.*, 2019). Ensuring appropriate patient selection was key, and, although sample collection was at times challenging, over the course of the study, 22 cell lines were collected in total, four of which were essential in optimisation and 16 of which were included in the conditioned media and co-culture experiments resulting in end-point experimental data. The two discrete populations are important as the majority of published *in vivo* and *in vitro* work examine cell lines often taken from young, healthy female volunteers undergoing elective cosmetic procedures. Whilst there are a few studies emerging with ADSCs

taken from patients with cancer, they represent the minority and as clinical studies often lag behind in power, duration of study or adequate numbers, it is important to address the gap that exists.

Reviewing three ADSC isolation protocols initially was to ensure that the protocol selected was appropriately considered given our advancing understanding of this novel stem cell population. The interest in ADSCs and evolving methods of isolation meant that the selected protocol had to meet a number of requirements while providing a reliable and robust method to isolate ADSCs from patient samples. The isolation technique chosen was ultimately the simplest and one that was initially described in 2001 (Zuk *et al.*, 2001). Whilst there have been numerous derivations and potential improvements purported in subsequent papers, it proved the most cost effective, reliable, and repeatable. Importantly, it produced a cell population that was plastically adherent in culture, demonstrated trilineage differentiation, and maintained crucial CD markers, monitored by flow cytometry for the duration of the study. Being able to reliably characterise the isolated cell populations as ADSCs throughout the study was key given the scarcity of patients and value that each cell line represented.

Establishing a reliable fluorophore panel to monitor the cell population for the duration of the study was a cornerstone of the quality control (QC) process. The size of the fluorophore panel initially posed some challenges with regards to fluorescence spillover emissions, as the fluorophores chosen did not entirely adhere to the tight range of emissions detected by the Novocyte flow cytometer. However, after the creation of a compensation matrix, the panel worked well and provided regular confirmation during the study that the cells were retaining their characteristic MSC phenotype. Once established, each cell line could be run at early and late passage across three tubes; no stain, positive and negative, meaning only 3×10^5 cells were required for each run. The panel chosen is comparable to those described in the literature, and while there are a significant range of additional CD markers that could be chosen if cost were not an issue, the panel used for this study is sufficiently broad and encompasses a range of positive and negative fluorophores to ensure that the

cell line retained their MSC potential throughout the duration of cell culture (Banie *et al.*, 2008; Cook *et al.*, 2008; Nan *et al.*, 2013).

While the limitations of cell lines are understood (Burdall *et al.*, 2003; Vargo-Gogola and Rosen, 2007), they form a vital part of our understanding and development of experimental models and will likely always have a vital role in research, and are invaluable models for investigating the dysregulation of the hallmarks of cancer (Vargo-Gogola and Rosen, 2007). Breast cancer is known to be a complex and heterogenous disease which has posed numerous challenges when attempting to cultivate predictable cell lines for use in experimental studies. BT-20 was the first breast cancer cell line established in 1958 and predominated for the following two decades prior to the widespread establishment of additional cell lines, which included the MD Anderson and SUM series (Cailleau, Olivé and Cruciger, 1978; Holliday and Speirs, 2011) and those created by the Michigan Cancer Foundation (Soule *et al.*, 1973).

Established in 1973, the oestrogen receptor positive (ER+) MCF-7 cell line remains one of the most commonly studied breast cancer cell lines in the world today (Jordan and Levenson, 1997; Holliday and Speirs, 2011). The ER+ subtype of breast cancer accounts for up to 75% of new cancer that is diagnosed, illustrating the significant clinical relevance of this unique cell line. Its clinical application further demonstrated by the role the MCF-7 cell line played in the development and subsequent trials of the selective oestrogen receptor down-regulator Fulvestrant (Faslodex®, AstraZeneca, USA) for treating ER+ recurrent metastatic breast cancer (Osborne, Hobbs and Clark, 1985; Gottardis, Robinson and Jordan, 1988; Howell *et al.*, 2005; American Cancer Society, 2019; Mesa-Eguiagaray *et al.*, 2020). The change in breast cancer classification based on molecular characteristics has resulted in an evolving clinical assessment and treatment approach (Prat *et al.*, 2015; Jiang *et al.*, 2016; McDonald *et al.*, 2016). As such, choosing a cell line which reflects not only the most common histological diagnosis, but better reflects the hormone receptor and metabolic subtypes is important to ensure cell models are clinically representative. The two ER+ cell lines chosen for this study (MCF-7 and T47D) are both widely researched and have features in line with

common clinical pathology for patients newly diagnosed with breast cancer (Forman *et al.*, 2014; Siegel, Miller and Jemal, 2016; Sung *et al.*, 2021). The addition of T47D to act as comparative marker in key co-culture assays provides the opportunity to determine if commonalities exist in a cell line with a similar hormone receptor profile or if the findings are unique to the MCF-7 line.

In establishing the assays for measuring each of the identified hallmarks of cancer (invasion, migration, morphology, bioenergetics, protein expression and proliferation), there were experiments that benefitted from the use of manufactured kits or inserts. They ensured repeatability and reliability (e.g., the cytokine antibody array and ELISA Kits), and offered a non-damaging method of measuring cellular migration (IBIDI cell culture insert). These inserts prevented the cellular damage as caused by traditional scratch assays whilst providing a standardised gap and improved repeatability. The optimisation of more complex assays such as the Seahorse Extracellular Flux Analyser allowed for a greater level of analysis, of the extracellular acidification rate (ECAR) and oxygen consumption (OCR) rate in co-culture. This is a developing area within the scientific literature, examining the metabolic abnormalities and altered phenotype within ER+ breast cancer cell lines (including MCF-7) which may confer drug resistance to oestrogen receptor antagonists (e.g. Tamoxifen) (Fiorillo *et al.*, 2017).

Abnormal cellular metabolism was described as one of the defining features by Warburg, when examining the glucose metabolism of cancer cells and their mitochondria (Warburg, Wind and Negelein, 1927a). While the 'Warburg effect' is still used today to describe the altered glucose dependant metabolism and resulting lactate production, our ability to examine the intricacies in cellular and metabolic function has expanded. Many studies are now finding that some cancer mitochondria are functional, and this effect is not consistent across all tumour types (Potter, Newport and Morten, 2016). A flexibility in their overall functionality may be responsible for some of the varied findings that can be specific to individual cancers and tumour types. Furthermore, emerging cancer hallmarks have been suggested to include dysregulated cellular energetics as

there are studies demonstrating symbiotic populations within the cancer who rely on lactate as their energy source, essentially working in tandem with their hypoxic counterparts (Semenza, 2008; Feron, 2009; Kennedy and Dewhirst, 2010).

The variability in oxygenation within tumours has long been recognised with aberrant cellular growth and areas of hypoxia visible on radiological imaging with different theories suggested for the intrinsic causes of acute and chronic hypoxia (Macklin *et al.*, 2020). Irrespective of tumour type and stage, the presence of hypoxia and necrosis within solid tumours has been shown to be an independent risk factor for poor prognosis (Wilson and Hay, 2011; Coates, Skwarski and Higgins, 2019). The promotion of genetic instability, neoangiogenesis, invasion and metastatic spread has been linked to hypoxic states within cancer, so gaining a better understanding of the dysregulated metabolic function is essential (Graeber *et al.*, 1996; Carmeliet *et al.*, 1998; Pennacchiotti *et al.*, 2003; Bhandari *et al.*, 2019). The use of the Seahorse XF Analyser provided the opportunity to examine in detail the metabolic response to non-contact co-culture with ADSCs from two patient populations through real-time measurement of OCR and ECAR. The optimisation of this assay and use of CellTak™ meant that the data was robust and cell numbers were quantifiable throughout the assay and comparable across the various patients. Although this was one of the more complex assays to optimise, the understanding of the cellular behaviour as a result of non-contact co-culture with MCF-7 and T47D allows for a greater understanding of one of the emerging cancer hallmarks.

3.4.1 Conclusions

This chapter describes a broad and well evidenced range of assays to measure the established and emerging hallmarks of cancer using several low-tech and more novel techniques as influenced by ADSCs. The isolation technique is well supported in the literature and produced a reliable cell population that were characterised as ADSCs and met the minimum criteria for MSCs. Utilising ADSCs isolated from patients with breast cancer, provides a unique opportunity to examine their behaviour and effect on the hallmark traits of cancer whilst comparing them with ADSCs isolated from the group most cited in the literature. Examining the conditioned media and non-contact co-culture effects of ADSCs on MCF-7s, provides an opportunity to understand their interaction in greater detail. The use of a second ER+ cell line (T47D) for key co-culture assays (invasion, migration, proliferation, and bioenergetics) provides the opportunity to validate the MCF-7 findings. This enabled a comparison to determine if the effects were specific to one cell line, or analogous with a second cell line with similar hormone receptor status.

This study is one of very few that directly compares primary cell lines taken from two clinically different patient groups and aims to contribute to a developing research area regarding patient safety. In view of the disparity between clinical and basic science research, it is important to critically examine possible confounding factors which may ultimately affect patient choice. The majority of the laboratory studies which focus on ADSCs taken from healthy patients, demonstrate a range of adverse impacts on breast cancer growth and progression in both cell culture and animal models (Gespach *et al.*, 2014; Ning *et al.*, 2014; Fujisaki *et al.*, 2015; Wu *et al.*, 2019). Conversely, clinical studies which examine women undergoing lipofilling to the breast following cancer resection, do not show a higher rate of recurrence (Brenelli *et al.*, 2014; Maione *et al.*, 2015; Batista *et al.*, 2016; Silva-Vergara *et al.*, 2016). By meeting the chapter aims and optimising the assays to evaluate the hallmarks of cancer, the measurement of both the indirect (Chapter Four) and co-culture (Chapter Five) effects of two ADSC populations can be affectively assessed on the hallmarks of two ER+ breast cancer cell lines.

Chapter Four

Evaluating the Indirect Effect of ADSC Conditioned Media from Healthy and Cancer Patients on the Neoplastic Traits of MCF-7 Cells

4.1 Introduction

ADSCs have been shown to secrete a variety of exosomes, protein cytokines, and additional active factors which promote normal cell function in response to inflammation and cellular injury (Cai *et al.*, 2020). However, it is through these paracrine effects, that ADSCs have the potential to support the development and progression of breast cancer (Trivanović *et al.*, 2014; Fujisaki *et al.*, 2015; Kruger *et al.*, 2018; Wu *et al.*, 2019). Media conditioned by ADSCs has the advantage of being cell free, more suitable for storage and resuscitation, and has in recent years been the focus of numerous scientific studies (Cai *et al.*, 2020; Ajit and Gopalankutty, 2021; Montero-Vilchez *et al.*, 2021). The evaluation of the indirect effects of ADSCs on the hallmarks of breast cancer utilising conditioned media, has previously been described as an essential part of experimental modelling (Weigand *et al.*, 2016; Koellensperger *et al.*, 2017; Teufelsbauer *et al.*, 2019). As discussed in Section 3.1 the difference in effects of ADSCs isolated from patients with breast cancer when compared with their healthy counterparts on the neoplastic traits of MCF-7 cells is of specific interest. The optimised endpoint experiments detailed in Chapter Three aim to represent the cancer hallmarks as defined in Chapter One (Section 1.4), and enable the neoplastic traits of the MCF-7 cells to be measured. Utilising a conditioned media model provides an important baseline understanding of the way ADSCs isolated from women with breast cancer may differ in their effect on MCF-7 cells, compared with their healthy counterparts.

4.1.1 Chapter Aims

The aim of this chapter is to evaluate the effects of ADSC conditioned media from two different patient populations on the neoplastic traits of MCF-7 growth and progression in a dose dependant fashion, and to determine if there is any difference between the two ADSC patient groups. This allows for the indirect effect of ADSCs taken from healthy patients to be compared with those taken from patients with ER+ breast cancer, who are currently undergoing treatment.

This will be achieved by meeting the objectives below:

1. Determine the effect of conditioned media taken from ADSCs isolated from healthy and cancer patients on the neoplastic traits of MCF-7 cancer growth and progression to include
 - a. Proliferation
 - b. Migration
 - c. Invasion
 - d. Morphology
 - e. Cytokine/Chemokine expression profiles
2. Determine if there are any differences in the effects of ADSC conditioned media on MCF-7 cancer growth and progression between the two patient groups (healthy and cancer).

4.2 Methods

4.2.1 Sample Collection

As described previously (Section 2.4), intra operative samples were collected from two patient groups. Patients used in the conditioned media work include ADSC005, 011, 012, 020, 021 and 022, which were healthy women who had never had cancer. ADSC 008, 009, 010, 013, 014, 015, 016, 017, 018 and 019, which were women diagnosed with ER+ breast cancer currently on systemic hormone therapy.

4.2.2 ADSC Isolation and Characterisation

As previously described in Section 2.7.1, ADSCs were isolated using the chosen protocol (Zuk *et al.*, 2001) and characterised using the fluorophore panel previously noted (Section 2.10) at early and late passage (p2 and p8) to ensure MSC potential was maintained prior to use in the experiments. Downstream analysis of flow cytometry was performed using FlowJo version 1.3 (Oregon, USA).

4.2.3 MCF-7 Cell Line

Authenticated breast cancer MCF-7 cells were obtained from ATCC and cultured in standard conditions and passaged when 80% confluent as outlined previously in the Methods (Section 2.3).

4.2.4 Tissue Culture

MCF-7 cells were cultured as described in Section 2.6, and ADSCs isolated from healthy and cancer patients were cultured as described in Section 2.7. ADSCs were all grown to 70% confluence before being passaged as described in (Section 2.7.1) and both ADSCs and MCF-7s were cultured for 14 days prior to any use in experimentation once removed from liquid nitrogen (Section 2.9.3).

4.2.5 Cell Counting

Cell counting and viability were calculated using the Countess™ automated cell counter (Life Technologies, UK) as described in Chapter Two (Section

2.8). The total live cell count (via trypan blue exclusion) was used for downstream experimentation inclusive of applicable dilution factor.

4.2.6 Conditioned Media

Conditioned media was prepared as described in Section 2.12 before being combined with fresh media in different ratios (Table 2.4). This allowed varying concentrations (0, 25, 50, 75 and 100%) of conditioned media to be used to establish if there was a dose dependant effect of the ADSC conditioned media on the hallmarks of MCF-7 cancer growth and progression. Unless otherwise stated, data shown is from technical replicates (n=3) at two time points (p2 and p8) across separate experiments with patients taken from two patient groups (healthy n=6 and cancer n=10) and data is expressed as the mean \pm SEM.

4.2.7 Proliferation

Proliferation of MCF-7s in response to varying concentrations of conditioned media was measured continuously using the RTCA iCELLigence instrument (ACEA Bioscience, UK now part of Agilent, UK) as described in Section 2.14.1, with experiments performed in triplicate at early (p2) and late (p8) passage and values were expressed as cell index (CI).

4.2.8 Migration

As detailed in Section 2.14.3, MCF-7 cells were seeded into cell culture inserts (IBIDI, Germany) prior to treatment with varying concentrations of conditioned media. Serial photographs were then used over the next 48 hours to observe the rate of closure of the standardised 500 μ m gap. The experiment was performed in triplicate at early (p2) and late (p8) passage, with results displayed as gap remaining and rate of gap closure.

4.2.9 Invasion

The assay to quantify invasion was conducted using the collagen inserts as described in Section 2.14.5 at early (p2) and late (p8) passage and repeated in triplicate. Following the stain and extraction protocol (Section 2.14.5), results were measured as absorbance at 560 nm using a microplate reader (POLARstar Omega, BMG Labtech, Germany).

4.2.10 Morphology

As described in Section 2.14.7 changes in MCF-7 morphology were measured after treatment with varying concentrations of conditioned media at early (p2) and late (p8) passage. Plates were read on the INCELL Analyser 2000 which took a series of 300 photographs (fields of view) using a high-performance CCD camera from each well for analysis.

4.2.11 Cytokine/Chemokine Expression Profiles

The measurements IL-6, VEG-F, and MCP-1, from the cell free culture media was performed using the sandwich ELISA technique as described in Section 2.15.1 following the manufacturer's instructions. Media was harvested from MCF-7 cells at 4 hours and 24 hours following treatment with ADSC conditioned media at early (p2) and late (p8) passage. Final plates were read at 450 nm using a plate reader (POLARstar Omega, Germany) and final protein concentration calculated in relation to the standard curve.

4.2.12 Data Analysis

4.2.12.1 Proliferation

Statistical analysis was performed using GraphPad Prism version 9.1.0, after exporting the file into RTCA Data Analysis Software 1.0 (ACEA Bioscience, UK). A one-way ANOVA was used to compare proliferation of each concentration of conditioned media against the untreated group (0%). All experiments were replicated in triplicate across both patient groups (n=6 healthy, n=10 cancer). Significant values were taken as $p < 0.05$ graphically denoted as * $p \leq 0.05$, ** $p \leq 0.01$, *** $p \leq 0.001$, **** $p \leq 0.0001$. Adhesion was calculated as the change in cell index divided by the change in time ($\Delta CI/\Delta T$) and a two-way ANOVA with multiple comparison tests was applied.

4.2.12.2 Migration

Images captured on a light microscope (Zeiss, Axiovert 40C) at x10 magnification were assessed visually initially before the gap was measured using ImageJ to quantify the gap remaining from the original 500 micron starting point as described previously (Section 2.14.3). Statistical analysis was

performed using GraphPad Prism version 9.1.0, after exporting the file into RTCA Data Analysis Software 1.0 (ACEA Bioscience, UK). A two-way ANOVA was used to compare different concentrations of conditioned media against the control (0%) across both patient groups (healthy and cancer). All experiments were repeated in triplicate across all concentrations of conditioned media at both early (p2) and late (p8) passage.

4.2.12.3 Invasion

Data quantified using extracted stain as previously described in Chapter Two (Section 2.14.5). Statistical analysis was performed using GraphPad Prism version 9.1.0 after exporting the data from the plate reader into MS Excel. A two-way ANOVA was used to compare different concentrations of conditioned media against the control (0%) across both patient groups (healthy and cancer). Data shown is from technical replicates (n=3) at two time points (p2 and p8) across separate experiments with patients taken from two patient groups (healthy n=6 and cancer n=10) and data is expressed as the mean \pm SEM.

4.2.12.4 Morphology

Data generated using the CellProfiler™ image analysis software version 3.1.5 (USA) was analysed using GraphPad Prism version 9.1.0 to compare the effects of different concentrations of ADSC CM from the two patient populations on the morphology of MCF-7 cells. A two-way ANOVA was used, with data from technical replicates (n=3) at two time points (p2 and p8) across separate experiments with patients taken from two patient groups (healthy n=6 and cancer n=10) and data is expressed as the mean \pm SEM.

4.2.12.5 Cytokine Expression Profiles

Statistical analysis was performed using GraphPad Prism version 9.1.0 after exporting the data from the plate reader into MS excel. A two-way ANOVA was used to compare the concentrations of different detected proteins in the media against the control (0%). Significant values were taken as $p < 0.05$ graphically denoted as * $p \leq 0.05$, ** $p \leq 0.01$, *** $p \leq 0.001$.

4.3 Results

Following reliable isolation, characterisation, and culture of ADSCs taken from the two different patient groups (healthy and those with ER+ breast cancer) (Section 3.3.2), it was important to initially assess the indirect effect of the ADSC CM on the hallmarks of cancer using the ER+ MCF-7 cell line. CM experiments were therefore utilised to examine the indirect effect of ADSC CM from the two different patient groups on the neoplastic traits of the MCF-7 cell line, to understand the baseline effects prior to commencing any non-contact co-culture work.

4.3.1 Increasing Concentrations of Healthy ADSC CM Significantly Increases the Rate of MCF-7 Proliferation at All Concentrations

To determine the effects of ADSC conditioned media from both healthy and cancer patients on proliferation, MCF-7 cell lines were treated with varying concentrations of conditioned media (25, 50, 75 and 100%) with 0% acting as the control. Proliferation, and maximum cell index were evaluated using the automated and continuous ACEA Biosciences iCELLigence system as previously described (Section 2.14.1). Cell adhesion was then defined as the change in cell index divided by the change in time ($\Delta CI/\Delta T$) to provide an indicator of the rate of adhesion to the bottom of the EL-8 plate. This was done at early (p2) and late (p8) passage and real time analysis was performed continuously for 48 hours. By measuring the change in electrical impedance on the bottom of each well, it was possible to quantify cell index values, which indicated an increase in cell number and density (Figure 4.1, A and B). This is more visually apparent when examining the growth curves over the first 24 hours (Figure 4.1, C and D). Comparing the two patient groups at early passage (p2), there was an increase in proliferation at all concentrations of ADSC conditioned media taken from healthy patients (25, 50, 75 and 100%) when compared with the 0% control ($p \leq 0.0001$). Comparatively, when MCF-7s were treated with ADSC conditioned media from patients with cancer, there was an increase only at lower concentrations of conditioned media (25% and 50%) when compared with the 0% control ($p \leq 0.0001$).

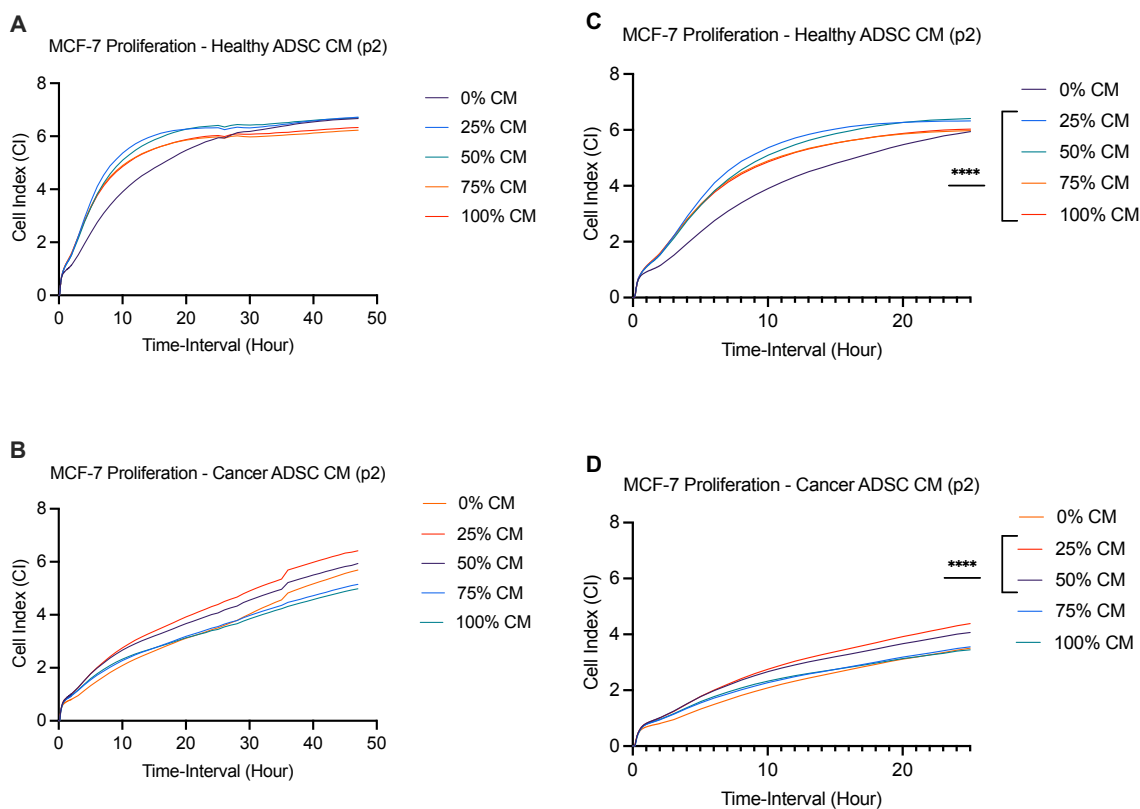


Figure 4.1: CM from healthy patient ADSCs at early passage (p2), increase the rate of MCF-7 proliferation when compared with the control across all concentrations.

MCF-7 cells treated with media that had been conditioned by ADSCs isolated from healthy patients (A and C) or those with breast cancer (B and D) for 48 hours. Examining the first 24 hours in more detail (C and D), these graphs demonstrate more clearly the difference in rates of proliferation between MCF-7 cells treated with CM taken from healthy patients (C) and cancer patients (D) compared with the control. (C) There is a statistically significant increase in MCF-7 proliferation with cells treated with healthy ADSC CM across all concentrations (25, 50, 75 and 100%) compared with the 0% control (**** $p \leq 0.0001$). (D) Comparatively, MCF-7s treated with ADSC CM from cancer patients, demonstrate a statistically significant increase in MCF-7 proliferation only at lower concentrations (25 and 50%) compared with the 0% control (**** $p \leq 0.0001$). Statistical significance (**** $p \leq 0.0001$) comparing proliferation to the control was evaluated using a one-way ANOVA. Data from $n=3$ technical replicates of $n=6$ healthy patients and $n=10$ cancer patients.

The effect of ADSC conditioned media from both patient groups (healthy and cancer) on MCF-7 proliferation noted at early passage (p2) (Figure 4.1), was similarly reflected at late passage (p8) (Figure 4.2). There was a comparable

trend in the significance when comparing MCF-7s treated with conditioned media from healthy patients (A and C), at all concentrations (25, 50, 75 and 100%) compared to the control (0%) ($p \leq 0.0001$). As illustrated in Figure 4.2 (B and D) (p8 cancer), MCF-7 proliferation was only increased significantly at lower concentrations (25 and 50%) when compared with the control (0%) ($p \leq 0.0001$).

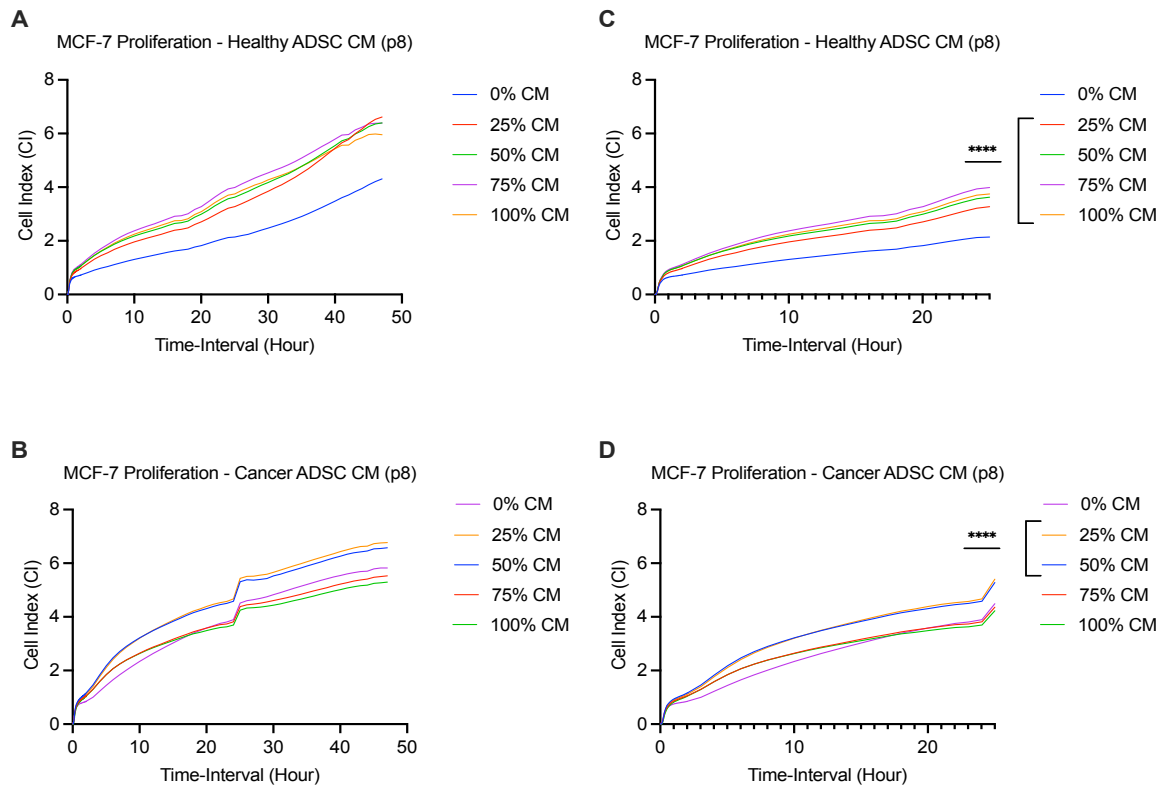


Figure 4.2: CM from healthy and cancer ADSCs at late passage (p8) influence rates of MCF-7 proliferation over 48 hours.

MCF-7 cells treated with media conditioned by ADSCs isolated from healthy patients (A and C) or those with breast cancer (B and D) for 48 hours. (A and C) MCF-7s treated with healthy ADSC CM demonstrated increased proliferation at all concentrations (25, 50, 75 and 100%) compared with the control (0%) ($****p \leq 0.0001$). (C) Examining proliferation over an adjusted 24 hour time-period makes it more visually apparent. (B and D) MCF-7s treated with cancer ADSC CM only showed increased rates of proliferation at 25% and 50% CM concentrations ($****p \leq 0.0001$). (D). Data from $n=3$ technical replicates of $n=6$ healthy patients and $n=10$ cancer patients. Of note, the disruption at all concentrations seen in graph B at approximately 23 hours is due to a faulty transmitter component which caused a recurrent disconnection between the instrument and the iPad after being active for 24 hours. While readings continued and there was no loss of data, once we became aware of the issue, a new component was ordered, and once the transmitter was replaced, there were no further signal interruptions.

Cell adhesion, which is defined as the change in cell index divided by the change in time ($\Delta CI/\Delta T$), was measured using sequential readings taken every 60 seconds for the first 120 minutes. These values are generated from the moment cells begin to adhere to the surface of the uncoated well, providing an indicator as to the rate of MCF-7 adhesion treated with differing concentrations of conditioned media (Figure 4.3). Although MCF-7 cells treated with healthy patient ADSC CM show increased rates of adhesion within the first 120 minutes, this is not statistically significant at either early (p2) or late passage (p8). It is therefore not possible to elucidate any significance regarding the rate at which MCF-7 cells adhere to the bottom of the EL8 well (uncoated plastic), when treated with ADSC CM (25, 50, 75 and 100%) from either healthy or cancer patients when compared to the control (0%).

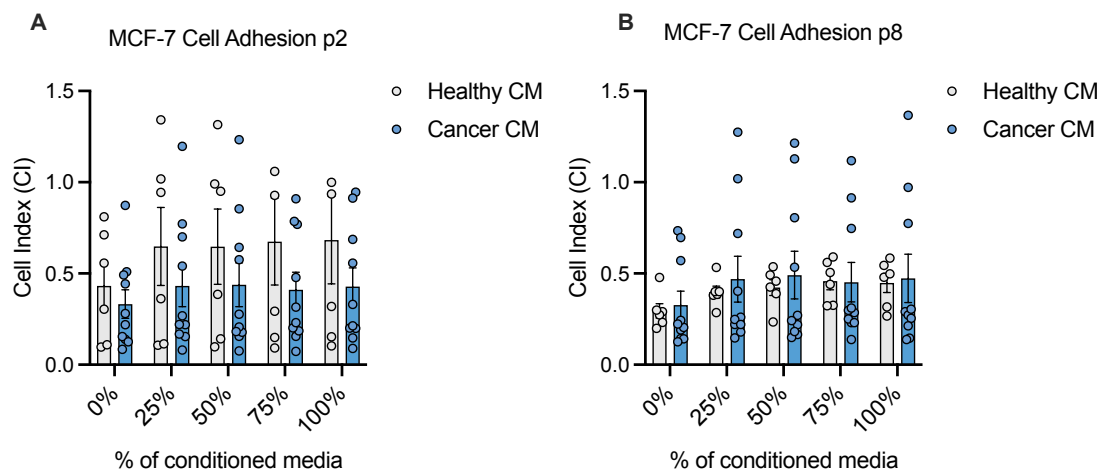


Figure 4.3: CM from healthy and cancer patients has no effect of real-time rate of MCF adhesion at either early (p2) or late (p8) passage.

MCF-7 cells treated with ADSC CM from healthy (light grey) and cancer patients (blue) were monitored every 60 second for the first 120 minutes using the iCELLigence at early (p2) (A) and late (p8) (B) passage following treatment with varying concentrations of conditioned media (25, 50, 75 and 100%) and compared against a control (0%). Although not statistically significant, there is an apparent increase in rate of adhesion onto the bottom of the EL8 well noted with increasing concentrations of healthy ADSC CM at early passage (p2) when compared with both the control and cancer ADSC CM. This change is not as apparent at late passage (p8). Data shown is from technical replicates (n=3) at two time points (p2 and p8) across separate experiments with patients taken from two patient groups (healthy n=6 and cancer n=10) and data is expressed as the mean \pm SEM.

4.3.2 Increasing Concentrations of ADSC CM From Healthy and Cancer Patients Does Not Significantly Affect the Rate of MCF-7 Migration

It was important to understand how the addition of ADSC CM affected the migration of MCF-7 cells, and whether the increase in proliferation was reflected in the rate of migration in either patient group. MCF-7 migration was analysed as previously described (Section 2.14.3) using the IBIDI cell culture inserts which created a standardised 500 µm gap that was then monitored with serial photographs over 48 hours. The rate of MCF-7 gap closure was compared for each concentration of ADSC CM (25, 50, 75 and 100%) against the control (0%) and the patient groups (healthy and ER+ breast cancer) were compared against each other. The gap was measured at five points using Image J as described previously (Section 2.17.1) across each of the three time points to ascertain the gap remaining and quantify the percentage by which the gap had been narrowed.

Visually, using the photographs to assess the rate of closure over 48 hours, there initially appeared to be a dose dependant effect in relation to the percentage of conditioned media that was used to treat the MCF-7 cells (Figure 4.4 and 4.5). MCF-7 cells appeared to migrate and close the gap more quickly with higher concentrations of ADSC CM from healthy patients when compared with cancer. However, when analysing all replicates across both patient groups (healthy n=6 and cancer n=10), a two-way ANOVA analysis comparing the patient groups at different concentrations of conditioned media did not demonstrate significance across either patient group over the full range of CM concentrations (Figure 4.6).

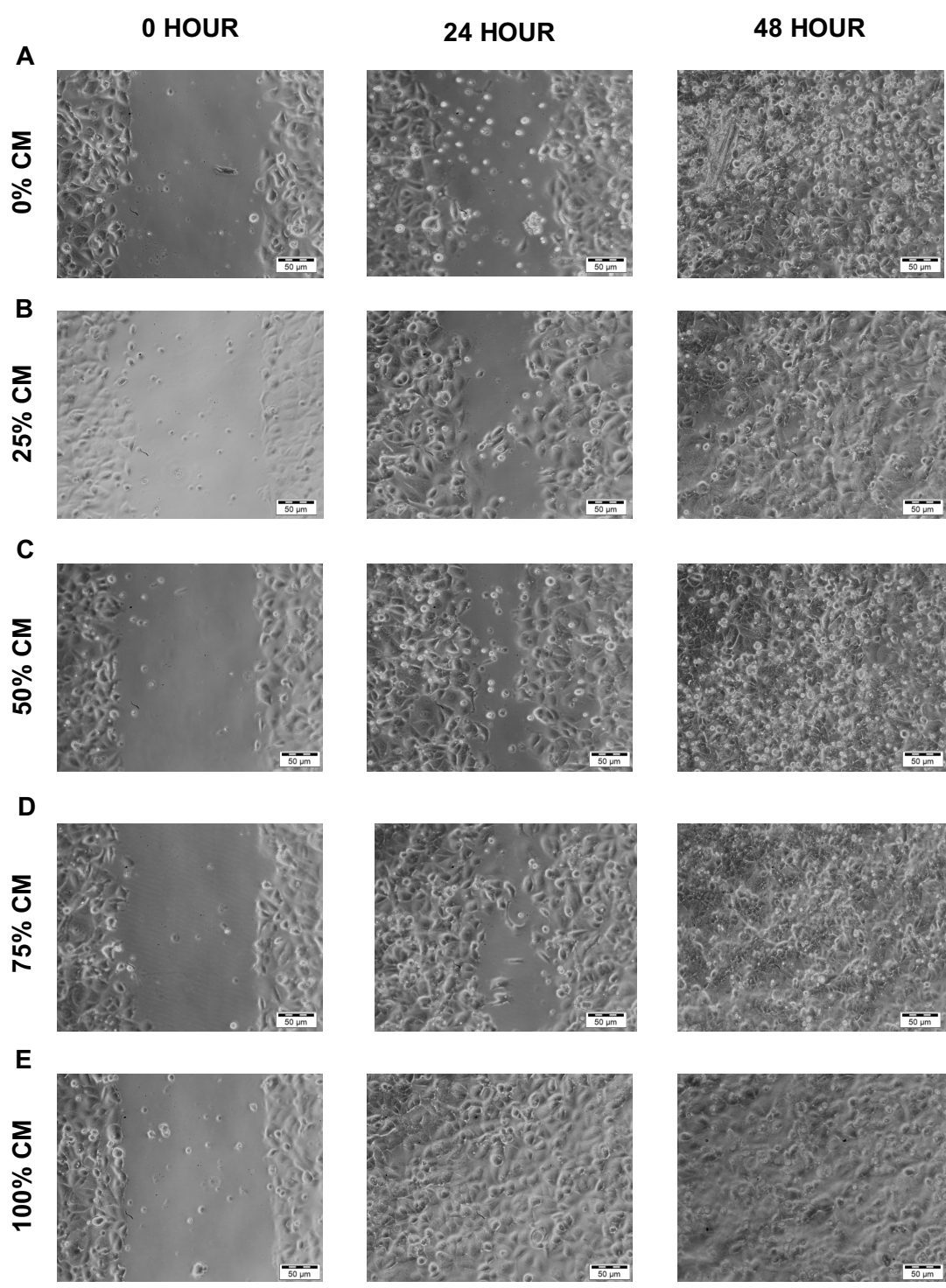


Figure 4.4: Rate of MCF-7 gap closure when treated with ADSC CM from a healthy patient when compared with the control (0%).

Images taken at x10 magnification on a light microscope (Zeiss, Axiovert 40C) of MCF-7 cells treated with various concentrations of ADSC CM (B to D) from a healthy patient at early passage (p2) and when compared with the control (A) (0%).

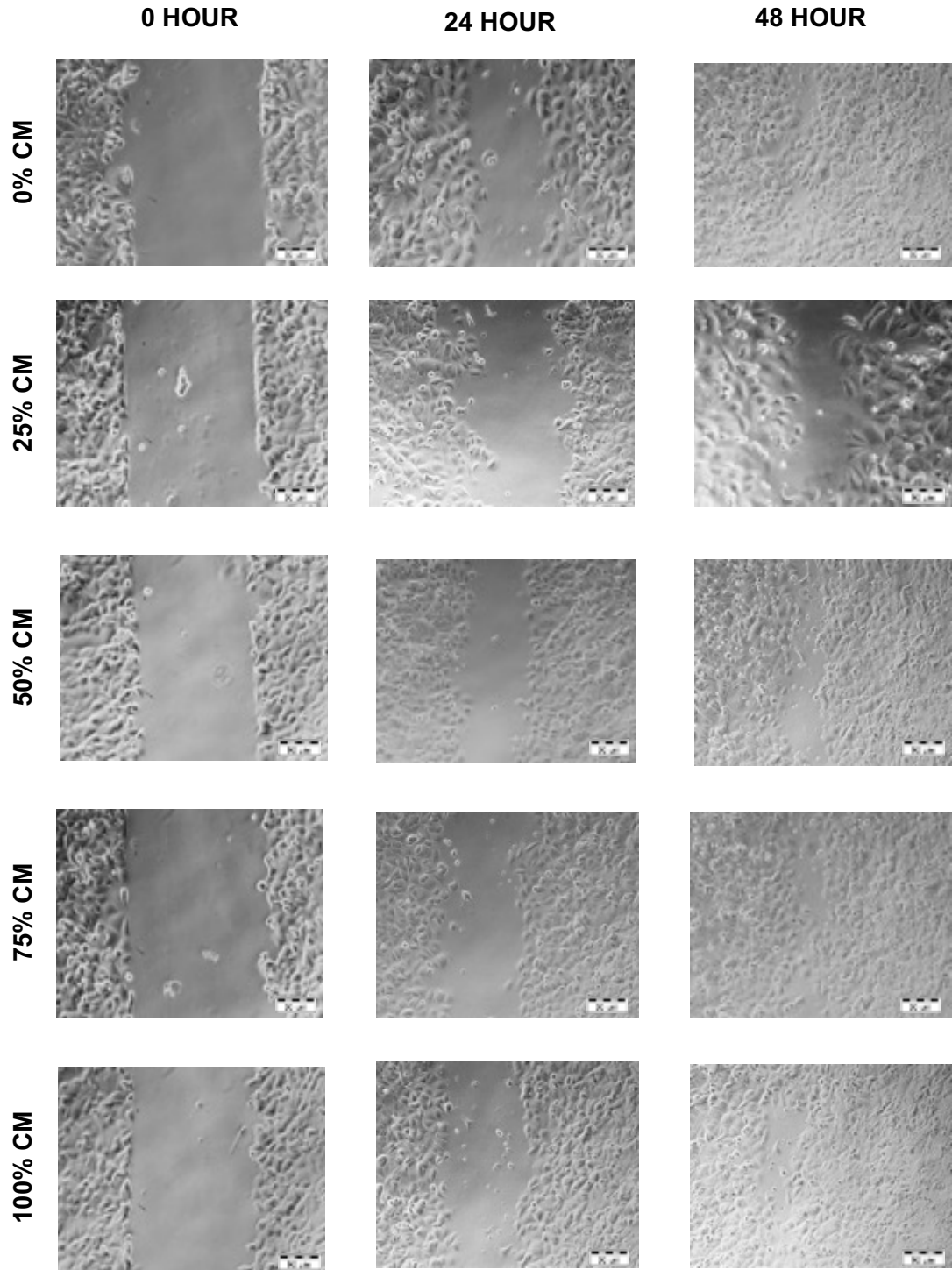


Figure 4.5: Rate of MCF-7 gap closure when treated with ADSC CM from a cancer patient when compared with the control (0%).

Images taken at x10 magnification on a light microscope (Zeiss, Axiovert 40C) of MCF-7 cells treated with various concentrations of ADSC CM (B to D) from a cancer patient at early passage (p2) and when compared with the control (A) (0%).

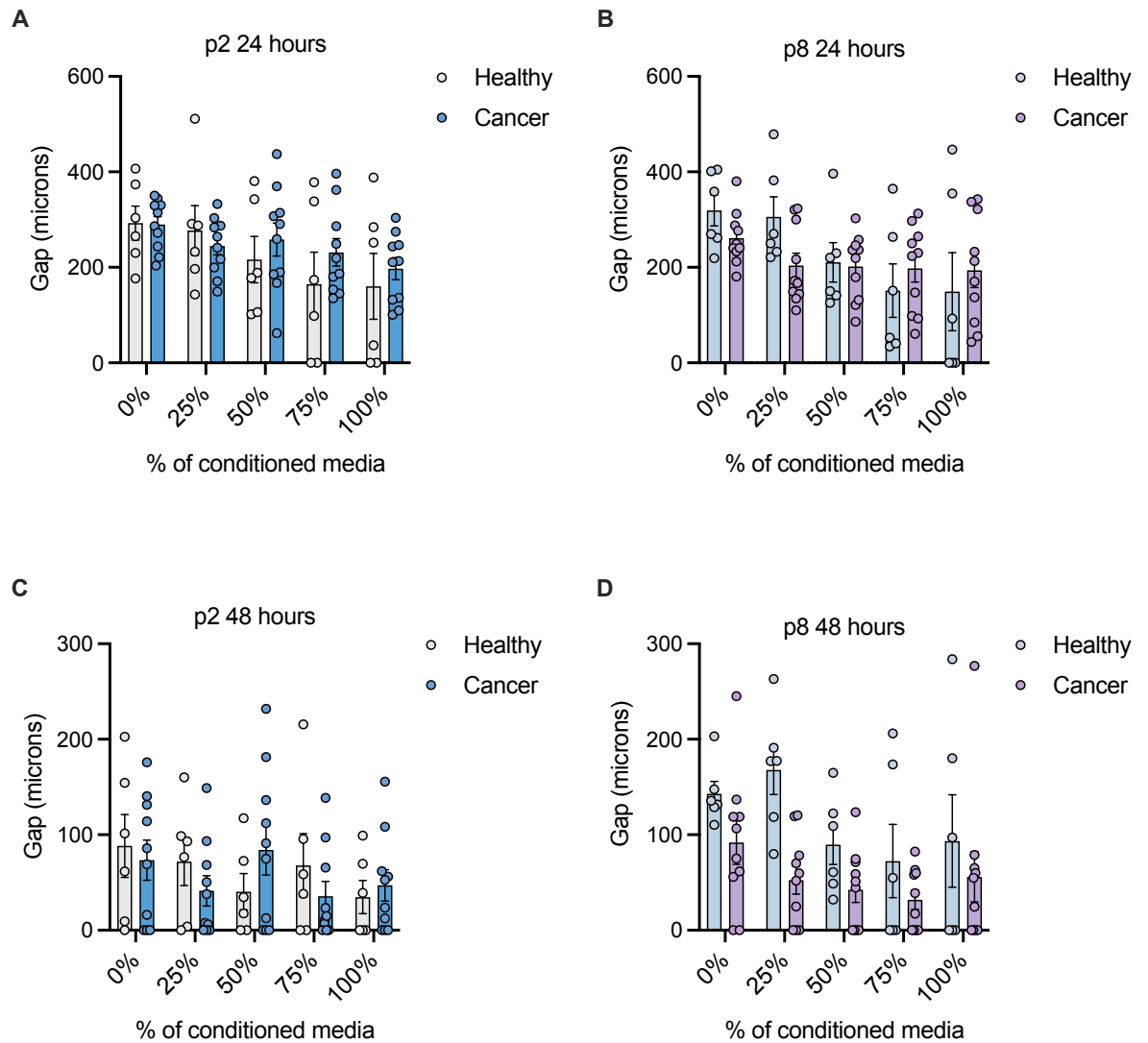


Figure 4.6: Analysis of gap remaining after 24 and 48 hours of treatment with ADSC CM from healthy and cancer patients at early and late passage.

These graphs represent the gap remaining following removal of the IBIDI insert and treatment with MCF-7s with varying concentrations of ADSC CM from both healthy and cancer patients, at early (p2) (A and C) and late (p8) (B and D) passage. The general trend appears to be a reduction in gap (microns) over time at higher concentrations of conditioned media (A-D). However, a two-way ANOVA demonstrates that statistical significance has not been reached e.g., 24 hour migration at p2 (A) Healthy 0% vs 100% $p=0.1155$. Data shown is from technical replicates ($n=3$) at two time points (p2 and p8) across separate experiments with patients taken from two patient groups (healthy $n=6$ and cancer $n=10$) and data is expressed as the mean \pm SEM.

4.3.3 Increasing Concentrations of ADSC CM from Healthy Patients Only Significantly Increases the Rate of MCF-7 Invasion at Early and Late Passage (p2 and p8)

The ability to invade through the basement membrane and potential to metastasise to distant anatomical locations is one of the defining hallmarks of cancer (Hanahan and Weinberg, 2011). As the MCF-7 cell line is derived from a malignant pleural effusion, there is already an established metastatic potential (Soule *et al.*, 1973). It was therefore important to understand the indirect effect that ADSC CM derived from two distinct patient groups had on MCF-7 invasion at early (p2) and late (p8) passage. As described previously (Section 2.14.5), the use of a collagen insert served as a surrogate for human basement membrane to establish any change in MCF-7 invasion when compared with the control (0% CM) and to compare the effect on invasion of ADSC conditioned media taken from two clinically discrete patient groups.

As shown in (Figure 4.7, A and B), MCF-7s treated with ADSC CM from healthy patients only at early passage (p2) suggested a general trend of increased invasion at higher concentrations of conditioned media (75% and 100%) when compared with CM derived from patients with cancer. A two-way ANOVA (healthy n=6, cancer n=10) demonstrated there was a statistically significant increase in invasion when observing MCF-7s treated with 75% and 100% healthy ADSC CM ($p=0.0218$ and $p=0.0100$). This is mirrored in the photographs of the stained collagen inserts at p2, showing an increase in number of MCF-7 cells invading at higher concentrations of healthy CM (75% and 100%) when compared with the control (0%) (Figure 4.8, A, D and E).

At late passage (p8) there was a statistically significant increase in MCF-7 invasion when treated with healthy ADSC CM only, at 75% and 100% compared with the control (0%) ($p=0.0017$ and $p<0.0001$) as determined by a two-way ANOVA (healthy n=6, cancer n=10). Additionally, there was a statistically significant difference that saw an increase in MCF-7 invasion at all concentrations of healthy ADSC CM when compared with cancer ADSC CM (Figure 4.7, B) (25% CM $p=0.0402$, 50% CM $p=0.014$, 75% and 100% CM $p<0.0001$). This is similarly reflected in the images captured with the light

microscope of the stained collagen inserts at p8 (Figure 4.9) showing an increase in the number of MCF-7 cells invading into the membrane at higher concentrations of healthy ADSC CM when compared with cancer ADSC CM. Treatment of MCF-7 cells with media conditioned by ADSCs isolated from patients with breast cancer failed to have an effect on invasion at early (p2) or late (p8) passage, across all concentrations.

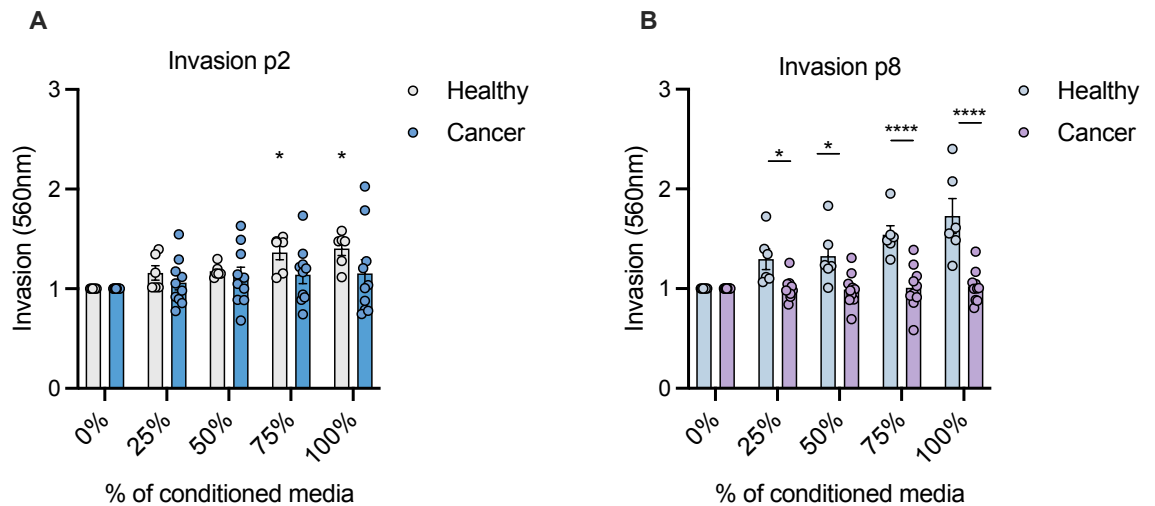


Figure 4.7: Media conditioned by healthy ADSCs increases MCF-7 invasion at late passage (p8) at all concentrations (25-100%).

Extracting the stain bound to the invading MCF-7 cells from each of the collagen membranes allowed rate of invasion to be quantified by measuring absorbance in a standard plate reader at 560nm. A: The number of MCF-7 cells that invaded through the membrane was increased at early passage (p2) in the healthy ADSC CM group compared with the 0% control 75% $p=0.0218$ and 100% $p=0.0100$. B: At late passage (p8) MCF-7 cells are more invasive at all concentrations of healthy ADSC media (25, 50, 75 and 100%) when compared with the control and ADSC CM derived from cancer patients (25% CM $p=0.0402$, 50% CM $p=0.014$, 75% and 100% CM (* $p<0.05$, **** $p\leq 0.0001$)). Data shown is from technical replicates ($n=3$) at two time points (p2 and p8) across separate experiments with patients taken from two patient groups (healthy $n=6$ and cancer $n=10$) and data is expressed as the mean \pm SEM.

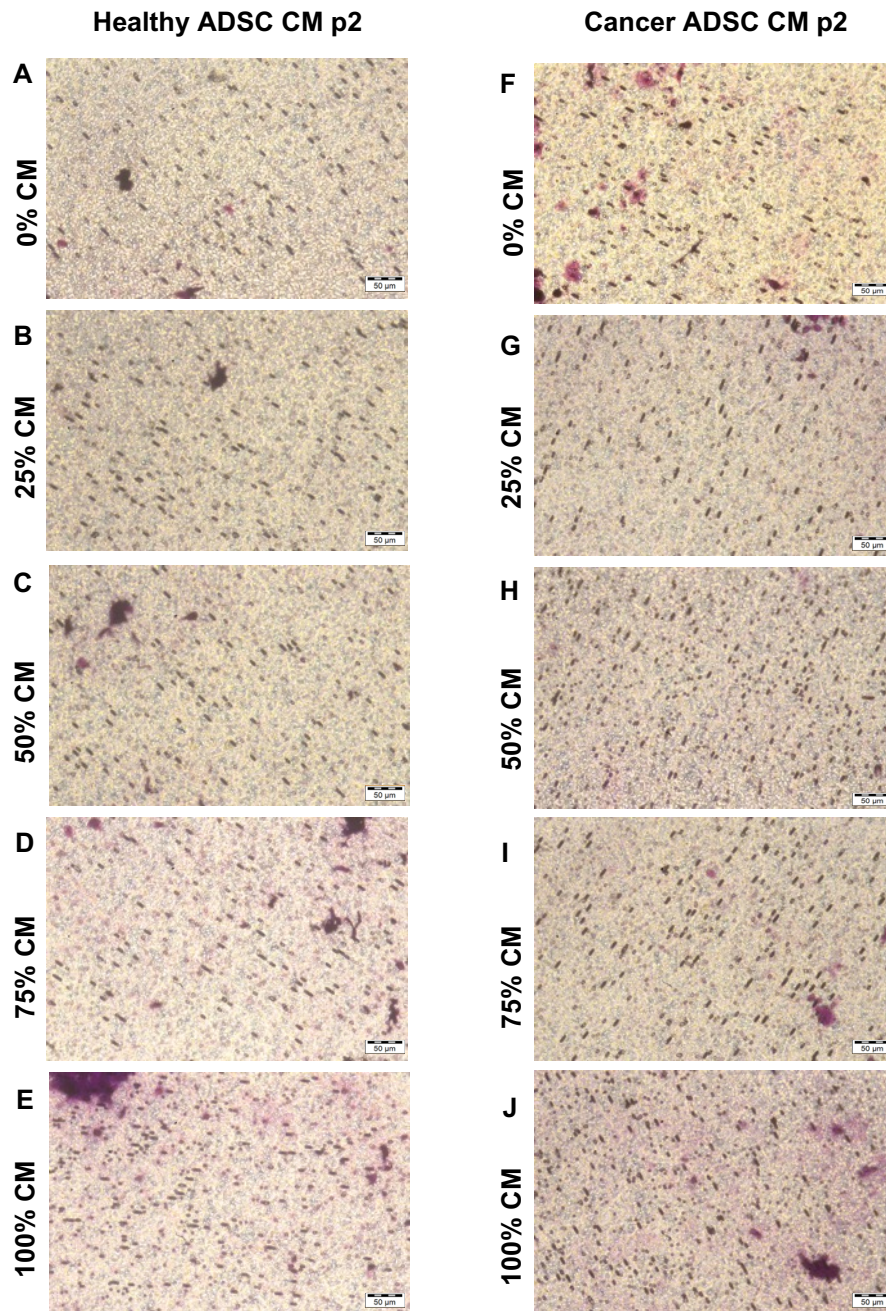


Figure 4.8: MCF-7 cells demonstrate increased invasion at early passage (p2) when treated with healthy ADSC CM at higher concentrations (75% and 100%) when compared with the control (0%).

(A – J) stained invasion inserts taken at x10 magnification on a light microscope (Zeiss, Axiovert 40C). (B) (C) (D) and (E) show MCF-7s treated with healthy CM compared against (A) the control. (G) (H) (I) and (J) show MCF-7s treated with cancer CM compared against (F) the control. (D and E) It is possible to see increasing numbers of MCF-7 cells (purple dots) invading through the insert when treated with higher concentrations (75% and 100%) of healthy ADSC CM versus (A) the control. (G – J) MCF-7s treated with increasing concentrations of cancer CM did not meet statistical significance versus (F) the control. Data from n=3 technical replicates of n=6 healthy patients and n=10 cancer patients.

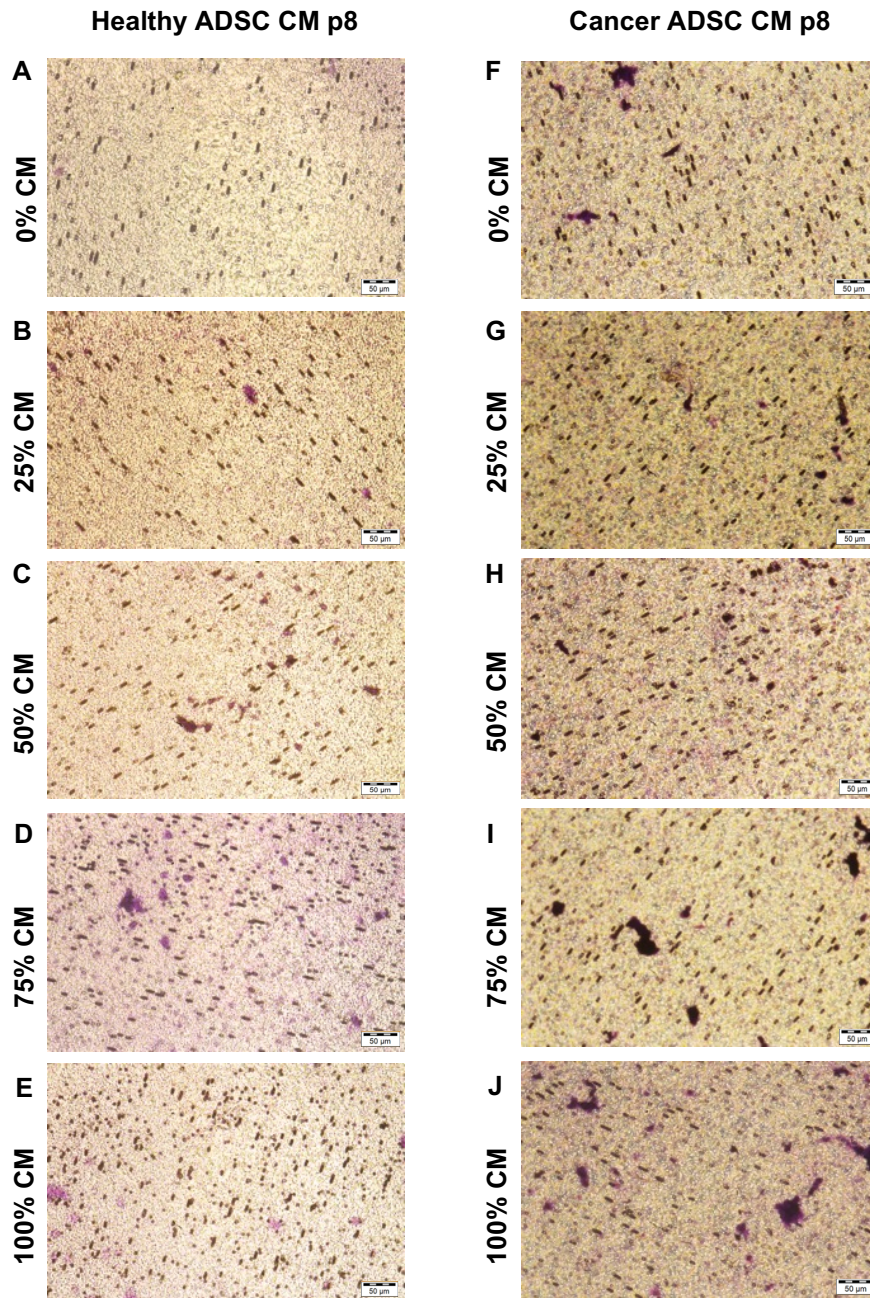


Figure 4.9: MCF-7 cells demonstrate increased invasion at late passage (p8) when treated with healthy ADSC CM at all concentrations when compared with cancer ADSC CM and the control (0%).

(A - J) stained invasion inserts taken at x10 magnification on a light microscope (Zeiss, Axiovert 40C). (B) (C) (D) and (E) show MCF-7s treated with healthy CM compared against (A) the control. (G) (H) (I) and (J) show MCF-7s treated with cancer CM compared against (F) the control. (B - E) It is possible to see increasing numbers of MCF-7 cells (purple dots) invading through the insert when treated with all concentrations of healthy ADSC CM versus (A) the control. (G - J) MCF-7s treated with increasing concentrations of cancer CM did not meet statistical significance when compared with (F) the control. Data from n=3 technical replicates of n=6 healthy patients and n=10 cancer patients.

4.3.4 Increasing Concentrations of ADSC CM Does Not Significantly Alter MCF-7 Nuclei or Cellular Morphology

The morphological change induced by pleiotropically acting transcription factors (e.g., *SNAIL*, *SLUG*, *TWIST* and *ZEB1/2*) include the loss of adhesion and tight junctions resulting in a cellular distortion from an epithelial/polygonal type to spindle/fibroblast like morphology (Lazebnik, 2010; Hanahan and Weinberg, 2011). This loss of cellular adhesion and increased motility is implicated in the increased propensity of a cell line to migrate and invade (Yuan *et al.*, 2015). It was therefore useful to visualise MCF-7 cells after treatment with ADSC media from the two patient groups at varying concentrations to ascertain if there was any effect of ADSC CM on the morphology of MCF-7 cells after 24 hours. As previously described (Section 2.14.7) MCF-7 cells that were treated with a range of ADSC CM from two different patient populations were fixed in 4% PFA before being stained with 1 ml of Hoechst working solution before being imaged on the INCELL Analyser 2000. As shown in Figure 4.10 each of the DAPI and Brightfield images captured by the INCELL 2000 were loaded into the CellProfiler™ image analysis software which were then used to calculate nuclear and cellular area and perimeter, solidity, and eccentricity.

At both early and late passage (p2 and p8) there was no statistically significant difference in the area or perimeter of either the MCF-7 cellular area or perimeter, or nuclei area or perimeter, when comparing ADSC CM from either patient group as determined by a two-way ANOVA (Figure 4.11). A Dunnett's multiple comparison test confirmed that there was no statistically significant difference in any of the cellular or nuclear measurement when compared with the 0% control. Similarly cellular eccentricity showed no statistically significant change at early or late passage for either MCF-7 cells treated with ADSC CM from either healthy or cancer patients or when comparing the effect of conditioned media against the 0% control (Figure 4.12).

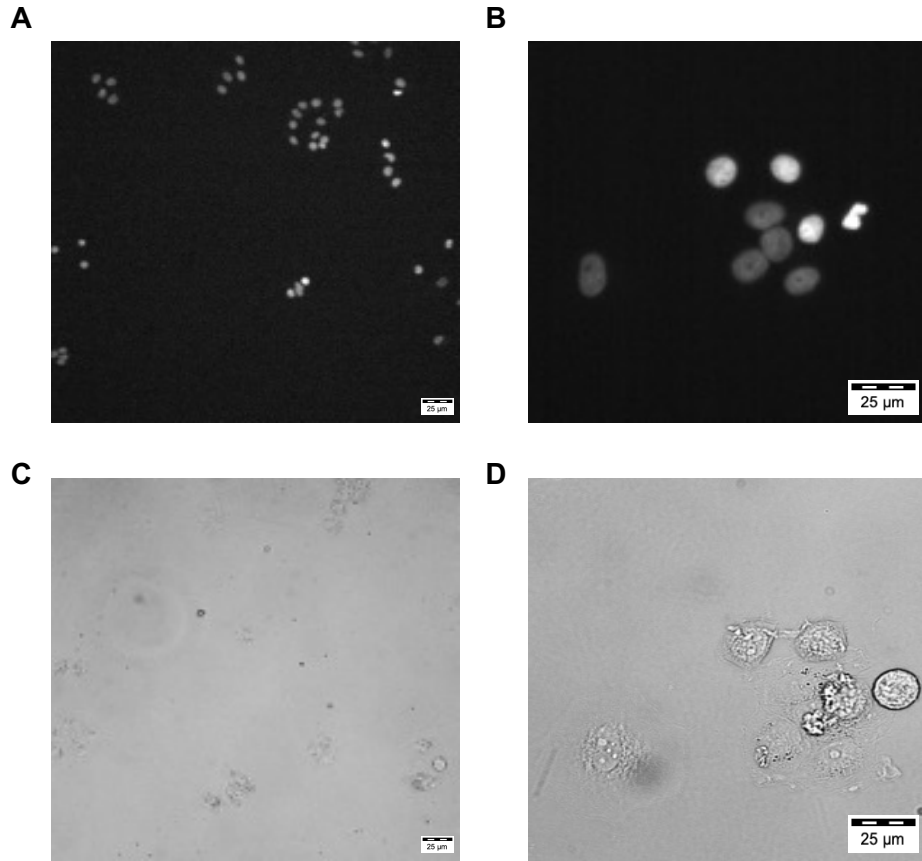


Figure 4.10: MCF-7 Cells imaged with the INCELL 2000 Analyzer (DAPI and Brightfield views).

(A and B) DAPI and (C and D) Brightfield images taken of MCF-7 cells following 24 hours of incubation with healthy ADSC CM (100%). Both the x10 magnification (A and C) and x20 magnification (B and D) allow visualisation of cellular structure, however the 20 times magnification images (B and D) better demonstrate the cellular and nuclear morphology which is comparable to the control group (0% - not shown). Data from n=3 technical replicates of n=6 healthy patients and n=10 cancer patients.

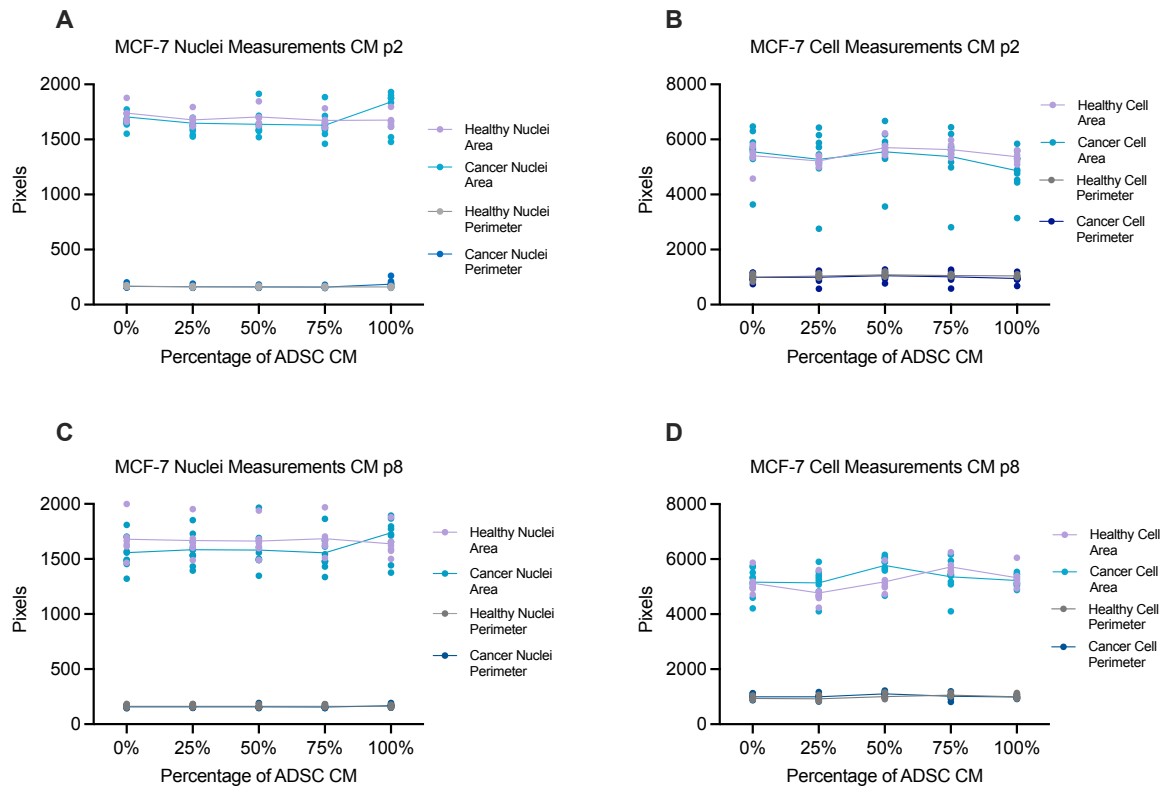


Figure 4.11: MCF-7 cell measurements of both nuclei and cellular morphology demonstrate no change at increasing concentrations of ADSC CM.

Analysis of both MCF-7 nuclei area (A and C) and perimeter (B and D) at both early (A and B) and late (C and D) passage (p2 and p8) demonstrate no statistically significant morphological difference between MCF-7s treated with ADSC CM from either patient group. Data from n=3 technical replicates of n=6 healthy patients and n=10 cancer patients.

Data analysis of the CellProfiler™ results also did not reveal any statistically significant change in MCF-7 nuclear form factor or solidity at either time point (p2 or p8) at any concentration of ADSC CM which was similarly reflected in the lack of statistically significant change observed in cellular solidity (Appendix Two).

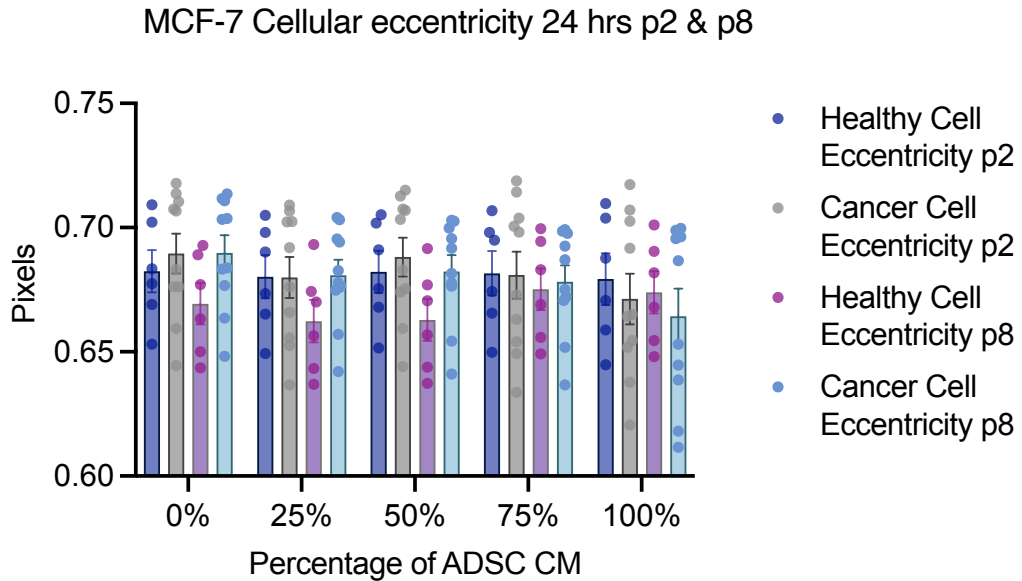


Figure 4.12: MCF-7 cells incubated with ADSC CM for 24 hours demonstrated no change in cellular eccentricity at early or late passage (p2 and p8).

Analysis of MCF-7 cellular eccentricity at both early and late passage (p2 and p8) demonstrate no statistically significant morphological difference between MCF-7s treated with ADSC CM from either patient group. As demonstrated by a two-way ANOVA, each experiment was repeated in triplicate for each biological replicate (n=6 healthy and n=10 cancer).

4.3.5 Increased Concentrations of ADSC CM Increases the Quantity of IL-6, VEG-F and MCP-1 Available to MCF-7 Cells

As previously described in Chapter One, the link between IL-6, EMT induction and angiogenesis is widely discussed and has been shown to play a role in the progression and invasion of ER+ breast cancer. Similarly, ER+ breast cancer relies on pro-angiogenic stimulators such as VEG-F and chemotactic proteins such as MCP-1 to promote migration, growth, and progression. It has previously been demonstrated that there is a statistically significant increase in MCF-7 invasion and proliferation when treated with high concentrations of ADSC CM media from healthy and cancer patients (Figures 4.1, 4.2 and 4.7 - 4.9). It was therefore important to ascertain the indirect effect of different concentrations of ADSC CM from the two patient groups (healthy and cancer) on MCF-7 cytokine and protein production. ADSCs secrete IL-6, MCP-1 and VEG-F at varying concentrations into the media, so quantifying the baseline protein production prior to evaluating MCF-7 response was an important step, to determine if there was any difference between patient groups (Figure 4.13).

By quantifying baseline concentrations in the media, it was possible to determine if the increase in invasion and proliferation were in part because of increased growth factor availability. It was important to also examine the concentrations over time, as a decrease in detectable protein might therefore indicate utilisation by the MCF-7 cells.

The media conditioned by the ADSCs for 24 hours as previously described (Section 2.12) demonstrated a statistically significant difference in baseline IL-6 and MCP-1 production at late passage (p8) as illustrated in Figure 4.13. A two-way ANOVA comparing healthy, and cancer ADSC IL-6 production found a statistically significant increase in IL-6 cytokine quantities produced by the healthy population when compared with the cancer; 2272.94 pg/mL compared with 1037.09 pg/mL (mean \pm SEM) ($p=0.0026$). There was a similar significance between healthy and cancer ADSC MCP-1 production, with the healthy population producing twice as much as the ADSCs derived from cancer patients; 222.015 pg/mL compared with 103.342 pg/mL (mean \pm SEM) ($p=0.0096$). The levels of VEG-F were comparable between both patient groups with no statistically significant difference at either passage. MCF-7 cells were subsequently incubated with ADSC CM from the two patient populations (healthy and cancer) and analysed at both the 4 and 24 hour timepoints as previously described (Section 2.15.1).

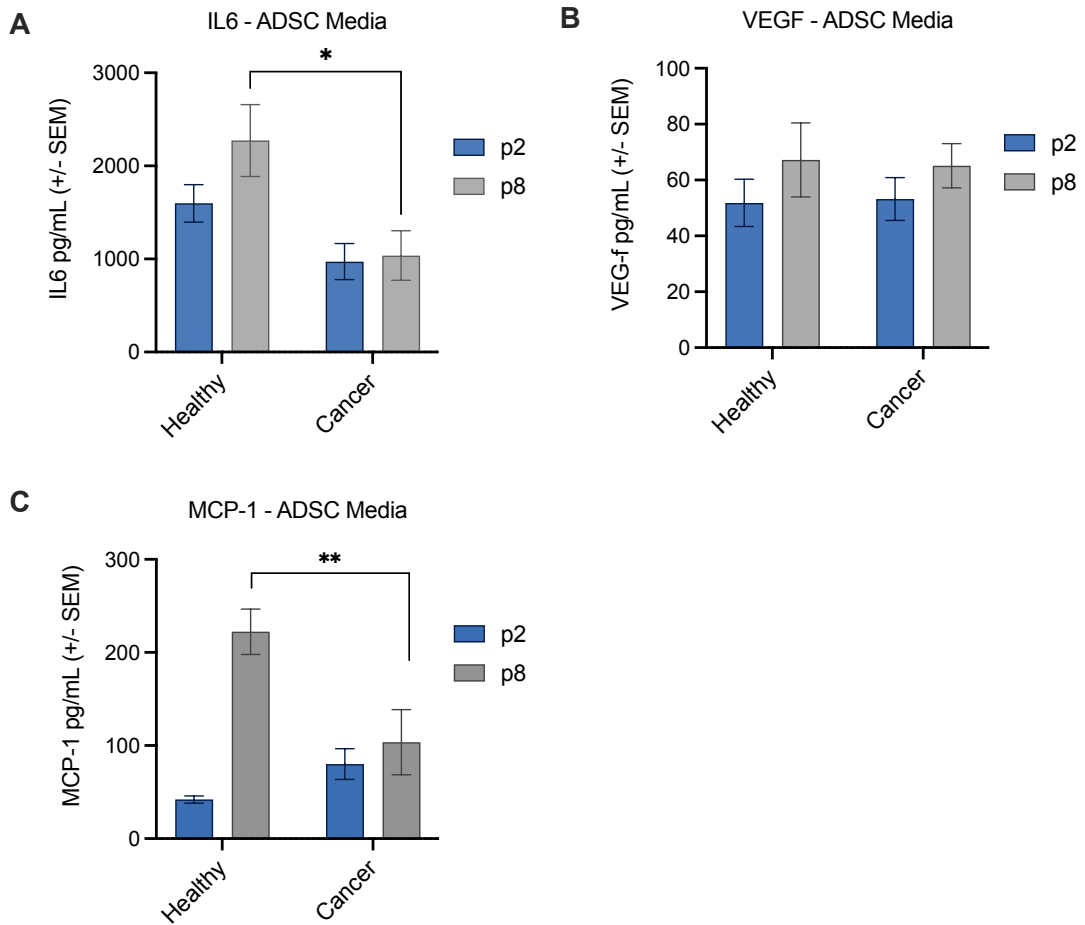


Figure 4.13: ADSCs isolated from healthy patients secrete higher levels of IL-6 and MCP-1 when compared with ADSCs isolated from patient with breast cancer.

(A) There was a statistically significant increase in IL-6 detected in the media of healthy ADSCs after 24 hours when compared with media conditioned by cancer ADSCs at late passage (p8) * $p=0.0026$. (B) There was no statistically significant increase in VEG-F detected in the ADSC media from either the healthy or cancer patient group, at either passage (p2 or p8). (C) There was a statistically significant increase in MCP-1 detected in the media of healthy ADSCs after 24 hours when compared with media conditioned by cancer ADSCs at late passage (p8) ** $p=0.0096$. Results as determined by a two-way ANOVA, data is from technical replicates ($n=3$) from biological replicates ($n=6$ healthy and $n=6$ cancer) with data expressed as mean \pm SEM.

As expected, in the media taken from MCF-7 cells treated with increasing concentrations of ADSC CM from both patient groups, there was an increase in the quantity of IL-6 detected (Figure 4.13), however this appears to be dilutional, rather than being related to a conditioned media effect. The same relationship is observed for both VEG-F (Figure 4.14) and MCP-1 (Figure

4.15), as the media removed from the MCF-7 cells incubated with higher concentrations of ADSC CM shows higher concentrations of detectable protein. While statistically the difference in IL-6, VEG-F and MCP-1 concentrations between 0% and 100% ADSC CM are significant as demonstrated by a two-way ANOVA, there is limited value in analysing the results in this manner. More useful is the observed difference in concentrations of proteins detected over the assay time (4 and 24 hours). During this 20-hour gap, there is a discernible decline in quantities of IL-6 and VEG-F detected in the MCF-7 media (Figure 4.13 and Figure 4.14). This was seen at each concentration of ADSC CM from both patient groups, indicating potential utilisation by the MCF-7 cells.

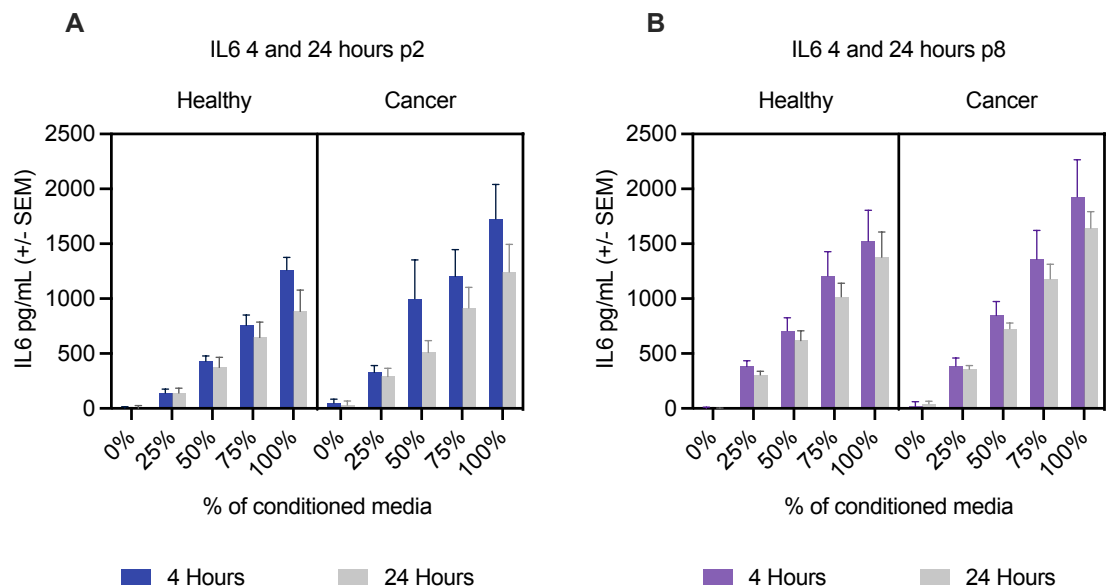


Figure 4.14: Concentrations of IL-6 detected in MCF-7 media are related to percentage of ADSC CM at early and late passage.

Detectable concentrations of IL-6 in the MCF-7 media following treatment with ADSC CM from healthy and cancer patients at early (A) and late (B) passage. There is a dilutional effect of the protein detected, related to percentage of conditioned media being used to treat the MCF-7 cells. Highest concentrations of IL-6 are seen when MCF-7s are treated with 100% ADSC CM (i.e., no dilution), at 4 and 24 hours of MCF-7 contact time with media conditioned by ADSCs from healthy and cancer patients. There is a general decline in quantity detected between the two time points (4 and 24 hours), this is not statistically significant. Data from n=3 technical replicates of n=6 healthy patients and n=10 cancer patients.

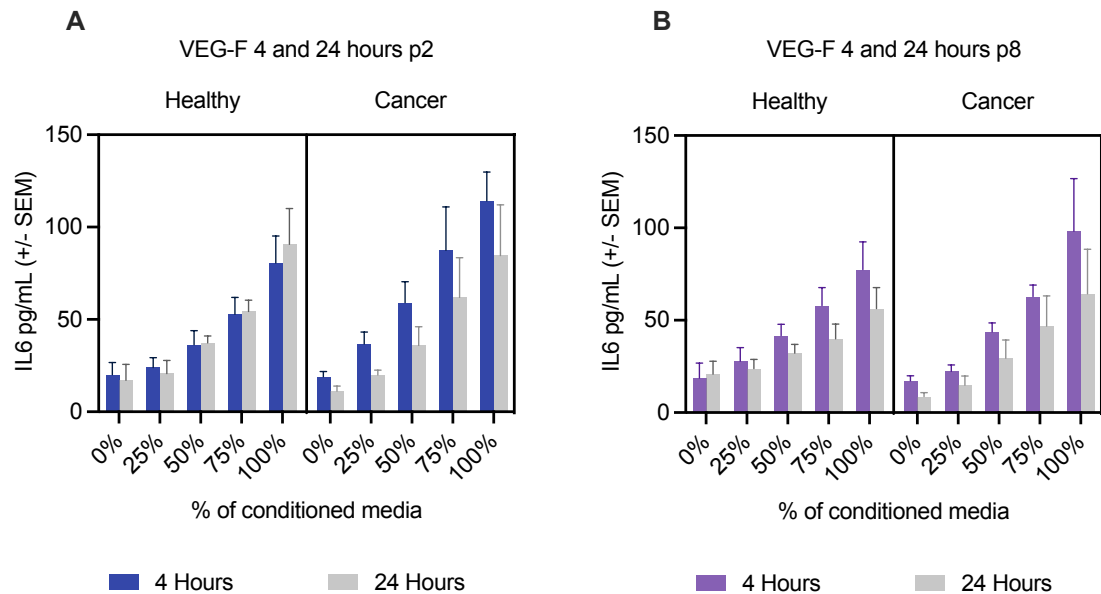


Figure 4.15: Concentrations of VEG-F detected in MCF-7 media are related to percentage of ADSC CM at early and late passage.

Detectable concentrations of VEG-F in the MCF-7 media following treatment with ADSC CM from healthy and cancer patients at early (A) and late (B) passage. There is a dilutional effect of the protein detected, related to percentage of conditioned media being used to treat the MCF-7 cells. Highest concentrations of VEG-F are seen when MCF-7s are treated with 100% ADSC CM (i.e., no dilution), at 4 and 24 hours of MCF-7 contact time with media conditioned by ADSCs from healthy and cancer patients. There is a general decline in quantity detected between the two time points (4 and 24 hours), this is not statistically significant. Data from n=3 technical replicates of n=6 healthy patients and n=10 cancer patients.

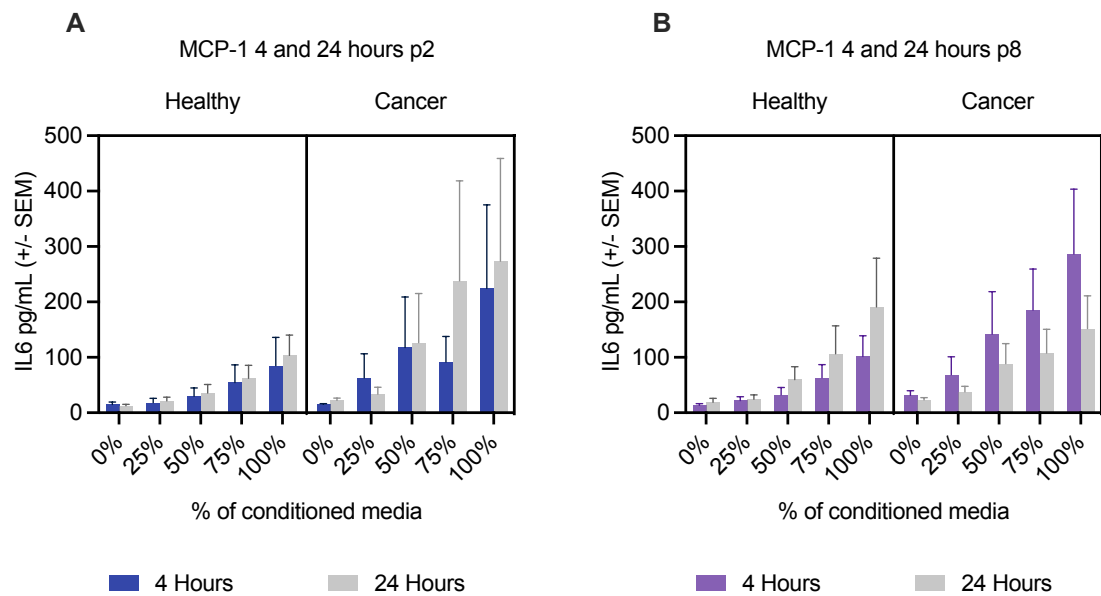


Figure 4.16: Concentrations of MCP-1 detected in MCF-7 media are related to percentage of ADSC CM at early and late passage.

Detectable concentrations of MCP-1 in the MCF-7 media following treatment with ADSC CM from healthy and cancer patients at early (A) and late (B) passage. There is a dilutional effect of the protein detected, related to percentage of conditioned media being used to treat the MCF-7 cells. Highest concentrations of MCP-1 are seen when MCF-7s are treated with 100% ADSC CM (i.e., no dilution), at 4 and 24 hours of MCF-7 contact time with media conditioned by ADSCs from healthy and cancer patients. There is a general decline in quantity detected between the two time points (4 and 24 hours), this is not statistically significant. Data from n=3 technical replicates of n=6 healthy patients and n=10 cancer patients.

The large error bars noted in both VEG-F and MCP-1 concentrations quantified using the ELISA method as previously described (Section 2.15.1) is likely owing to the biological variability of patient samples which has prevented statistical significance being achieved despite a clear visible trend of increased detectable concentrations at higher percentages of CM.

4.4 Discussion

Numerous studies have attempted to recreate components of the breast micro-environment to better understand the complex interplay between ADSCs, the associated extracellular matrix (ECM) and breast cancer (Fujisaki *et al.*, 2015; Teufelsbauer *et al.*, 2019). The use of conditioned media to evaluate the indirect effect prior to co-culture is well described, as this aims to mimic breast cancer response to native ADSCs found within adjacent tissue giving an indication of the indirect biological interaction (Weigand *et al.*, 2016). Much of the foundation underpinning the initial understanding of ADSC characterisation, function and interaction with breast cancer originates primarily from ADSCs isolated from healthy women undergoing cosmetic procedures or routine surgery (Jotzu *et al.*, 2011; D'Esposito *et al.*, 2012; Ning *et al.*, 2014; Koellensperger *et al.*, 2017; Visweswaran *et al.*, 2018; Teufelsbauer *et al.*, 2019; Wu *et al.*, 2019; Garroni *et al.*, 2021). Many of these studies have laid the foundation for much of the expected behaviour between ADSCs and breast cancer cell lines, both indirectly and directly.

As understanding of this unique cell population has developed, there is now a greater acceptance that there may be numerous factors that influence ADSC behaviour and intrinsic function. There has been an increased interest in isolating ADSCs from either tumour adjacent breast parenchyma or distant adipose tissue in women undergoing breast cancer resections to gain a more representative population of MSCs for study (Dieudonne *et al.*, 2002; Weigand *et al.*, 2016; Varghese *et al.*, 2017; Schmid *et al.*, 2018). However, while the choice of patient may have become more clinically representative, sample collection is usually at the time of primary resection and prior to the commencement of any systemic therapy. The extended use of systemic anti-oestrogen receptor antagonists or aromatase inhibitors such as Tamoxifen or Letrozole has the potential to influence the behaviour of the ADSC population within the patient (Pike *et al.*, 2015; Varghese *et al.*, 2017). Numerous factors such as advancing age, smoking status, obesity and additional co-morbidities have been demonstrated to influence the behaviour and function of ADSCs isolated from peripheral adipose tissue (Algire, Medrikova and Herzig, 2013; Aiwei *et al.*, 2015; Barwinska *et al.*, 2018; Kruger *et al.*, 2018; Tsai *et al.*, 2018).

It is therefore prudent to consider the lasting effect that systemic therapies may have on patients ADSCs, and that sample collection timing may need adjustment to ensure the cells isolated are truly representative of the patient population being studied. In view of potential differences between ADSCs isolated from healthy patients with limited co-morbidities and those from women with breast cancer, who have undergone systemic treatment, it is increasingly important to clarify the clinical application of the cell culture model in experimental design. This is partially being addressed in the literature with a broader patient selection and varied anatomical location of MSC harvest being chosen. However, using ADSCs isolated from cancer adjacent tissue can only elucidate the interplay between the complex tumour environment and co-located native breast ADSCs. As a model for post resection and post treatment reconstruction it is limited, not only by anatomical location as it pertains to reconstruction, but by lack of systemic and neoadjuvant treatment exposure.

In addition to cell source, when considering experimental design to ascertain the impact of ADSC CM on MCF-7 cells, precedent is set by numerous studies which describe the use of varying concentrations of CM on the cell population of interest (Trivanović *et al.*, 2014; L. Li *et al.*, 2020). However, as expected there are a number of variations with regards to cell confluence, contact time with the ADSC cells to define the media as conditioned, and a range of processing techniques described prior to its use (Trivanović *et al.*, 2014; Kengelbach-Weigand *et al.*, 2019; Plangger *et al.*, 2021). In addition, it was essential to consider the choice of patients and MSC source to accurately reflect the anatomical region most likely to be used for reconstruction after breast-conserving surgery (BCS). With those factors in mind, the experimental design aimed to reflect the clinical picture as closely as possible with the choice of patient groups (Section 3.3.1) and anatomical harvest site for ADSCs. Similarly, when conditioning the media, balancing ADSC cell confluence, contact time and post conditioning processing alongside timing of use in experiments was carefully considered. Allowing 24 hours for media to condition, removing cellular debris as potential confounders and treating MCF-7 cells in a dose dependant fashion provided a greater level of detail and

significantly more data points. Accepting that there are always opportunities for experimental design development, the rationale behind each choice provides a solid framework for the experimental assays chosen. The data outlined in this chapter primarily serves as a baseline understanding to delineate the indirect impact of ADSC CM from two different patient groups (healthy and breast cancer patients) on the neoplastic traits of MCF-7 growth and progression.

Initially focusing on the assays that established an effect on hallmark measures, there is a significant difference in the rate of proliferation of MCF-7 cells treated with higher concentrations of ADSC CM from healthy patients, when compared with both the control (0%), and ADSC CM from patients with breast cancer. This is demonstrated when comparing rates of proliferation over 48 hours, at both early and late passage (p2 and p8), at all concentrations of conditioned media (25, 50, 75, 100%). As might be expected in the context of the literature, there was a statistically significant increase in the proliferation rate of MCF-7 treated with healthy ADSC CM when compared with the control (0%) ($p \leq 0.0001$). The effect of media conditioned by ADSCs isolated from patient with cancer had a less predictable effect, with an increase in proliferation was only seen in MCF-7s treated at lower concentrations (25 and 50%) and was not demonstrated at higher concentrations (75% and 100%) at either passage (p2 and p8). The influence of ADSC CM from patients with cancer was not as predictable and the difference between the two groups was further highlighted by measuring MCF-7 invasion. At early passage (p2) the increased MCF-7 invasion was noted at higher concentrations of ADSC CM from healthy patients (75 and 100%) ($p < 0.05$). This was more apparent at late passage (p8) across all concentrations (25, 50, 75 and 100%) CM when compared with ADSC CM from cancer patients and the control (0%). While these findings are reflected in the literature with regards to the effects of healthy ADSC CM on breast cancer proliferation and invasion, the lack of effect on invasion and wholly inconsistent effect of the cancer ADSC CM on proliferation is a novel finding (Fujisaki *et al.*, 2015; Teufelsbauer *et al.*, 2019; Plangger *et al.*, 2021).

There are a number of mechanisms theorised to contribute to increased rates of proliferation and invasion, including EMT induction facilitated by increased IL-6 and MCP-1 (Fujisaki *et al.*, 2015; Gallo *et al.*, 2018; Wu *et al.*, 2019). Protein analysis of the ADSC media prior to its use in the CM experiments demonstrated significantly higher quantities of IL-6 and MCP-1 only produced by ADSCs isolated from healthy patients (Figure 4.13). Although there was an increase in the quantity of IL-6 and VEG-F detected when MCF-7 cells were treated with ADSC CM from both patient groups, this appeared to be related to dilution of conditioned media rather than a true effect on the cells. It is therefore potentially more useful to look at the general trend over time with regards to the quantities detected. At both p2 and p8, between the 4 and 24 hour time points, there was a reduction in the levels of all three proteins detected (IL-6, VEG-F and MCP-1). The reduction in cytokine/chemokine levels may have therefore represent utilisation by the MCF-7 cells, which could be viewed in the context of the neoplastic traits of breast cancer previously discussed in Chapter One. As illustrated in Section 1.4.6, IL-6 has been shown to influence epithelial mesenchymal transition (EMT) induction, so increased rates of proliferation and invasion, seen especially in the MCF-7 groups treated with ADSC CM from healthy patients may be in part influenced by this. Further work to explore the influence of ADSC CM on MCF-7 EMT markers (E-cadherin, N-cadherin and Vimentin) utilising qRT-PCR would allow a greater level of understanding as to the influence of ADSC CM on adhesion, invasion and migration of MCF-7 cells, by quantifying key proteins in the context of IL-6 and MCP-1 values detected using ELISA. While beyond the scope of this work, it would be interesting to evaluate in the context of the results and may provide more clarity as to why ADSCs from patients with cancer resulted in more muted effects.

There are however, a number of hallmark measures that were not significantly influenced by the addition of ADSC CM from either healthy or cancer patients. The literature generally indicated, as would be expected given the change in invasion and proliferation, that ADSCs and ADSC CM increases the rate of MCF-7 migration (Yuan *et al.*, 2015; Wu *et al.*, 2019; Garroni *et al.*, 2021). The photographs capturing migration initially appeared to show an increase in gap

closure rate when MCF-7 cells were treated with higher concentrations of healthy ADSC CM (Figure 4.4). When the distances were measured over 48 hours, across all replicates this was not statistically significant, and it would be important to ascertain whether the time points chosen were adequate. More frequent gap closure assessment below 24 hours may have yielded a significant result. It will be important to examine whether a non-contact co-culture model produces comparable results or if the trend that is seen with increased gap closure becomes statistically significant when both cell populations are co-located and able to interact. Similarly, with regards cellular morphology, changes observed in the literature are often as a result of extended treatment with conditioned media or non-contact co-culture, i.e., in excess of 48 hours (Xu *et al.*, 2012; Abramczyk *et al.*, 2015; Lee, Jung and Koo, 2015). MCF-7 morphology remained unchanged regardless of CM concentration or patient population during the brief time period of assessment. This data may therefore simply represent the baseline information against which to measure an effect. Characterisation and extended culture would be required to observe the true impact of ADSC CM on cellular and nuclear morphology. While the rest of the assays were complete within 48 hours, observed changes in cell morphology and structure are more likely to require a greater observation time-period, and the lack of significance does not provide conclusive evidence either way.

This chapter has demonstrated that there is a statistically significant difference between the ADSC CM from healthy and cancer patients and their effects on the neoplastic traits of the MCF-7 cell line. The increased rates of proliferation, invasion and increased concentration of key cytokines not only reflects what is seen in the literature with regards to ADSCs from healthy patients but demonstrate a contrast between the two patient populations. For all assays, it is essential to compare these findings with the effect of co-locating ADSCs, using non-contact co-culture to better understand if there is a component of cell-cell communication not accounted for in these assays. This will also hopefully provide result confirmation, as it would be anticipated that significant changes in cancer traits seen during CM experiments would be reflected in co-culture experiments. The addition of a second ER+ breast cancer cell line

(T47D) also serves as an additional opportunity to ascertain if the results seen with MCF-7s are specific to this line or shared with other lines with a similar hormone profile.

4.4.1 Conclusions

This chapter demonstrates the novel approach to patient selection and emerging differences in the neoplastic traits of MCF-7 cells when treated with varying concentrations of conditioned media from two distinct patient populations (healthy and cancer). Establishing the indirect effect initially has allowed the two patient groups to be compared with the control and with each other across a number of assays designed to measure the neoplastic traits of the MCF-7 cell line. Although the isolation and characterisation of ADSCs as described previously (Section 3.3.1) is comparable, there are key differences emerging between the effects attributed to the patient groups as illustrated by the effect on MCF-7 rates of proliferation and invasion. MCF-7 cells demonstrated increased rates of proliferation at all concentrations of ADSC CM from healthy patients. Whilst this effect was seen in the group treated with ADSC CM from cancer patients, it was less marked and at comparably lower concentrations. The contrast between the two patient populations was more marked when examining MCF-7 invasion. At both early and late passage only ADSC CM from healthy patients had any effect on invasion, compared with the control. This clear difference in results is attributed to the patient selection and intrinsic difference between the ADSC populations isolated. The focus of the next phase of experiments was to ascertain whether these findings are reflected in co-culture models when there is an opportunity for the two cell populations to influence each other.

Chapter Five

Using Non-Contact Co-Culture to Evaluate the Effect of Co-Locating ADSCs From Healthy and Cancer Patients on the Neoplastic Traits of MCF-7 and T47D Cell Lines

5.1 Introduction

As discussed in Chapter Four, there are differences emerging in the effect of ADSCs isolated from patients with cancer, on the neoplastic traits of MCF-7 cells, when compared to their healthy counterparts. Media conditioned by ADSCs isolated from cancer patients, failed to produce comparable effects on the rate of MCF-7 proliferation and invasion, when compared with conditioned media from healthy ADSCs. Building on this foundation, using non-contact co-culture models provides an opportunity to interrogate the effect, that co-locating ADSCs isolated from healthy and cancer patients, has on the hallmark traits of ER+ breast cancer. Evaluating the effects of co-locating ADSCs on ER+ breast cancer lines utilising co-culture, has previously been described as an essential part of experimental modelling (Yu *et al.*, 2008; Xu *et al.*, 2012; Fujisaki *et al.*, 2015; Wu *et al.*, 2019). The use of non-contact co-culture systems to measure the effect of ADSCs on a range of cancer cell lines is well established (Heneweer *et al.*, 2005; Strassburg *et al.*, 2016; Koellensperger *et al.*, 2017; Preisner *et al.*, 2018b). Unlike the conditioned media experiments detailed in Chapter Three, non-contact co-culture models allow for the diffusion of secreted cytokines and signalling proteins, providing the opportunity to measure real-time cell-cell interaction. As discussed in Chapter One, the use of the MCF-7 cell line is clinically representative enabling findings to be directly compared with a significant proportion of the scientific literature. However, utilising a second ER+ cell line with comparable hormone receptors (T47D) enables key hallmark measures to be validated (Holliday and Speirs, 2011; Aiwei *et al.*, 2015; Fujisaki *et al.*, 2015; Gao *et al.*, 2019). This provides a further opportunity to ascertain whether effects observed are cell line specific, or more widely related to the ER+ receptor status. Analogous findings in both the MCF-7 and T47D cell lines would be expected in a cell-model which was clinically representative.

5.1.1 Chapter Aims

The aim of this chapter is to evaluate the effect of co-locating ADSCs isolated from healthy and cancer patients on the neoplastic traits of MCF-7 and T47D breast cancer cell lines utilising non-contact co-culture.

This will be achieved by meeting the objectives below:

1. Determine the effect of co-locating ADSCs isolated from healthy and cancer patients on the neoplastic traits of MCF-7 and T47D cancer growth and progression to include:
 - a. Proliferation (MCF-7 and T47D)
 - b. Migration (MCF-7 and T47D)
 - c. Invasion (MCF-7 and T47D)
 - d. Morphology (MCF-7)
 - e. Cytokine/Chemokine expression Profiles (MCF-7)
 - f. Bioenergetics (MCF-7 and T47D)

2. Determine if there are any differences in the effects of ADSCs from each patient group (healthy and cancer) on MCF-7 and T47D cancer growth and progression.

5.2 Methods

5.2.1 Sample Collection

As described previously (Section 2.7), samples were collected from two patient groups. Sample collection was completed as described in Chapter Two (section 2.4). Patients used in the co-culture work include ADSC005, 011, 012, 020, 021 and 022, which were healthy women who had never had cancer. ADSC 008, 009, 010, 017, 018 and 019, which were women diagnosed with ER+ breast cancer currently on systemic hormone therapy.

5.2.2 ADSC Isolation and Characterisation

As previously described (Section 2.7.1), ADSCs were isolated using the chosen protocol (Zuk *et al.*, 2001) and characterised using the fluorophore panel previously noted (Section 2.10) at late passage (p8) to ensure MSC potential was maintained prior to use in the experiments. Downstream analysis of flow cytometry was performed using FlowJo version 1.3 (Oregon, USA).

5.2.3 MCF-7 Cell line

Authenticated breast cancer MCF-7 cells were obtained from ATCC and cultured in standard conditions and passaged when 80% confluent as mentioned in Chapter Two (Section 2.6).

5.2.4 T47D Cell line

Authenticated breast cancer T47D cells were obtained from ATCC and cultured in standard conditions and passaged when 80% confluent as mentioned in Chapter Two (Section 2.6).

5.2.5 Tissue Culture

As previously described in Section 2.6, the cell lines (MCF-7 and T47D) and primary cells (ADSCs) were cultured in standard culture conditions, and maintained at 37°C, 5% CO₂ throughout. ADSCs were all grown to 70% confluence before being passaged as described in Section 2.7 and both ADSCs, MCF-7s and T47Ds were cultured for 14 days prior to any use in experimentation once removed from liquid nitrogen (Section 2.9).

5.2.6 Cell Counting

Cell counting and viability were calculated using the Countess™ automated cell counter (Life Technologies, UK) as described in the methods (Section 2.8). The total live cell count (via trypan blue exclusion) was used for downstream experimentation inclusive of applicable dilution factor.

5.2.7 Co-Culture Inserts

As previously described in Section 2.13 ADSCs from healthy and cancer patients were seeded into the appropriate 0.4µm transwell insert at the timings specified for use in the experiments. Unless otherwise stated, data shown is from technical replicates (n=3) at late passage (p8) across separate experiments with patients taken from two patient groups (healthy n=6 and cancer n=6) with an internal control and data is expressed as the mean ± SEM.

5.2.8 Proliferation

To determine whether ER+ breast cancer (MCF-7 and T47D) proliferated differently when co-cultured with ADSCs isolated from patients with and without breast cancer, EL-16 transwell inserts were used to create non-contact co-culture models and enable continuous measurement of proliferation using a real time cellular impedance assay. Rates of proliferation of both MCF-7 and T47D cells were measured continuously using the RTCA iCELLigence instrument (ACEA Bioscience, UK now part of Agilent, UK) as described in methods Section 2.14.2 with experiments performed in triplicate at late (p8) passage and values were expressed as cell index (CI).

5.2.9 Migration

As described in Chapter Two (Section 2.14.4), an IBIDI insert was used to create a standardised 500 µm gap prior to the transfer of the transwell co-culture insert. Serial photographs were then used over the next 48 hours to observe the rate of gap closure, and the experiment was performed in triplicate at late passage (p8), with results displayed as gap remaining and rate of gap closure.

5.2.10 Invasion

The effect of non-contact co-culture of MCF-7 and T47D with ADSCs from healthy and cancer patients was conducted using the Collagen Invasion Assay as described (Section 2.14.6). This experiment was performed at late passage (p8) and repeated in triplicate. Following the stain and extraction protocol described in Section 2.14.6, results were measured as absorbance at 560 nm using a microplate reader (POLARstar Omega, BMG Labtech, Germany).

5.2.11 Bioenergetics

Metabolic analysis of MCF-7 and T47D cells were carried out using the Seahorse XFe24 analyser (Seahorse Bioscience, USA) as described in Section 2.16. Both ECAR and OCR measurement were performed for MCF-7 and T47D cells using an adherent cell monolayer within a transient micro chamber. The experiment was performed at late passage (p8) and the experiment was repeated in triplicate with an internal control.

5.2.12 Morphology

Morphological changes to the cell or nucleus were measured as detailed in Section 2.14.8, with MCF-7 cells co-cultured with ADSCs from healthy and cancer patients, suspended in 0.4 µm transwell inserts at late passage (p8). Plates were read on the INCELL Analyser 2000 which took a series of 300 photographs (fields of view) from each well for analysis.

5.2.13 Cytokine/Chemokine Expression Profiles

The measurements of the three specific proteins that had been identified (IL-6, VEG-F, and MCP-1), from the cell free culture media was performed using the sandwich ELISA technique as described in Section 2.15.2. Media was harvested from MCF-7 cells at 4 hours and 24 hours following non-contact co-culture with ADSCs from both patient groups (healthy and cancer) at late (p8) passage. Final plates were read at 450 nm using a plate reader (POLARstar Omega, Germany) and analysed as outlined in Section 2.17.4.

5.2.14 Data Analysis

5.2.14.1 Proliferation

Statistical analysis was performed as described in Section 2.17.1. A two-way ANOVA was used to compare proliferation of ADSCs co-cultured with either MCF-7 and T47D, from both patient groups (healthy and cancer) against the control. All experiments were replicated in triplicate across both patient groups (MCF-7 n=6 healthy, n=6 cancer and T47D n=3 healthy, n=3 cancer) and a Dunnett's multiple comparison test was applied. Adhesion was calculated as the change in cell index divided by the change in time ($\Delta CI/\Delta T$) and a two-way ANOVA with multiple comparison tests was applied. Significant values were taken as $p < 0.05$ graphically denoted as * $p \leq 0.05$, ** $p \leq 0.01$, *** $p \leq 0.001$, **** $p \leq 0.0001$.

5.2.14.2 Migration

Images were analysed as described in Section 2.17.2. Statistical analysis was performed using GraphPad Prism version 9.1.0, after exporting the file into RTCA Data Analysis Software 1.0 (ACEA Bioscience, UK). A two-way ANOVA was used to compare different co-culture conditions against the control across both patient groups (healthy and cancer). All experiments were repeated in triplicate at late (p8) passage.

5.2.14.3 Invasion

Data quantified using extracted stain as previously described in the methods (Section 2.14.6). Statistical analysis was performed as described in Section 2.17.3. A two-way ANOVA was used to compare different co-culture conditions against the control across both patient groups (healthy and cancer). Data shown is from technical replicates (n=3) at late passage (p8) across separate experiments with patients taken from two patient groups (healthy n=6 and cancer n=6) and data is expressed as the mean \pm SEM.

5.2.14.4 Bioenergetics

Metabolic analysis of MCF-7 and T47D cells was carried out as described in Section 2.17.6. using the Seahorse Extracellular Flux Analyzer XFe24

(Seahorse Bioscience) as described in the methods (Section 2.16). Statistical analysis was performed using GraphPad Prism version 9.1.0 and data shown is from technical replicates (n=3) at one time point (p8) across separate experiments with patients taken from two patient groups (healthy n=6 and cancer n=6) with data expressed as the mean \pm SEM.

5.2.14.5 Morphology

Data was generated as described in Section 2.17.5, and statistical analysis performed using GraphPad Prism version 9.1.0 to compare the effects of non-contact co-culture of ADSCs from the two patient populations on the morphology of MCF-7 cells. A two-way ANOVA was used, with data from technical replicates (n=3) at p8 across separate experiments with patients taken from two patient groups (healthy n=6 and cancer n=6) and data is expressed as the mean \pm SEM.

5.2.14.6 Cytokine Expression Profiles

Statistical analysis was performed as described in Section 2.17.4 using GraphPad Prism version 9.1.0. A two-way ANOVA was used to compare the concentrations of different detected proteins in the media against the control. Significant values were taken as $p < 0.05$ graphically denoted as * $p \leq 0.05$, ** $p \leq 0.01$, *** $p \leq 0.001$ and **** $p \leq 0.0001$.

5.3 Results

Building on the conditioned media experiments (see Chapter Four), it was important to assess the effect of co-locating ADSCs and ER+ breast cancer cell lines by utilising a non-contact co-culture model. ADSCs from two patient populations (healthy and cancer) were co-cultured with either MCF-7 or T47D cell lines to assess the effect the adult MSC population had on the neoplastic traits of cancer growth and progression. This was the second part of the cell-based model to examine the reciprocal effects of ADSCs from different patient groups and ER+ breast cancer cell lines.

5.3.1 Co-Culturing MCF-7 Cells with ADSCs Isolated from Healthy Patients Significantly Increases the Rate of MCF-7 Proliferation

To establish the effects of ADSCs isolated from both healthy and cancer patients on the proliferation of MCF-7 cells a non-contact co-culture model was used to study the reciprocal effects. The transwell insert enabled cell-cell interaction whilst allowing continuous monitoring the MCF-7 cell line. There was a control for each experimental replicate with proliferation and maximum cell index evaluated using the automated and continuous ACEA Biosciences iCELLigence system as previously described (Section 2.14.2). This was done at late (p8) passage and real time analysis was performed continuously for 48 hours by measuring the change in electrical impedance on the bottom of each well with increasing cell index values indicating an increase in cell number and density (Figure 5.1). Cell adhesion was then defined as the change in cell index divided by the change in time ($\Delta CI/\Delta T$) to provide an indicator of the rate of adhesion to the bottom of the EL-8 plate within the first 120 minutes (Figure 5.2). Comparing the two patient groups, there is a significant increase in the rate of proliferation of MCF-7 cells co-cultured with ADSCs isolated from healthy patients versus those with cancer and the control (** $p \leq 0.01$) (Figure 5.1). This is more visually apparent when examining the rate of proliferation over the first 24 hours as illustrated in Figure 5.1, image B.

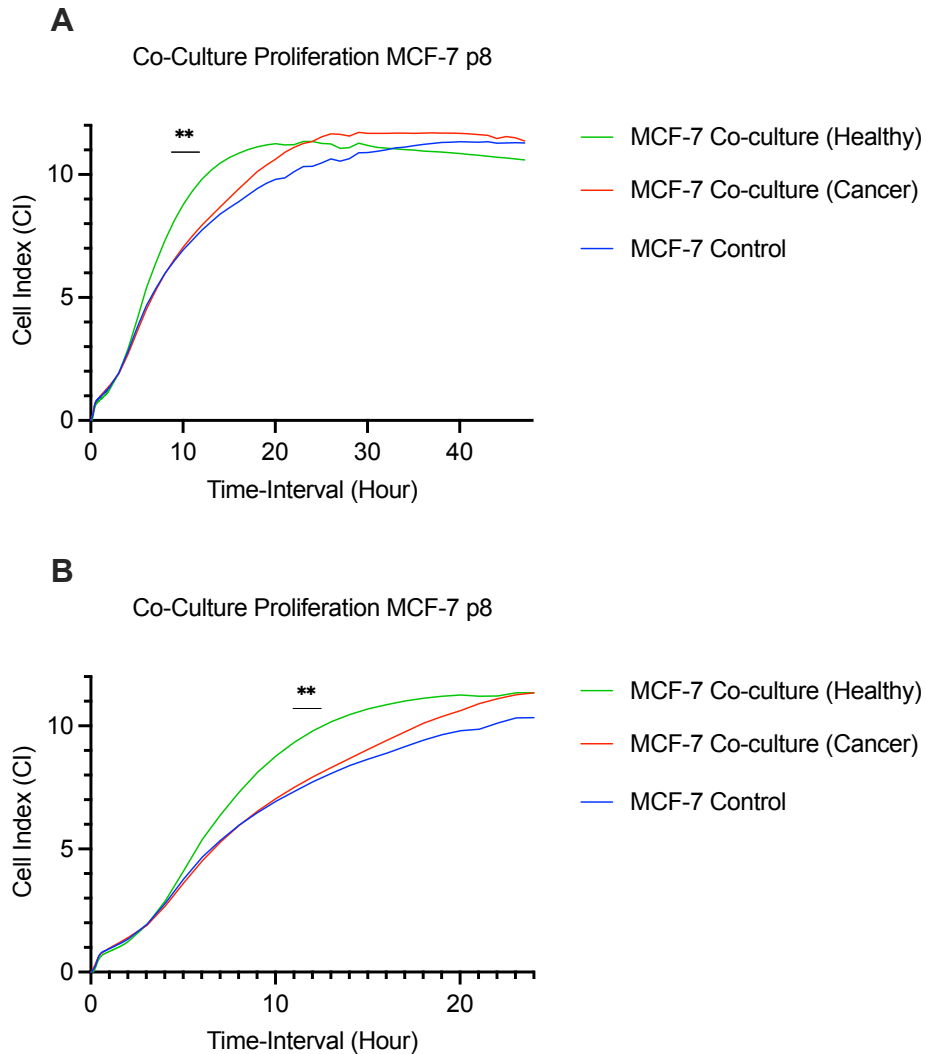


Figure 5.1: MCF-7 cells co-cultured with ADSCs isolated from healthy patients proliferate at an increased rate when compared with ADSCs isolated from patients with cancer.

(A) MCF-7 proliferation over 48 hours, co-cultured with ADSCs from healthy patients (n=6), patients with breast cancer (n=6) or on their own as a control. (B) MCF-7 proliferation over the first 24 hours of the same three MCF-7 conditions to provide additional detail in the differences in rates of proliferation. As demonstrated in both A and B, there is a statistically significant increase in the rate of proliferation noted (green graph) in the MCF-7 population that is co-cultured with ADSCs isolated from healthy patients compared with the control $**p \leq 0.01$. There is no significant difference between the MCF-7 population co-cultured with ADSCs isolated from patients with breast cancer and the control. Statistical significance comparing proliferation to the control was evaluated using a one-way ANOVA. Data from n=3 technical replicates of n=6 healthy patients and n=6 cancer patients.

Cell adhesion is defined as the change in cell index divided by the change in time ($\Delta CI/\Delta T$). This was measured using readings taken at regular intervals, every 60 seconds for the first 120 minutes of the experiment. As previously

described (Section 2.14.2), the readings commence immediately after the EL-8 plate is placed back into the iCELLigence reader and the experiment is initiated. The electrical impedance increases as more cells adhere to the uncoated well surface and reduce the rate of signal conduction. A higher cell index value signifying that an increased number of cells have adhered to the well within the first two hours, providing an indicator as to the rate of MCF-7 adhesion. MCF-7 cells co-cultured with healthy ADSCs only adhered at a slower rate within the first two hours when compared with the control (Figure 5.2) which was statistically significant ($*p<0.05$).

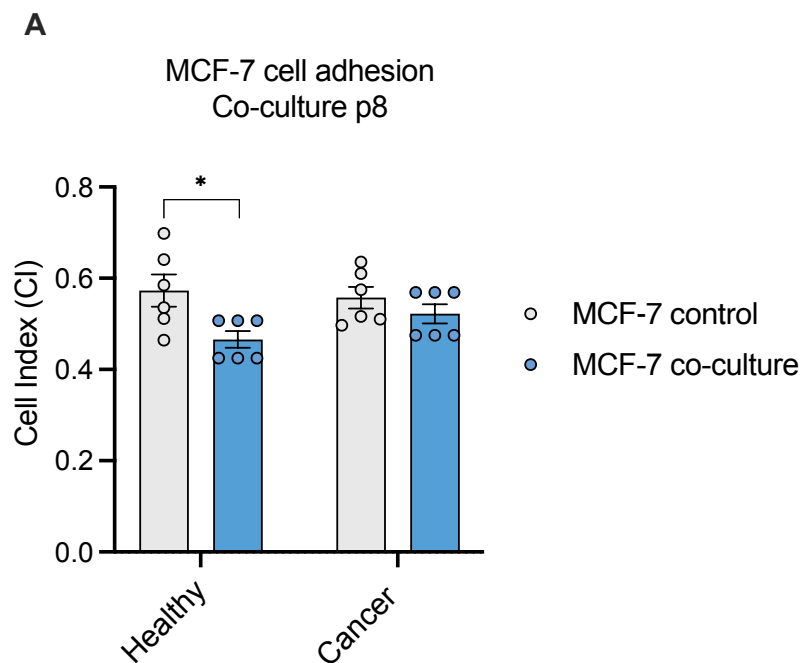


Figure 5.2: MCF-7 cells co-cultured with ADSCs isolated from healthy patients are less adherent in cell culture compared with the control.

(A) MCF-7 cells co-cultured with healthy patients (n=6) are less adherent, as demonstrated by the CI after 120 minutes, when compare with the control. There is no difference in the adhesion noted in the MCF-7 cells co-cultured with ADSCs isolated from patients with cancer (n=6) when compared with the control. $*p<0.05$ Statistical significance comparing proliferation to the control was evaluated using a two-way ANOVA. Data from n=3 technical replicates.

5.3.2 Co-Culturing T47D Cells with ADSCs Isolated from Healthy Patients and Patients with Cancer Significantly Increases the Rate of T47D Proliferation

To establish the effects of ADSCs isolated from both healthy and cancer patients on the proliferation of T47D cells a non-contact co-culture model was used to study the reciprocal effects. The transwell insert enabled cell-cell interaction whilst allowing continuous monitoring of the T47D cell line, and enabled comparison with the MCF-7 results. As with the MCF-7 experiment, there was a control for each experimental replicate with proliferation and maximum cell index evaluated using the automated and continuous ACEA Biosciences iCELLigence system as previously described (Section 2.14.2). This was done at late (p8) passage and real time analysis was performed continuously for 48 hours by measuring the change in electrical impedance on the bottom of each well with increasing cell index values indicating an increase in cell number and density (Figure 5.3). Cell adhesion was then defined as the change in cell index divided by the change in time ($\Delta CI/\Delta T$) to provide an indicator of the rate of adhesion to the bottom of the EL-8 plate within the first 120 minutes (Figure 5.4). Comparing the two patient groups, there is a significant increase in the rate of proliferation of T47D cells co-cultured with both ADSCs isolated from healthy patients (n=3) and cancer patients (n=3) versus the control (****p \leq 0.0001). This is more visually apparent when examining the rate of proliferation over the first 24 hours as illustrated in Figure 5.3, image B.

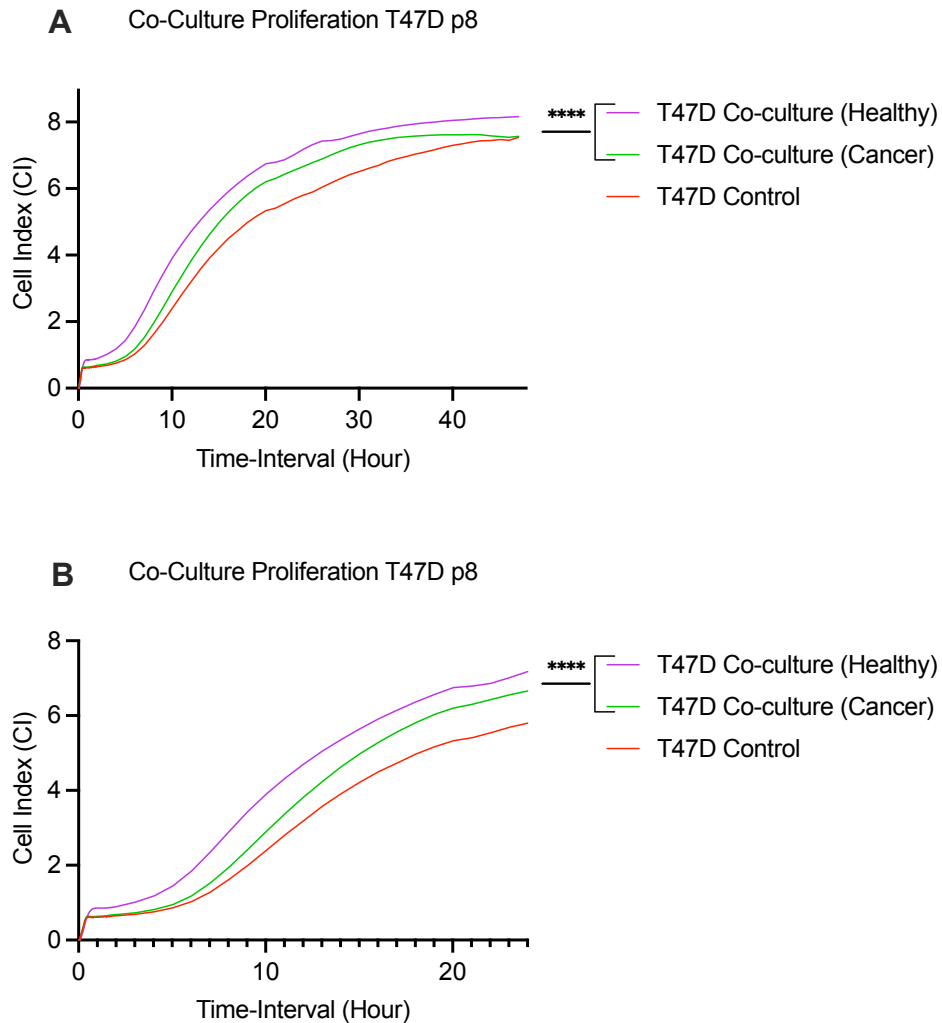


Figure 5.3: T47D cells co-cultured with ADSCs isolated from healthy and cancer patients proliferate at an increased rate when compared with the control.

(A) T47D proliferation over 48 hours, co-cultured with ADSCs from healthy patients (n=3), patients with breast cancer (n=3) or on their own as a control. (B) T47D proliferation over the first 24 hours of the same three T47D conditions to provide additional detail in the differences in rates of proliferation. As demonstrated in both A and B, there is a statistically significant increase in the rate of proliferation noted in the T47D population that is co-cultured with ADSCs isolated from healthy patients and from patients with cancer when compared with the control **** $p \leq 0.0001$. Statistical significance comparing proliferation to the control was evaluated using a one-way ANOVA. Data from n=3 technical replicates.

As seen with the MCF-7 co-culture experiments, there was a significant change in the rate of T47D cell adhesion within the first 120 minutes only when the cell line was co-cultured with ADSCs isolated from healthy patients (Figure 5.4). The higher CI value within the control population demonstrating an

increased number of cells adhering to the well within the two hours after the experiment was commenced. This clearly demonstrates that T47D cells exhibited reduced adherence following co-culture, a comparable finding across both ER+ cell lines.

A

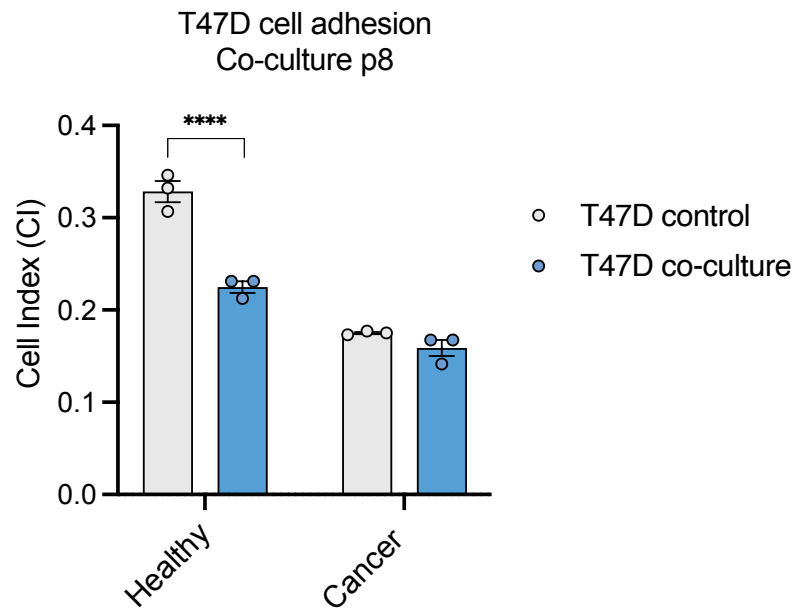


Figure 5.4: T47D cells co-cultured with ADSCs isolated from healthy patients are less adherent in cell culture compared with the control.

(A) T47D cells co-cultured with healthy patients (n=3) are less adherent, as demonstrated by the CI after 120 minutes, when compared with the control. There is no difference in the adhesion noted in the T47D cells co-cultured with ADSCs isolated from patients with cancer (n=3) when compared with the control. **** $p \leq 0.0001$ Statistical significance comparing proliferation to the control was evaluated using a two-way ANOVA. Data from n=3 technical replicates.

5.3.3 Co-Culturing MCF-7 Cells with ADSCs Isolated from Healthy Patients Significantly Increases the Rate of MCF-7 Migration

It was important to ascertain if there were any effects on the rate of MCF-7 migration when co-cultured with ADSCs from either patient group (healthy and cancer) as the experiment in Chapter Four (Section 4.3.2) highlighted a potential limitation regarding time points observed. As previously described (Section 2.14.4), the IBIDI cell culture inserts were used to create a standardised 500 μm gap that was then monitored with serial photographs

over 48 hours after commencing the experiment. A transwell co-culture insert seeded with ADSCs isolated from either healthy (n=6) or cancer patients (n=6) were suspended over the MCF-7 cells to allow cell-cell interaction whilst maintaining the ability to monitor the gap on the bottom of the well. For each patient there was a control, and the experiment was repeated in triplicate at late passage (p8) to enable a difference in migration to be evaluated. The rate of gap closure was measured and a visual difference in MCF-7 migration was observed only in the group co-cultured with ADSCs isolated from healthy patients (Figure 5.5). The complete closure of the gap after 24 hours was apparent from the photographic analysis, and this was statistically significant when analysing all replicates across both patient groups with the associated controls as calculated using a two-way ANOVA * $p \leq 0.05$, *** $p \leq 0.001$ (Figure 5.6).

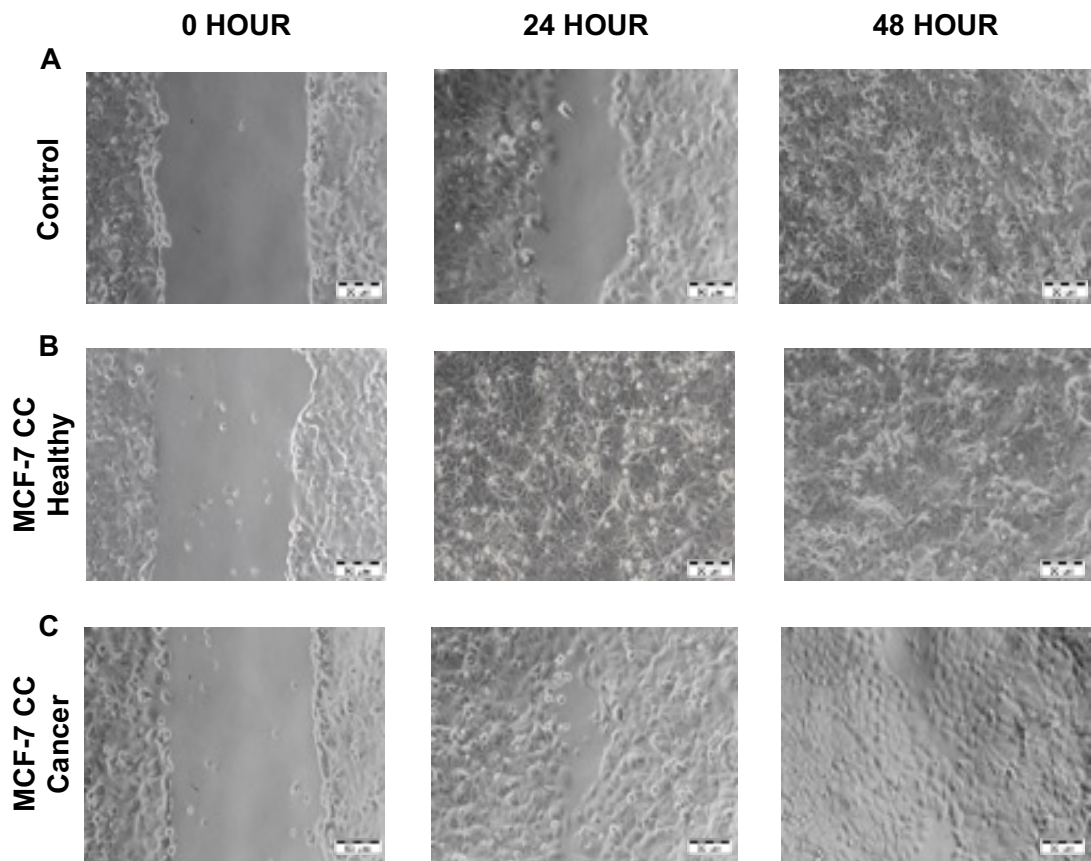


Figure 5.5: MCF-7 cells demonstrate increased migration when co-cultured with ADSCs isolated from healthy patients.

Images taken over 48 hours at x10 magnification on a light microscope (Zeiss, Axiovert 40C) of (A) the MCF-7 control, (B) MCF-7 cells co-cultured with ADSCs isolated from a healthy patient and (C) MCF-7 cells co-cultured with ADSCs from a patient with breast cancer. The 500 μm gap is closed within the first 24 hours when MCF-7 cells are co-cultured with ADSCs isolated from healthy patients (B). While all three are closed at 48 hours, the closure at 24 hours is statistically significant (see next figure) when compared with the control (A) and with ADSCs isolated from patients with breast cancer (C). The experiment was repeated in triplicate, at late passage (p8) with ADSCs isolated from healthy (n=6) and breast cancer (n=6) patients.

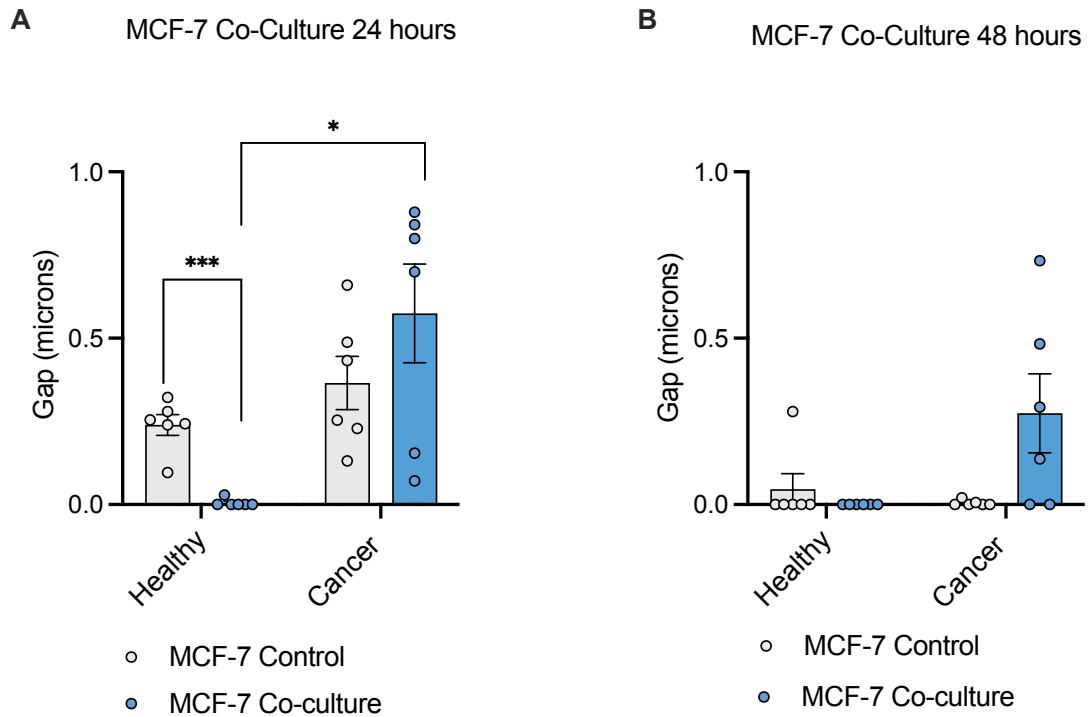


Figure 5.6: MCF-7 cells co-cultured with ADSCs isolated from healthy patients demonstrate an increased rate of migration.

Gap remaining following removal of the IBIDI insert and co-culture of MCF-7s with ADSCs from both healthy and cancer patients at 24 hours (A) and 48 hours (B). As demonstrated visually in Figure 5.7, the obliteration of the gap at 24 hours is statistically significant as demonstrated by a two-way ANOVA * $p \leq 0.05$, *** $p \leq 0.001$. (A) MCF-7 migration when co-cultured with healthy ADSCs is significantly increased compared with both the control group ($p=0.0006$) and with the MCF-7s co-cultured with ADSCs isolated from patients with breast cancer ($p=0.0177$). Data is shown from technical replicates ($n=3$) at late passage (p8) from two patient groups ($n=6$ healthy and $n=6$ cancer) and data is expressed as the mean \pm SEM.

5.3.4 Co-Culturing T47D Cells with ADSCs from Healthy and Cancer Patients Does Not Significantly Affect the Rate of Migration

It was important to ascertain the effect of non-contact co-culture with ADSCs from various patient groups on T47D migration as a comparison to the findings noted with the MCF-7 cell line. As described previously (Section 2.14.4) and as with the MCF-7 experiments, an IBIDI insert was used to create a standardised 500 μm gap that was monitored using serial photographs over 48 hours. The gap was repeatedly measured at set intervals using Image J to ascertain the gap remaining and quantify the percentage by which the gap had been narrowed. The rate of T47D migration was visually slower in comparison

to the MCF-7 cell line (Figure 5.7) across all conditions and neither the photographs nor image analysis demonstrate any significance as determined by a two-way ANOVA (Figure 5.8). The experiment was repeated in triplicate, at late passage (p8) across two patient groups (healthy n=3 and cancer n=3), with a control (no co-culture).

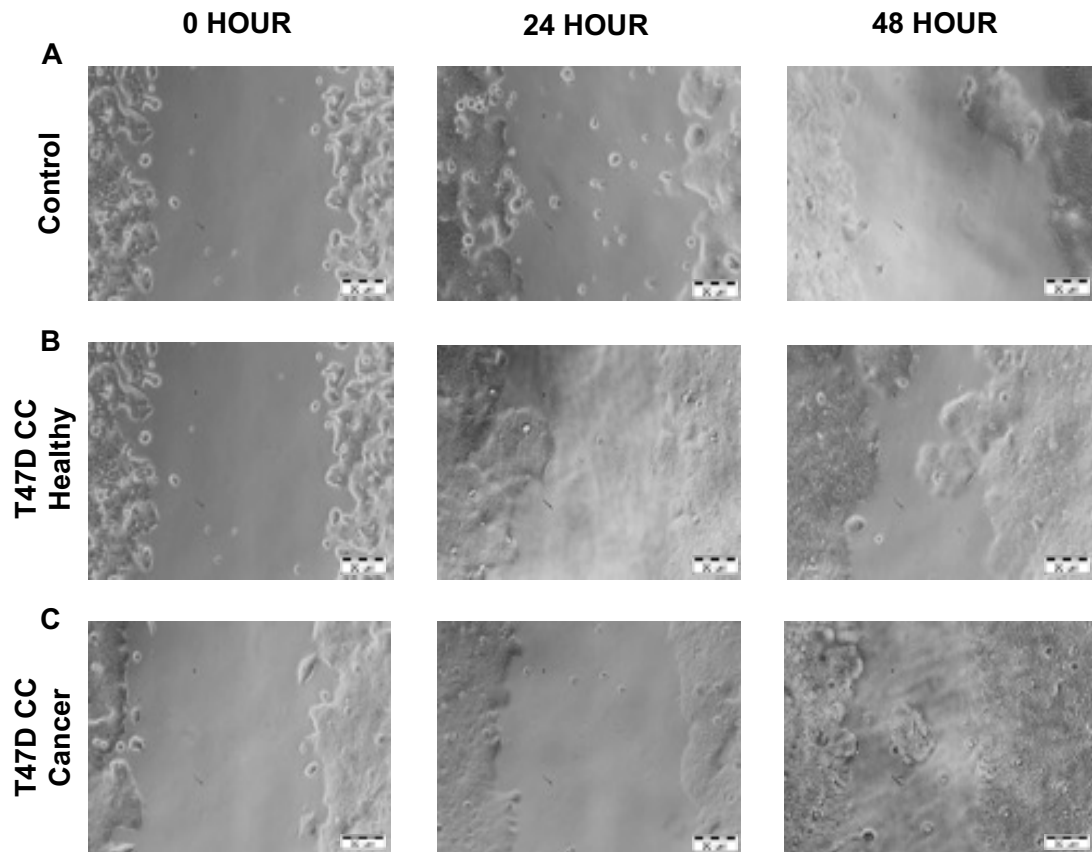


Figure 5.7: There is no change in T47D migration observed when cells are co-cultured with ADSCs from either healthy or cancer patients.

Images taken over 48 hours at x10 magnification on a light microscope (Zeiss, Axiovert 40C) of T47D cells co-cultured with ADSCs isolated from a healthy patient (B), patient with breast cancer (C) and the control (A). There is a gap visible at all time points (0, 24 and 48 hours) and all co-culture and control conditions. The experiment was repeated in triplicate, at late passage (p8) with ADSCs isolated from healthy (n=3) and breast cancer (n=3) patients.

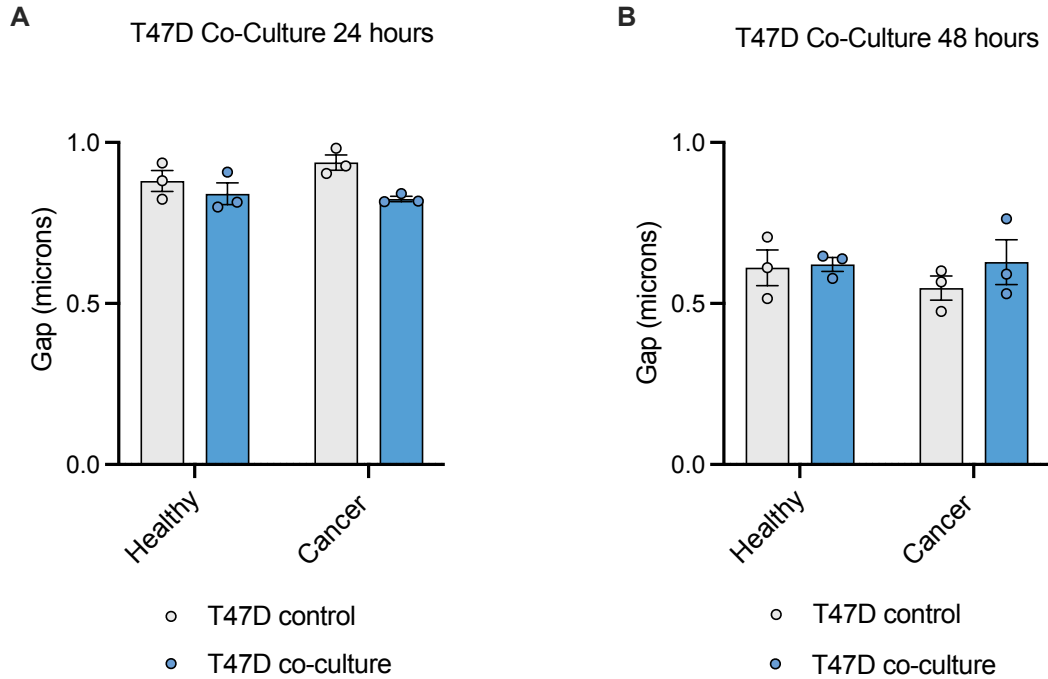


Figure 5.8: There is no change in T47D migration observed when cells are co-cultured with ADSCs from either healthy or cancer patients.

Gap remaining following removal of the IBIDI insert and co-culture of T47D with ADSCs from both healthy and cancer patients at 24 hours (A) and 48 hours (B). As demonstrated visually in Figure 5.9, the gap remains after 48 hours in all three groups and none of them were statistically significant. Data is shown from technical replicates (n=3) at late passage (p8) from two patient groups (n=3 healthy and n=3 cancer) and data is expressed as the mean \pm SEM.

5.3.5 Co-Culturing MCF-7 Cells with ADSCs Isolated from Healthy Patients, Significantly Increases the Rate of Invasion

It was important to understand if the effects noted during the conditioned media experiments (Section 4.3.3) were reflected in the non-contact co-culture model, as invasion through the basement membrane is a defining cancer hallmark (Hanahan and Weinberg, 2011; Jiang *et al.*, 2015). Utilising the non-contact co-culture model enabled the non-contact cell-cell interaction between ADSCs from two patient groups to be evaluated determining if there was any change in the rate of MCF-7 invasion at late passage (p8). As previously described (Section 2.14.6), the use of a collagen insert served as a surrogate for human basement membrane seeded above ADSCs isolated from healthy and cancer patients to enable non-contact, cell-cell interaction and allowing the effect on invasion to be quantified. As shown in Figure 5.9, only MCF-7s

co-cultured with ADSCs isolated from healthy patients demonstrated statistically significant increases in invasion when compared with the control ($p < 0.0001$) as determined by a two-way ANOVA (healthy $n=6$, cancer $n=6$). This is similarly reflected in the times ten magnification images captured with the light microscope of the stained collagen inserts at p8 (Figure 5.10) showing an increase in the number of MCF-7 cells invading into the membrane when co-cultured with ADSCs from cancer patients and the control.

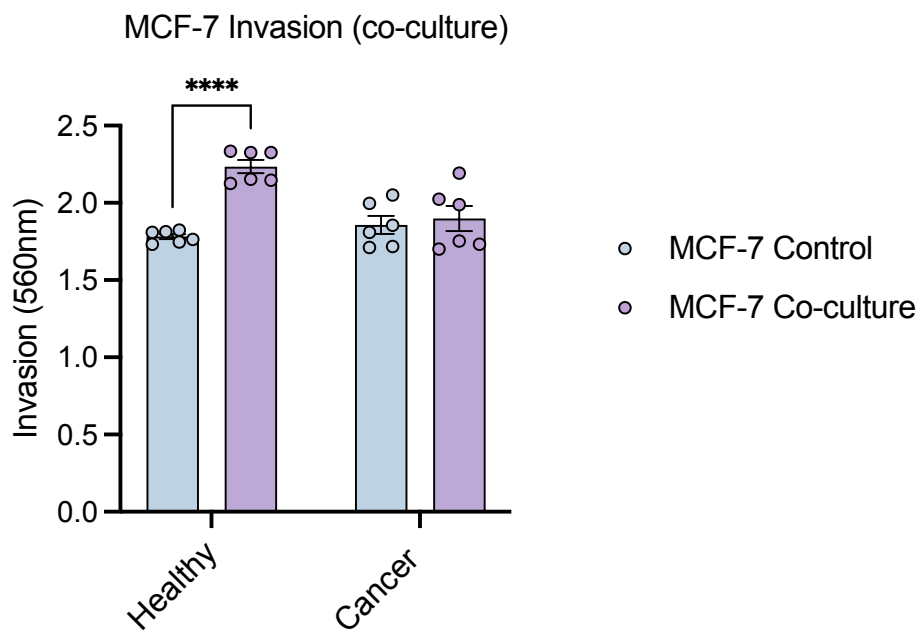


Figure 5.9: Co-culturing MCF-7 cells with healthy ADSCs increases invasion at late passage (p8).

Extracting the stain bound to the invading MCF-7 cells from each of the collagen membranes allowed rate of invasion to be quantified by measuring absorbance in a standard plate reader at 560nm. The number of MCF-7 cells that invaded through the membrane was increased in the group co-cultured with ADSCs isolated from healthy patients only when compared with the 0% control **** $p \leq 0.0001$ as determined by a two-way ANOVA. Data is shown from technical replicates ($n=3$) at late passage (p8) from two patient groups ($n=6$ healthy and $n=6$ cancer) and data is expressed as the mean \pm SEM.

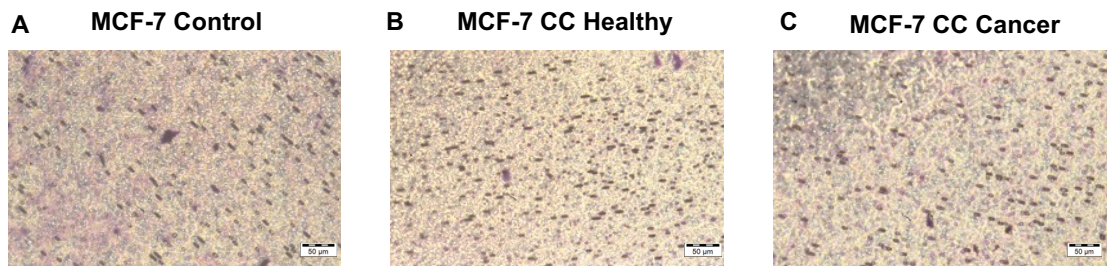


Figure 5.10: MCF-7 cells demonstrate increased invasion when co-cultured ADSCs isolated from healthy patients when compared with the control.

A-C show images of stained invasion inserts taken at x10 magnification on a light microscope (Zeiss, Axiovert 40C) after 24 hours of non-contact co-culture with ADSCs from healthy patients (B) and patients with cancer (C). The control group (A) are in standard culture conditions alone. There is an increased number of stained MCF-7 cells (purple dots) visible on the insert that was in the co-culture environment with healthy ADSCs (B) compared with the control (A). Data is shown from technical replicates (n=3) at late passage (p8) from two patient groups (n=6 healthy and n=6 cancer).

5.3.6 Co-Culturing T47D Cells with ADSCs Isolated from Healthy Patients, Significantly Increases the Rate of Invasion

Similarly to the MCF-7 cell line, the luminal A ER+ PR+ and HER2- T47D cell line was established from a metastatic pleural effusion, thus illustrating its established metastatic potential (Holliday and Speirs, 2011). The results from co-culture with the MCF-7 cell line demonstrate an increased rate of invasion with ADSCs isolated from healthy patients and the same effect is seen with this cell line. As shown in Figure 5.11, only T47D cells co-cultured with ADSCs isolated from healthy patients demonstrated statistically significant increases in invasion when compared with the control ($p < 0.0001$) as determined by a two-way ANOVA (healthy n=3, cancer n=3). This is similarly reflected in the times ten magnification images captured with the light microscope of the stained collagen inserts at p8 (Figure 5.12) showing an increase in the number of T47D cells invading into the membrane when co-cultured with ADSCs from cancer patients and the control.

T47D Invasion (co-culture)

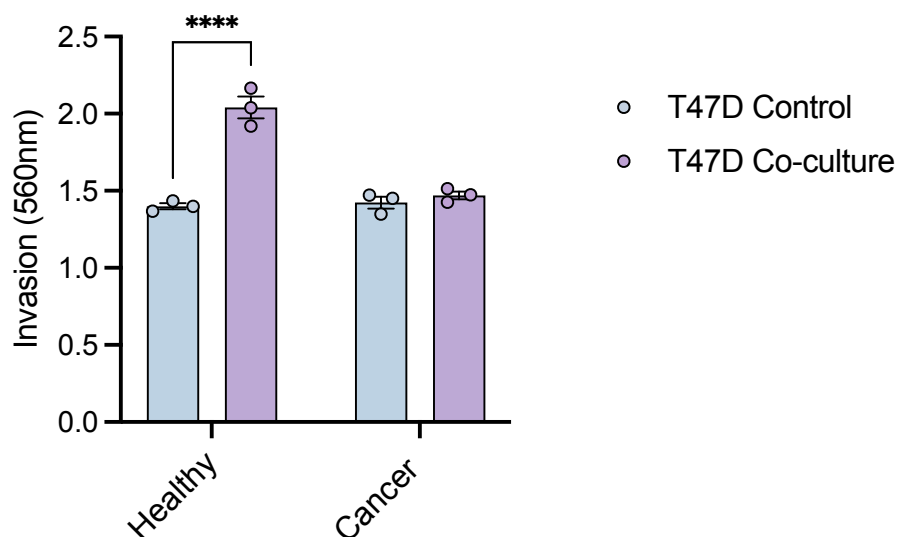


Figure 5.11: Co-culturing T47D cells with healthy ADSCs increases invasion at late passage (p8).

Extracting the stain bound to the invading T47D cells from each of the collagen membranes allowed rate of invasion to be quantified by measuring absorbance in a standard plate reader at 560nm. The number of T47D cells that invaded through the membrane was increased at late passage (p8) in the group co-cultured with ADSCs isolated from healthy patients compared with the 0% control **** $p \leq 0.0001$ as determined by a two-way ANOVA Data is shown from technical replicates (n=3) at late passage (p8) from two patient groups (n=3 healthy and n=3 cancer).

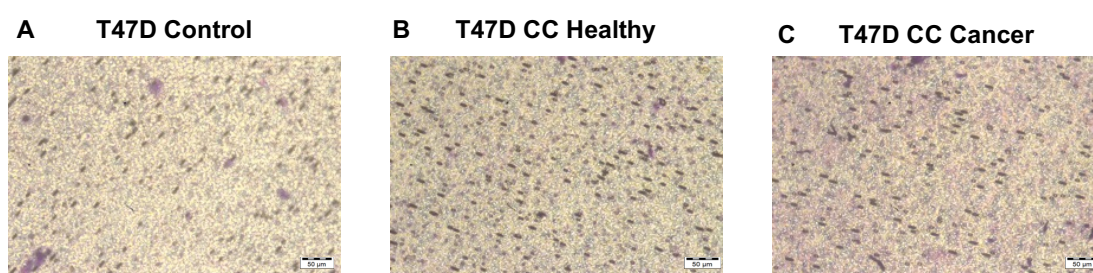


Figure 5.12: T47D cells demonstrate increased invasion when co-cultured ADSCs isolated from healthy patients when compared with the control.

A-C Images of stained invasion inserts taken at x10 magnification on a light microscope (Zeiss, Axiovert 40C) with T47D cells after 24 hours of non-contact co-culture with ADSCs from healthy patients (B) and patients with cancer (C). The control group (A) are in standard culture conditions. There is an increased number of stained T47D cells (purple dots) visible on the insert that was in the co-culture environment with healthy ADSCs (B) compared with the control (A). Data is shown from technical replicates (n=3) at late passage (p8) from two patient groups (n=3 healthy and n=3 cancer).

5.3.7 Utilising the Seahorse XF Extracellular Flux Analyser Enabled Real-Time Metabolic and Glycolytic Interrogation

The complexity of cancer metabolism has been described within the literature and is briefly outlined in Chapter One. Rather than all abnormally proliferating tumours following a common pathway, it is accepted that as our understanding of cellular bioenergetics evolves there are a number of diverse metabolic strategies that support sustained tumour growth (Hanahan and Weinberg, 2011; Intlekofer and Finley, 2019; Shin and Koo, 2021). The use of the Seahorse XF extracellular flux analyser allowed the real-time measurement of glycolytic and mitochondrial function of MCF-7 and T47D cells in response to a series of timed injections (oligomycin, FCCP, rotenone/antimycin A) (Appendix Three). As described previously in the methods (Section 2.16) the two energy-producing metabolic pathways, glycolysis and oxidative phosphorylation (OXPHOS), are directly correlated to the extracellular acidification rate (ECAR; mpH/min) and oxygen consumption rate (OCR; pmole/min) respectively and were able to be simultaneously measured in a single assay (Figure 2.16). From these assays, the various respiratory parameters could be calculated and compared with the control to ascertain the effect of co-culturing ADSCs from healthy (n=6) and cancer (n=6) patients on the OCR and ECAR of MCF-7 cells. T47D cells were used as a comparative cell line with a smaller patient subset to validate the MCF-7 results (n=3 healthy and n=3 cancer).

5.3.8 MCF-7 Cells That Were Co-Cultured with ADSCs from Healthy and Cancer Patients Were Increasingly Metabolically Active Compared with the MCF-7 Control

As previously described in the methods (Section 2.16) following 24 hours of non-contact co-culture with ADSCs isolated from healthy and cancer patients, the MCF-7 cells were removed and immediately run on the Seahorse XF^e analyser to evaluate oxidative phosphorylation (OXPHOS) which correlates with oxygen consumption rate (OCR; pmole/min). From these data the additional respiratory parameters as outlined could be calculated as previously discussed (Section 3.3.4.7). MCF-7 cells co-cultured with ADSCs isolated from healthy and cancer patients were increasingly metabolically active when

compared with the baseline control group of MCF-7s (Figure 5.13). Non-mitochondrial respiration was the only equivocal parameter, with no difference between either co-culture group or the control. There was a statistically significant increase in basal respiration ($p=0.0134$ healthy and $p=0.0177$ cancer), ATP linked production ($p=0.0177$ healthy and $p=0.0171$ cancer), proton leak ($p=0.0079$ healthy and $p=0.0127$ cancer), maximal respiration ($p=0.165$ healthy and $p=0.0320$ cancer) and spare respiratory capacity ($p=0.0149$ healthy and $p=0.0469$ cancer), as determined by one-way ANOVA with data expressed as mean \pm SEM and asterisks denoting * $p \leq 0.05$, ** $p \leq 0.01$.

The glycolytic potential of MCF-7s directly correlated to the extracellular acidification rate (ECAR; mpH/min) measured following the series of timed injections of oligomycin, FCCP and rotenone/antimycin-A. There was a significant increase in basal glycolysis ($p=0.0034$) and maximal glycolysis ($p=0.0281$) observed in MCF-7 cells that had been co-cultured with ADSCs isolated from healthy patients only compared with the control population (Figure 5.14). The MCF-7 cells co-cultured with ADSCs isolated from patients with cancer did not show statistical significance in glycolytic potential as determined by one-way ANOVA with data expressed as mean \pm SEM and asterisks denoting * $p \leq 0.05$, ** $p \leq 0.01$.

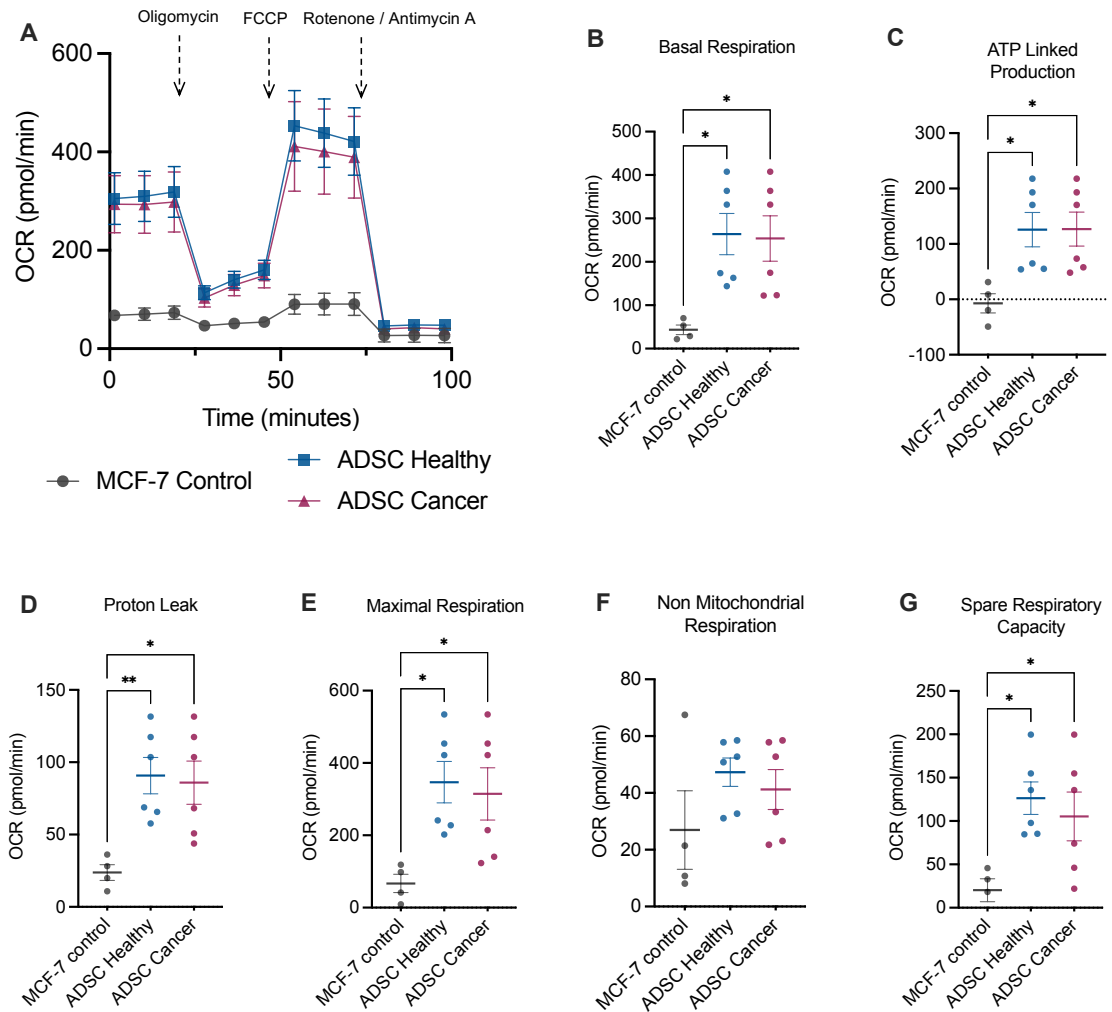


Figure 5.13: MCF-7 cells demonstrate increased metabolic activity when co-cultured with ADSCs from healthy and cancer patients when compared with the control.

(A) OCR (pmol/min) profile following non-contact co-culture of MCF-7 cells with ADSCs from healthy (n=6) and cancer (n=6) against a control. The oxygen consumption rate is determined using sequential injections of oligomycin, FCCP and rotenone/antimycin-A as indicated (arrows) from which the respiratory parameters can be calculated (shown in subsequent graphs). (B) Basal respiration, (C) ATP-linked production, (D) Proton leak, (E) Maximal respiration, (F) Non-mitochondrial respiration, (G) Spare respiratory capacity. Data as determined by one-way ANOVA with data expressed as mean \pm SEM and asterisks denoting * $p \leq 0.05$, ** $p \leq 0.01$ of co-culture experiments undertaken at late passage (p8). Technical replicates (n=3) across two patient groups (healthy n=6 and cancer n=6).

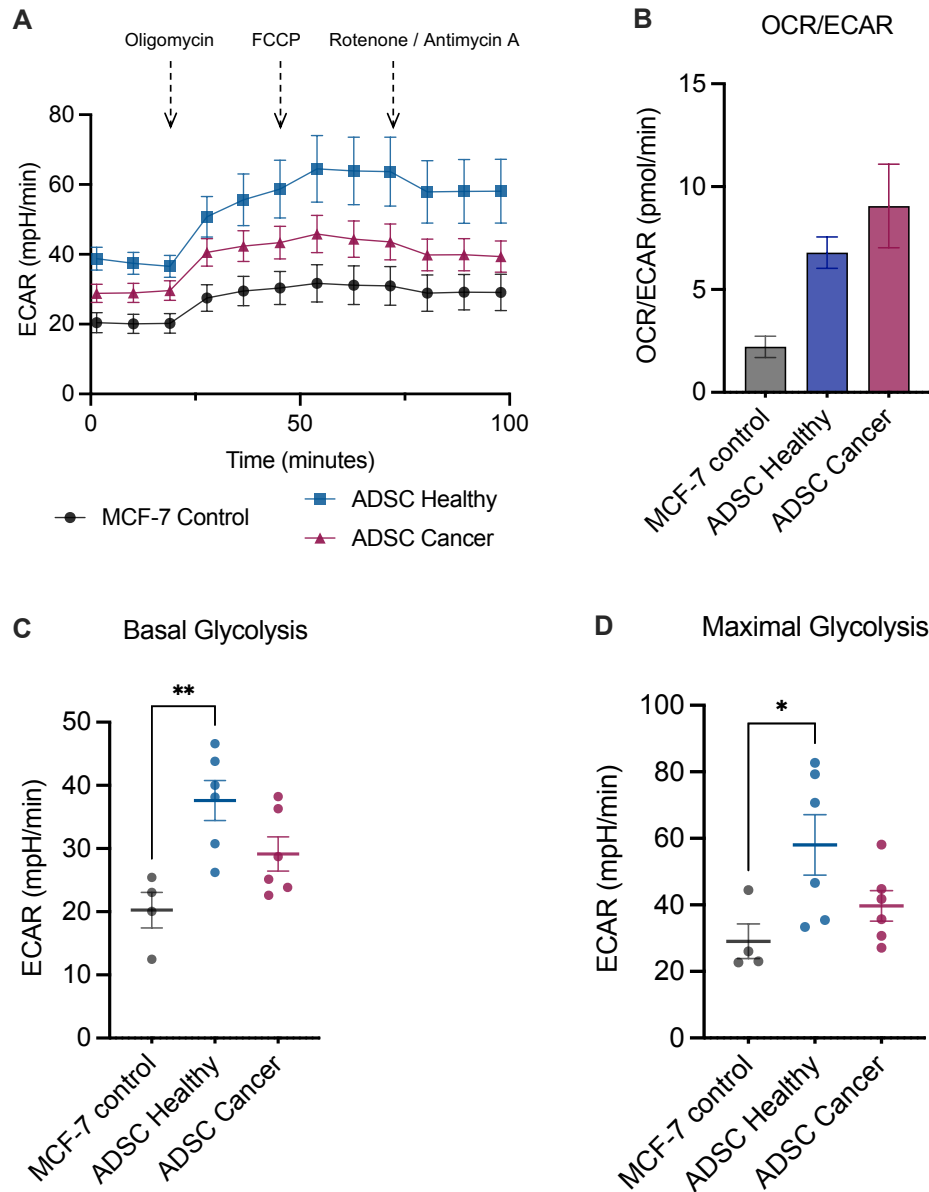


Figure 5.14: MCF-7 cells demonstrate increased basal and maximal glycolysis when co-cultured with ADSCs from healthy patients.

(A) ECAR (mpH/min) profile following non-contact co-culture of MCF-7 cells with ADSCs from healthy and cancer patients against a control. The glycolytic stress test is determined using sequential injections of oligomycin, FCCP and rotenone/antimycin-A as indicated (arrows) from which the glycolytic parameters can be calculated (B-D). (B) OCR/ECAR ratio determined using basal respiration and glycolysis to identify any disparity in metabolic function. (C) Basal glycolysis (D) Maximal glycolysis. Data as determined by one-way ANOVA with data expressed as mean \pm SEM and asterixis denoting * $p \leq 0.05$, ** $p \leq 0.01$ of co-culture experiments undertaken at late passage (p8). Technical replicates (n=3) across two patient groups (healthy n=6 and cancer n=6).

5.3.9 T47D cells that were co-cultured with ADSCs from healthy patients were increasingly metabolically active compared with the T47D control

As with the MCF-7 experiments detailed above the experiments were repeated with a smaller sample size (healthy n=3 and cancer n=3) to determine whether the metabolic changes observed as a result of co-culture were reflected in a second ER+ breast cancer cell line. T47D cells co-cultured with ADSCs isolated from healthy patients only were increasingly metabolically active when compared with the baseline control group of T47D cells (Figure 5.15). Spare respiratory capacity was the only equivocal parameter, with no difference between either co-culture group and the control. There was a statistically significant increase in basal respiration ($p=0.0009$), ATP linked production ($p=0.0325$), proton leak ($p=0.0007$), maximal respiration ($p=0.0409$) and non-mitochondria respiration ($p=0.0008$), as determined by one-way ANOVA with data expressed as mean \pm SEM and asterisks denoting * $p \leq 0.05$, *** $p \leq 0.001$. T47D cells co-cultured with ADSCs isolated from cancer patients were comparable to the control group with no statistical significance demonstrated in response to any of the timed injections (oligomycin, FCCP and rotenone/antimycin-A).

The glycolytic potential of T47Ds directly correlated to the extracellular acidification rate (ECAR; mpH/min) measured following the series of timed injections of oligomycin, FCCP and rotenone/antimycin-A. There was a significant increase in basal glycolysis ($p=0.0428$) and maximal glycolysis ($p=0.0234$) observed in T47D cells that had been co-cultured with ADSCs isolated from healthy patients only compared with the control population (Figure 5.16). The T47D cells co-cultured with ADSCs isolated from patients with cancer did not show statistical significance in glycolytic potential as determined by one-way ANOVA with data expressed as mean \pm SEM and asterisks denoting * $p \leq 0.05$.

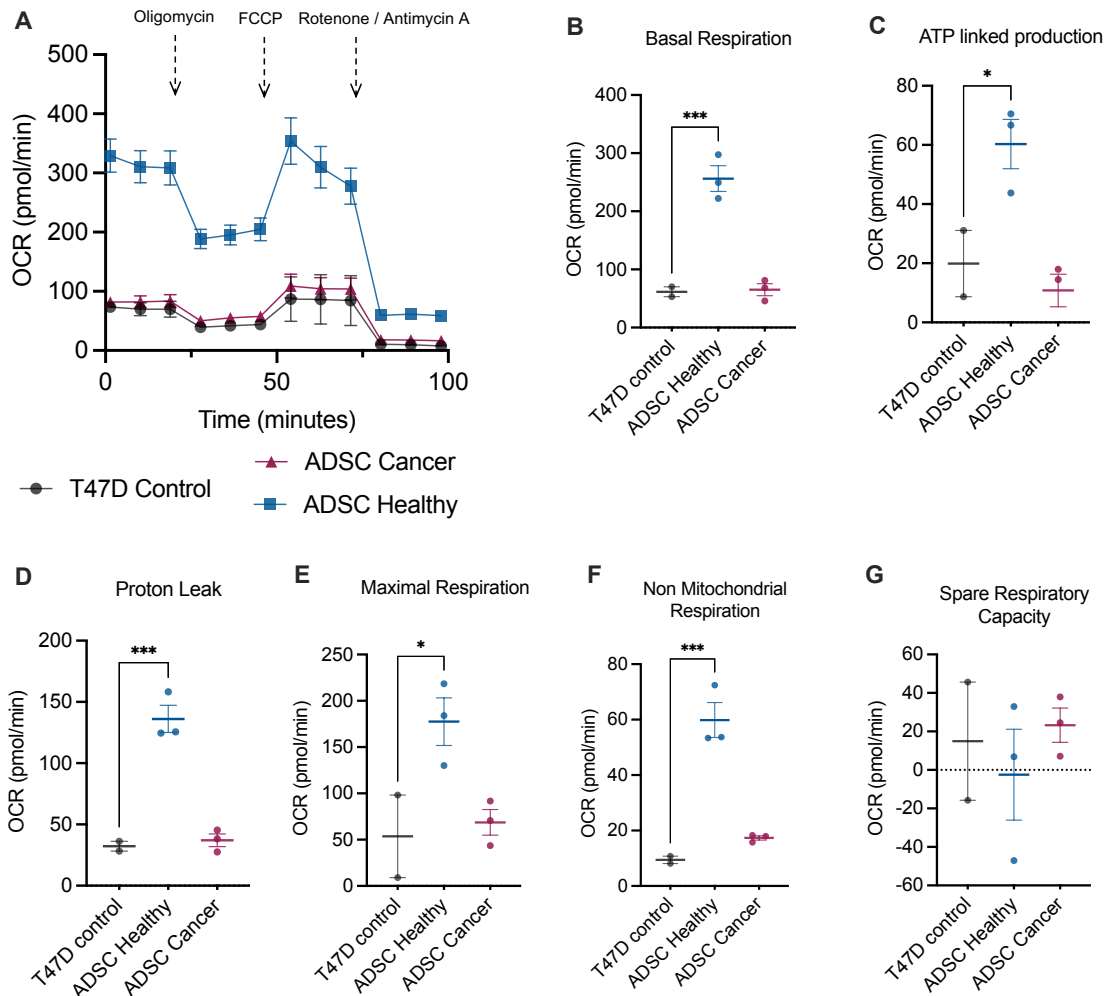


Figure 5.15: T47D cells demonstrate increased metabolic activity when co-cultured with ADSCs from healthy patients when compared with the control.

(A) OCR (pmol/min) profile following non-contact co-culture of T47D cells with ADSCs from healthy and cancer patients against a control. The oxygen consumption rate is determined using sequential injections of oligomycin, FCCP and rotenone/antimycin-A as indicated (arrows) from which the respiratory parameters can be calculated (shown in subsequent graphs). (B) Basal respiration, (C) ATP-linked production, (D) Proton leak, (E) Maximal respiration, (F) Non-mitochondrial respiration, (G) Spare respiratory capacity. Data as determined by one-way ANOVA with data expressed as mean \pm SEM and asterisks denoting * $p \leq 0.05$, *** $p \leq 0.001$ of co-culture experiments undertaken at late passage (p8). Technical replicates (n=3) across two patient groups (healthy n=3 and cancer n=3).

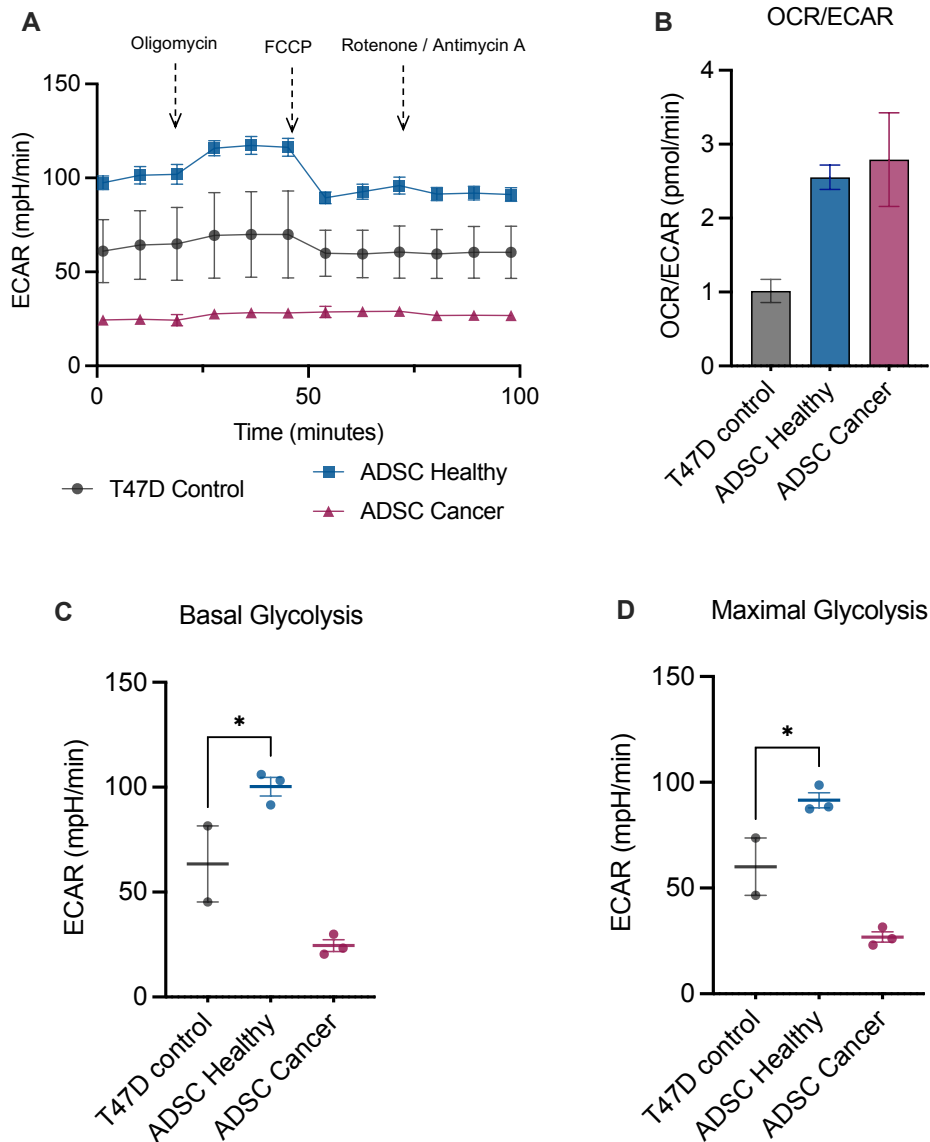


Figure 5.16: T47D cells demonstrate increased basal and maximal glycolysis when co-cultured with ADSCs from healthy patients.

(A) ECAR (mpH/min) profile following non-contact co-culture of T47D cells with ADSCs from healthy and cancer patients against a control. The glycolytic stress test is determined using sequential injections of oligomycin, FCCP and rotenone/antimycin-A as indicated (arrows) from which the glycolytic parameters can be calculated (B-D). (B) OCR/ECAR ratio determined using basal respiration and glycolysis to identify any disparity in metabolic function. (C) Basal glycolysis (D) Maximal glycolysis. Data as determined by one-way ANOVA with data expressed as mean \pm SEM and asterisks denoting * $p \leq 0.05$ of co-culture experiments undertaken at late passage (p8). Technical replicates (n=3) across two patient groups (healthy n=3 and cancer n=3).

5.3.10 Co-Culturing MCF-7 Cells with ADSCs from Healthy and Cancer Patients Does Not Significantly Alter MCF-7 Nuclei or Cellular Morphology

The morphological changes induced within the tumour cell architecture reflect the numerous abnormalities occurring within the nuclei and cytoplasm (Baba and Cătoi, 2007). Unlike healthy cells, neoplastic cells demonstrate disorganised architecture, loss of tissue polarity and failure of apoptosis and cell cycle arrest (Kenny *et al.*, 2007; Hanahan and Weinberg, 2011). The abnormalities of tumour cell morphology has been shown to correlate with gene expression, and loss of essential structural adhesion molecules such as E-cadherin which is important in the development of advanced neoplastic disease (Hajra, Chen and Fearon, 2002; Kenny *et al.*, 2007). Building on the conditioned media experiments, it was therefore important to establish if ADSCs isolated from two different patient populations (healthy and cancer), influenced the MCF-7 nuclei and cellular morphology in a non-contact co-culture model.

As previously outlined (Section 2.14.8) MCF-7 cells were co-cultured with ADSCs isolated from either healthy patients or patients with cancer for 4 and 24 hours. The MCF-7s cells were fixed in 4% PFA before being stained with 1 ml of Hoechst working solution before being imaged on the INCELL Analyser 2000. The DAPI and Brightfield images captured by the INCELL 2000 (Figure 5.17) were then loaded into the CellProfiler™ image analysis software which was used to measure nuclear and cellular area and perimeter, solidity, and eccentricity. Non-contact co-culture of MCF-7 cells with ADSCs isolated from both healthy and cancer patients failed to demonstrate any statistically significant difference in nuclei or cellular area after 4 or 24 hours as determined by a two-way ANOVA (Figure 5.18) (n=6 healthy and n=6 cancer). A Tukey's multiple comparison test confirmed there was no statistically significant difference in any of the cellular or nuclear measurements when compared with the control. Similarly, an analysis of 4 and 24 hour cellular eccentricity showed no statistically significant change at late passage (p8) for MCF-7 cells co-cultured with ADSCs from either patient group (Figure 5.19).

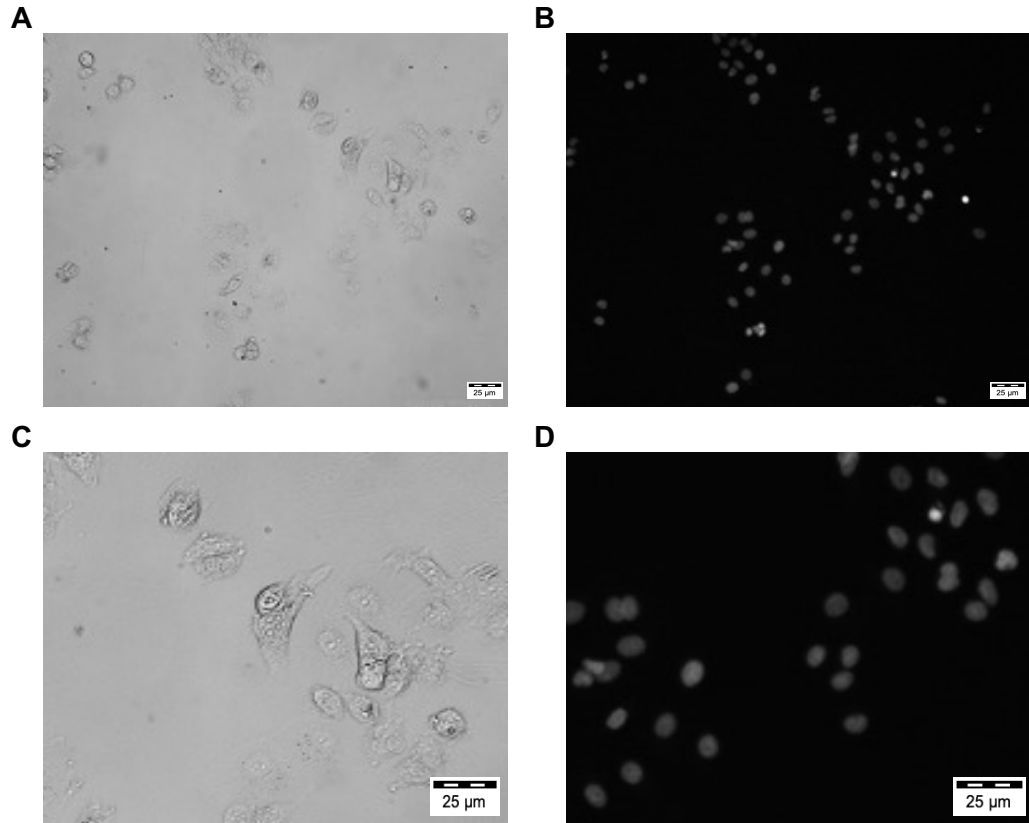


Figure 5.17: MCF-7 Cells imaged with the INCELL 2000 Analyzer (DAPI and Brightfield views).

(A and C) Brightfield and (B and C) DAPI images taken of MCF-7 cells following 24 hours of non-contact co-culture with ADSCs isolated from a healthy patient. Both the x10 magnification (A and B) and x20 magnification (C and D) allow visualisation of cellular structure, however the 20 times magnification images (C and D) better demonstrate the cellular and nuclear morphology which is comparable to the control group (not shown). Technical replicates (n=3) across two patient groups (healthy n=6 and cancer n=6)

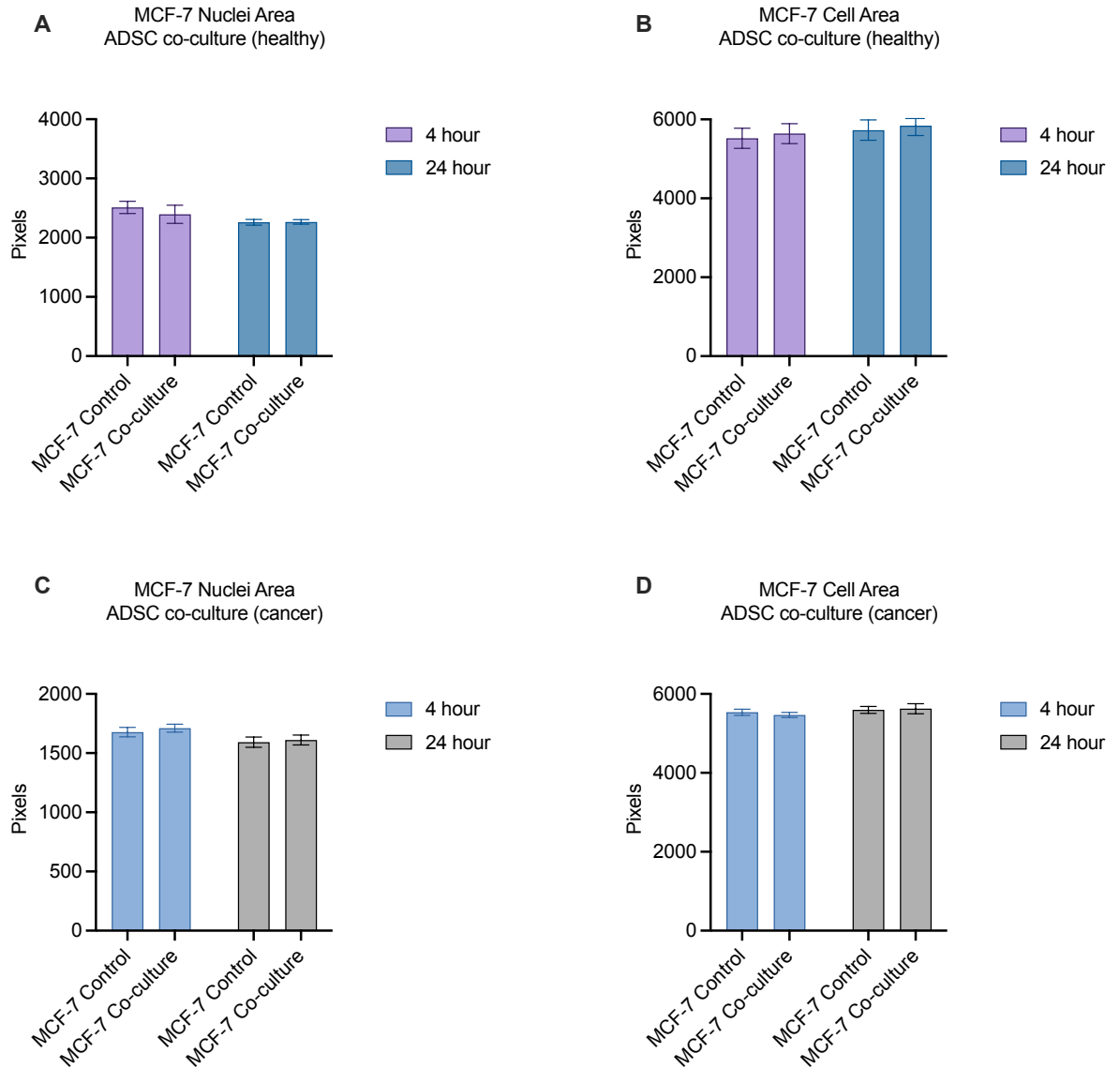


Figure 5.18: MCF-7 cell measurements of both nuclei and cellular area demonstrate no change following co-culture with ADSCs from healthy and cancer patients.

Analysis of both MCF-7 nuclei area (A and C) and cellular area (B and D) following 4 and 24 hours of non-contact co-culture at late passage (p8). Neither group demonstrates a statistically significant morphological difference in MCF-7 cells following co-culture with ADSCs isolated from healthy or cancer patients. Technical replicates (n=3) across two patient groups (healthy n=3 and cancer n=3).

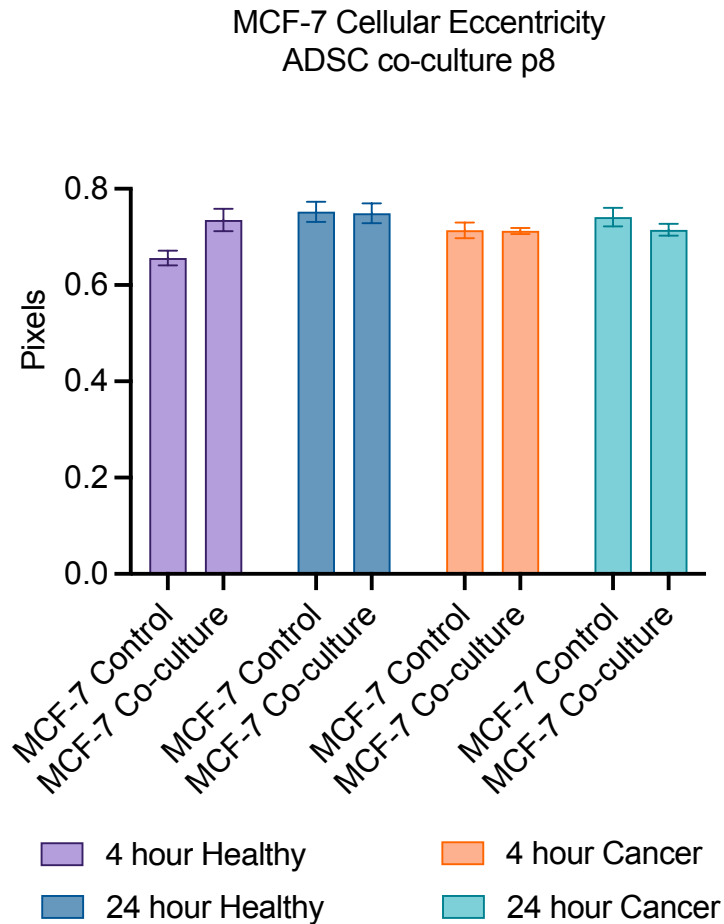


Figure 5.19: MCF-7 cells co-cultured with ADSCs from healthy and cancer patients demonstrated no change in cellular eccentricity at late passage (p8). Analysis of MCF-7 cellular eccentricity at late passage (p8) demonstrates no statistically significant morphological difference between MCF-7s co-cultured with ADSCs isolated from either patient group (healthy and cancer). As demonstrated by a two-way ANOVA, each experiment was repeated in triplicate for each biological replicate (n=6 healthy and n=6 cancer).

5.3.11 Non-Contact Co-Culture of MCF-7 Cells with ADSCs from Healthy and Cancer Patients Increases the Quantity of IL-6 Available

As detailed in Chapter One (Section 1.4.6) IL-6 has been shown to increase migration and invasion of breast cancer through an established role in epithelial-mesenchymal-transition (EMT) induction and angiogenesis. Clinically, there is a correlation between increased serum levels of IL-6 and advanced tumour stage which represents poorer prognosis and reduced patient survival. As demonstrated previously (Section 4.3.5), healthy ADSCs cultured alone produce greater quantities of IL-6 compared with their cancer

patient counterparts (Figure 4.12). Given the significant potential impact of IL-6 on the neoplastic traits of the MCF-7 cell line, it was important to examine the effect non-contact co-culture with ADSCs from two different patient populations (healthy and cancer) had on the detectable concentration of IL-6 after 4 and 24 hours. As illustrated in Figure 5.20 (A), co-culturing MCF-7 cells with ADSCs from both healthy and cancer patients significantly increased the concentration of IL-6 available to MCF-7 cells detected in the media at 4 hours (healthy $p=0.0033$ and cancer $p=0.0230$). This trend became more contrasted over the subsequent 20 hours, and at the 24 hour time point, there was significantly more IL-6 available to MCF-7 cells that were co-cultured with ADSCs isolated from healthy patients ($p=0.0004$) only (Figure 5.23 (B)).

The significance was not seen in the group which co-cultured MCF-7 cells with ADSCs isolated from cancer patients ($p=0.2910$ – not significant) which again demonstrated a continued lack of effect by this cell population. In contrast to the conditioned media experiments, IL-6 concentrations detected in the media increased between the two time points indicating one of the cell populations was producing additional IL-6 during the observed time-period (24 hours). Data is expressed as mean \pm SEM and asterisks denoting * $p \leq 0.05$, ** $p \leq 0.01$, *** $p \leq 0.001$, with results as determined from a two-way ANOVA with post hoc Tukey's multiple comparison test comparing the co-culture of ADSCs isolated from healthy ($n=6$) and cancer ($n=6$) patients against a control, in triplicate.

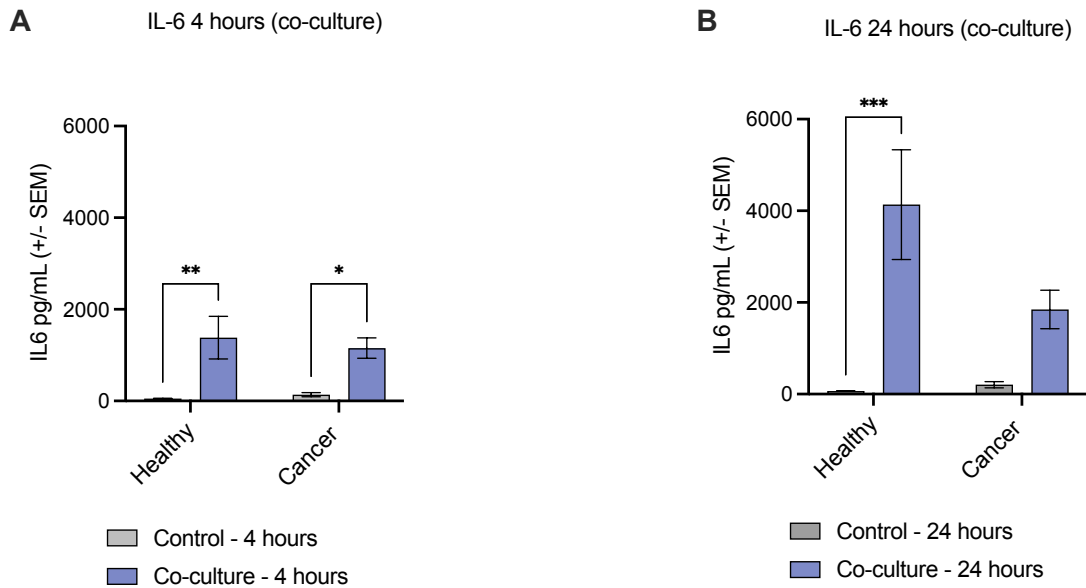


Figure 5.20: MCF-7s co-cultured with ADSCs isolated from healthy patients had statistically significant increases in IL-6 concentration detected in the culture media.

IL-6 levels detected in the media following non-contact co-culture of ADSCs from healthy and cancer patients after 4 hours (A) and 24 hours (B). (A) Co-culturing MCF-7 cells with ADSCs from both healthy and cancer patients at the early time point (4 hours) show a statistically significant increase in IL-6 detected within the media. (B) At 24 hours however, only the MCF-7 group co-cultured with ADSCs isolated from healthy patients is significant, with the detectable IL-6 concentration doubling in 20 hours. Experiments were performed at late passage (p8) in triplicate with an internal control using ADSCs isolated from healthy (n=6) and cancer (n=6) patients. Data expressed as mean \pm SEM; * $p \leq 0.05$, ** $p \leq 0.01$, *** $p \leq 0.001$.

5.3.12 Non-Contact Co-Culture of MCF-7 Cells with ADSCs from Healthy Patients Increases the Quantity of VEG-F Available

The role of VEG-F in tumour angiogenesis, resistance to apoptosis and dysregulated hyperplastic growth is well described in the literature and outlined in Section 1.2.5. Similar to IL-6, there are published studies describing VEG-F levels as clinically relevant markers for breast cancer tumour burden, with elevated concentrations indicative of advanced nodal disease and disseminated malignancy. As observed in the conditioned media experiments, there was an increase in detectable levels of VEG-F with increasing concentrations of conditioned media, which reduced between the 4 and 24 hour time points. Appreciating the essential role this signalling protein plays in the cancer microenvironment it was important to understand if co-locating

MCF-7 cells and ADSCs from two patient groups (healthy and cancer) affected any change in the levels of VEG-F protein detected in the media. As illustrated in Figure 5.21, there is a statistically significant increase in detectable levels of VEG-F in the media when MCF-7 cells are co-cultured with ADSCs isolated from healthy patients only (4 hours $p < 0.0001$ and 24 hours $p = 0.0023$).

In contrast to the conditioned media experiments and in keeping with the results seen in the IL-6 data, the quantity of VEG-F detected in the media significantly increased over time from 206.77 pg/mL at 4 hours to 393.92 pg/mL at 24 hours (mean \pm SEM) in the MCF-7 group co-cultured with ADSCs from healthy patients. Data is expressed as mean \pm SEM and asterix denoting ** $p \leq 0.01$ and **** $p \leq 0.0001$, with results as determined from a two-way ANOVA with post hoc Tukey's multiple comparison test comparing the co-culture of ADSCs isolated from healthy (n=6) and cancer (n=6) patients against a control, in triplicate.

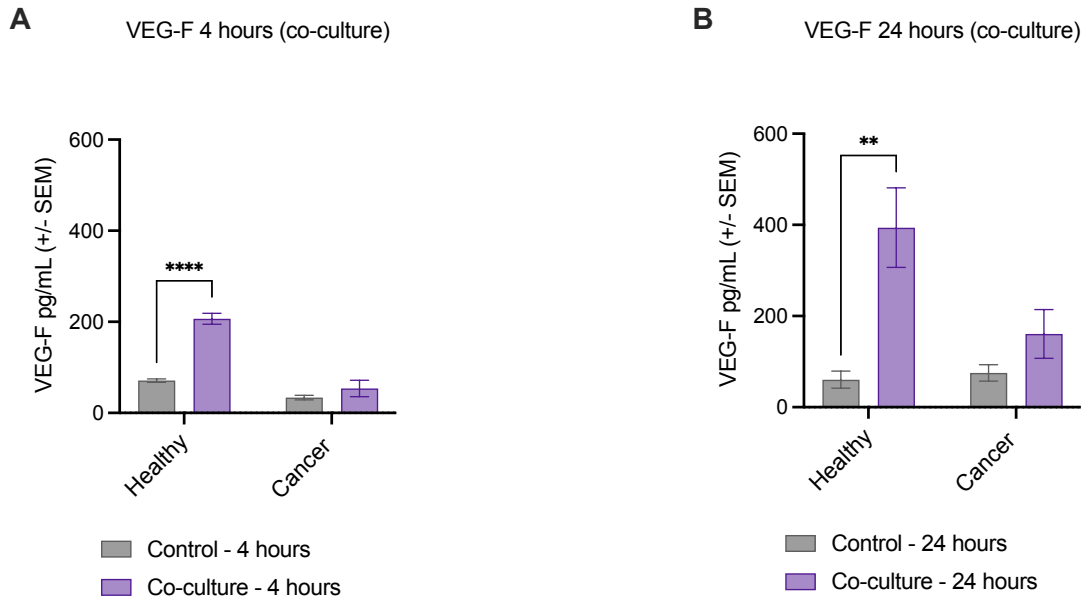


Figure 5.21: MCF-7s co-cultured with ADSCs isolated from healthy patients had statistically significant increases in VEG-F concentration detected in the culture media.

VEG-F levels detected in the media following non-contact co-culture of ADSCs from healthy and cancer patients after 4 hours (A) and 24 hours (B). (A) Co-culturing MCF-7 cells with ADSCs from healthy patients at the early time point (4 hours) show a statistically significant increase in VEG-F detected within the media. (B) At 24 hours this significance is maintained in the MCF-7 group co-cultured with ADSCs isolated from healthy patients, with the detectable IL-6 concentration almost doubling in 20 hours. Experiments were performed at late passage (p8) in triplicate with an internal control using ADSCs isolated from healthy (n=6) and cancer (n=6) patients. Data expressed as mean \pm SEM; ** $p \leq 0.01$, **** $p \leq 0.0001$.

5.3.13 Non-Contact Co-Culture of MCF-7 Cells with ADSCs from Healthy Patients Increases the Quantity of MCP-1 Available

The independent influence that chemokines such as MCP-1 (CCL2) exert on the development and progression of breast cancer has been outlined in Section 1.3.2. Its increased expression by breast cancer tumours and interaction with other pro-inflammatory chemokines support a significant association with advanced stage breast cancer. It was essential to compare the non-contact co-culture interaction between MCF-7 cells and ADSCs isolated from healthy and breast cancer patients with the conditioned media experiments, which were not statistically significant. As illustrated in Figure 5.22, there was a statistically increased concentration of MCP-1 detected in the media after 24 hours of non-contact co-culture between MCF-7 cells and

ADSCs isolated from healthy patients only ($p=0.0252$). In contrast to the conditioned media experiments and in keeping with the results seen in both the IL-6 and VEG-F experiments, the quantity of MCP-1 detected in the media significantly increased over time from 88.905 pg/mL at 4 hours to 563.632 pg/mL at 24 hours (mean \pm SEM) in the MCF-7 group co-cultured with ADSCs from healthy patients. Data is expressed as mean \pm SEM and asterisks denoting * $p < 0.05$ with results as determined from a two-way ANOVA with post hoc Tukey's multiple comparison test comparing the co-culture of ADSCs isolated from healthy ($n=6$) and cancer ($n=6$) patients against a control, in triplicate.

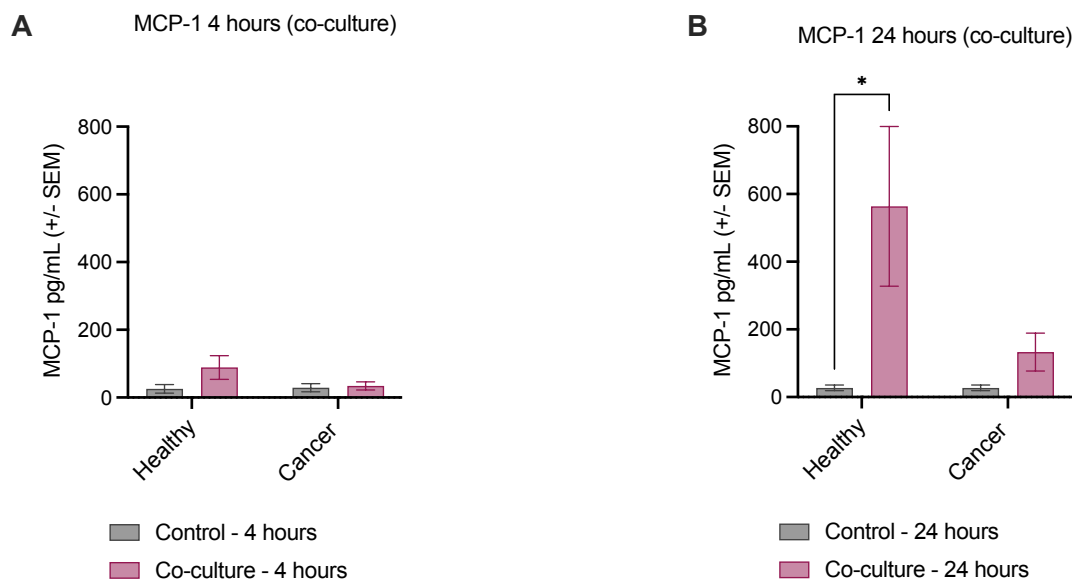


Figure 5.22: MCF-7s co-cultured with ADSCs isolated from healthy patients had statistically significant increases in MCP-1 concentration detected in the culture media.

Graphs demonstrating MCP-1 levels detected in the media following non-contact co-culture of ADSCs from healthy and cancer patients after 4 hours (A) and 24 hours (B). (A) Co-culturing MCF-7 cells with ADSCs from healthy and cancer patients at the early time point (4 hours) fails to show a statistically significant difference of MCP-1 concentrations in the media. (B) At 24 hours there is a statistically significant increase in the MCF-7 group co-cultured with ADSCs isolated from healthy patients, with the detectable MCP-1 concentration increasing by a factor of six in 20 hours. Experiments were performed at late passage (p8) in triplicate with an internal control using ADSCs isolated from healthy ($n=6$) and cancer ($n=6$) patients. Data expressed as mean \pm SEM; * $p < 0.05$.

5.4 Discussion

Interrogating the complex interactions and molecular events that drive the neoplastic traits of ER+ breast cancer cell lines *in vitro* requires the utilisation of complementary experimental methodologies. Considering the importance of ADSCs and their potential influence on breast cancer tumour progression, establishing a suitable model for examining their effects on the neoplastic traits of MCF-7 cells was key. Furthermore, it was important to establish if there was a difference in effect on the neoplastic traits of MCF-7 and T47D cells between patient groups (healthy and cancer). Described in the literature as a powerful tool to simplify and examine complex cancer mechanisms and interaction, the non-contact co-culture model outlined in the methods and optimised for use (Section 3.3.4.8) has provided a greater depth of understanding of how patient selection can potentially influence the effect of ADSCs on the neoplastic traits of MCF-7s (Arrigoni *et al.*, 2016). The transwell non-contact co-culture system enabled the experimental assays conducted in Chapter Four to be repeated with the addition of the ADSC cells isolated from different patient groups (healthy and cancer) allowing indirect and co-culture results to be effectively compared by keeping the cell populations separate. The inclusion of a second ER+ cell line (T47D) provided the opportunity to corroborate some of the key hallmark measures of neoplasia and establish whether the effects of ADSCs were limited to MCF-7 cells only or if there was an effect on other breast cancer lines. This formed an important part of experimental validation in the context of the clinical environment as over 70% of new breast cancers diagnosed are ER+ (Rosenberg, Barker and Anderson, 2015; Patel and Bihani, 2018; Mesa-Eguiagaray *et al.*, 2020).

Discussing first the assays that established an effect on the hallmark measures of cancer, there was an interesting trend that emerged between the two patient groups (healthy and cancer) seen across a range of experiments. Identified as one of the most fundamental cancer hallmarks, sustained and persistent proliferation leading to dysregulated tumour growth is a defining feature of neoplastic disease (Hanahan and Weinberg, 2000; Yaswen *et al.*, 2015). When co-cultured with ADSCs isolated from healthy patients only, MCF-7 cells demonstrated increased rates of proliferation when compared with both the

control and MCF-7 cells co-cultured with ADSCs isolated from cancer patients at late passage (p8) ($p \leq 0.01$). This was mirrored in the increased rate of MCF-7 migration and closure of the 500 μm gap which was statistically significant only in the group co-cultured with healthy ADSCs ($p \leq 0.001$). Interestingly, when ADSCs from both patient populations (healthy and cancer) were co-cultured with T47D cells, there was a significant increase in proliferation in both groups compared with the control ($p \leq 0.000$). However, although both patient groups increased the rate of T47D proliferation, the co-culture group with ADSCs isolated from healthy patients demonstrated the greatest increase in proliferation overall (Figure 5.3). These findings are mirrored in the scientific literature which similarly find co-culturing MCF-7 and T47D cells with healthy ADSCs increase the rate of proliferation and migration (Devarajan *et al.*, 2012; Zhang *et al.*, 2013; Yuan *et al.*, 2015; Teufelsbauer *et al.*, 2019; Plava *et al.*, 2020; Plangger *et al.*, 2021). However, the lack of statistically significant effect on MCF-7 proliferation and migration when co-cultured with ADSCs isolated from cancer patients is a novel finding. Rather than confirming the results so often referenced in the scientific literature, these ADSCs do not significantly contribute to the neoplastic traits of ER+ cell lines, and patient factors may well be a contributing feature.

Examining the difference between the two patient groups in more detail and their effects on both ER+ cell lines, the observed changes in cellular adhesion better illustrate the potential differences between the two patient groups. As outlined in Section 1.4.6, changes in cellular adhesion are an essential component of the invasion-metastasis cascade resulting in disseminated malignancy (Manabe *et al.*, 2003; Xie *et al.*, 2012; Ziegler *et al.*, 2014). The metastatic spread of breast cancer and increased risk of cancer recurrence is directly linked to reduced patient survival and is a substantial contributing factor to deaths related to breast cancer (Carioli *et al.*, 2017; Sun *et al.*, 2017; Fridrichova and Zmetakova, 2019). Both MCF-7 and T47D cells demonstrated a reduced rate of adhesion when co-cultured with ADSCs isolated from healthy patients only ($p \leq 0.05$ and $p \leq 0.0001$ respectively) and this was not seen in co-culture with ADSCs isolated from breast cancer patients. This is a critical discriminator and gives an additional level of detail in addition to increased

proliferation and migration in isolation, highlighting the importance of viewing these results in the context of the development and progression of cancer. The metastatic potential of both the MCF-7 and T47D cell line is well established as they are both isolated from malignant pleural effusions, it was therefore interesting to see there was a statistically significant increase in the invasion of both MCF-7 and T47D cells when co-cultured with ADSCs isolated from healthy patients only ($p \leq 0.0001$). In the context of the literature, reduced adhesion, EMT induction, release of pro-tumorigenic factors, increased proliferation, migration and invasion are all inextricably linked and observed in co-culture models utilising healthy ADSCs with ER+ cell lines such as MCF-7 (Zhang *et al.*, 2013; Ziegler *et al.*, 2014; Gallo *et al.*, 2018; Wu *et al.*, 2019; Li *et al.*, 2020).

If the literature applied uniformly to the interaction between all ADSCs regardless of their patient origin and ER+ breast cancer cell lines, similar results would have been seen in both patient groups (healthy and cancer), which this chapter clearly demonstrates is not the case. Uniquely, as illustrated with the proliferation, migration and invasion assays, there is a lack of significant effect when co-culturing MCF-7 and T47D cells with ADSCs isolated from cancer patients. This is critical, as these results demonstrate an apparent divergence in effect on the neoplastic traits of ER+ breast cancer when the co-culture includes ADSCs isolated from cancer patients who are completing systemic hormone treatment. Even studies that isolate ADSCs from women with breast cancer have a tendency to obtain samples from a patient population that was pre-systemic treatment, which resulted in ADSCs that behaved comparably to those isolated from healthy patients (Yuan *et al.*, 2015; Weigand *et al.*, 2016). Comparisons between laboratory studies and the clinical studies regarding safety of FFT post-BCS must better address the patient group being treated in order to create an analogous cell-based model which can be used to interrogate the effect. It is insufficient to compare ADSCs isolated from breast cancer patients with those isolated from healthy patients if they are isolated from tumour adjacent tissue at the initial commencement of their treatment (Jotzu *et al.*, 2011; Trivanović *et al.*, 2014; Schmid *et al.*, 2018). It is well established as outlined in Chapter One (Section 1.2) that MSCs track

to sites of inflammation and when co-located with neoplastic cells have the significant potential to support and amplify tumour growth and progression. Isolating and characterising native breast ADSCs at tumour adjacent sites, establishing a change in their phenotype or function simply corroborates findings in the literature and tells us little about the clinical picture with relation to reconstruction in the post treatment breast (Lazebnik, 2010; Hanahan and Weinberg, 2011; Losken *et al.*, 2011; Joyce *et al.*, 2015; Schweizer *et al.*, 2015; Dothel *et al.*, 2016).

For an ADSC and ER+ cancer cell-based model of the breast environment to have real world clinical application it must be directly representative of the women for whom FFT is a part of their treatment journey. Patients selected for primary cell line harvest for inclusion in laboratory-based studies must be post-BCS, have completed their (neo)adjuvant chemo-radiotherapy where applicable and be commenced on hormone receptor therapy. It is also essential to remember the anatomical location of harvest has a bearing on ADSC function, which limits the applicability of ADSCs isolated from tumour adjacent breast tissue as a model for the microenvironment alone, as this is not the tissue type that will be used to reconstruct the breast post operatively (Engels *et al.*, 2013; Rey *et al.*, 2019; Trivanović *et al.*, 2020). Women undergoing FFT post-BCS predominantly have adipose tissue harvested from their abdomen and processed before it is injected into the contour deformity within the breast to restore volume. The ADSCs used in this present study are all isolated from the anatomical region (abdomen) that would be utilised for reconstruction lending greater weight to the applicability of the results to clinical picture.

A range of ADSC secreted factors have been shown to support proliferation, enhance migration, induce phenotypic change and increase the invasive potential of breast cancer either separately or in combination (Kucerova *et al.*, 2011; Zimmerlin *et al.*, 2011; Trivanović *et al.*, 2016; L. Li *et al.*, 2020). As discussed in Section 1.4.6, IL-6 has been shown to induce an EMT phenotype in breast cancer cells and is associated with increased migration and invasion (Axel *et al.*, 2009; Fujisaki *et al.*, 2015). The clinical significance of this is further

illustrated as high serum levels of IL-6 have been shown to correlate with advanced tumour stage, nodal disease and distant metastasis with a poor clinical outcome (Salgado *et al.*, 2003; Ravishankaran and Karunanithi, 2011; Ma *et al.*, 2017; Noman *et al.*, 2017). Initially (after four hours) there was a significant increase in quantity of IL-6 detected in the media following co-culture of MCF-7 cells with ADSCs isolated from both healthy and cancer patients. However, after 24 hours only the group co-cultured with ADSCs isolated from healthy patients demonstrated a significant increase in the quantity of IL-6 ($p \leq 0.001$). This correlates with the assays examining MCF-7 adhesion and invasion, which found the group co-cultured with healthy ADSCs was less adherent and more invasive when compared with the control. Similar findings were noted when quantifying the levels of VEG-F and MCP-1 (CCL2) in the media after co-culture with ADSCs isolated from healthy patients.

As outlined previously (Section 1.4.5 and 1.4.6) both of these proteins are important in sustained breast cancer growth and similarly to IL-6, high serum levels of VEG-F has been shown clinically to correlate with disseminated malignancy and advanced nodal disease in patients diagnosed with breast cancer (Leek *et al.*, 1996; Rykala *et al.*, 2011; Aleskandarany *et al.*, 2015). The chemokine MCP-1 (CCL2) has also been shown to contribute to the recruitment of tumour associated macrophages (TAM) and demonstrates pro-tumorigenic activities, supporting angiogenesis and increased vascularity (Soria *et al.*, 2008; Hembruff *et al.*, 2010; Liubomirski *et al.*, 2019). At both measured time points (4 and 24 hours) there was a statistically significant increase in VEG-F detected following MCF-7 co-culture with ADSCs isolated from healthy patients only compared with the control ($p \leq 0.0001$ and $p \leq 0.01$ respectively). Quantities of MCP-1 were also significantly raised in the healthy only co-culture group at the 24 hour time point ($p < 0.05$). The lack of key cytokine and protein production by ADSCs isolated from patients with cancer clearly demonstrates an impairment of function and production of these key proteins which are essential in the support of tumorigenesis. A parallel study in the literature examining comparatively poor FFT retention in women taking tamoxifen found reduced VEG-F production by ADSCs with increasing doses of the oestrogen receptor antagonist (Pike *et al.*, 2015). While not conclusive,

it indicates that a host of patient factors, including systemic hormone therapies might play a part in the protein production and excretion capability of ADSCs, which may partially explain the difference in cytokine expression profiles.

The ability of cancer cells to acquire and utilise nutrients in often complex and dynamic environments to sustain essential processes and perpetuating growth has been defined as an emerging cancer hallmark (Hanahan and Weinberg, 2011; Sancho, Barneda and Heeschen, 2016). Accepting that cancer metabolism is more complex than initially described by Warburg, numerous features of cancer-associated metabolic reprogramming are theorised to contribute to the complex metabolic changes observed within cancer (Pavlova and Thompson, 2016; Potter, Newport and Morten, 2016). As described previously (Section 2.16) the two energy-producing metabolic pathways, glycolysis and oxidative phosphorylation (OXPHOS), are directly correlated to the extracellular acidification rate (ECAR; mpH/min) and oxygen consumption rate (OCR; pmole/min) respectively and were able to be simultaneously measured in a single assay using the Seahorse XF extracellular flux analyser.

For MCF-7 cells co-cultured with ADSCs isolated from both healthy and cancer patients, basal OCR was higher when compared with the control reflecting a more energetic state. The increase in proton leak may indicate a lower OXPHOS efficiency in response to the increased metabolic demands of the MCF-7 cells co-cultured with both ADSC populations, however this metabolic process is still being actively utilised. Increased glucose utilisation (ECAR) and resultant threefold increase in OCR/ECAR ratio potentially suggests an increased reliance on mitochondria for energy production and higher mitochondrial content in MCF-7s as indicated by increased ATP levels. The increased MCF-7 metabolic activity noted within both co-culture groups (healthy and cancer) demonstrates robust metabolic (OCR) and glycolytic (ECAR) activity which may be counterintuitive when assuming blanket application of the Warburg effect (Liberti and Locasale, 2016; Potter, Newport and Morten, 2016). It would suggest a move away from OXPHOS towards glycolysis, however the MCF-7 cell line appears to respire well when cells were co-cultured with ADSCs from both healthy and cancer patients which is in line

with findings within the literature (Zhang *et al.*, 2012; Radde *et al.*, 2015). The upregulated metabolic activity is a potential indicator for increased cellular proliferation, which is more starkly reflected within the T47D cell line which was used for result validation and comparison. An increase in OCR and ECAR was noted when T47D cells were co-cultured with ADSCs from healthy patients only, compared with the control, which is stark contrast to the MCF-7 co-culture group. The T47D group co-cultured with ADSCs isolated from patients with cancer were comparable to the control, with an increasing reliance on OXPHOS for metabolism with low basal and maximal glycolysis. This difference in ADSC behaviour is potentially linked to patient factors and the effects of systemic hormone therapy, which importantly has the potential to reduce the ability of ADSCs from cancer patients to successfully support ongoing metabolic requirements of ER+ breast cancer.

There were two hallmark measures that were not significantly influenced by non-contact co-culture with ADSCs from healthy and cancer patients, which were largely down to experimental duration. Similarly, to the conditioned media experiments detailed in Chapter Four (Section 4.3.4), MCF-7 cellular morphology was not significantly altered following 24 hours of non-contact co-culture with either patient group (healthy or cancer). This was entirely expected given the published evidence that indicates cancer cell line (MCF-7 or T47D) morphological changes often result only after extended periods of time in culture (in excess of five to seven days) (Ponti *et al.*, 2005; Xu *et al.*, 2012; Kuhbier *et al.*, 2014; Garroni *et al.*, 2021). As surmised from reviewing the conditioned media data in addition to the co-culture results, this assay, although designed to run alongside the other experiments, needs to be repeated over a greater time period to conclusively determine whether non-contact co-culture of ADSCs from either patient group would affect MCF-7 morphology. Using the second cell line (T47D) to validate the results would be advantageous to determine if non-contact co-culture would elicit any of the structural changes noted in the literature in either ER+ cell line.

While MCF-7 migration was found to be significantly increased when co-cultured with ADSCs isolated from healthy patients, the significance did not

extend to the T47D cell line. Observationally, there was a fundamental difference in the migration characteristics of the T47D cells which were noted to be slower growing in standard tissue culture conditions when compared with the MCF-7 cell line. It was apparent after completion of the replicates, that these cells migrate at a lower rate compared with MCF-7 cells and a longer period of observation is likely required to establish the presence of statistical significance. Additionally there are a range of advantages and limitations of monolayer and co-culture models widely discussed in the literature, while the non-contact co-culture model utilised in this chapter enables paracrine mechanisms to be measured, heterotypic interactions resulting from direct cell contact cannot be elucidated (Arrigoni *et al.*, 2016; Oliveira-Ferrer *et al.*, 2020). In re-designing some of the assays to measure the neoplastic hallmarks over an extended time period, the model to interrogate cell-cell interaction could be reviewed to examine the additional opportunities for observing the effects of ADSCs from two different patient groups on different ER+ cell lines.

These experiments have afforded a unique opportunity to directly compare a single MSC population (ADSCs) isolated from two distinct patient groups (healthy and cancer) on the neoplastic traits of two ER+ breast cancer lines (MCF-7 and T47D). The expectation based on the scientific literature is that the co-location of ADSCs within the microenvironment of breast cancer, either indirectly or directly, creates pro-tumorigenic conditions which support ongoing tumour development (Jotzu *et al.*, 2011; Lee, Jung and Koo, 2015; Koellensperger *et al.*, 2017; Plava *et al.*, 2020). While this was seen within the non-contact co-culture experiments conducted utilising ADSCs isolated from healthy patients, the results were significantly different when examining the group co-cultured with ADSCs isolated from patients with breast cancer and undergoing systemic therapy. While there was a marginal increase in the rate of T47D proliferation co-cultured with ADSCs from cancer patient compared with the control in the group co-cultured with healthy ADSCs, the increase in proliferation was greater across the whole time period of observation. Importantly, there was no change in the rate of T47D adhesion which was reduced in both ER+ cell lines when co-cultured with ADSCs isolated from healthy patients. This is important because it differentiates the two patient

groups from each other and demonstrates, for the first time that ADSCs are not all uniformly capable of supporting the neoplastic progression of ER+ breast cancer.

Clinically the question has centred on safety, which is a key component of any pre- and post-treatment counselling between a clinician and their patient. Patients want to understand and be able to quantify their expected disease-free survival and risk of locoregional recurrence with any course of treatment. Reconstruction post breast cancer resection has become intrinsically linked to treatment and in response to national guidance established following reporting from four successive audits, forms an early part of the patient discussion (Jeevan *et al.*, 2011, 2014). While established methods of reconstruction involving implants and free tissue transfer have long track records from which to draw complication rates, FFT does not have a comparable legacy of safety (Critchley *et al.*, 2013; Petit *et al.*, 2013; Chaput *et al.*, 2014). Initial concerns regarding detection of recurrence in the post FFT breast related to imaging modality efficacy has been discussed previously (Section 1.6.13). However the discovery of an MSC population within adipose tissue (ADSCs) that had the potential to negatively impact the neoplastic traits of breast cancer and increase the rate of recurrence pivoted the debate (Delay *et al.*, 2009; Fraser, Hedrick and Cohen, 2011; Singla, 2016). The clinical studies aiming to reassure the surgical community at large and in turn the patient population undergoing FFT, repeatedly reported no difference in recurrence risk following the procedure post-BCS (Petit *et al.*, 2013; Maione *et al.*, 2015; Cohen *et al.*, 2019; Piccotti *et al.*, 2021). As detailed in Section 1.7.3, their limitations centre around limited follow up, lack of conclusive outcomes and inability to effectively explain their incongruency with the ever-growing volume of contrary laboratory-based studies expressing concerns. Notwithstanding the need to design and execute more robust cohort studies examining FFT post-BCS, the scientific studies examining the clinical question at hand must robustly defend its choice of primary cell section and culture conditions under which it attempts to interrogate this urgent clinical query regarding the safety of FFT in the microenvironment of breast cancer.

5.4.1 Conclusions

This chapter has built on the experimental methods initially utilised to examine the indirect effects of ADSC conditioned media on the neoplastic hallmarks of MCF-7 cells (Chapter Four). It examined the effect of co-locating ADSCs isolated from different patient groups (healthy and cancer) on MCF-7 cells utilising non-contact co-culture. There is a clear difference in the neoplastic hallmark measures when comparing MCF-7 cells that are co-cultured with ADSCs isolated from healthy patients versus patients with cancer being treated with systemic therapy. This unique finding, for the first time demonstrates the differences in the effects of ADSCs from different patient populations on the neoplastic traits of two ER+ breast cancer cell lines. There was a significant increase in migration and invasion, with reduction in adhesion and raised concentrations of key cytokines linked with EMT induction and advanced disease (IL-6, VEG-F and MCP-1) in MCF-7 cells co-cultured with ADSCs isolated from healthy patients only. The increased metabolic activity similarly reflected a significant difference in the way different ADSC populations interact with MCF-7 cells which was also reflected in the additional ER+ cell line (T47D). The intrinsic differences between ADSCs isolated from healthy patients and patients with breast cancer may account for the differences noted in the neoplastic traits observed with both MCF-7 and T47D cell lines in co-culture.

The most obvious difference between the two groups is the sustained use of hormone therapy as part of their long-term treatment for ER+ breast cancer. While not in itself conclusive, this chapter has effectively demonstrated a divergence of behaviour for ADSCs isolated from cancer patients being treated with long term hormone therapy compared with those isolated from healthy patients. This contrasts with the expected effects as demonstrated by numerous laboratory-based scientific studies examining ADSC interaction with breast cancer, which illustrates the potential for refining the cell-based research model to better reflect the clinical picture. The inclusion of the second ER+ cell line for the key hallmark measures of proliferation, adhesion, invasion, migration, and bioenergetics demonstrated the significant influence of healthy ADSCs in co-culture was seen in more than one ER+ cell line.

Representing over 70% of all new breast cancer diagnoses, it was essential to demonstrate comparability between the experimental assays and clinical landscape (Holliday and Speirs, 2011; Millar *et al.*, 2011; Dai *et al.*, 2016; McDonald *et al.*, 2016).

This chapter has demonstrated that patient factors have the potential to affect not only the ADSC function but the way in which they interact in the cancer microenvironment and their effect on the neoplastic traits of ER+ cell lines. In contrast to previous studies, these results demonstrate a potential reason for the disparity between many scientific and clinical papers. Demonstrating that ADSCs isolated from patients with cancer may fundamentally interact differently than those isolated from healthy patients or those not yet commenced on systemic treatment. To meaningfully contribute to the debate regarding the safety of FFT post-BCS, further work is required to create cell models that more accurately reflects the patient group likely to undergo this type of reconstruction.

Chapter Six

General Discussion

6.1 Overview

The rising global incidence of breast cancer makes it the most common malignancy diagnosed annually world-wide, with in excess of 55,000 new cases in the UK each year alone (Pashayan *et al.*, 2020; Sung *et al.*, 2021). The advances in radiological imaging, nationwide screening programmes and the range of (neo)adjuvant treatments available means, more women than ever before are being diagnosed at an earlier stage, with improved survival (Public Health England, 2016; Pashayan *et al.*, 2020). The evolution of breast cancer surgery and its role in disease management has changed significantly since the original oncological procedure was described and popularised by Halstead in the late 1800s (Cotlar, Dubose and Rose, 2003). Technique refinement and the advancement of BCS has occurred in partnership with the developments made in radiotherapy, chemotherapy, hormone therapy, and imaging modalities for monitoring lymph node basins and distant sites of potential disease spread (Asgeirsson *et al.*, 2005; Asselain *et al.*, 2018; Gu *et al.*, 2021). A greater appreciation of the intrinsic molecular subtypes of cancer and hormone receptor status has led to a more detailed understanding of how different tumour types behave and their responses to targeted treatments (Dai *et al.*, 2016; Plichta *et al.*, 2020). With an increasingly clinically focused risk model, patients are now presented with a greater range of options regarding their surgical treatment pathway than was previously possible, and conversations regarding breast mound reconstruction happen at the earliest possible opportunity (Jeevan *et al.*, 2011, 2014).

Alongside the shift in resectional surgery, breast reconstruction had to rapidly adapt as the defects resulting from oncological clearance reduced in volume, posing a unique surgical challenge. While the post-mastectomy breast required the replacement of larger volumes of skin and soft tissue making it amenable to free flap reconstruction, small to medium volume defects presented surgeons with more nuanced volume loss requiring replacement.

The use of adipose tissue as FFT or lipofilling provided an ideal autologous reconstructive option which had the advantage of low donor site morbidity and ability for the technique to be repeated as a day case procedure. However, after initial introduction in the 1980s, concerns regarding patient safety primarily centred around the reliable radiological detection of recurrence, meant until evidence demonstrated that imaging could reliably delineate between benign fat necrosis and cancer, this technique was essentially abandoned (Gutowski *et al.*, 2009; Fatah *et al.*, 2012). Despite advancements in imaging, the discovery in 2001 of an adult MSC population characterised as ADSCs within adipose tissue raised questions about the impact of co-locating this progenitor population within the micro-environment of breast cancer (Zuk *et al.*, 2001, 2002). Numerous scientific studies demonstrated the pro-tumorigenic effects of ADSCs on breast cancer, and with tighter clinical margins and early breast reconstruction, questions regarding patient safety and suitability of this technique for volume replacement was raised (Dirat *et al.*, 2011; Young Park, Sung Hong and Sung-Hyun, 2013; Wu *et al.*, 2019; Atiya *et al.*, 2020; T. Li *et al.*, 2020).

Initially the *in vivo* and *in vitro* work utilised ADSCs isolated from healthy patients, and while more recent studies have aimed to include ADSCs isolated from breast cancer patients, they rarely include ADSCs harvested from patients commenced on systemic therapy, who have completed their surgical treatment. In response to these scientific papers, the clinical studies aimed to address the potentially limited laboratory-based models by interrogating breast cancer patient data establishing comparatively low rates of locoregional recurrence post FFT (Riggio, Bordoni and Nava, 2013; Maione *et al.*, 2015; Batista *et al.*, 2016; Fertsch *et al.*, 2017). Although the clinical studies generally demonstrated no increased risk, two identified an association between FFT and increased rates of local recurrence in patients with intraepithelial neoplasia (Petit *et al.*, 2012, 2013). However, it is generally accepted that the limited follow up time within the clinical studies, small patient numbers, and single centre focus, limited the power calculations and definitive conclusions that could be drawn from these papers. Systematic reviews have highlighted the limitations of the current evidence base preventing conclusive validation of

FFT safety, instead suggesting larger population studies with an extended follow up period are required (Cohen *et al.*, 2019; Piccotti *et al.*, 2021). Similarly, scientific studies are attempting to address the clinical comparability of their studies to better reflect the breast microenvironment and develop a greater understanding of how ADSCs behave and contribute to potential recurrence (Thitilertdecha *et al.*, 2020; Challapalli *et al.*, 2021; Fang *et al.*, 2021; Plangger *et al.*, 2021). With this contrasting evidence base, there was an opportunity to more closely examine of the key gaps between the scientific and clinical research studies, to better understand why the disparity might exist.

With the aim to create a cell-based model that more closely represented the patient population undergoing FFT post-BCS, this thesis set out to establish whether there was a disparity in effects exerted by ADSCs from different patient populations (healthy and cancer) on the neoplastic traits of ER+ breast cancer. By examining ADSCs isolated from two distinct patient populations, it was possible to discern whether the lack of congruence between the laboratory and clinically based studies was in part due to patient selection for the *in vivo* and *in vitro* work. This study therefore began by identifying a patient group that would most accurately represent the clinical question being raised regarding the safety of FFT in the breast microenvironment and a control group representing the cell population widely examined in the literature. Subsequently, women with ER+ breast cancer who were currently subject to systemic treatment and undergoing breast reconstruction were identified for inclusion in the research. It was felt that isolating ADSCs from this group would provide a much more representative population for study. It would also enable direct comparison with ADSCs isolated from healthy women, which were widely reported in the literature to support the progression of breast cancer. Ensuring the ADSCs population could be reliably isolated and characterised for use in the study (Chapter Three) was vital prior to examining the indirect (Chapter Four) and co-culture (Chapter Five) effects of ADSCs isolated from both healthy and cancer patients on the neoplastic traits of the MCF-7 and later, T47D breast cancer lines. The results were examined, and conclusions were drawn regarding any differences observed in the patient groups and how

that may have influenced the results of the experiments designed to measure the hallmark traits of ER+ breast cancer.

6.2 Conclusions Made from ADSC Optimisation and Patient Selection

As described in Chapter Three, ADSCs were successfully isolated and characterised using a reliable and widely accepted published protocol, which was ultimately based on the original technique first described in 2001 (Zuk *et al.*, 2001). Proving the most consistent and cost effective method, ADSCs were reliably isolated and subsequently characterised by assessing plastic adherence, cell phenotype and trilineage differentiation potential (Dominici *et al.*, 2006; Bourin *et al.*, 2013). Established tissue ethics ensured that patient samples could be collected for the duration of the project and although sample collection was at times challenging, over the course of the study, 22 cell lines were collected. Of these, four were essential in optimisation with 16 included in the final conditioned media (Chapter Three), and 12 included in the co-culture experiments (Chapter Four) resulting in end-point experimental data. Phenotypic characterisation posed a challenge given the size of the panel being used (nine fluorophores) and managing fluorescent spillover emissions required several different fluorophore combinations and compensation matrix reviews before arriving at a final optimised panel. While the configuration of an optimised panel bore cost and time implications, it provided a level of confirmational assurance at regular intervals throughout the study that the cell populations being used remained as ADSCs and was ultimately essential.

Clear patient recruitment parameters were vital for this thesis, to ensure the research effectively addressed the current evidentiary gap in the literature. As previously outlined, the ADSC source in many *in vivo* and *in vitro* studies that originally highlighted safety concerns regarding FFT and the breast cancer microenvironment derived their primary cell lines from healthy women (Yuan *et al.*, 2015; Schmid *et al.*, 2018; Visweswaran *et al.*, 2018; Teufelsbauer *et al.*, 2019; Wu *et al.*, 2019; Plangger *et al.*, 2021). While latterly there has been a shift towards examining ADSCs harvested from tumour adjacent tissue or generally from women with breast cancer, the timing of tissue harvest often entirely precludes the cells from systemic therapy exposure (Weigand *et al.*,

2016; Schmid *et al.*, 2018; Rey *et al.*, 2019). In this thesis, isolating ADSCs from patients with ER+ breast cancer, at the point of reconstruction, while commenced on long term systemic hormone therapy, ensured that the primary cells harvested were representative of the patient group central to the safety debate.

The hypothesis postulated in this thesis anticipated a divergence in effect when examining ADSCs derived from cancer patients on the neoplastic traits of MCF-7 cells compared with healthy ADSCs. The inclusion of a healthy patient ADSC group enabled comparison not only with the ADSC group isolated from cancer patients, but also the literature as a form of additional experimental validation. While patient selection was important, considerations were also made regarding anatomical location from where the samples were taken. Patients undergoing FFT to the breast post-BCS often have adipose tissue harvested from the abdomen, which is also a common anatomical site chosen for larger free flap reconstruction (e.g., DIEP flap). As such, it was crucial to collect lipoaspirate or *en bloc* samples from the abdomen of both healthy and cancer patients to ensure that anatomical location was representative. This was an essential consideration, prior to the commencement of comparative analysis between patient groups (healthy and cancer), as it was important to establish comparability between the cell-based model being designed and the clinical question being examined.

While it was established that the patient-derived cell lines could be reliably isolated and characterised, it was important to ensure that the breast cancer cell line chosen for the study was similarly reflective of the clinical picture. It was critical to balance the suitability of the cell line to ensure that it reflected the subtype and hormone receptor status of the majority of breast cancers diagnosed. The use of the ER+ luminal A cell lines MCF-7 and T47D reflected the histopathological and hormone receptor status of approximately 70% of new breast cancers diagnosed, which made them ideal cell lines for use in the study (Dai *et al.*, 2016; Jiang *et al.*, 2016). Their widespread use and citations in the literature, make them two of the most commonly used breast cancer cell lines in laboratory based research to date (Jordan and Levenson, 1997;

Holliday and Speirs, 2011). Accepting the limitations that come along with an immortalised cell line for use in research, their well-established track record as a surrogate line for breast cancer in the lab ensured that the results from this study could be directly compared with the literature.

6.3 The Creation of a Clinically Relevant Cell-Based Model

There are numerous studies that have attempted to re-create the breast microenvironment and design a model for approximating the types of cell-based interaction between ADSCs and breast cancer cell lines. While the limitations of *in vivo* and *in vitro* models are regularly debated, there is no doubt as to their advantages and application to enhance our understanding of vital cellular mechanisms. The utilisation of a range of experimental approaches within this thesis was important to robustly assess the indirect, and co-location effect of ADSCs from healthy and cancer patients on the neoplastic traits of MCF-7 and T47D cells. As one of the primary aims of this study, experiments were designed to create a more clinically analogous cell-based model to more accurately reflect the patient group undergoing FFT post-BCS. Understanding the indirect influence that the ADSCs from each patient group had on the MCF-7 cells prior to co-culture was an important part of the experimental design. It was the primary opportunity to observe baseline behaviour of ADSCs isolated from different patient groups (healthy and patients with breast cancer) and ascertain how representative the experimental assays were at assessing the neoplastic traits of cancer.

As a simulation for the surgical setting, treatment of MCF-7s with conditioned media approximates the indirect effects of relocated ADSCs within the wider breast microenvironment. Supported by studies in the literature, ADSCs are known to exert a general indirect effect on the surrounding tissue having the potential to induce or support malignant change. It was useful to ascertain if patient factors such as systemic therapy affected the inherent way in which the ADSC behave and indirectly influence ER+ breast cancer, prior to enabling cell-cell communication. Chapter Four provided the first opportunity to compare the indirect effects of ADSC CM from two distinct patient groups (healthy and cancer) on the neoplastic traits of MCF-7 cells. Forming the first

part of a two-stage cell-based model, to fully evaluate the role patient selection has on the ADSC populations isolated and their indirect effect on the neoplastic traits of cancer. Using a variety of concentrations of conditioned media produced a broader range of data points for each cell line, affording greater detail regarding the influence of ADSCs on the hallmark traits being observed.

The utilisation of the non-contact co-culture model in Chapter Five, built on the work done with conditioned media (Chapter Four) to observe the co-culture effects of ADSCs from healthy and cancer patients on the neoplastic traits of MCF-7 and T47D cells. With this cell model analogous for the co-location of ADSCs within the microenvironment containing (residual) breast cancer. It was also an opportunity to observe the effects of ADSCs from healthy and cancer patients in a second ER+ cell line (T47D) to establish whether any effects seen were specific to just MCF-7 cells or shared in a second cell line with common hormone receptor characteristics. If patient factors play a role in the interaction between ADSCs isolated from patients with cancer and the MCF-7 cell line, it would be reasonable to assume these effects would also be reflected in a second cell line with a similar hormone profile.

6.4 Measuring the Effect of ADSCs Isolated from Healthy and Cancer Patients on the Neoplastic Traits of MCF-7 and T47D Cells

Assessing the hallmarks of cancer as indicative of a wider disease process, it is helpful to view the results from this thesis as a collective, rather than individual measures. While the hypothesis central to this work was prompted by the disparity between the clinical and scientific studies, it has been clearly established that there are a range of expected interactions between ADSCs and ER+ breast cancer. Beginning with the most basic measurement of disease growth, proliferation of MCF-7 cells was both indirectly (CM) and directly (co-culture) increased when interacting with healthy ADSCs. Reflected in the T47D cell line, co-culture demonstrated the greatest increase in proliferation when co-located and able to communicate with ADSCs isolated from healthy patients. Importantly there was also a significant reduction in rate of adhesion when both MCF-7 and T47D cells were co-cultured with healthy

ADSCs only. This speaks, at least partly, to a potential neoplastic change within the cell lines, and when viewed in context of the rest of the results, indicates a possible development and progression of the cancer phenotype. There was a statistically significant increase in the rate of migration within the first 24 hours, when MCF-7 cells were co-cultured with ADSCs isolated from healthy patients only. ADSCs isolated from patients with cancer failed to have an impact and were comparable to the control. It was possible to see a divergence in the way ADSCs from each patient group influenced both MCF-7 and T47D cells, with clear differences in effect becoming apparent.

The same trends were again seen with invasion, showing a statistically significant increase when MCF-7 cells were conditioned and both MCF-7 and T47D cells were co-cultured with healthy ADSCs. The experimental assays involving healthy patients confirmed not only what has been found in the literature, but also that the assays chosen adequately functioned as surrogate measures for the cancer hallmarks. These results however were simply confirmational, and it was important to remember that although they were positive findings, they were already widely corroborated. Crucially however, these findings were not observed in the MCF-7 group treated with ADSC CM from patients with breast cancer undergoing systemic hormone treatment, which was a novel finding. While a variety of factors could have influenced this difference, for the first time it has been possible to establish a discrepancy in the way in which ADSCs from different patient groups indirectly affect the neoplastic traits of ER+ breast cancer. Similarly, the lack of effect on MCF-7 proliferation and invasion when co-cultured with cancer ADSC CM, while not conclusive, alludes to a disparity in ADSC function or behaviour which affects their baseline function.

It was important to build on the idea that ADSCs isolated from patients with cancer might operate at a functional deficit compared with those isolated from healthy patients. Protein analysis of the ADSC media demonstrated a statistically significant difference in baseline IL-6 and MCP-1 production between healthy and cancer patients, with only ADSCs isolated from healthy patients producing significantly higher quantities. The lack of significance for

ADSCs isolated from patients with cancer may imply a dysfunction in either synthesis, or release of essential proteins. Numerous factors have been shown in the literature to affect protein production, with increasing doses of Tamoxifen linked to reduced VEG-F levels and decreased cell viability (Pike *et al.*, 2015; Varghese *et al.*, 2017). ADSC exposure to systemic cancer and hormone therapy may therefore in part account for the reduction in baseline IL-6 and MCP-1 production by the ADSC population isolated from patients with breast cancer. There were significant increases in quantities of IL-6 and VEG-F detected when cells were treated with increasing concentrations of ADSC CM (25, 50, 75 and 100%) from both patient populations. However, this was hardly surprising when they were compared with the very low concentrations produced by the MCF-7 control. Over the 24 hour time period, the quantities of protein detected decreased, which may represent either utilisation by the MCF-7 cells or degradation in the media. Importantly, no quantity of CM from either patient group (healthy or cancer) resulted in an increase in protein production. It was difficult therefore, to attribute any real significance to the CM experiments at early and late passage (p2 and p8) without looking at the trends from the co-culture experiments. In contrast, there was only a significant increase in protein quantities detected when healthy ADSCs were co-cultured with MCF-7 cells. Interestingly, this group demonstrated an increase in production of IL-6, VEG-F and MCP-1 between the 4 and 24 hour time points. This potentially demonstrates even indirectly, a level of advantageous cell-cell communication only observed between the MCF-7 and healthy ADSCs which resulted in up-regulated cytokine production.

As an emerging cancer hallmark, the metabolic changes observed in both MCF-7 and T47D cells utilising the Seahorse XF extracellular flux analyser was very interesting. MCF-7 and T47D cells co-cultured with healthy ADSCs demonstrated a higher level of baseline metabolism. MCF-7 cells when co-cultured with both ADSC populations demonstrated globally increased OXPHOS parameters (basal and maximal respiration, rate of proton leak, ATP linked production and spare respiratory capacity). MCF-7 ECAR values were noted to be highest after FCCP injection which may be related to the increased rate of mitochondrial proton leak, as FCCP can cause mitochondrial

depolarisation, and utilising electron microscopy techniques could be useful in evaluating structural changes within MCF-7 mitochondria (Moon *et al.*, 2005). This future work would be interesting to undertake alongside extended conditioned media and co-culture work to establish whether ADSCs from either patient population affects the nuclei or cellular structure or morphology (Xu *et al.*, 2012; Ferraro *et al.*, 2019; Liubomirski *et al.*, 2019).

In the context of the safety debate regarding FFT post-BCS and potential for increasing the risk of locoregional recurrence, it is easy to understand the reticence to endorse the safety of this procedure given these results (Zhang *et al.*, 2013; Ziegler *et al.*, 2014; Gallo *et al.*, 2018; Wu *et al.*, 2019; L. Li *et al.*, 2020). As reinforced within the literature, ADSCs isolated from healthy patients influence the neoplastic traits of ER+ breast cancer cell lines resulting in increased rates of proliferation, migration, invasion, alongside aberrant production of EMT inducers (Chen *et al.*, 2015; Schweizer *et al.*, 2015; Trivanović *et al.*, 2016; Wu *et al.*, 2019). While there is an emerging understanding that ADSCs isolated from tumour adjacent tissue or breast cancer patients at the time of their oncological resections may behave differently in co-culture, they do not entirely reflect the clinical picture for patients undergoing reconstruction (Dirat *et al.*, 2011; Trivanović *et al.*, 2014; Thitilertdecha *et al.*, 2020).

There is therefore a lack of data that accurately reflects the patient group undergoing FFT post-BCS following commencement of systemic therapy. The experimental data from the MCF-7 and T47D co-culture with ADSCs isolated from healthy patients (Chapter 5) reflects those findings in the literature. What is unique however is the lack of effect exerted by the ADSC population isolated from patients with breast cancer undergoing systemic treatment. If the literature applied uniformly to the interaction between all ADSCs and ER+ breast cancer cell lines, similar results would have been seen in both patient groups (healthy and cancer). This data clearly demonstrates, however that this is not the case, and may provide some clarity as to why the clinical studies which focus exclusively on breast cancer patients, fail to see an increase in the rate of locoregional recurrence. This difference in ADSC behaviour could

be linked to patient factors such as the effects of systemic hormone therapy, which importantly has the potential to reduce the ability of ADSCs from cancer patients to successfully support ongoing metabolic requirements of ER+ breast cancer. This novel finding, not previously described in the literature provides an opportunity to develop this research area to enable a more representative cell model to be designed to better interrogate the interaction of ADSCs and breast cancer as a model of the post-BCS breast. Importantly it provides some additional context with which to view the current published evidence, both lab based and clinical studies, to better contextualise the evidence for patients being counselled for FFT post-BCS.

6.5 Future Work

This thesis has summarised a range of experimental approaches designed to interrogate whether patient selection influences the ways in which ADSCs effect the hallmark traits of two ER+ breast cancer cell lines (MCF-7 and T47D). Resulting in an alternative ADSC source recommended as part of a cell-based model to better understanding the post-BCS breast microenvironment. Further research would aim initially to address the gaps remaining from this study before going on to develop the research interest in the context of FFT post-BCS and long-term clinical safety. Primarily the research would aim to conclusively investigate any effects that ADSCs isolated from healthy and cancer patients might have on the nuclei and cellular morphology of MCF-7 cells through an extended period of co-culture (up to 14 days). In re-designing the assay to measure this neoplastic hallmark over an extended time period, the model to interrogate cell-cell interaction could be reviewed to examine the additional opportunities for observing the effects of ADSCs on different ER+ cell lines.

While the non-contact co-culture model utilised in this study enabled paracrine mechanisms to be measured, heterotypic interactions resulting from direct cell contact cannot be elucidated and would potentially have a bearing on cellular morphology and phenotype, which would be of great interest. Further work to explore the influence of ADSC CM and co-culture on MCF-7 and T47D EMT markers (E-cadherin, N-cadherin, and Vimentin) utilising qRT-PCR would

provide a greater level of detail regarding the influence of ADSCs from healthy and cancer patients on adhesion, invasion, and migration of these cell lines. This would provide an additional opportunity to compare the quantification of key proteins in the context of IL-6, VEG-F and MCP-1 values detected using ELISA. As metastatic disease is the leading cause of breast cancer-related death, further work to examine the underlying mechanisms driving EMT is vital. ADSC secreted extracellular vesicles (exosomes) have been shown to promote upregulated neovascularisation, tumour growth and invasion through protein kinase B (AKT) and ERK activation (An et al., 2019; Fridrichova and Zmetakova, 2019; Hinz and Jücker, 2019). Protein kinase B (AKT) is linked to and regulates numerous cancer hallmarks as described in Chapter One, and this is in part thought to be linked to upstream interactions between the cell-surface protein integrin- β 3 (Wen et al., 2019). Further work to isolate the secreted exosomes, using published protocols, from healthy and cancer ADSC populations, would enable their effects on the EMT regulators of various ER+ breast cancer cell lines to be observed (Lin, Wang and Zhao, 2013; Villagrasa *et al.*, 2015). Following topical treatment of the MCF-7 and T47D cells with the ADSC exosomes, in addition to the end point experiments described in this study, protein extraction for analysis would provide a greater understanding of potential upstream regulators of EMT. MCF-7 and T47D cells would be collected and lysed for protein to allow AKT, ERK and integrin- β 3 expression to be quantified utilising western blot and qRT-PCR.

The focus of this study has been on the effects of ADSCs on the neoplastic traits of MCF-7 and latterly T47D cells, it would be prudent to fully investigate the ADSC populations isolated from both patient groups to determine their intrinsic behaviours. Gaining a greater understanding of their baseline function including their bioenergetics and cellular morphology to compare with any changes after co-culture, would be an invaluable opportunity to better understand this unique cell population. Changes in cellular morphology are the result of numerous cell-cell and cell-matrix interactions within the tumour microenvironment involving the ECM, of which collagen is a major component (Kyriakopoulou *et al.*, 2020). In addition to structural changes, interaction with the predominant ECM remodelling enzyme matrix metalloproteinases

(MMPs) is seen in the formation of invadopodia which use MMP deposition to induce ECM degradation, facilitating invasion (Kessenbrock, Plaks and Werb, 2010; Eddy et al., 2017). Culturing MCF-7 and T47D cells within a type I collagen-based 3D matrix prior to treatment with ADSC CM and non-contact co-culture allows the cell lines to be subsequently imaged using scanning electron microscope (SEM). These images will provide a more detailed view of cellular phenotype and morphology, enabling the identification of invadopodia, tunnelling nanotubes (TNTs) and bridge like cytoplasmic processes formed by the MCF-7 and T47D cells, which are all features of invading cells. In addition to the SEM, following the end point experiments, MCF-7 and T47D cells could be collected for RNA isolation and assessment before reverse transcription. The genes of interest (*MMP7*, *MT1-MMP*, and *ACTB*) could then be quantified using RT-PCR analysis as these are often implicated in the morphological change and progression of breast cancer. The hope would be to attain a more detailed understanding of the potential mechanisms underlying why MCF-7 and T47D cells behave differently when co-located with ADSCs isolated from cancer patients, compared with their healthy counterparts. The potential impact on the patient safety debate is significant, if factors affecting ADSC function and by extension, their interaction in the breast microenvironment are better understood, and could therefore be better explained to patients. If upon restarting routine surgical services within the NHS there was the opportunity for further sample collection, the hope would be to increase the sample size to account for patient variability and increase study power.

In parallel to experimental optimisation aimed at better delineating the effect of ADSCs isolated from patients with breast cancer versus healthy patients, it is prudent to also examine the shortcomings within the clinical studies. Their limited patient numbers and relatively short follow up times, mean that despite a lack of clinical evidence demonstrating an increased risk of breast cancer recurrence following FFT, the procedure cannot be validated. As patient safety remains of paramount importance and central to this debate, a large population-based study is required to examine the long-term effects of FFT post-BCS. Without this, patient information, pre-operative counselling, and

considerations regarding follow up are left to the discretion of the clinical team, without the backing of a robust evidence base. As part of a recent pathway to portfolio grant achieved during this research study, in conjunction with the Secure Anonymised Information Linkage (SAIL) database, a large retrospective cohort study has been designed and initial data extraction has been undertaken. The study will look at multiple anonymised datasets covering the whole population of Wales over a 20 year period to identify women who underwent FFT to the breast. This population will then be analysed and utilising linked databases, any patients who then go on to develop breast cancer or are diagnosed with recurrence will be identified. The incidence of developing cancer for the total cohort will be calculated and logistic regression used to identify risk factors associated with its development. The aim of the study will be two-fold, firstly to establish whether FFT post-BCS increases the risk of breast cancer recurrence compared with traditional reconstruction or no reconstruction. Secondly, whether FFT to the breast for cosmetic purposes (i.e., not as part of an oncological reconstruction) increases the lifetime risk of developing breast cancer compared with patients having never undergone FFT.

6.6 Conclusion

Aiming to create a clinically representative model to study the effects of ADSCs on the hallmarks of ER+ breast cancer, this thesis has identified a two-part cell-based model which more accurately represents the patient population in question. The core concern has been that ADSCs in the breast micro-environment have the potential to negatively influence residual or recurrent microscopic disease. However, these studies fail to recognise the potential effects that patient factors may have on the function of ADSCs isolated for experimental use, limiting their clinical application. Mindful of the contrary outcomes between both the scientific and clinical studies, this work uniquely examines a patient population not widely studied. ADSCs from patients with breast cancer, commenced on systemic therapy were successfully isolated and characterised. Comparing their effects (indirectly and co-culture) on ER+ breast cancer alongside healthy ADSCs, which are routinely used in cell-based

models of the breast microenvironment, provided an incredible opportunity to observe a divergence in behaviour.

This thesis demonstrates that ADSCs isolated from patients with ER+ breast cancer, who have completed their surgical and (neo)adjuvant treatment, and are taking long term hormone therapy, have a markedly different effect on ER+ breast cancer compared with their healthy counterparts. Unlike ADSCs isolated from healthy women, those isolated from patients with cancer on systemic hormone treatment failed to significantly influence key neoplastic traits in either MCF-7 and later, T47D cells. Utilising a second ER+ breast cancer cell line during the co-culture experiments (Chapter Five) provided validation that these unique findings were comparable across cell lines with shared hormone receptor profiles. Recognising therefore, the potential limitations in applying the results from traditional cell-based scientific studies which use healthy ADSCs, to the clinical context and without considering the ADSC source. This study suggests that ADSCs isolated from patients with breast cancer, commenced on systemic treatment, may more accurately represent patients undergoing FFT post-BCS. It is therefore suggested that when choosing ADSC cell lines for use in studies examining the safety of lipofilling to breast, this patient group be considered over healthy volunteers undergoing cosmetic procedures.

Appendix One

ADSC isolation protocols trialled prior to the selection of the protocol that was used for the duration of the study.

Tables A1.1: ADSC isolation protocol number two being trialled for inclusion in the study.

Protocol	Two
Paper	Adipose-derived stem cells: Isolation, expansion and differentiation (Bunnell, Mette, <i>et al.</i> , 2008)
Materials	FBS (Atlanta Biological, Atlanta, GA), alpha-MEM and L-glutamine; (Mediatech, Herndon, VA) Pen/strep, collagenase type I
Cell lines	ADSCs, elective procedures, lipoaspirate, Human
Harvest	Needle biopsy or liposuction aspirate
Isolation and Culture	<ol style="list-style-type: none"> 1. Lipoaspirate is washed (5 times) with equal amount of PBS (with 5% pen/strep) 2. Place on a sterile culture plate and digest the ECM with 0.075% collagenase (type 1) prepared in PBS buffer with 2% pen/strep 3. Mince the sample using two scalpels and pipette using a 25- or 50-ml pipette several times to further facilitate digestion. 4. Incubate for 30 minutes at 37°C and 5% CO₂ 5. Neutralise enzyme activity with adding 5 ml of α-MEM containing 20% heat inactivated foetal bovine serum (FBS) (equal volume) 6. Pipette the sample up and down to further disintegrate aggregates of the adipose tissue 7. Transfer to a 50 ml tube (avoiding the solid aggregates) 8. Centrifuge at 2000xg for 5 minutes to get the SVF 9. Shake vigorously to thoroughly mix the cells and pellet 10. Centrifuge at 2000xg for 5 minutes to get the SVF 11. Aspirate all the collagenase solution above the pellet without disturbing the cells 12. Re-suspend in 1 ml of lysis buffer, incubate for 10 min on ice 13. Wash with 20 ml of PBS/2% pen/strep 14. Centrifuge at 2000xg for 5 minutes to get pellet 15. Aspirate the supernatant and re-suspend the cell pellet in a maximum of 3 ml of stromal medium (α-MEM, 20% FBS, 1% L-glutamine, 1% pen/strep) 16. Filter through a 70mm cell strainer 17. Wash the cell strainer with an additional 2 ml of stromal medium to obtain any additional cells 18. Plate the sample containing the cells in a lysine coated culture plate and incubate at 37°C, 5% CO₂. [Inoculate the cells in a single well of a 12-well plate for an amount of about 500 mg of adipose tissue or in a single well of a 24 well plate for an amount of 250–150 mg of adipose tissue]. 19. Maintain cells at sub-confluence levels (80%) to prevent spontaneous differentiation

Protocols selected from the literature describing different techniques for isolating ADSCs from human adipose tissue. Protocol two expands on principles in protocol one and uses coated plates to select for ADSCs to increase MSC yield.

Tables A1.2: ADSC isolation protocols number three being trialled for inclusion in the study.

Protocol	Three
Paper	Pooled human platelet lysate versus foetal bovine serum—investigating the proliferation rate, chromosome stability and angiogenic potential of human adipose tissue-derived stem cells intended for clinical use (Trojahn Kølle <i>et al.</i> , 2013)
Materials	Collagenase NB 4 Standard Grade (SERVA), (DMEM) (PAA Laboratories Pasching, Austria), 1% penicillin-streptomycin (GIBCO-Invitrogen, Taastrup, Denmark), 1% GlutaMAX (GIBCO-Invitrogen) and 10% of pHPL. In addition, 2 IU/mL preservative-free heparin (LEO Pharma, Ballerup, Denmark)
Cell lines	ADSCs, elective procedures, lipoaspirate, Human (four healthy female patients)
Harvest	Liposuction (breast and inner thigh) – Vibrast device
Isolation and Culture	<ol style="list-style-type: none"> 1. Wash lipoaspirate with PBS saline 2. Centrifuge at 300g for 5 minutes at room temperature 3. Incubate at 37°C for 45-60 minutes with Collagenase NB 4 Standard Grade (SERVA) 4. Neutralise the enzyme activity by adding cell DMEM supplemented with either 10% FBS or 10% pHPL 5. Filtered through a 100-mm filter 6. Centrifuge for 10 min at 1200g at room temperature 7. Resuspend in DMEM in 50 ml tubes 8. Filter through a 70-mm filter 9. Centrifuge for 10 min at 1200g at room temperature 10. Count the cells in the pellet (using an automated cell counter) 11. Seed in 175-cm² flasks at a density of approximately 85 000 cells/cm² in culture medium (DMEM, 1% pen/strep, 1% GlutaMAX, 10% pHPL) – 2 IU/mL preservative free heparin was added to the pHPL-supplemented media 12. Incubated for 4 days in a humidified atmosphere that contained 95% air and 5% CO₂ at 37°C. After the first day of cultivation, the non-adherent cells were discarded, the cell culture flasks were carefully rinsed with PBS and the medium was replaced.

Protocols selected from the literature describing three different techniques for isolating ADSCs from human adipose tissue. Protocol three endeavours to isolate ADSCs that are suitable for use in clinical trials and are isolated with GMP in mind.

Appendix Two

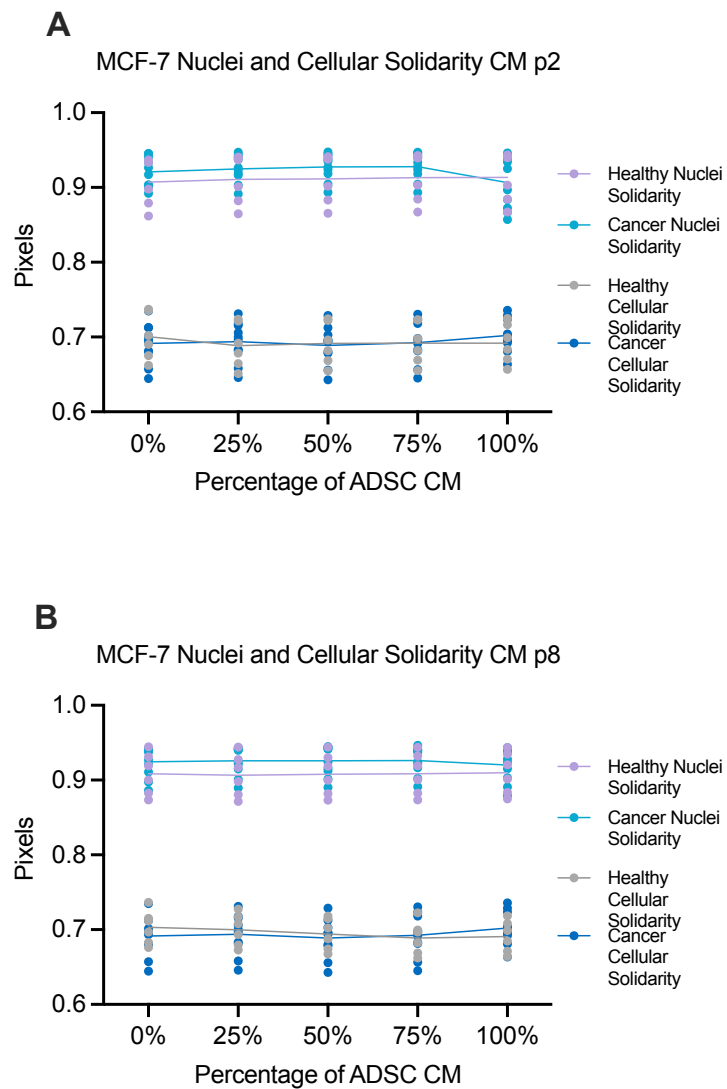


Figure A2.1 MCF-7 cell measurements of both nuclei and cellular solidarity demonstrate no change at increasing concentrations of ADSC CM.

Analysis of both MCF-7 nuclei and cellular solidarity at p2 (A) and p8 (B) demonstrate no statistically significant morphological difference between MCF-7s treated with ADSC CM from either patient group (n=6 healthy and n=10 cancer).

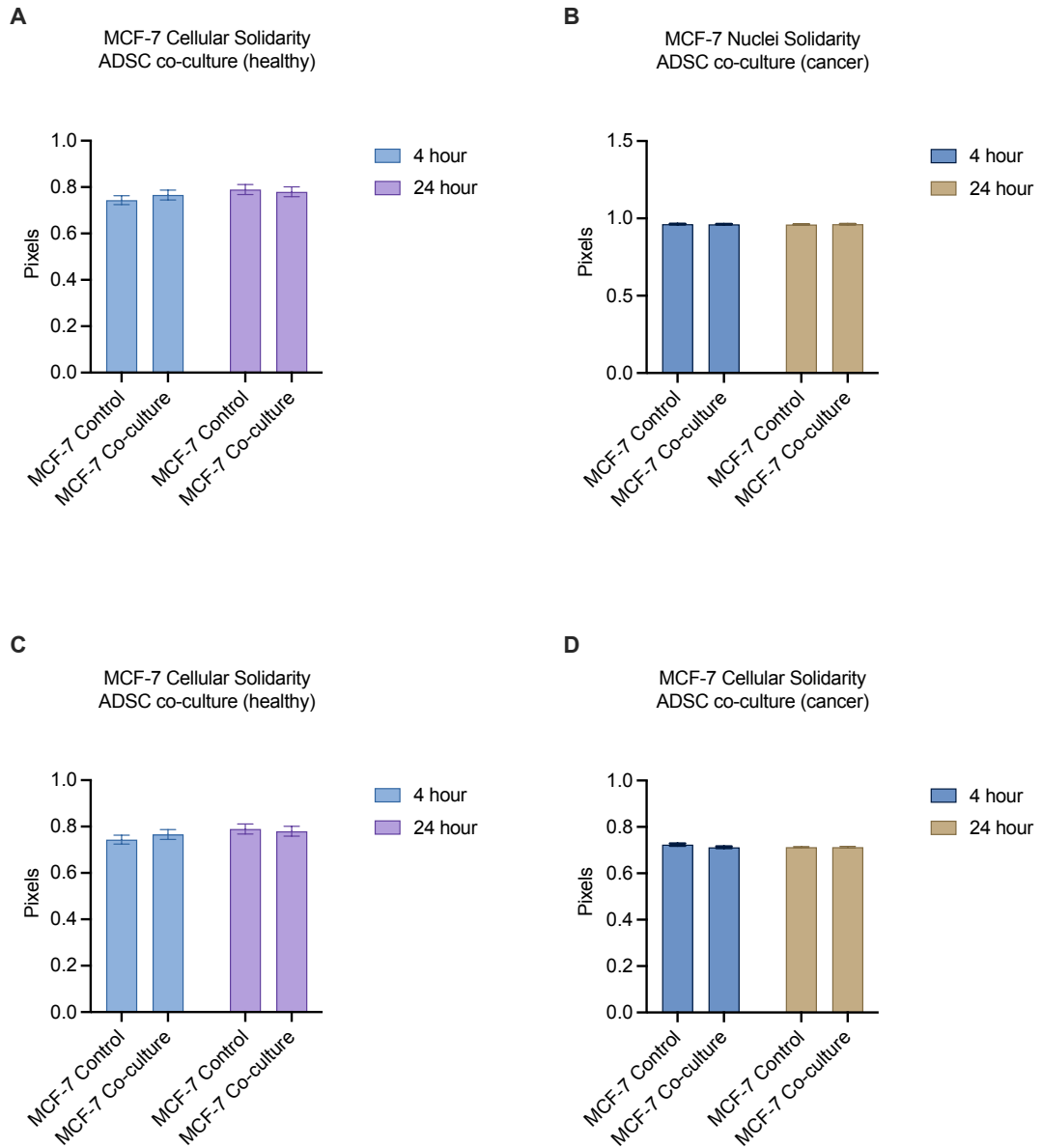


Figure A2.2: MCF-7 cell measurements of both nuclei and cellular solidarity demonstrate no change following co-culture with ADSCs from healthy and cancer patients.

Analysis of both MCF-7 cellular solidarity (A and C) and nuclei solidarity (B and D) following 4 and 24 hours of non-contact co-culture at late passage (p8). Neither group demonstrates a statistically significant morphological difference in MCF-7 cells following co-culture with ADSCs isolated from healthy or cancer patients (n=6 healthy and n=6 cancer).

Appendix Three

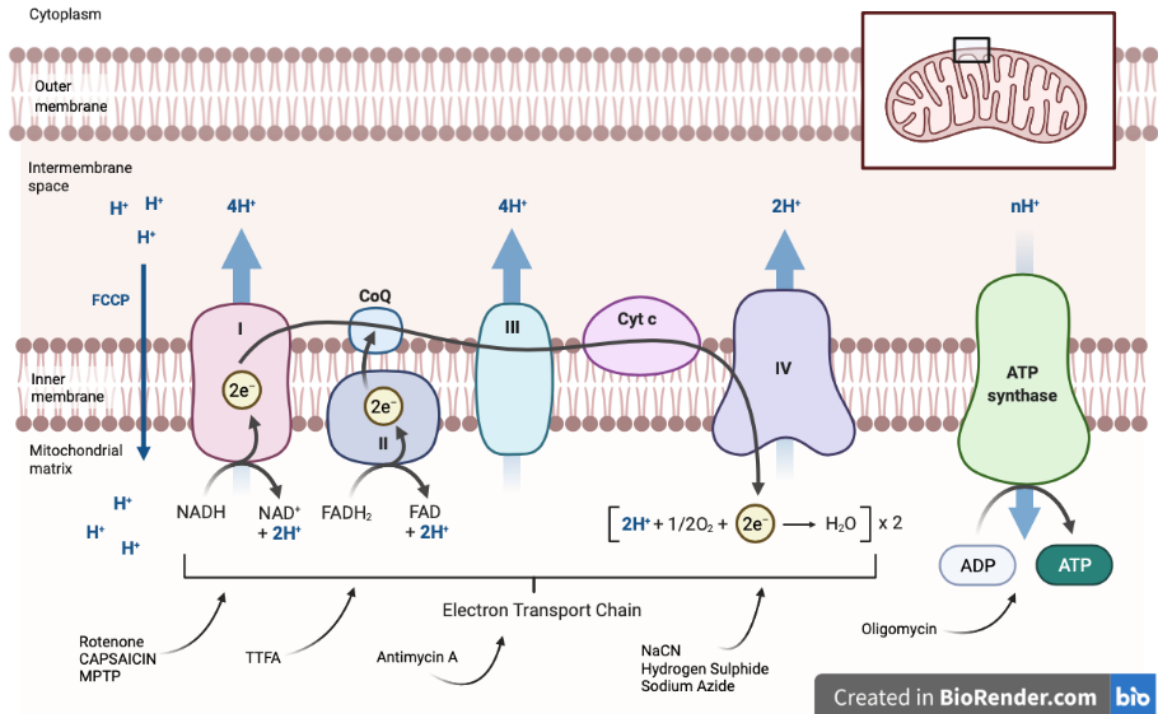


Figure A3.1 Graphical representation of the mitochondrial electron transport chain.

Utilising a series of electron transfers to generate cellular ATP, this graphical representation demonstrates at what point each of the timed injections (oligomycin, FCCP, rotenone/antimycin A) act, allowing the real-time measurement of glycolytic and mitochondrial function of MCF-7 and T47D cells. Created in BioRender.com

Appendix Four

Publications

Thomson (née Combellack)

Related Papers

Combellack EJ, Jessop ZM, Naderi N, Griffin M, Dobbs T, Ibrahim A, Evans S, Burnell S, Doak SH, Whitaker IS. Adipose regeneration and implications for breast reconstruction: update and the future. *Gland Surg*. 2016 Apr;5(2):227-41. doi: 10.3978/j.issn.2227-684X.2016.01.01. PMID: 27047789; PMCID: PMC4791352.

Naderi N, Combellack EJ, Griffin M, Sedaghati T, Javed M, Findlay MW, Wallace CG, Mosahebi A, Butler PE, Seifalian AM, Whitaker IS. The regenerative role of adipose-derived stem cells (ADSC) in plastic and reconstructive surgery. *Int Wound J*. 2017 Feb;14(1):112-124. doi: 10.1111/iwj.12569. Epub 2016 Feb 1. PMID: 26833722; PMCID: PMC7949873.

Al-Himdani S, Jessop ZM, Al-Sabah A, Combellack E, Ibrahim A, Doak SH, Hart AM, Archer CW, Thornton CA, Whitaker IS. Tissue-Engineered Solutions in Plastic and Reconstructive Surgery: Principles and Practice. *Front Surg*. 2017 Feb 23;4:4. doi: 10.3389/fsurg.2017.00004. PMID: 28280722; PMCID: PMC5322281.

Presentations

Thomson E. Adipose Derived Stem Cells (ADSCs) and the breast microenvironment: the implications of patient selection. Fat graft symposium BEAULI, Berlin, Germany (2022). Invited speaker (faculty)

Thomson E, Doak, S, Whitaker IS. Mimicking the breast microenvironment to investigate the interaction between Adipose Derived Stem Cells (ADSCs) and ER+ breast cancer cell lines (MCF-7 & T47D): Implications for the safety of fat

grafting. 32nd EURAPS Annual Meeting, Naples, Italy (2022). Podium presentation

Combella E, Doak, S, Whitaker IS. The safety of fat grafting: examining the interaction between adipose derived stem cells (ADSC) and MCF-7 breast cancer cells. Winter BAPRAS, Monaco (2019). Podium presentation

Combella E, Burnell S, Al-Sabah A, Doak, S, Whitaker IS. Interaction of Adipose Stem Cells (ADSC) & MCF-7s in the breast microenvironment: A pilot study. CST Academic day, Cardiff, UK (2017). Podium presentation

Burnell S⁺, Combella E^{*}, Doak S, Whitaker IS. Examining the Interaction Between Adipose Derived Stem Cells (ADSC) and MCF-7 Breast Cancer Cells Using Co-Culture Technique. TERMIS, Kyoto, Japan (2018). Poster presentation. *First author ⁺Presenter.

Bibliography

- Abaan, O. D. *et al.* (2013) 'The Exomes of the NCI-60 Panel: a Genomic Resource for Cancer Biology and Systems Pharmacology', *Cancer Research*, 15(73(14)), pp. 4372–4382. doi: 10.1158/0008-5472.CAN-12-3342.The.
- Abramczyk, H. *et al.* (2015) 'The role of lipid droplets and adipocytes in cancer. Raman imaging of cell cultures: MCF10A, MCF7, and MDA-MB-231 compared to adipocytes in cancerous human breast tissue', *Analyst*, 140(7), pp. 2224–2235. doi: 10.1039/c4an01875c.
- Abramsson, A., Lindblom, P. and Betsholtz, C. (2003) 'Endothelial and nonendothelial sources of PDGF-B regulate pericyte recruitment and influence vascular pattern formation in tumors', *Journal of Clinical Investigation*, 112(8), pp. 1142–1151. doi: 10.1172/JCI200318549.
- Adams, J. and Cory, S. (2007) 'The Bcl-2 apoptotic switch in cancer development and therapy', *Oncogene*, 26, pp. 1324–1337. doi: 10.1038/sj.onc.1210220.
- Aird, W. C. (2008) 'Endothelium in health and disease', *Pharmacological Reports*, 60(1), pp. 139–143.
- Aiwei, Y. B. *et al.* (2015) 'Adipocyte hypoxia promotes epithelial-mesenchymal transition-related gene expression and estrogen receptor-negative phenotype in breast cancer cells', *Oncology Reports*, 33(6), pp. 2689–2694. doi: 10.3892/or.2015.3880.
- Ajit, A. and Gopalankutty, A. I. (2021) 'Adipose-derived stem cell secretome as a cell-free product for cutaneous wound healing', *3 Biotech*. Springer International Publishing, 11(9), pp. 1–19. doi: 10.1007/s13205-021-02958-7.
- Akino, T. *et al.* (2009) 'Cytogenetic abnormalities of tumor-associated endothelial cells in human malignant tumors', *American Journal of Pathology*, 175(6), pp. 2657–2667. doi: 10.2353/ajpath.2009.090202.
- Akiyama, K. *et al.* (2012) 'Tumor endothelial cells acquire drug resistance by MDR1 up-regulation via VEGF signaling in tumor microenvironment', *American Journal of Pathology*. Elsevier Inc., 180(3), pp. 1283–1293. doi: 10.1016/j.ajpath.2011.11.029.
- Akram, M. *et al.* (2017) 'Awareness and current knowledge of breast cancer', *Biological Research*. BioMed Central, 50(1), pp. 1–23. doi: 10.1186/s40659-017-0140-9.

- Aleskandarany, M. A. *et al.* (2015) 'Molecular Mechanisms Underlying Lymphovascular Invasion in Invasive Breast Cancer', *Pathobiology*, 82(3–4), pp. 113–123. doi: 10.1159/000433583.
- Algire, C., Medrikova, D. and Herzig, S. (2013) 'White and brown adipose stem cells: From signaling to clinical implications', *Biochimica et Biophysica Acta - Molecular and Cell Biology of Lipids*. Elsevier B.V., 1831(5), pp. 896–904. doi: 10.1016/j.bbali.2012.10.001.
- American Cancer Society (2019) *Breast Cancer Facts & Figures 2019-2020*, Atlanta: American Cancer Society, Inc. doi: 10.1007/978-3-030-30766-0_24.
- An, Y. *et al.* (2019) 'Exosomes from Adipose-Derived Stem cells (ADSCs) overexpressing miR-21 Promote Vascularization of Endothelial Cells', *Scientific Reports*, 9, p. 12861. doi: 10.1073/pnas.1608384113.
- Angeloni, V. *et al.* (2017) 'Polyurethane foam scaffold as in vitro model for breast cancer bone metastasis', *Acta Biomaterialia*. Acta Materialia Inc., 63, pp. 306–316. doi: 10.1016/j.actbio.2017.09.017.
- Arrigoni, C. *et al.* (2016) 'In vitro co-culture models of breast cancer metastatic progression towards bone', *International Journal of Molecular Sciences*, 17(9). doi: 10.3390/ijms17091405.
- Asgeirsson, K. S. *et al.* (2005) 'Oncological and cosmetic outcomes of oncoplastic breast conserving surgery', *European Journal of Surgical Oncology*, 31(8), pp. 817–823. doi: 10.1016/j.ejso.2005.05.010.
- Asprițoiu, V. M. *et al.* (2021) 'Epigenetic Regulation of Angiogenesis in Development and Tumors Progression: Potential Implications for Cancer Treatment', *Frontiers in Cell and Developmental Biology*. doi: 10.3389/fcell.2021.689962.
- ASPRS (1987) 'Report on autologous fat transplantation', *Plast Surg Nurs*, 7(4), pp. 140–1.
- Asselain, B. *et al.* (2018) 'Long-term outcomes for neoadjuvant versus adjuvant chemotherapy in early breast cancer: meta-analysis of individual patient data from ten randomised trials', *The Lancet Oncology*, 19(1), pp. 27–39. doi: 10.1016/S1470-2045(17)30777-5.
- Atiya, H. *et al.* (2020) 'Mesenchymal Stem Cells in the Tumor Microenvironment', *Advances in Experimental Medicine and Biology*, 1234(February), pp. 31–42. doi: 10.1007/978-3-030-37184-5_3.

- Attwell, D. *et al.* (2016) 'What is a pericyte?', *Journal of Cerebral Blood Flow and Metabolism*, 36(2), pp. 451–455. doi: 10.1177/0271678X15610340.
- Axel, A. E. *et al.* (2009) 'Interleukin-6 induces an epithelial–mesenchymal transition phenotype in human breast cancer cells', *Oncogene*. Nature Publishing Group, 28(33), pp. 2940–2947. doi: 10.1038/onc.2009.180.
- Baba, A. and Cătoi, C. (2007) 'TUMOR CELL MORPHOLOGY', in *Comparative Oncology*. Bucharest (RO): The Publishing House of the Romanian Academy. Available at: <https://www.ncbi.nlm.nih.gov/books/NBK9553/#top>.
- Bachmann, S. *et al.* (2020) 'Interacting adipose-derived stem cells and microvascular endothelial cells provide a beneficial milieu for soft tissue healing', *Molecular Biology Reports*. Springer Netherlands, 47(1), pp. 111–122. doi: 10.1007/s11033-019-05112-y.
- Baeriswyl, V. and Christofori, G. (2009) 'The angiogenic switch in carcinogenesis', *Seminars in Cancer Biology*, 19(5), pp. 329–337. doi: 10.1016/j.semcancer.2009.05.003.
- Bajaj, J., Diaz, E. and Reya, T. (2020) 'Stem cells in cancer initiation and progression', *Journal of Cell Biology*, 219(1), pp. 1–12. doi: 10.1083/jcb.201911053.
- Balkwill, F. and Mantovani, A. (2001) 'Inflammation and cancer: Back to Virchow?', *Lancet*, 357(9255), pp. 539–545. doi: 10.1016/S0140-6736(00)04046-0.
- Banie, L. *et al.* (2008) 'Defining Stem and Progenitor Cells within Adipose Tissue', *Stem Cells and Development*, 17(6), pp. 1053–1063. doi: 10.1089/scd.2008.0117.
- Banyard, D. A. *et al.* (2015) 'Implications for human adipose-derived stem cells in plastic surgery', *Journal of Cellular and Molecular Medicine*, 19(1), pp. 21–30. doi: 10.1111/jcmm.12425.
- Barbarestani, M. *et al.* (2006) 'Evaluation of human breast adenocarcinoma (MCF-7) cells proliferation in co-culture with human adipocytes in three dimensional collagen gel matrix: Norepinephrine as a lipolytic factor', *Iranian Biomedical Journal*, 10(3), pp. 125–131.
- Barbato, L. *et al.* (2019) 'Cancer Stem Cells and Targeting Strategies', *Cells*, 8(8), p. 926. doi: 10.3390/cells8080926.

- Bartoschek, M. *et al.* (2018) 'Spatially and functionally distinct subclasses of breast cancer-associated fibroblasts revealed by single cell RNA sequencing', *Nature Communications*. Springer US, 9(1). doi: 10.1038/s41467-018-07582-3.
- Barwinska, D. *et al.* (2018) 'Cigarette Smoking Impairs Adipose Stromal Cell Vasculogenic Activity and Abrogates Potency to Ameliorate Ischemia', *Stem Cells*, 36(6), pp. 856–867. doi: 10.1002/stem.2813.
- Batista, B. N. *et al.* (2016) 'Lipofilling of the Breast Does Not Increase the Risk of Recurrence of Breast Cancer', *Plastic and Reconstructive Surgery*, 138(6), pp. 1068e-1069e. doi: 10.1097/prs.0000000000002794.
- Baum, M. (2013) 'Modern concepts of the natural history of breast cancer: A guide to the design and publication of trials of the treatment of breast cancer', *European Journal of Cancer*. Elsevier Ltd, 49(1), pp. 60–64. doi: 10.1016/j.ejca.2012.07.005.
- Bellei, B. *et al.* (2017) 'Maximizing non-enzymatic methods for harvesting adipose-derived stem from lipoaspirate: Technical considerations and clinical implications for regenerative surgery', *Scientific Reports*. Springer US, 7(1), pp. 1–15. doi: 10.1038/s41598-017-10710-6.
- Berdasco, M. and Esteller, M. (2010) 'Aberrant Epigenetic Landscape in Cancer: How Cellular Identity Goes Awry', *Developmental Cell*, 19(5), pp. 698–711. doi: 10.1016/j.devcel.2010.10.005.
- Bertheau, P. *et al.* (2013) 'P53 in breast cancer subtypes and new insights into response to chemotherapy', *Breast*. Elsevier Ltd, 22(S2), pp. S27–S29. doi: 10.1016/j.breast.2013.07.005.
- Berthois, Y., Katzenellenbogen, J. A. and Katzenellenbogen, B. S. (1986) 'Phenol red in tissue culture media is a weak estrogen: Implications concerning the study of estrogen-responsive cells in culture', *Proceedings of the National Academy of Sciences of the United States of America*, 83(8), pp. 2496–2500. doi: 10.1073/pnas.83.8.2496.
- Bertolini, F., Petit, J. Y. and Kolonin, M. G. (2015) 'Stem cells from adipose tissue and breast cancer: Hype, risks and hope', *British Journal of Cancer*. Nature Publishing Group, 112(3), pp. 419–423. doi: 10.1038/bjc.2014.657.
- Berx, G. *et al.* (1995) 'E-cadherin is a tumor/invasion suppressor gene mutated in human lobular breast cancers', *The EMBO Journal*, 14(24), pp. 6107–6115.

doi: 10.1136/mp.54.2.91.

Berx, G. and van Roy, F. (2009) 'Involvement of members of the cadherin superfamily in cancer.', *Cold Spring Harbor perspectives in biology*, 1(6). doi: 10.1101/cshperspect.a003129.

Bhandari, V. *et al.* (2019) 'Molecular landmarks of tumor hypoxia across cancer types', *Nature Genetics*. Springer US, 51(2), pp. 308–318. doi: 10.1038/s41588-018-0318-2.

Bhowmick, N. A., Neilson, E. G. and Moses, H. L. (2004) 'Stromal fibroblasts in cancer initiation and progression', *Nature*, 432(7015), pp. 332–337. doi: 10.1038/nature03096.

Biazús, J. V. *et al.* (2015) 'Immediate reconstruction with autologous fat transfer following breast-conserving surgery', *Breast Journal*, 21(3), pp. 268–275. doi: 10.1111/tbj.12397.

Blondeel, P. N. and Christiaens, M. R. (2002) '1025 Recent refinements in free flap breast reconstruction: The deep inferior epigastric perforator (DIEP) free flap anastomosed to the internal mammary artery', *European Journal of Cancer*, 31, p. S215. doi: 10.1016/0959-8049(95)96273-g.

Boire, A. *et al.* (2005) 'PAR1 Is a Matrix Metalloprotease-1 Receptor that Promotes Invasion and Tumorigenesis of Breast Cancer Cells', 120, pp. 303–313. doi: 10.1016/j.cell.2004.12.018.

Bourin, P. *et al.* (2013) 'Stromal cells from the adipose tissue-derived stromal vascular fraction and culture expanded adipose tissue-derived stromal/stem cells: A joint statement of the International Federation for Adipose Therapeutics and Science (IFATS) and the International So', *Cytotherapy*. Elsevier Inc, 15(6), pp. 641–648. doi: 10.1016/j.jcyt.2013.02.006.

Boussari, O. *et al.* (2018) 'A new approach to estimate time-to-cure from cancer registries data', *Cancer Epidemiology*. Elsevier, 53(September 2017), pp. 72–80. doi: 10.1016/j.canep.2018.01.013.

Bowen, J. E. (2015) 'Technical Issues in Harvesting and Concentrating Stem Cells (Bone Marrow and Adipose)', *PM and R*, 7(4), pp. S8–S18. doi: 10.1016/j.pmrj.2015.01.025.

Brenelli, F. *et al.* (2014) 'Oncological safety of autologous fat grafting after breast conservative treatment: A prospective evaluation', *Breast Journal*, 20(2), pp. 159–165. doi: 10.1111/tbj.12225.

- Browall, M. *et al.* (2018) 'Physical Activity During and After Adjuvant Treatment for Breast Cancer: An Integrative Review of Women's Experiences', *Integrative Cancer Therapies*, 17(1), pp. 16–30. doi: 10.1177/1534735416683807.
- Bunnell, B. A., Flaate, M., *et al.* (2008) 'Adipose-derived stem cells: Isolation, expansion and differentiation', *Methods*, 45(2), pp. 115–120. doi: 10.1016/j.ymeth.2008.03.006.
- Bunnell, B. A., Mette, F., *et al.* (2008) 'Adipose-derived stem cells: Isolation, expansion and differentiation', *Methods*, 45(2), pp. 115–120. doi: 10.1016/j.ymeth.2008.03.006.Adipose-derived.
- Burdall, S. E. *et al.* (2003) 'Breast cancer cell lines: Friend or foe?', *Breast Cancer Research*, 5(2), pp. 89–95. doi: 10.1186/bcr577.
- Busser, H. *et al.* (2014) 'Isolation of Adipose-Derived Stromal Cells', *Stem Cells and Development*, 23(19), pp. 2390–2400. doi: 10.1089/scd.2014.0071.
- Byrd, T. *et al.* (2015) 'Polystyrene microspheres enable 10-color compensation for immunophenotyping of primary human leukocytes', *Cytometry Part A*, 87(11), pp. 1038–1046. doi: 10.1002/cyto.a.22717.
- Cai, Y. *et al.* (2020) 'Therapeutic applications of adipose cell-free derivatives: A review', *Stem Cell Research and Therapy*. *Stem Cell Research & Therapy*, 11(1), pp. 1–16. doi: 10.1186/s13287-020-01831-3.
- Cailleau, R., Olivé, M. and Cruciger, Q. V. J. (1978) 'Long-term human breast carcinoma cell lines of metastatic origin: Preliminary characterization', *In Vitro*, 14(11), pp. 911–915. doi: 10.1007/BF02616120.
- Carioli, G. *et al.* (2017) 'Trends and predictions to 2020 in breast cancer mortality in Europe', *Breast*. Elsevier Ltd, 36(2017), pp. 89–95. doi: 10.1016/j.breast.2017.06.003.
- Carmeliet, P. *et al.* (1998) 'Role of HIF-1 α in hypoxia-mediated apoptosis, cell proliferation and tumour angiogenesis', *Nature*, 394(6692), pp. 485–490. doi: 10.1038/28867.
- Carneiro, B. A. and S. El-Deiry, W. (2020) 'Targeting apoptosis in cancer therapy', *Nat Rev Clin Oncol*, 17(7), pp. 395–417. doi: 10.1038/s41571-020-0341-y.Targeting.
- Caul, S. and Broggio, J. (2019) *Cancer registration statistics, England 2017*, Office for National Statistics. Available at:

<https://www.ons.gov.uk/peoplepopulationandcommunity/healthandsocialcare/conditionsanddiseases/bulletins/cancerregistrationstatisticsengland/2017>.

Cavallaro, U. and Christofori, G. (2004) 'Cell adhesion and signalling by cadherins and Ig-CAMs in cancer', *Nature Reviews Cancer*, 4(2), pp. 118–132. doi: 10.1038/nrc1276.

Cerottini, J. C., Liénard, D. and Romero, P. (1996) 'Recognition of tumor-associated antigens by T-lymphocytes: Perspectives for peptide-based vaccines', *Annals of Oncology*, 7(4), pp. 339–342. doi: 10.1093/oxfordjournals.annonc.a010598.

Challapalli, R. S. *et al.* (2021) 'Effect of Breast Cancer and Adjuvant Therapy on Adipose-Derived Stromal Cells: Implications for the Role of ADSCs in Regenerative Strategies for Breast Reconstruction', *Stem Cell Reviews and Reports*. *Stem Cell Reviews and Reports*, 17(2), pp. 523–538. doi: 10.1007/s12015-020-10038-1.

Chaput, B. *et al.* (2014) 'Another suspected case of breast cancer recurrence after lipofilling? Remain cautious', *Journal of Plastic, Reconstructive and Aesthetic Surgery*. Elsevier, 67(8), pp. 1156–1157. doi: 10.1016/j.bjps.2014.03.027.

Chen, D. *et al.* (2015) 'Paracrine factors from adipose-mesenchymal stem cells enhance metastatic capacity through Wnt signaling pathway in a colon cancer cell co-culture model', *Cancer Cell International*. *Cancer Cell International*, 15(1), pp. 1–13. doi: 10.1186/s12935-015-0198-9.

Chen, D. S. and Mellman, I. (2013) 'Oncology meets immunology: The cancer-immunity cycle', *Immunity*, 39(1), pp. 1–10. doi: 10.1016/j.immuni.2013.07.012.

Chen, Y.-J. *et al.* (2016) 'Isolation and Differentiation of Adipose-Derived Stem Cells from Porcine Subcutaneous Adipose Tissues', *Journal of Visualized Experiments*, (109), pp. 1–10. doi: 10.3791/53886.

Cheng, N. *et al.* (2005) 'Loss of TGF- β type II receptor in fibroblasts promotes mammary carcinoma growth and invasion through upregulation of TGF- α -, MSP- and HGF-mediated signaling networks', *Oncogene*, 24(32), pp. 5053–5068. doi: 10.1038/sj.onc.1208685.

Cheng, N. *et al.* (2008) 'TGF- β signaling deficient fibroblasts enhance Hepatocyte Growth Factor signaling in mammary carcinoma cells to promote

scattering and invasion', *Molecular Cancer Research*, 6(10), pp. 1521–1533. doi: 10.1158/1541-7786.MCR-07-2203.TGF-

Cherubino, M. *et al.* (2011) 'Adipose-derived stem cells for wound healing applications', *Annals of Plastic Surgery*, 66(2), pp. 210–215. doi: 10.1097/SAP.0b013e3181e6d06c.

Chirappapha, P. *et al.* (2015) 'Evaluation of lipofilling safety in elderly patients with breast cancer', *Plastic and Reconstructive Surgery - Global Open*, 3(7), pp. 1–7. doi: 10.1097/GOX.0000000000000411.

Cho, J. A. *et al.* (2012) 'Exosomes from breast cancer cells can convert adipose tissue-derived mesenchymal stem cells into myofibroblast-like cells', *International Journal of Oncology*, 40(1), pp. 130–138. doi: 10.3892/ijo.2011.1193.

Coates, J. T., Skwarski, M. and Higgins, G. S. (2019) 'Targeting tumour hypoxia: Shifting focus from oxygen supply to demand', *British Journal of Radiology*, 92(1093), pp. 1–3. doi: 10.1259/bjr.20170843.

Coecke, S. *et al.* (2005) 'Guidance on good cell culture practice: A Report of the Second ECVAM Task Force on good cell culture practice', *ATLA Alternatives to Laboratory Animals*, 33(3), pp. 261–287. doi: 10.1177/026119290503300313.

Cohen, S. *et al.* (2019) 'Lipofilling after breast conserving surgery: A comprehensive literature review investigating its oncologic safety', *Gland Surgery*, 8(5), pp. 569–580. doi: 10.21037/gs.2019.09.09.

Coletta, S. *et al.* (2021) 'Tumor cells and the extracellular matrix dictate the pro-tumoral profile of macrophages in CRC', *Cancers*, 13(20), pp. 1–19. doi: 10.3390/cancers13205199.

Combella, E. J. *et al.* (2016) 'Background: breast cancer and the need for reconstruction', *Gland Surg*, 5(2), pp. 227–241. doi: 10.3978/j.issn.2227-684X.2016.01.01.

Comşa, Ş., Cîmpean, A. M. and Raica, M. (2015) 'The story of MCF-7 breast cancer cell line: 40 Years of experience in research', *Anticancer Research*, 35(6), pp. 3147–3154.

Cook, M. M. *et al.* (2021) 'Everolimus Plus Exemestane Treatment in Patients with Metastatic Hormone Receptor-Positive Breast Cancer Previously Treated with CDK4/6 Inhibitor Therapy', *Oncologist*, 26(2), pp. 101–106. doi:

10.1002/onco.13609.

Cook, T. G. *et al.* (2008) 'IFATS Collection: Human Adipose Tissue-Derived Stem Cells Induce Angiogenesis and Nerve Sprouting Following Myocardial Infarction, in Conjunction with Potent Preservation of Cardiac Function', *Stem Cells*, 27(1), pp. 230–237. doi: 10.1634/stemcells.2008-0273.

Cooper, J. (2012) 'Cell line profile MCF-7 (ECACC Catalogue no.86012803)', *European Collection of Authenticated Cell Cultures*, 7(86012803), pp. 1–2.

Costantini, M. *et al.* (2013) 'Radiological findings in mammary autologous fat injections: A multi-technique evaluation', *Clinical Radiology*, 68(1), pp. 27–33. doi: 10.1016/j.crad.2012.05.009.

Cotlar, A. M., Dubose, J. J. and Rose, D. M. (2003) 'History of surgery for breast cancer: Radical to the sublime', *Current Surgery*, 60(3), pp. 329–337. doi: 10.1016/S0149-7944(02)00777-8.

Coussens, L. M. and Werb, Z. (2002) 'Inflammation and cancer', *Nature*, 420, pp. 860–867. doi: 10.1186/s12199-018-0740-1.

Critchley, A. C. *et al.* (2013) 'Current Controversies in Breast Cancer Surgery', *Clinical Oncology*. Elsevier Ltd, 25(2), pp. 101–108. doi: 10.1016/j.clon.2012.10.009.

Cserni, G. *et al.* (2018) 'The new TNM-based staging of breast cancer', *Virchows Archiv*. Virchows Archiv, 472(5), pp. 697–703. doi: 10.1007/s00428-018-2301-9.

D'Esposito, V. *et al.* (2012) 'Adipocyte-released insulin-like growth factor-1 is regulated by glucose and fatty acids and controls breast cancer cell growth in vitro', *Diabetologia*, 55(10), pp. 2811–2822. doi: 10.1007/s00125-012-2629-7.

Dai, X. *et al.* (2016) 'Cancer hallmarks, biomarkers and breast cancer molecular subtypes', *Journal of Cancer*, 7(10), pp. 1281–1294. doi: 10.7150/jca.13141.

Debald, M. *et al.* (2017) 'Lipofilling effects after breast cancer surgery in post-radiation patients: an analysis of results and algorithm proposal', *European Journal of Plastic Surgery*. European Journal of Plastic Surgery, 40(5), pp. 447–454. doi: 10.1007/s00238-017-1311-1.

Delay, E. *et al.* (2009) 'Fat Injection to the Breast: Technique, Results, and Indications Based on 880 Procedures Over 10 Years', *Aesthetic Surgery Journal*. American Society for Aesthetic Plastic Surgery, Inc., 29(5), pp. 360–

376. doi: 10.1016/j.asj.2009.08.010.

Devarajan, E. *et al.* (2012) 'Epithelial-mesenchymal transition in breast cancer lines is mediated through PDGF-D released by tissue-resident stem cells', *International Journal of Cancer*, 131(5), pp. 1023–1031. doi: 10.1002/ijc.26493.

DeVita, V. T. and Rosenberg, S. A. (2012) 'Two Hundred Years of Cancer Research', *New England Journal of Medicine*, 366(23), pp. 2207–2214. doi: 10.1056/nejmra1204479.

Dieudonne, M. N. *et al.* (2002) 'Leptin mediates a proliferative response in human MCF7 breast cancer cells', *Biochemical and Biophysical Research Communications*, 293(1), pp. 622–628. doi: 10.1016/S0006-291X(02)00205-X.

Dirat, B. *et al.* (2011) 'Cancer-associated adipocytes exhibit an activated phenotype and contribute to breast cancer invasion', *Cancer Research*, 71(7), pp. 2455–2465. doi: 10.1158/0008-5472.CAN-10-3323.

Domenis, R. *et al.* (2015) 'Adipose tissue derived stem cells: In vitro and in vivo analysis of a standard and three commercially available cell-assisted lipotransfer techniques', *Stem Cell Research and Therapy*, 6(1), pp. 1–15. doi: 10.1186/scrt536.

Dominici, M. *et al.* (2006) 'Minimal criteria for defining multipotent mesenchymal stromal cells. The International Society for Cellular Therapy position statement', *Cytotherapy*, 8(4), pp. 315–317. doi: 10.1080/14653240600855905.

Donnenberg, V. S. *et al.* (2010) 'Localization of CD44 and CD90 positive cells to the invasive front of breast tumors', *Cytometry Part B - Clinical Cytometry*, 78(5), pp. 287–301. doi: 10.1002/cyto.b.20530.

Dossus, L. and Benusiglio, P. R. (2015) 'Lobular breast cancer: Incidence and genetic and non-genetic risk factors', *Breast Cancer Research*, 17(1), pp. 1–8. doi: 10.1186/s13058-015-0546-7.

Dothel, G. *et al.* (2016) 'Mesenchymal stromal cell-based therapy: Regulatory and translational aspects in gastroenterology', *World Journal of Gastroenterology*, 22(41), pp. 9057–9068. doi: 10.3748/wjg.v22.i41.9057.

Duffy, S. W. *et al.* (2020) 'Effect of mammographic screening from age 40 years on breast cancer mortality (UK Age trial): final results of a randomised,

controlled trial', *The Lancet Oncology*. The Author(s). Published by Elsevier Ltd. This is an Open Access article under the CC BY-NC-ND 4.0 license, 21(9), pp. 1165–1172. doi: 10.1016/S1470-2045(20)30398-3.

Durrechou, Q. *et al.* (2020) 'Management of immune checkpoint inhibitor toxicities', *Cancer Management and Research*, 12, pp. 9139–9158. doi: 10.2147/CMAR.S218756.

Dvorak, H. F. *et al.* (1995) 'Vascular permeability factor/vascular endothelial growth factor, microvascular hyperpermeability, and angiogenesis', *American Journal of Pathology*, 146(5), pp. 1029–1039.

Ekmektzoglou, K. A. *et al.* (2009) 'Breast cancer: From the earliest times through to the end of the 20th century', *European Journal of Obstetrics and Gynecology and Reproductive Biology*, 145(1), pp. 3–8. doi: 10.1016/j.ejogrb.2009.03.017.

Engels, P. E. *et al.* (2013) 'Harvest site influences the growth properties of adipose derived stem cells', *Cytotechnology*, 65(3), pp. 437–445. doi: 10.1007/s10616-012-9498-2.

Evan, G. and Littlewood, T. (1998) 'A matter of life and cell death', *Science*, 281(5381), pp. 1317–1322. doi: 10.1126/science.281.5381.1317.

Evan, G., Lowe, S. and Cepero, E. (2004) 'Intrinsic tumour suppression', *Nature*, 432(NOVEMBER), pp. 1–9. Available at: [papers://5680c084-7e9d-4370-be57-26c320af1685/Paper/p109%0Ahttp://dialnet.unirioja.es/servlet/articulo?codigo=1042932%0Ahttp://file//localhost\(null\)%0Apapers3://publication/uuid/252871BA-EE6A-486E-8050-E261D2908C1B](https://papers://5680c084-7e9d-4370-be57-26c320af1685/Paper/p109%0Ahttp://dialnet.unirioja.es/servlet/articulo?codigo=1042932%0Ahttp://file//localhost(null)%0Apapers3://publication/uuid/252871BA-EE6A-486E-8050-E261D2908C1B).

Evans, D. G. R. *et al.* (2016) 'Breast cancer risk feedback to women in the UK NHS breast screening population', *British Journal of Cancer*. Nature Publishing Group, 114(9), pp. 1045–1052. doi: 10.1038/bjc.2016.56.

Fang, J. *et al.* (2021) 'Adipose tissue-derived stem cells in breast reconstruction: a brief review on biology and translation', *Stem Cell Research and Therapy*. Stem Cell Research & Therapy, 12(1), pp. 1–13. doi: 10.1186/s13287-020-01955-6.

Fatah, F. *et al.* (2021) 'Adipose tissue-derived stem cells in breast reconstruction: a brief review on biology and translation', *Stem Cell Research and Therapy*. Stem Cell Research & Therapy, 12(1), pp. 1–13. doi: 10.1186/s13287-020-01955-6.

Fatah, F. *et al.* (2012) *Lipomodelling Guidelines for Breast Surgery, Joint Guidelines from the Association of Breast Surgery, the British Association of Plastic, Reconstructive and Aesthetic Surgeons, and the British Association of*

Aesthetic Plastic Surgeons.

- Feron, O. (2009) 'Pyruvate into lactate and back: From the Warburg effect to symbiotic energy fuel exchange in cancer cells', *Radiotherapy and Oncology*. Elsevier Ireland Ltd, 92(3), pp. 329–333. doi: 10.1016/j.radonc.2009.06.025.
- Ferrara, N. (2009) 'Vascular endothelial growth factor', *Arteriosclerosis, Thrombosis, and Vascular Biology*, 29(6), pp. 789–791. doi: 10.1161/ATVBAHA.108.179663.
- Ferraro, D. A. *et al.* (2019) 'Endothelial cell-derived nidogen-1 inhibits migration of SK-BR-3 breast cancer cells', *BMC Cancer*. BMC Cancer, 19(1), pp. 1–13. doi: 10.1186/s12885-019-5521-8.
- Fertsch, S. *et al.* (2017) 'Increased risk of recurrence associated with certain risk factors in breast cancer patients after DIEP-flap reconstruction and lipofilling-a matched cohort study with 200 patients', *Gland Surgery*, 6(4), pp. 315–323. doi: 10.21037/gs.2017.03.11.
- Fidler, I. J. (2003) 'The pathogenesis of cancer metastasis: the "seed and soil" hypothesis revisited', *Nat Rev Cancer*, 3(6), pp. 453–8. doi: 10.1097/00006454-199103000-00027.
- Fiorillo, M. *et al.* (2017) 'Mitochondrial "power" drives tamoxifen resistance: NQO1 and GCLC are new therapeutic targets in breast cancer', *Oncotarget*, 8(12), pp. 20309–20327. doi: 10.18632/oncotarget.15852.
- Fiorillo, M. *et al.* (2018) 'The ER-alpha mutation Y537S confers Tamoxifen-resistance via enhanced mitochondrial metabolism, glycolysis and Rho-GDI/PTEN signaling: Implicating TIGAR in somatic resistance to endocrine therapy', *Aging*, 10(12), pp. 4000–4023. doi: 10.18632/aging.101690.
- Fisher, B. *et al.* (2002) 'Twenty-Year Follow-up of a Randomized Trial Comparing Total Mastectomy, Lumpectomy, and Lumpectomy plus Irradiation for the Treatment of Invasive Breast Cancer', *New England Journal of Medicine*, 347(16), pp. 1233–1241. doi: 10.1056/nejmoa022152.
- Fisusi, F. A. and Akala, E. O. (2019) 'Drug Combinations in Breast Cancer Therapy', *Pharmaceutical Nanotechnology*, 7(1), pp. 3–23. doi: 10.2174/2211738507666190122111224.
- Fitoussi, A. *et al.* (2009) 'Reconstruction mammaire secondaire par lipomodelage exclusif', *Annales de Chirurgie Plastique et Esthétique*, 54(4), pp. 374–378. doi: 10.1016/j.anplas.2008.10.009.

- Forman, D. *et al.* (2014) 'Cancer incidence and mortality worldwide: Sources, methods and major patterns in GLOBOCAN 2012', *International Journal of Cancer*, 136(5), pp. E359–E386. doi: 10.1002/ijc.29210.
- Foulds, C. E. (2018) 'Disrupting a negative feedback loop drives endocrine therapy-resistant breast cancer', *Proceedings of the National Academy of Sciences of the United States of America*, 115(33), pp. 8236–8238. doi: 10.1073/pnas.1811263115.
- Fragomeni, S. M., Sciallis, A. and Jeruss, J. S. (2018) 'Molecular subtypes and local-regional control of breast cancer', *Surg Oncol Clin N Am*, 27(1), pp. 95–120. doi: 10.1016/j.soc.2017.08.005.Molecular.
- Fraser, J. K. *et al.* (2006) 'Fat tissue: an underappreciated source of stem cells for biotechnology', *Trends in Biotechnology*, 24(4), pp. 150–154. doi: 10.1016/j.tibtech.2006.01.010.
- Fraser, J. K., Hedrick, M. H. and Cohen, S. R. (2011) 'Oncologic Risks of Autologous Fat Grafting to the Breast', *Aesthetic Surgery Journal*, 31(1), pp. 68–75. doi: 10.1177/1090820x10390922.
- Fridrichova, I. and Zmetakova, I. (2019) 'MicroRNAs Contribute to Breast Cancer Invasiveness', *Cells*, 8(11). doi: 10.3390/cells8111361.
- Fu, C. and Jiang, A. (2018) 'Dendritic Cells and CD8 T Cell Immunity in Tumor Microenvironment', *Frontiers in immunology*, 9(December), p. 3059. doi: 10.3389/fimmu.2018.03059.
- Fujisaki, K. *et al.* (2015) 'Cancer-mediated adipose reversion promotes cancer cell migration via IL-6 and MCP-1', *Breast Cancer Research and Treatment*, 150(2), pp. 255–263. doi: 10.1007/s10549-015-3318-2.
- Fukumura, D. *et al.* (1998) 'Tumor induction of VEGF promoter activity in stromal cells', *Cell*, 94(6), pp. 715–725. doi: 10.1016/S0092-8674(00)81731-6.
- Funes, J. M. *et al.* (2007) 'Transformation of human mesenchymal stem cells increases their dependency on oxidative phosphorylation for energy production', *Proceedings of the National Academy of Sciences of the United States of America*, 104(15), pp. 6223–6228. doi: 10.1073/pnas.0700690104.
- Gabos, Z. *et al.* (2010) 'The association between biological subtype and locoregional recurrence in newly diagnosed breast cancer', *Breast Cancer Research and Treatment*, 124(1), pp. 187–194. doi: 10.1007/s10549-010-

1135-1.

Gallo, M. *et al.* (2018) 'RANTES and IL-6 cooperate in inducing a more aggressive phenotype in breast cancer cells', *Oncotarget*, 9(25), pp. 17543–17553. doi: 10.18632/oncotarget.24784.

Gao, X. *et al.* (2019) 'PIM1 is responsible for IL-6-induced breast cancer cell EMT and stemness via c-myc activation', *Breast Cancer*. Springer Japan, 26(5), pp. 663–671. doi: 10.1007/s12282-019-00966-3.

Gao, Y. *et al.* (2020) 'CD63+ Cancer-Associated Fibroblasts Confer Tamoxifen Resistance to Breast Cancer Cells through Exosomal miR-22', *Advanced Science*. doi: 10.1002/advs.202002518.

Gardner, A. and Ruffell, B. (2016) 'Dendritic Cells and Cancer Immunity', *Trends in Immunology*, 37(12), pp. 855–865. doi: 10.1016/j.it.2016.09.006.Dendritic.

Garroni, G. *et al.* (2021) 'Adipo-derived stem cell features and mcf-7', *Cells*, 10(7), pp. 1–16. doi: 10.3390/cells10071754.

Gatzemeier, W. and Bruce Mann, G. (2013) 'Which sentinel lymph-node (SLN) positive breast cancer patient needs an axillary lymph-node dissection (ALND) - ACOSOG Z0011 results and beyond', *Breast*. Elsevier Ltd, 22(3), pp. 211–216. doi: 10.1016/j.breast.2013.02.001.

Gazet, J.-C. *et al.* (2001) 'Estrogen-receptor-directed neoadjuvant therapy for breast cancer: Results of a randomised trial using formestane and methotrexate, mitozantrone and mitomycin C (MMM) chemotherapy', *Annals of Oncology*, 12, pp. 685–691. doi: 10.1023/A.

Gespach, C. P. *et al.* (2014) 'Cancer-Associated Adipose Tissue Promotes Breast Cancer Progression by Paracrine Oncostatin M and Jak/STAT3 Signaling', *Cancer Research*, 74(23), pp. 6806–6819. doi: 10.1158/0008-5472.can-14-0160.

Goel, S. *et al.* (2016) 'Overcoming Therapeutic Resistance in HER2-Positive Breast Cancers with CDK4/6 Inhibitors', *Cancer Cell*. Elsevier Inc., 29(3), pp. 255–269. doi: 10.1016/j.ccell.2016.02.006.

Goldar, S. *et al.* (2015) 'Molecular mechanisms of apoptosis and roles in cancer development and treatment', *Asian Pacific Journal of Cancer Prevention*, 16(6), pp. 2129–2144. doi: 10.7314/APJCP.2015.16.6.2129.

Gottardis, M. M., Robinson, S. P. and Jordan, V. C. (1988) 'Estradiol-

stimulated growth of MCF-7 tumors implanted in athymic mice: A model to study the tumorigenic action of tamoxifen', *Journal of Steroid Biochemistry*, 30(1–6), pp. 311–314. doi: 10.1016/0022-4731(88)90113-6.

Gøtzsche, P. C. and Jørgensen, K. J. (2013) 'Screening for breast cancer with mammography', *Cochrane Database of Systematic Reviews*, 2013(6). doi: 10.1002/14651858.CD001877.pub5.

Gourdon, D. *et al.* (2012) 'Implanted adipose progenitor cells as physicochemical regulators of breast cancer', *Proceedings of the National Academy of Sciences*, 109(25), pp. 9786–9791. doi: 10.1073/pnas.1121160109.

Graeber, T. G. *et al.* (1996) 'Hypoxia-mediated selection of cells with diminished apoptotic potential in solid tumours', *Nature*, pp. 88–91. doi: 10.1038/379088a0.

Greuter, T. *et al.* (2020) 'Malignancies in Inflammatory Bowel Disease', *Digestion*, 101(Suppl1), pp. 136–145. doi: 10.1159/000509544.

Grivennikov, S. I., Greten, F. R. and Karin, M. (2010) 'Immunity, Inflammation, and Cancer', *Cell*. Elsevier Inc., 140(6), pp. 883–899. doi: 10.1016/j.cell.2010.01.025.

Groen, J. W. *et al.* (2016) 'Autologous fat grafting in cosmetic breast augmentation: A systematic review on radiological safety, complications, volume retention, and patient/surgeon satisfaction', *Aesthetic Surgery Journal*, 36(9), pp. 993–1007. doi: 10.1093/asj/sjw105.

Grotting, J. C., Beckenstein, M. S. and Arkoulakis, N. S. (2003) 'The art and science of autologous breast reconstruction', *Breast Journal*, 9(5), pp. 350–360. doi: 10.1046/j.1524-4741.2003.09527.x.

Grujic, D. *et al.* (2021) 'Well-being, depression, and anxiety following oncoplastic breast conserving surgery versus modified radical mastectomy followed by late breast reconstruction', *International Journal of Environmental Research and Public Health*, 18(17). doi: 10.3390/ijerph18179320.

Grünherz, L. *et al.* (2020) 'Donor site aesthetics and morbidity after DIEP flap breast reconstruction—A retrospective multicenter study', *Breast Journal*, 26(10), pp. 1980–1986. doi: 10.1111/tbj.14003.

Gu, L. *et al.* (2021) 'Comparing Hypofractionated With Conventional Fractionated Radiotherapy After Breast-Conserving Surgery for Early Breast

Cancer: A Meta-Analysis of Randomized Controlled Trials', *Frontiers in Oncology*, 11(October), pp. 1–12. doi: 10.3389/fonc.2021.753209.

Guan, J. and Chen, J. (2013) 'Mesenchymal stem cells in the tumor microenvironment', *Biomedical Reports*, 1(4), pp. 517–521. doi: 10.3892/br.2013.103.

Gudjonsson, T. *et al.* (2005) 'Myoepithelial cells: their origin and function in breast morphogenesis and neoplasia.', *Journal of mammary gland biology and neoplasia*, 10(3), pp. 261–272. doi: 10.1007/s10911-005-9586-4.

Guppy, M. *et al.* (2002) 'Contribution by different fuels and metabolic pathways to the total ATP turnover of proliferating MCF-7 breast cancer cells', *Biochemical Journal*, 364(1), pp. 309–315. doi: 10.1042/bj3640309.

Guterres, A. N. and Villanueva, J. (2020) 'Targeting telomerase for cancer therapy', *Oncogene*. Springer US, 39(36), pp. 5811–5824. doi: 10.1038/s41388-020-01405-w.

Gutowski, K. A. *et al.* (2009) 'Current applications and safety of autologous fat grafts: A report of the ASPS Fat Graft Task Force', *Plastic and Reconstructive Surgery*, 124(1), pp. 272–280. doi: 10.1097/PRS.0b013e3181a09506.

Hajmoussa, G. and Harmsen, M. C. (2017) 'Assessment of Energy Metabolic Changes in Adipose Tissue-Derived Stem Cells', *Methods Mol Biol*, 1553, pp. 55–65. doi: 10.1007/978-1-4939-6756-8.

Hajra, K. M., Chen, D. Y. S. and Fearon, E. R. (2002) 'The SLUG zinc-finger protein represses E-cadherin in breast cancer', *Cancer Research*, 62(6), pp. 1613–1618.

Hanahan, D. and Folkman, J. (1996) 'Models and molecular mechanisms of blood vessel co-option by cancer cells', *Cell*, 86(3), pp. 353–364. doi: 10.1016/S0092-8674(00)80108-7.

Hanahan, D. and Weinberg, R. A. (2000) 'The Hallmarks of Cancer', *Cell*, 100, pp. 57–70.

Hanahan, D. and Weinberg, R. A. (2011) 'Hallmarks of cancer: The next generation', *Cell*. Elsevier Inc., 144(5), pp. 646–674. doi: 10.1016/j.cell.2011.02.013.

Hanson, S. E., Kim, J. and Hematti, P. (2013) 'Comparative analysis of adipose-derived mesenchymal stem cells isolated from abdominal and breast tissue', *Aesthetic Surgery Journal*, 33(6), pp. 888–898. doi:

10.1177/1090820X13496115.

Hao, Y. *et al.* (2021) 'Effect of long-term weight gain on the risk of breast cancer across women's whole adulthood as well as hormone-changed menopause stages: A systematic review and dose–response meta-analysis', *Obesity Research and Clinical Practice*, 15(5), pp. 439–448. doi: 10.1016/j.orcp.2021.08.004.

Hao, Y., Baker, D. and Dijke, P. Ten (2019) 'TGF- β -mediated epithelial-mesenchymal transition and cancer metastasis', *International Journal of Molecular Sciences*, 20(11). doi: 10.3390/ijms20112767.

Harrod, A. *et al.* (2017) 'Genomic modelling of the ESR1 Y537S mutation for evaluating function and new therapeutic approaches for metastatic breast cancer', *Oncogene*. Nature Publishing Group, 36(16), pp. 2286–2296. doi: 10.1038/onc.2016.382.

Hembruff, S. L. *et al.* (2010) 'Loss of transforming growth factor- β signaling in mammary fibroblasts enhances CCL2 secretion to promote mammary tumor progression through macrophage-dependent and -independent mechanisms', *Neoplasia*. Neoplasia Press, Inc., 12(5), pp. 425–433. doi: 10.1593/neo.10200.

Heneweer, M. *et al.* (2005) 'Co-culture of primary human mammary fibroblasts and MCF-7 cells as an in vitro breast cancer model', *Toxicological Sciences*, 83(2), pp. 257–263. doi: 10.1093/toxsci/kfi025.

Hermann, R. E. *et al.* (1985) 'Results of Conservative Operations for Breast Cancer', *Archives of Surgery*, 120(6), pp. 746–751. doi: 10.1001/archsurg.1985.01390300084015.

Hicks, D. G. and Lester, S. C. (2016) 'Histology of Normal Breast', *Diagnostic Pathology: Breast*, pp. 4–13. doi: 10.1016/b978-0-323-37712-6.50007-7.

Hida, K. and Maishi, N. (2018) 'Abnormalities of tumor endothelial cells and cancer progression', *Oral Science International*. Japanese Stomatological Society, 15(1), pp. 1–6. doi: 10.1016/S1348-8643(17)30041-1.

Hoeijmakers, J. H. J. (2001) 'The consequences of DNA injury Genome maintenance mechanisms for preventing cancer', *Nature*, 411(6835), pp. 366–374.

Holliday, D. L. and Speirs, V. (2011) 'Choosing the right cell line for breast cancer research', *Breast cancer research*, 13(4), pp. 1–7. Available at:

<http://download.springer.com/static/pdf/110/art%253A10.1186%252Fbcr2889.pdf?originUrl=http%3A%2F%2Fbreast-cancer-research.biomedcentral.com%2Farticle%2F10.1186%2Fbcr2889&token2=exp=1494268443~acl=%2Fstatic%2Fpdf%2F110%2Fart%25253A10.1186%25252Fbcr2889.pdf>.

Holm, J. *et al.* (2017) 'Assessment of breast cancer risk factors reveals subtype heterogeneity', *Cancer Research*, 77(13), pp. 3708–3717. doi: 10.1158/0008-5472.CAN-16-2574.

Hortobagyi, G. N. *et al.* (2016) 'Ribociclib as First-Line Therapy for HR-Positive, Advanced Breast Cancer', *New England Journal of Medicine*, 375(18), pp. 1738–1748. doi: 10.1056/nejmoa1609709.

Howell, A. *et al.* (2005) 'Fulvestrant versus anastrozole for the treatment of advanced breast carcinoma: A prospectively planned combined survival analysis of two multicenter trials', *Cancer*, 104(2), pp. 236–239. doi: 10.1002/cncr.21163.

Hussain, S. P. and Harris, C. C. (2007) 'Inflammation and cancer: An ancient link with novel potentials', *International Journal of Cancer*, 121(11), pp. 2373–2380. doi: 10.1002/ijc.23173.

Hynes, N. E. and MacDonald, G. (2009) 'ErbB receptors and signaling pathways in cancer', *Current Opinion in Cell Biology*, 21(2), pp. 177–184. doi: 10.1016/j.ceb.2008.12.010.

Intlekofer, A. M. and Finley, L. W. S. (2019) 'Metabolic signatures of cancer cells and stem cells', *Nature Metabolism*, 1(2), pp. 177–188. doi: 10.1038/s42255-019-0032-0.Metabolic.

Iqbal, J., Chong, P. Y. and Tan, P. H. (2013) 'Breast cancer stem cells: An update', *Journal of Clinical Pathology*, 66(6), pp. 485–490. doi: 10.1136/jclinpath-2012-201304.

Iyyanki, T. *et al.* (2015) 'Harvesting technique affects adipose-derived stem cell yield', *Aesthetic Surgery Journal*, 35(4), pp. 467–476. doi: 10.1093/asj/sju055.

Jackson, S. P. and Bartek, J. (2009) 'The DNA-damage response in human biology and disease', *Nature*, 461(7267), pp. 1071–1078. doi: 10.1038/nature08467.

Jeevan, R. *et al.* (2011) *National Mastectomy and Breast Reconstruction Audit*,

The NHS Information Centre.

Jeevan, R. *et al.* (2014) 'Findings of a national comparative audit of mastectomy and breast reconstruction surgery in England', *Journal of Plastic, Reconstructive and Aesthetic Surgery*. Elsevier Ltd, 67(10), pp. 1333–1344. doi: 10.1016/j.bjps.2014.04.022.

Jiang, G. *et al.* (2016) 'Comprehensive comparison of molecular portraits between cell lines and tumors in breast cancer', *BMC Genomics*. BMC Genomics, 17(Suppl 7). doi: 10.1186/s12864-016-2911-z.

Jiang, W. G. *et al.* (2015) 'Tissue invasion and metastasis: Molecular, biological and clinical perspectives', *Seminars in Cancer Biology*, 35, pp. S244–S275. doi: 10.1016/j.semcancer.2015.03.008.

Jiang, Y., Xie, Q. L. and Chen, R. (2021) 'Breast Cancer Incidence and Mortality in Relation to Hormone Replacement Therapy Use Among Postmenopausal Women: Results From a Prospective Cohort Study', *Clinical Breast Cancer*. Elsevier Inc., pp. 1–8. doi: 10.1016/j.clbc.2021.06.010.

Johnson, J. *et al.* (2016) 'Targeting the RB-E2F pathway in breast cancer', *Oncogene*. Nature Publishing Group, 35(37), pp. 4829–4835. doi: 10.1038/onc.2016.32.

Jordan, V. C. and Levenson, A. S. (1997) 'MCF-7: The First Hormone-responsive Breast Cancer Cell Line', *Cancer Research*, 57(20), pp. 3071–3078.

Jose, C., Bellance, N. and Rossignol, R. (2011) 'Choosing between glycolysis and oxidative phosphorylation: A tumor's dilemma?', *Biochimica et Biophysica Acta - Bioenergetics*. Elsevier B.V., 1807(6), pp. 552–561. doi: 10.1016/j.bbabi.2010.10.012.

Josiah, D. T. *et al.* (2010) 'Adipose-derived stem cells as therapeutic delivery vehicles of an oncolytic virus for glioblastoma', *Molecular Therapy*. The American Society of Gene & Cell Therapy, 18(2), pp. 377–385. doi: 10.1038/mt.2009.265.

Jotzu, C. *et al.* (2011) 'Adipose tissue derived stem cells differentiate into carcinoma-associated fibroblast-like cells under the influence of tumor derived factors', *Cellular Oncology*, 34(1), pp. 55–67. doi: 10.1007/s13402-011-0012-1.

Joyce, C. W. *et al.* (2015) 'Fat grafting: A citation analysis of the seminal

articles', *Plastic and Reconstructive Surgery - Global Open*, 3(1), pp. 15–24. doi: 10.1097/GOX.0000000000000269.

Ju, Y. S. et al. (2014) 'Origins and functional consequences of somatic mitochondrial DNA mutations in human cancer', *eLife*, 3, pp. 1–28. doi: 10.7554/eLife.02935.

Kalluri, R. and Zeisberg, M. (2006) 'Fibroblasts in cancer', *Nature Reviews Cancer*, 6(5), pp. 392–401. doi: 10.1038/nrc1877.

Kalstrup, J. et al. (2021) 'Immediate direct-to-implant breast reconstruction with acellular dermal matrix: Evaluation of complications and safety', *The Breast*, 60, pp. 192–198. doi: 10.1016/j.breast.2021.10.006.

Kengelbach-Weigand, A. et al. (2019) 'Plasticity of patient-matched normal mammary epithelial cells is dependent on autologous adipose-derived stem cells', *Scientific Reports*. Springer US, 9(1), pp. 1–14. doi: 10.1038/s41598-019-47224-2.

Kennedy, K. M. and Dewhirst, M. W. (2010) 'Tumor metabolism of lactate: The influence and therapeutic potential for MCT and CD147 regulation', *Future Oncology*, 6(1), pp. 127–148. doi: 10.2217/fon.09.145.

Kenny, P. A. et al. (2007) 'The morphologies of breast cancer cell lines in three-dimensional assays correlate with their profiles of gene expression', *Molecular Oncology*, 1(1), pp. 84–96. doi: 10.1016/j.molonc.2007.02.004.

Kessenbrock, K., Plaks, V. and Werb, Z. (2010) 'Matrix Metalloproteinases: Regulators of the Tumor Microenvironment', *Cell*, 141(1), pp. 52–67. doi: 10.1016/j.cell.2010.03.015.

Kidd, S. et al. (2009) 'Direct Evidence of Mesenchymal Stem Cell Tropism for Tumor and Wounding Microenvironments using In Vivo Bioluminescence Imaging', *Stem Cells*, 27(10), pp. 2614–2623. doi: 10.1002/stem.187.Direct.

Koellensperger, E. et al. (2017) 'The impact of human adipose tissue-derived stem cells on breast cancer cells: Implications for cell-assisted lipotransfers in breast reconstruction', *Stem Cell Research and Therapy*. Stem Cell Research & Therapy, 8(1), pp. 1–19. doi: 10.1186/s13287-017-0579-1.

Kønig, S. M. et al. (2019) 'Alterations of the interactome of Bcl-2 proteins in breast cancer at the transcriptional, mutational and structural level', *PLoS Computational Biology*, 15(12), pp. 1–28. doi: 10.1371/journal.pcbi.1007485.

Krag, D. et al. (2010) 'Sentinel-lymph-node resection compared with

conventional axillary-lymph-node dissection in clinically node-negative patients with breast cancer: overall survival findings from the NSABP B-32 randomised phase 3 trial', *Lancet Oncology*, 11(10), pp. 927–33. doi: 10.1016/S1470-2045(10)70207-2.Sentinel-lymph-node.

Kronowitz, S. J. (2012) 'State of the art in breast reconstruction', *Current Breast Cancer Reports*, 4(2), pp. 119–131. doi: 10.1007/s12609-012-0078-4.

Kronowitz, S. J. *et al.* (2016) 'Lipofilling of the Breast Does Not Increase the Risk of Recurrence of Breast Cancer: A Matched Controlled Study', *Plastic and Reconstructive Surgery*, 137(2), pp. 385–393. doi: 10.1097/01.prs.0000475741.32563.50.

Kruger, M. J. *et al.* (2018) 'ADSC-conditioned media elicit an ex vivo anti-inflammatory macrophage response', *Journal of Molecular Endocrinology*, 61(4), pp. 173–184. doi: 10.1530/JME-18-0078.

Kucerova, L. *et al.* (2011) 'Interaction of human adipose tissue-derived mesenchymal stromal cells with breast cancer cells', *Neoplasma*, 5, pp. 361–370. doi: 10.4149/neo.

Kuhbier, J. W. *et al.* (2014) 'Observed changes in the morphology and phenotype of breast cancer cells in direct co-culture with adipose-derived stem cells', *Plastic and Reconstructive Surgery*, 134(3), pp. 414–423. doi: 10.1097/PRS.0000000000000525.

Kyriakopoulou, K. *et al.* (2020) 'EGFR/ER β -Mediated Cell Morphology and Invasion Capacity Are Associated with Matrix Culture Substrates in Breast Cancer', *Cells*, 9(10). doi: 10.3390/cells9102256.

Lazebnik, Y. (2010) 'What are the hallmarks of cancer?', *Nature Reviews Cancer*. Nature Publishing Group, 10(4), pp. 232–233. doi: 10.1038/nrc2827.

Lee, J., Park, S. and Roh, S. (2015) 'Transdifferentiation of mouse adipose-derived stromal cells into acinar cells of the submandibular gland using a co-culture system', *Experimental Cell Research*. Academic Press Inc., 334(1), pp. 160–172. doi: 10.1016/j.yexcr.2015.03.006.

Lee, Y. K., Jung, W. H. and Koo, J. S. (2015) 'Adipocytes can induce epithelial-mesenchymal transition in breast cancer cells', *Breast Cancer Research and Treatment*. Springer US, 153(2), pp. 323–335. doi: 10.1007/s10549-015-3550-9.

Leek, R. D. *et al.* (1996) 'Association of Macrophage Infiltration with

Angiogenesis and Prognosis in Invasive Breast Carcinoma', *Cancer Research*, 56(16), pp. 4625–4629.

Lemmon, M. A. and Schlessinger, J. (2010) 'Cell signaling by receptor tyrosine kinases', *Cell*, 141(7), pp. 1117–1134. doi: 10.1016/j.cell.2010.06.011.

Li, C. Y. *et al.* (2015) 'Comparative analysis of human mesenchymal stem cells from bone marrow and adipose tissue under xeno-free conditions for cell therapy', *Stem Cell Research and Therapy*. ???, 6(1). doi: 10.1186/s13287-015-0066-5.

Li, L. *et al.* (2020) 'Conditioned medium from human adipose-derived mesenchymal stem cell culture prevents uvb-induced skin aging in human keratinocytes and dermal fibroblasts', *International Journal of Molecular Sciences*, 21(1). doi: 10.3390/ijms21010049.

Li, R. *et al.* (2009) 'Interleukin 6 secreted from adipose stromal cells promotes migration and invasion of breast cancer cells', *Oncogene*, 28(30), pp. 2745–2755. doi: 10.1038/onc.2009.130.

Li, T. *et al.* (2020) 'Adipose-derived mesenchymal stem cells and extracellular vesicles confer antitumor activity in preclinical treatment of breast cancer', *Pharmacological Research*. Elsevier, 157(April), p. 104843. doi: 10.1016/j.phrs.2020.104843.

Liberti, M. V and Locasale, J. W. (2016) 'The Warburg Effect : How Does it Benefit Cancer Cells?', *Trends Biochem Sci*, 41(3), pp. 211–218. doi: 10.1016/j.tibs.2015.12.001.The.

Lin, R., Wang, S. and Zhao, R. C. (2013) 'Exosomes from human adipose-derived mesenchymal stem cells promote migration through Wnt signaling pathway in a breast cancer cell model', *Molecular and Cellular Biochemistry*, 383(1–2), pp. 13–20. doi: 10.1007/s11010-013-1746-z.

Liu, L. *et al.* (2020) 'Comparing hypofractionated to conventional fractionated radiotherapy in postmastectomy breast cancer: A meta-analysis and systematic review', *Radiation Oncology*. Radiation Oncology, 15(1), pp. 1–15. doi: 10.1186/s13014-020-1463-1.

Liu, M. *et al.* (2017) 'Adipose-Derived Mesenchymal Stem Cells from the Elderly Exhibit Decreased Migration and Differentiation Abilities with Senescent Properties', *Cell Transplantation*, 26(9), pp. 1505–1519. doi: 10.1177/0963689717721221.

- Liu, S. *et al.* (2006) 'Hedgehog signaling and Bmi-1 regulate self-renewal of normal and malignant human mammary stem cells', *Cancer Research*, 66(12), pp. 6063–6071. doi: 10.1158/0008-5472.CAN-06-0054.
- Liu, S. *et al.* (2010) 'Synergistic Angiogenesis Promoting Effects of Extracellular Matrix Scaffolds and Adipose-Derived Stem Cells During Wound Repair', *Tissue Engineering Part A*, 17(5–6), pp. 725–739. doi: 10.1089/ten.tea.2010.0331.
- Liubomirski, Y. *et al.* (2019) 'Tumor-stroma-inflammation networks promote pro-metastatic chemokines and aggressiveness characteristics in triple-negative breast cancer', *Frontiers in Immunology*, 10(APR), pp. 1–24. doi: 10.3389/fimmu.2019.00757.
- Locke, M., Windsor, J. and Dunbar, P. R. (2009) 'Human adipose-derived stem cells: Isolation, characterization and applications in surgery', *ANZ Journal of Surgery*, 79(4), pp. 235–244. doi: 10.1111/j.1445-2197.2009.04852.x.
- Losken, A. *et al.* (2011) 'Autologous fat grafting in secondary breast reconstruction', *Annals of Plastic Surgery*, 66(5), pp. 518–522. doi: 10.1097/SAP.0b013e3181fe9334.
- Losken, A. and Jurkiewicz, M. J. (2002) 'History of breast reconstruction', *Breast Disease*, 16(2), pp. 3–9. doi: 10.3233/BD-2002-16102.
- Lucar, O., Keith Reeves, R. and Jost, S. (2019) 'A natural impact: NK cells at the intersection of cancer and HIV disease', *Frontiers in Immunology*, 10(AUG). doi: 10.3389/fimmu.2019.01850.
- Ma, Y. *et al.* (2017) 'IL-6, IL-8 and TNF- α levels correlate with disease stage in breast cancer patients', *Advances in Clinical and Experimental Medicine*, 26(3), pp. 421–426. doi: 10.17219/acem/62120.
- Macklin, P. S. *et al.* (2020) 'Recent advances in the biology of tumour hypoxia with relevance to diagnostic practice and tissue-based research', *Journal of Pathology*, 250(5), pp. 593–611. doi: 10.1002/path.5402.
- Magnoni, F. *et al.* (2020) 'Axillary surgery in breast cancer: An updated historical perspective', *Seminars in Oncology*. Elsevier Inc., 47(6), pp. 341–352. doi: 10.1053/j.seminoncol.2020.09.001.
- Mai, P. L. *et al.* (2016) 'Risks of first and subsequent cancers among TP53 mutation-carriers in the NCI LFS cohort', *Cancer*, 122(23), pp. 3673–3681. doi: 10.1002/cncr.30248.Risks.

- Maione, L. *et al.* (2015) 'Autologous Fat Graft by Needle: Analysis of Complications after 1000 Patients', *Annals of Plastic Surgery*, 74(3), pp. 277–280. doi: 10.1097/SAP.000000000000050.
- Maishi, N. and Hida, K. (2017) 'Tumor endothelial cells accelerate tumor metastasis', *Cancer Science*, 108(10), pp. 1921–1926. doi: 10.1111/cas.13336.
- Manabe, Y. *et al.* (2003) 'Mature adipocytes, but not preadipocytes, promote the growth of breast carcinoma cells in collagen gel matrix culture through cancer-stromal cell interactions', *Journal of Pathology*, 201(2), pp. 221–228. doi: 10.1002/path.1430.
- Manzotti, M. *et al.* (2011) 'The White Adipose Tissue Used in Lipotransfer Procedures Is a Rich Reservoir of CD34+ Progenitors Able to Promote Cancer Progression', *Cancer Research*, 72(1), pp. 325–334. doi: 10.1158/0008-5472.can-11-1739.
- Martin, E. C. *et al.* (2014) 'Preferential star strand biogenesis of pre-miR-24-2 targets PKC-alpha and suppresses cell survival in MCF-7 breast cancer cells', *Molecular Carcinogenesis*, 53(1), pp. 38–48. doi: 10.1002/mc.21946.
- Martin, M. *et al.* (1998) 'Energetic and morphological plasticity of C6 glioma cells grown on 3-D support; Effect of transient glutamine deprivation', *Journal of Bioenergetics and Biomembranes*, 30(6), pp. 565–578. doi: 10.1023/A:1020584517588.
- Masia, J. *et al.* (2015) 'Oncological safety of breast cancer patients undergoing free-flap reconstruction and lipofilling', *European Journal of Surgical Oncology*. Elsevier Ltd, 41(5), pp. 612–616. doi: 10.1016/j.ejso.2015.02.008.
- Massat, N. J. *et al.* (2016) 'Impact of screening on breast cancer mortality: The UK program 20 years on', *Cancer Epidemiology Biomarkers and Prevention*, 25(3), pp. 455–462. doi: 10.1158/1055-9965.EPI-15-0803.
- Maughan, K. L., Lutterbie, M. A. and Ham, P. S. (2010) 'Treatment of breast cancer', *American Family Physician*, 81(11), pp. 1339–1346. doi: 10.1056/nejm199810013391407.
- Mayor, S. (2012) 'A fifth of women with breast cancer have a recurrence, new UK figures show.', *BMJ (Clinical research ed.)*, 344(June), p. 4085. doi: 10.1136/bmj.e4085.
- McDonald, E. S. *et al.* (2016) 'Clinical diagnosis and management of breast

cancer', *Journal of Nuclear Medicine*, 57, pp. 9S-16S. doi: 10.2967/jnumed.115.157834.

Mesa-Eguiagaray, I. *et al.* (2020) 'Distinct temporal trends in breast cancer incidence from 1997 to 2016 by molecular subtypes: a population-based study of Scottish cancer registry data', *British Journal of Cancer*. Springer US, 123(5), pp. 852–859. doi: 10.1038/s41416-020-0938-z.

Millar, E. K. A. *et al.* (2011) 'Prediction of outcome of early ER breast cancer is improved using a biomarker panel, which includes Ki-67 and p53', *British Journal of Cancer*, 105(2), pp. 272–280. doi: 10.1038/bjc.2011.228.

Moiseeva, O. *et al.* (2009) 'Mitochondrial Dysfunction Contributes to Oncogene-Induced Senescence', *Molecular and Cellular Biology*, 29(16), pp. 4495–4507. doi: 10.1128/mcb.01868-08.

Mojallal, A. and Foyatier, J. L. (2004) 'Historical review of the use of adipose tissue transfer in plastic and reconstructive surgery', *Annales de Chirurgie Plastique Esthétique*. doi: 10.1016/j.anplas.2004.08.004.

Mokhatri-Hesari, P. and Montazeri, A. (2020) 'Health-related quality of life in breast cancer patients: Review of reviews from 2008 to 2018', *Health and Quality of Life Outcomes*. BioMed Central, 18(1), pp. 1–25. doi: 10.1186/s12955-020-01591-x.

Moltó García, R., González Alonso, V. and Villaverde Doménech, M. E. (2016) 'Fat grafting in immediate breast reconstruction. Avoiding breast sequelae', *Breast Cancer*, 23(1), pp. 134–140. doi: 10.1007/s12282-014-0541-3.

Montero-Vilchez, T. *et al.* (2021) 'Mesenchymal Stromal Cell-Conditioned Medium for Skin Diseases: A Systematic Review', *Frontiers in Cell and Developmental Biology*, 9(July). doi: 10.3389/fcell.2021.654210.

Moon, Y. *et al.* (2005) 'Mitochondrial membrane depolarization and the selective death of dopaminergic neurons by rotenone: Protective effect of coenzyme Q10', *Journal of Neurochemistry*, 93(5), pp. 1199–1208. doi: 10.1111/j.1471-4159.2005.03112.x.

Moreno-Sánchez, R. *et al.* (2007) 'Energy metabolism in tumor cells', *FEBS Journal*, 274(6), pp. 1393–1418. doi: 10.1111/j.1742-4658.2007.05686.x.

Moser, K. *et al.* (2011) 'Extending the age range for breast screening in England: Pilot study to assess the feasibility and acceptability of randomization', *Journal of Medical Screening*, 18(2), pp. 96–102. doi:

10.1258/jms.2011.011065.

Moses, C. *et al.* (2018) 'Hallmarks of cancer: The CRISPR generation', *European Journal of Cancer*. Elsevier Ltd, 93, pp. 10–18. doi: 10.1016/j.ejca.2018.01.002.

Muehlberg, F. L. *et al.* (2009) 'Tissue-resident stem cells promote breast cancer growth and metastasis', *Carcinogenesis*, 30(4), pp. 589–597. doi: 10.1093/carcin/bgp036.

Mullard, A. (2013) 'New checkpoint inhibitors ride the immunotherapy tsunami', *Nature Reviews Drug Discovery*. Nature Publishing Group, 12, pp. 489–492. doi: 10.1056/nejmoa1302369.

Murata, M. (2018) 'Inflammation and cancer', *Environmental Health and Preventive Medicine*. Environmental Health and Preventive Medicine, 23(1), pp. 1–8. doi: 10.1186/s12199-018-0740-1.

Naderi, N. *et al.* (2017) 'The regenerative role of adipose-derived stem cells (ADSC) in plastic and reconstructive surgery', *International Wound Journal*, 14(1), pp. 112–124. doi: 10.1111/iwj.12569.

Nagawa, H. *et al.* (2007) 'Leptin Augments Proliferation of Breast Cancer Cells via Transactivation of HER2', *Journal of Surgical Research*, 149(1), pp. 9–14. doi: 10.1016/j.jss.2007.10.012.

Nan, H. *et al.* (2013) 'Assessment of biological characteristics of adipose tissue-derived stem cells co-labeled with Molday ION Rhodamine BTM and green fluorescent protein in vitro', *Molecular Medicine Reports*, 8(5), pp. 1446–1452. doi: 10.3892/mmr.2013.1694.

Nano, M. T. *et al.* (2004) 'Breast volume replacement using the latissimus dorsi miniflap', *ANZ Journal of Surgery*, 74(3), pp. 98–104. doi: 10.1046/j.1445-2197.2003.02917.x.

Neuber, G. (1893) 'Ueber die Wiederanheilung vollständig vom Körper getrennter, die ganze Fettschicht enthaltender Hautstücke', *Zentralblatt Chir*, 30, p. 16.

Nguyen, R. *et al.* (2013) 'Quantifying spillover spreading for comparing instrument performance and aiding in multicolor panel design', *Cytometry Part A*, 83 A(3), pp. 306–315. doi: 10.1002/cyto.a.22251.

Nims, R. W. and Price, P. J. (2017) 'Best practices for detecting and mitigating the risk of cell culture contaminants', *In Vitro Cellular and Developmental*

- Biology - Animal*. In *In Vitro Cellular & Developmental Biology - Animal*, 53(10), pp. 872–879. doi: 10.1007/s11626-017-0203-9.
- Ning, H. *et al.* (2014) 'Conversion of adipose-derived stem cells into natural killer-like cells with anti-tumor activities in nude mice', *PLoS ONE*, 9(8). doi: 10.1371/journal.pone.0106246.
- Noman, A. S. *et al.* (2017) 'Serum sonic hedgehog (SHH) and interleukin-(IL-6) as dual prognostic biomarkers in progressive metastatic breast cancer', *Scientific Reports*, 7(1), pp. 1–12. doi: 10.1038/s41598-017-01268-4.
- Noor, L. *et al.* (2016) 'Imaging changes after breast reconstruction with fat grafting - Retrospective study of 90 breast cancer', *Pakistan Journal of Medical Sciences*, 32(1), pp. 8–12. doi: 10.12669/pjms.321.9460.
- Nurmik, M. *et al.* (2020) 'In search of definitions: Cancer-associated fibroblasts and their markers', *International Journal of Cancer*, 146(4), pp. 895–905. doi: 10.1002/ijc.32193.
- Oliveira-Ferrer, L. *et al.* (2020) 'Mechanisms of tumor-lymphatic interactions in invasive breast and prostate carcinoma', *International Journal of Molecular Sciences*, 21(2), pp. 1–15. doi: 10.3390/ijms21020602.
- Olivier, M. *et al.* (2006) 'The clinical value of somatic TP53 gene mutations in 1,794 patients with breast cancer', *Clinical Cancer Research*, 12(4), pp. 1157–1167. doi: 10.1158/1078-0432.CCR-05-1029.
- Orecchioni, S. *et al.* (2013) 'Complementary populations of human adipose CD34+ progenitor cells promote growth, angiogenesis, and metastasis of breast cancer', *Cancer Research*, 73(19), pp. 5880–5891. doi: 10.1158/0008-5472.CAN-13-0821.
- Osborne, C. K., Hobbs, K. and Clark, G. M. (1985) 'Effect of Estrogens and Antiestrogens on Growth of Human Breast Cancer Cells in Athymic Nude Mice', *Cancer Research*, 45(2), pp. 584–590.
- Palumbo, P. *et al.* (2015) 'In vitro evaluation of different methods of handling human liposuction aspirate and their effect on adipocytes and adipose derived stem cells', *Journal of Cellular Physiology*, 230(8), pp. 1974–1981. doi: 10.1002/jcp.24965.
- Pan, H. *et al.* (2017) '20-Year Risks of Breast-Cancer Recurrence After Stopping Endocrine Therapy At 5 Years', *New England Journal of Medicine*, 377(19), pp. 1836–1846. doi: 10.1056/NEJMoa1701830.

- Panchal, H. and Matros, E. (2017) 'Current trends in postmastectomy breast reconstruction', *Plastic and Reconstructive Surgery*, 140(5S), pp. 7S-13S. doi: 10.1097/PRS.0000000000003941.
- Pardoll, D. M. (2012) 'The blockade of immune checkpoints in cancer immunotherapy', *Nature Reviews Cancer*. Nature Publishing Group, 12(4), pp. 252–264. doi: 10.1038/nrc3239.
- Pashayan, N. *et al.* (2020) 'Personalized early detection and prevention of breast cancer: ENVISION consensus statement', *Nature Reviews Clinical Oncology*. Springer US, 17(11), pp. 687–705. doi: 10.1038/s41571-020-0388-9.
- Patel, H. K. and Bihani, T. (2018) 'Selective estrogen receptor modulators (SERMs) and selective estrogen receptor degraders (SERDs) in cancer treatment', *Pharmacology and Therapeutics*. The Authors, 186, pp. 1–24. doi: 10.1016/j.pharmthera.2017.12.012.
- Pavlova, N. N. and Thompson, C. B. (2016) 'Perspective The Emerging Hallmarks of Cancer Metabolism', *Cell Metabolism*. Elsevier Inc., 23(1), pp. 27–47. doi: 10.1016/j.cmet.2015.12.006.
- Pennacchietti, S. *et al.* (2003) 'Hypoxia promotes invasive growth by transcriptional activation of the met protooncogene', *Cancer Cell*, 3(4), pp. 347–361. doi: 10.1016/S1535-6108(03)00085-0.
- Pernas, S. *et al.* (2018) 'CDK4/6 inhibition in breast cancer: current practice and future directions', *Therapeutic Advances in Medical Oncology*, 10, pp. 1–15. doi: 10.1177/1758835918786451.
- Petit, J. Y. *et al.* (2012) 'Locoregional recurrence risk after lipofilling in breast cancer patients', *Annals of Oncology*, 23(3), pp. 582–588. doi: 10.1093/annonc/mdr158.
- Petit, J. Y. *et al.* (2013) 'Evaluation of fat grafting safety in patients with intra epithelial neoplasia: A matched-cohort study', *Annals of Oncology*. Elsevier Masson SAS, 24(6), pp. 1479–1484. doi: 10.1093/annonc/mds660.
- Petitprez, F. *et al.* (2020) 'The Tumor Microenvironment in the Response to Immune Checkpoint Blockade Therapies', *Frontiers in Immunology*, 11(May), pp. 1–11. doi: 10.3389/fimmu.2020.00784.
- Piccotti, F. *et al.* (2021) 'Lipofilling in breast oncological surgery: A safe opportunity or risk for cancer recurrence?', *International Journal of Molecular*

- Sciences*, 22(7). doi: 10.3390/ijms22073737.
- Pike, S. *et al.* (2015) 'In vitro effects of tamoxifen on adipose-derived stem cells', *Wound Repair and Regeneration*, 23(5), pp. 728–736. doi: 10.1111/wrr.12322.
- Plangger, A. *et al.* (2021) 'Interactions of BRCA1-mutated Breast Cancer Cell Lines with Adipose-derived Stromal Cells (ADSCs)', *Journal of Mammary Gland Biology and Neoplasia*. Springer US, (0123456789). doi: 10.1007/s10911-021-09493-4.
- Plava, J. *et al.* (2020) 'Permanent Pro-Tumorigenic Shift in Adipose Tissue-Derived Mesenchymal Stromal Cells Induced by Breast Malignancy', *Cells*, 9(2). doi: 10.3390/cells9020480.
- Plichta, J. *et al.* (2020) 'Implications for Breast Cancer Restaging Based on the 8th Edition AJCC Staging Manual', *Ann Surg*, 271(1), pp. 169–176. doi: 10.1097/SLA.0000000000003071.Implications.
- Ponti, D. *et al.* (2005) 'Isolation and in vitro propagation of tumorigenic breast cancer cells with stem/progenitor cell properties', *Cancer Research*, 65(13), pp. 5506–5511. doi: 10.1158/0008-5472.CAN-05-0626.
- Potter, M., Newport, E. and Morten, K. J. (2016) 'The Warburg effect: 80 years on', *Biochemical Society Transactions*, 44(5), pp. 1499–1505. doi: 10.1042/BST20160094.
- Prantl, L. *et al.* (2010) 'Adipose tissue-derived stem cells promote prostate tumor growth', *Prostate*, 70(15), pp. 1709–1715. doi: 10.1002/pros.21206.
- Prat, A. *et al.* (2015) 'Clinical implications of the intrinsic molecular subtypes of breast cancer', *Breast*, 24, pp. S26–S35. doi: 10.1016/j.breast.2015.07.008.
- Preisner, F. *et al.* (2018a) 'Impact of Human Adipose Tissue-Derived Stem Cells on Malignant Melanoma Cells in An In Vitro Co-culture Model', *Stem Cell Reviews and Reports*. Humana Press Inc., 14(1), pp. 125–140. doi: 10.1007/s12015-017-9772-y.
- Preisner, F. *et al.* (2018b) 'Impact of Human Adipose Tissue-Derived Stem Cells on Malignant Melanoma Cells in An In Vitro Co-culture Model', *Stem Cell Reviews and Reports*. Springer US, 14(1), pp. 125–140. doi: 10.1007/s12015-017-9772-y.
- Public Health England (2016) *Clinical guidance for breast cancer screening assessment (NHSBSP Publication No 49)*. Available at:

<https://www.gov.uk/government/publications/breast-screening-clinical-guidelines-for-screening-management>.

Public Health England (2018) *Breast screening. An easy guide about a health test for women aged 50 and over*. Available at: https://assets.publishing.service.gov.uk/government/uploads/system/uploads/attachment_data/file/765594/Easy_guide_to_breast_screening.pdf.

Public Health Scotland (2020) *Cancer Incidence in Scotland (to December 2018)*. Available at: <https://beta.isdscotland.org/find-publications-and-data/conditions-and-diseases/cancer/cancer-incidence-in-scotland/28-april-2020/>.

Public Health Wales (2021) *CANCER INCIDENCE IN WALES, 2002 – 2018 TECHNICAL GUIDE*. doi: 10.1002/1097-0142(19870401)59:7<1386::AID-CNCR2820590726>3.0.CO;2-B.

Qian, B. Z. *et al.* (2011) 'CCL2 recruits inflammatory monocytes to facilitate breast-tumour metastasis', *Nature*. Nature Publishing Group, 475(7355), pp. 222–225. doi: 10.1038/nature10138.

Radde, B. N. *et al.* (2015) 'Bioenergetic differences between MCF-7 and T47D breast cancer cells and their regulation by oestradiol and tamoxifen', *Biochemical Journal*, 465, pp. 49–61. doi: 10.1042/BJ20131608.

Ravishankaran, P. and Karunanithi, R. (2011) 'Clinical significance of preoperative serum interleukin-6 and C-reactive protein level in breast cancer patients', *World Journal of Surgical Oncology*, 9, pp. 1–6. doi: 10.1186/1477-7819-9-18.

Raynaud, C. M. *et al.* (2010) 'DNA damage repair and telomere length in normal breast, preneoplastic lesions, and invasive cancer', *American Journal of Clinical Oncology: Cancer Clinical Trials*, 33(4), pp. 341–345. doi: 10.1097/COC.0b013e3181b0c4c2.

Razavi, S. *et al.* (2013) 'Biochemical and Biophysical Research Communications Co-culture with neurotrophic factor secreting cells induced from adipose-derived stem cells: Promotes neurogenic differentiation', *Biochemical and Biophysical Research Communications*. Elsevier Inc., 440(3), pp. 381–387. doi: 10.1016/j.bbrc.2013.09.069.

Razmkhah, M. *et al.* (2010) 'Expression profile of IL-8 and growth factors in breast cancer cells and adipose-derived stem cells (ASCs) isolated from

breast carcinoma', *Cellular Immunology*. Elsevier Inc., 265(1), pp. 80–85. doi: 10.1016/j.cellimm.2010.07.006.

Rehnke, R. D. *et al.* (2018) 'Anatomy of the superficial fascia system of the breast: A comprehensive theory of breast fascial anatomy', *Plastic and Reconstructive Surgery*, 142(5), pp. 1135–1144. doi: 10.1097/PRS.0000000000004948.

Rey, F. *et al.* (2019) 'Adipose-derived stem cells from fat tissue of breast cancer microenvironment present altered adipogenic differentiation capabilities', *Stem Cells International*. Hindawi, 2019. doi: 10.1155/2019/1480314.

Reya, T. *et al.* (2001) 'Stem cells, cancer, and cancer stem cells', *Nature*, 414, pp. 105–111. doi: 10.5892/intech.csc.2011.0328.

Rhyu, M. S. (1995) 'Telomeres, Telomerase, and Immortality', *Journal of the National Cancer Institute*, 87(12), pp. 884–894. doi: 10.1001/jama.1903.02490060034003.

Riggio, E., Bordoni, D. and Nava, M. B. (2013) 'Oncologic surveillance of breast cancer patients after lipofilling', *Aesthetic Plastic Surgery*, 37(4), pp. 728–735. doi: 10.1007/s00266-013-0166-5.

Riordon, D. R. and Boheler, K. R. (2018) 'Immunophenotyping of Live Human Pluripotent Stem Cells by Flow Cytometry', *Methods in Molecular Biology*, (1722), pp. 127–149. doi: 10.1007/978-1-4939-7553-2.

Robiolle, C. *et al.* (2015) 'Évaluation De La Satisfaction Des Patientes De Leur Reconstruction Mammaire Après Mammectomie', *Annales de Chirurgie Plastique et Esthétique*. Elsevier Masson SAS, 60(3), pp. 201–207. doi: 10.1016/j.anplas.2014.02.003.

Rosenberg, P. S., Barker, K. A. and Anderson, W. F. (2015) 'Estrogen Receptor Status and the Future Burden of Invasive and in Situ Breast Cancers in the United States', *Journal of the National Cancer Institute*, 107(9), pp. 1–7. doi: 10.1093/jnci/djv159.

Rous, P. and Kidd, J. G. (1941) 'Conditional Neoplasms and Subthreshold Neoplastic States', *Journal of Experimental Medicine*, 73(3), pp. 365–390. doi: 10.1084/jem.73.3.365.

Rutherford, M. J. *et al.* (2013) 'How much of the deprivation gap in cancer survival can be explained by variation in stage at diagnosis: An example from

breast cancer in the East of England', *International Journal of Cancer*, 133(9), pp. 2192–2200. doi: 10.1002/ijc.28221.

Rutherford, M. J. *et al.* (2015) 'The impact of eliminating age inequalities in stage at diagnosis on breast cancer survival for older women', *British Journal of Cancer*. Nature Publishing Group, 112, pp. S124–S128. doi: 10.1038/bjc.2015.51.

Rykala, J. *et al.* (2011) 'Angiogenesis markers quantification in breast cancer and their correlation with clinicopathological prognostic variables', *Pathology and Oncology Research*, 17(4), pp. 809–817. doi: 10.1007/s12253-011-9387-6.

Salgado, R. *et al.* (2003) 'Circulating interleukin-6 predicts survival in patients with metastatic breast cancer', *International Journal of Cancer*, 103(5), pp. 642–646. doi: 10.1002/ijc.10833.

Sancho, P., Barneda, D. and Heeschen, C. (2016) 'Hallmarks of cancer stem cell metabolism', *British Journal of Cancer*. Nature Publishing Group, 114(12), pp. 1305–1312. doi: 10.1038/bjc.2016.152.

Sarfati, I. *et al.* (2011) 'Adipose-tissue grafting to the post-mastectomy irradiated chest wall: Preparing the ground for implant reconstruction', *Journal of Plastic, Reconstructive and Aesthetic Surgery*. Elsevier Ltd, 64(9), pp. 1161–1166. doi: 10.1016/j.bjps.2011.03.031.

Schäffler, A. and Büchler, C. (2007) 'Concise Review: Adipose Tissue-Derived Stromal Cells-Basic and Clinical Implications for Novel Cell-Based Therapies', *Stem Cells*, 25(4), pp. 818–827. doi: 10.1634/stemcells.2006-0589.

Schlosser, S. *et al.* (2012) 'Paracrine effects of mesenchymal stem cells enhance vascular regeneration in ischemic murine skin', *Microvascular Research*. Elsevier Inc., 83(3), pp. 267–275. doi: 10.1016/j.mvr.2012.02.011.

Schmid, R. *et al.* (2018) 'ADSCs and adipocytes are the main producers in the autotaxin-lysophosphatidic acid axis of breast cancer and healthy mammary tissue in vitro 11 Medical and Health Sciences 1112 Oncology and Carcinogenesis', *BMC Cancer*. BMC Cancer, 18(1), pp. 1–11. doi: 10.1186/s12885-018-5166-z.

Schmidt, M. E. *et al.* (2015) 'Effects of resistance exercise on fatigue and quality of life in breast cancer patients undergoing adjuvant chemotherapy: A randomized controlled trial', *International Journal of Cancer*, 137(2), pp. 471–

480. doi: 10.1002/ijc.29383.

Schon, K. and Tischkowitz, M. (2018) 'Clinical implications of germline mutations in breast cancer: TP53', *Breast Cancer Research and Treatment*. Springer US, 167(2), pp. 417–423. doi: 10.1007/s10549-017-4531-y.

Schweizer, R. *et al.* (2015) 'The Role of Adipose-Derived Stem Cells in Breast Cancer Progression and Metastasis', *Stem Cells International*, 2015, pp. 1–17. doi: 10.1155/2015/120949.

Semenza, G. L. (2008) 'Tumor metabolism: Cancer cells give and take lactate', *Journal of Clinical Investigation*, 118(12), pp. 3835–3837. doi: 10.1172/JCI37373.

Serpico, D., Molino, L. and Di Cosimo, S. (2014) 'MicroRNAs in breast cancer development and treatment', *Cancer Treatment Reviews*. Elsevier Ltd, 40(5), pp. 595–604. doi: 10.1016/j.ctrv.2013.11.002.

Sherr, C. J. and McCormick, F. (2002) 'The RB and p53 pathways in cancer', *Cancer Cell*, 2(2), pp. 103–112. doi: 10.1016/S1535-6108(02)00102-2.

Shien, T. and Iwata, H. (2020) 'Adjuvant and neoadjuvant therapy for breast cancer', *Japanese Journal of Clinical Oncology*, 50(3), pp. 225–229. doi: 10.1093/jjco/hyz213.

Shin, E. and Koo, J. S. (2021) 'Glucose Metabolism and Glucose Transporters in Breast Cancer', *Frontiers in Cell and Developmental Biology*, 9(September), pp. 1–18. doi: 10.3389/fcell.2021.728759.

Siegel, R. L., Miller, K. D. and Jemal, A. (2016) 'Cancer statistics, 2016', *CA Cancer J Clin*, 66, pp. 7–30. doi: 10.3322/caac.21551.

Silva-Vergara, C. *et al.* (2016) 'Oncological outcomes of lipofilling breast reconstruction: 195 consecutive cases and literature review', *Journal of Plastic, Reconstructive and Aesthetic Surgery*. Elsevier Ltd, 69(4), pp. 475–481. doi: 10.1016/j.bjps.2015.12.029.

Silva, K. R. *et al.* (2015) 'Stromal-vascular fraction content and adipose stem cell behavior are altered in morbid obese and post bariatric surgery ex-obese women', *Stem Cell Research and Therapy*. ???, 6(1), pp. 1–13. doi: 10.1186/s13287-015-0029-x.

Singh, R., Letai, A. and Sarosiek, K. (2019) 'Regulation of apoptosis in health and disease: the balancing act of BCL-2 family proteins', *Nat Rev Mol Cell Biol.*, 20(3), pp. 175–193. doi: 10.32388/j9r853.

- Singla, A. (2016) 'Protocol for Autologous Fat Grafting for Immediate Reconstruction of Lumpectomy Defects Following Surgery for Breast Cancer', *JMIR Research Protocols*, 5(3), p. e109. doi: 10.2196/resprot.5494.
- Smolková, K. *et al.* (2011) 'Waves of gene regulation suppress and then restore oxidative phosphorylation in cancer cells', *International Journal of Biochemistry and Cell Biology*, 43(7), pp. 950–968. doi: 10.1016/j.biocel.2010.05.003.
- Solinas, G. *et al.* (2009) 'Tumor-associated macrophages (TAM) as major players of the cancer-related inflammation', *Journal of Leukocyte Biology*, 86(5), pp. 1065–1073. doi: 10.1189/jlb.0609385.
- Somogyi, R. B. *et al.* (2015) 'Understanding the factors that influence breast reconstruction decision making in Australian women', *Breast*. Elsevier Ltd, 24(2), pp. 124–130. doi: 10.1016/j.breast.2014.11.013.
- Song, K. *et al.* (2015) 'Autophagy induction by leptin contributes to suppression of apoptosis in cancer cells and xenograft model: Involvement of p53/FoxO3A axis', *Oncotarget*, 6(9). doi: 10.18632/oncotarget.3347.
- Soria, G. *et al.* (2008) 'Concomitant expression of the chemokines RANTES and MCP-1 in human breast cancer: A basis for tumor-promoting interactions', *Cytokine*, 44(1), pp. 191–200. doi: 10.1016/j.cyto.2008.08.002.
- Soule, H. D. *et al.* (1973) 'A human cell line from a pleural effusion derived from a breast carcinoma', *Journal of the National Cancer Institute*, 51(5), pp. 1409–1416. doi: 10.1093/jnci/51.5.1409.
- Spaeth, E. L. *et al.* (2009) 'Mesenchymal stem cell transition to tumor-associated fibroblasts contributes to fibrovascular network expansion and tumor progression', *PLoS ONE*, 4(4). doi: 10.1371/journal.pone.0004992.
- Strassburg, S. *et al.* (2016) 'Adipose-Derived Stem Cells Support Lymphangiogenic Parameters In Vitro', *Journal of Cellular Biochemistry*, 10(November 2015), pp. 2620–2629. doi: 10.1002/jcb.25557.
- Strauss, D. C. and Thomas, J. M. (2010) 'Transmission of donor melanoma by organ transplantation', *The Lancet Oncology*. Elsevier Ltd, 11(8), pp. 790–796. doi: 10.1016/S1470-2045(10)70024-3.
- Streubel, B. *et al.* (2004) 'Lymphoma-Specific Genetic Aberrations in Microvascular Endothelial Cells in B-Cell Lymphomas', *New England Journal of Medicine*, 351(3), pp. 250–259. doi: 10.1056/nejmoa033153.

- Sturtz, G. P. *et al.* (2005) 'Outcome Analysis of Breast-Conservation Surgery and Immediate Latissimus Dorsi Flap Reconstruction in Patients with T1 to T2 Breast Cancer', *Plastic and Reconstructive Surgery*, 116(3), pp. 741–752. doi: 10.1097/01.prs.0000176251.15140.36.
- Suarez-Carmona, M. *et al.* (2017) 'EMT and inflammation: inseparable actors of cancer progression', *Molecular Oncology*, 11(7), pp. 805–823. doi: 10.1002/1878-0261.12095.
- Sun, Y. S. *et al.* (2017) 'Risk factors and preventions of breast cancer', *International Journal of Biological Sciences*, 13(11), pp. 1387–1397. doi: 10.7150/ijbs.21635.
- Sun, Z.-H. *et al.* (2021) 'Breast surgery for young women with early-stage breast cancer', *Medicine*, 100(18), pp. 1–10. doi: 10.1097/md.00000000000025880.
- Sung, H. *et al.* (2021) 'Global cancer statistics 2020: GLOBOCAN estimates of incidence and mortality worldwide for 36 cancers in 185 countries', *CA: A Cancer Journal for Clinicians*, 71(3), pp. 209–249. doi: 10.3322/caac.21660.
- Suzuki, K. *et al.* (2011) 'Mesenchymal stromal cells promote tumor growth through the enhancement of neovascularization', *Molecular Medicine*, 17(7–8), pp. 579–587. doi: 10.2119/molmed.2010.00157.
- Takeda, K. *et al.* (2021) 'Donor-Derived Neuroendocrine Carcinoma Transmission to Two Kidney Transplant Recipients Demonstrated by Short Tandem Repeat Analysis: A Case Report', *Transplantation Proceedings*. Elsevier Inc., 53(4), pp. 1337–1341. doi: 10.1016/j.transproceed.2021.03.002.
- Talmadge, J. E. and Fidler, I. J. (2010) 'AACR centennial series: The biology of cancer metastasis: Historical perspective', *Cancer Research*, 70(14), pp. 5649–5669. doi: 10.1158/0008-5472.CAN-10-1040.
- Tamai, S. (2009) 'History of Microsurgery', *Plastic and Reconstructive Surgery*, 124, pp. e282–e294. doi: 10.1097/PRS.0b013e3181bf825e.
- Tan, P. H. *et al.* (2020) 'The 2019 World Health Organization classification of tumours of the breast', *Histopathology*, 77(2), pp. 181–185. doi: 10.1111/his.14091.
- Taucher, S. *et al.* (2008) 'The potential risk of neoadjuvant chemotherapy in breast cancer patients-results from a prospective randomized trial of the Austrian Breast and Colorectal Cancer Study Group (ABCSCG-07)', *Breast*

Cancer Research and Treatment, 112(2), pp. 309–316. doi: 10.1007/s10549-007-9844-9.

Teufelsbauer, M. *et al.* (2019) 'Interaction of adipose-derived stromal cells with breast cancer cell lines', *Plastic and Reconstructive Surgery*, 144(2), pp. 207E-217E. doi: 10.1097/PRS.0000000000005839.

Thitilertdecha, P. *et al.* (2020) 'Extensive Characterization of Mesenchymal Stem Cell Marker Expression on Freshly Isolated and in Vitro Expanded Human Adipose-Derived Stem Cells from Breast Cancer Patients', *Stem Cells International*, 2020. doi: 10.1155/2020/8237197.

Tomlins, A. and Parker, S. (2016) *Guidelines for the management of breast cancer*, Breast Cancer Expert Advisory Group, NHS England. doi: 10.2165/00128413-200112820-00001.

Tompkins, K. D. and Thorburn, A. (2019) 'Regulation of apoptosis by autophagy to enhance cancer therapy', *Yale Journal of Biology and Medicine*, 92(4), pp. 707–718.

Tonini, T., Rossi, F. and Claudio, P. P. (2003) 'Molecular basis of angiogenesis and cancer', *Oncogene*, 22(43), pp. 6549–6556. doi: 10.1038/sj.onc.1206816.

Trenker, R. and Jura, N. (2020) 'Receptor Tyrosine Kinase activation: from the ligand perspective', *Curr Opin Cell Biol*, Apr(63), pp. 174–185. doi: 10.1016/j.physbeh.2017.03.040.

Tripathi, M., Billet, S. and Bhowmick, N. A. (2012) 'Understanding the role of stromal fibroblasts in cancer progression', *Cell Adhesion and Migration*, 6(3), pp. 231–235. doi: 10.4161/cam.20419.

Trivanović, D. *et al.* (2014) 'Characteristics of human adipose mesenchymal stem cells isolated from healthy and cancer affected people and their interactions with human breast cancer cell line MCF-7 in vitro', *Cell Biology International*, 38(2), pp. 254–265. doi: 10.1002/cbin.10198.

Trivanović, D. *et al.* (2016) 'Inflammatory cytokines prime adipose tissue mesenchymal stem cells to enhance malignancy of MCF-7 breast cancer cells via transforming growth factor- β 1', *IUBMB Life*, 68(3), pp. 190–200. doi: 10.1002/iub.1473.

Trivanović, D. *et al.* (2020) 'Adipogenesis in Different Body Depots and Tumor Development', *Frontiers in Cell and Developmental Biology*, 8(September), pp. 1–9. doi: 10.3389/fcell.2020.571648.

- Trojahn Kølle, S. F. *et al.* (2013) 'Pooled human platelet lysate versus fetal bovine serum-investigating the proliferation rate, chromosome stability and angiogenic potential of human adipose tissue-derived stem cells intended for clinical use', *Cytotherapy*. Elsevier Inc, 15(9), pp. 1086–1097. doi: 10.1016/j.jcyt.2013.01.217.
- Tsai, P. C. *et al.* (2018) 'Smoking induces coordinated DNA methylation and gene expression changes in adipose tissue with consequences for metabolic health 06 Biological Sciences 0604 Genetics', *Clinical Epigenetics*. Clinical Epigenetics, 10(1), pp. 1–21. doi: 10.1186/s13148-018-0558-0.
- Valković, T. *et al.* (1998) 'Expression of monocyte chemotactic protein-1 in human invasive ductal breast cancer', *Pathology Research and Practice*, 194(5), pp. 335–340. doi: 10.1016/S0344-0338(98)80057-5.
- Valles, G. J. *et al.* (2020) 'USP7 Is a Master Regulator of Genome Stability', *Frontiers in Cell and Developmental Biology*, 8(August), pp. 1–23. doi: 10.3389/fcell.2020.00717.
- Varghese, J. *et al.* (2017) 'Systematic review of patient factors affecting adipose stem cell viability and function: implications for regenerative therapy', *Stem cell research & therapy*. Stem Cell Research & Therapy, 8(1), p. 45. doi: 10.1186/s13287-017-0483-8.
- Vargo-Gogola, T. and Rosen, J. M. (2007) 'Modelling breast cancer: One size does not fit all', *Nature Reviews Cancer*, 7(9), pp. 659–672. doi: 10.1038/nrc2193.
- Vater, C., Kasten, P. and Stiehler, M. (2011) 'Culture media for the differentiation of mesenchymal stromal cells', *Acta Biomaterialia*. Acta Materialia Inc., 7(2), pp. 463–477. doi: 10.1016/j.actbio.2010.07.037.
- Veber, M. *et al.* (2011) 'Radiographic findings after breast augmentation by autologous fat transfer', *Plastic and Reconstructive Surgery*, 127(3), pp. 1289–1299. doi: 10.1097/PRS.0b013e318205f38f.
- Villagrasa, A. *et al.* (2015) 'Exosomes Derived from Breast Cancer Cells, Small Trojan Horses?', *Journal of Mammary Gland Biology and Neoplasia*, 19(3–4), pp. 303–313. doi: 10.1007/s10911-015-9332-5.
- Visweswaran, M. *et al.* (2018) 'The inhibitory influence of adipose tissue-derived mesenchymal stem cell environment and Wnt antagonism on breast tumour cell lines', *International Journal of Biochemistry and Cell Biology*.

Elsevier, 95(December 2017), pp. 63–72. doi: 10.1016/j.biocel.2017.12.013.

Voduc, K. D. *et al.* (2010) 'Breast cancer subtypes and the risk of local and regional relapse', *Journal of Clinical Oncology*, 28(10), pp. 1684–1691. doi: 10.1200/JCO.2009.24.9284.

Walcher, L. *et al.* (2020) 'Cancer Stem Cells—Origins and Biomarkers: Perspectives for Targeted Personalized Therapies', *Frontiers in Immunology*, 11(August), pp. 1–33. doi: 10.3389/fimmu.2020.01280.

Wang, G. *et al.* (2018) 'Co-culture system of hepatocytes and endothelial cells: two in vitro approaches for enhancing liver-specific functions of hepatocytes', *Cytotechnology*. Springer Netherlands, 70(4), pp. 1279–1290. doi: 10.1007/s10616-018-0219-3.

Wang, Z. *et al.* (2021) 'Osteogenic and angiogenic lineage differentiated adipose-derived stem cells for bone regeneration of calvarial defects in rabbits', *Journal of Biomedical Materials Research - Part A*, 109(4), pp. 538–550. doi: 10.1002/jbm.a.37036.

Warburg, O., Wind, F. and Negelein, E. (1927a) 'THE METABOLISM OF TUMORS IN THE BODY', *J Gen Physiol*, 7(8(6)), pp. 519–30. doi: 10.1136/bmj.1.3653.74-a.

Warburg, O., Wind, F. and Negelein, E. (1927b) 'The Metabolism of Tumours in the Body', *The journal of General Physiology*, 8(6), pp. 519–530.

Wei, H.-J. *et al.* (2015) 'Adipose-derived stem cells promote tumor initiation and accelerate tumor growth by interleukin-6 production', *Oncotarget*, 6(10). doi: 10.18632/oncotarget.3481.

Wei, Y. *et al.* (2010) 'Schwann-like cell differentiation of rat adipose-derived stem cells by indirect co-culture with Schwann cells in vitro', *Cell Proliferation*, 43(6), pp. 606–616. doi: 10.1111/j.1365-2184.2010.00710.x.

Weigand, A. *et al.* (2016) 'Selective isolation and characterization of primary cells from normal breast and tumors reveal plasticity of adipose derived stem cells', *Breast Cancer Research*. Breast Cancer Research, 18(1), pp. 1–20. doi: 10.1186/s13058-016-0688-2.

Weng, Y. S. *et al.* (2019) 'MCT-1/miR-34a/IL-6/IL-6R signaling axis promotes EMT progression, cancer stemness and M2 macrophage polarization in triple-negative breast cancer', *Molecular Cancer*. Molecular Cancer, 18(1), pp. 1–15. doi: 10.1186/s12943-019-0988-0.

- Węsierska-Gądek, J. *et al.* (2007) 'Phenol red in the culture medium strongly affects the susceptibility of human MCF-7 cells to roscovitine', *Cellular and Molecular Biology Letters*, 12(2), pp. 280–293. doi: 10.2478/s11658-007-0002-5.
- Wilson, W. R. and Hay, M. P. (2011) 'Targeting hypoxia in cancer therapy', *Nature Reviews Cancer*. Nature Publishing Group, 11(6), pp. 393–410. doi: 10.1038/nrc3064.
- Wu, S. *et al.* (2019) 'Human adipose-derived mesenchymal stem cells promote breast cancer MCF7 cell epithelial-mesenchymal transition by cross interacting with the TGF- β /Smad and PI3K/AKT signaling pathways', *Molecular Medicine Reports*, 19(1), pp. 177–186. doi: 10.3892/mmr.2018.9664.
- Xiao, G. *et al.* (2020) 'Gain-of-Function Mutant p53 R273H Interacts with Replicating DNA and PARP1 in Breast Cancer', *Cancer Research*, 80(3), pp. 394–405. doi: 10.1158/0008-5472.CAN-19-1036.Gain-of-Function.
- Xiao, T. *et al.* (2018) 'Estrogen-regulated feedback loop limits the efficacy of estrogen receptor–targeted breast cancer therapy', *Proceedings of the National Academy of Sciences of the United States of America*, 115(31), pp. 7869–7878. doi: 10.1073/pnas.1722617115.
- Xie, G. *et al.* (2012) 'IL-6-induced epithelial-mesenchymal transition promotes the generation of breast cancer stem-like cells analogous to mammosphere cultures', *International Journal of Oncology*, 40(4), pp. 1171–1179. doi: 10.3892/ijo.2011.1275.
- Xu, Q. *et al.* (2012) 'Mesenchymal stem cells play a potential role in regulating the establishment and maintenance of epithelial-mesenchymal transition in MCF7 human breast cancer cells by paracrine and induced autocrine TGF- β ', *International Journal of Oncology*, 41(3), pp. 959–968. doi: 10.3892/ijo.2012.1541.
- Yang, D. *et al.* (2013) 'Bcl-2 expression predicts sensitivity to chemotherapy in breast cancer: A systematic review and meta-analysis', *Journal of Experimental and Clinical Cancer Research*. Journal of Experimental & Clinical Cancer Research, 32(1), pp. 1–11. doi: 10.1186/1756-9966-32-105.
- Yang, J. *et al.* (2021) 'The Paradoxical Role of Cellular Senescence in Cancer', *Frontiers in Cell and Developmental Biology*, 9(August). doi:

10.3389/fcell.2021.722205.

Yang, X., Wang, H. and Jiao, B. (2017) 'Mammary gland stem cells and their application in breast cancer', *Oncotarget*, 8(6), pp. 10675–10691. doi: 10.18632/oncotarget.12893.

Yaswen, P. *et al.* (2015) 'Therapeutic targeting of replicative immortality', *Seminars in Cancer Biology*. Elsevier Ltd, 35, pp. S104–S128. doi: 10.1016/j.semcancer.2015.03.007.

Yin, L. *et al.* (2020) 'Triple-negative breast cancer molecular subtyping and treatment progress', *Breast Cancer Research*. Breast Cancer Research, 22(1), pp. 1–13. doi: 10.1186/s13058-020-01296-5.

Young Park, M. I. N., Sung Hong, Y. O. O. and Sung-Hyun, K. I. M. (2013) 'Adipose-derived stem cells induced EMT-like changes in H358 lung cancer cells', *Anticancer Research*, 33(10), pp. 4421–4430.

Yu, J. M. *et al.* (2008) 'Mesenchymal Stem Cells Derived from Human Adipose Tissues Favor Tumor Cell Growth in vivo', *Stem Cells and Development*, 17(3), pp. 463–474. doi: 10.1089/scd.2007.0181.

Yu, S. *et al.* (2017) 'The T47D cell line is an ideal experimental model to elucidate the progesterone-specific effects of a luminal A subtype of breast cancer', *Biochemical and Biophysical Research Communications*. Elsevier Ltd, 486(3), pp. 752–758. doi: 10.1016/j.bbrc.2017.03.114.

Yuan, J. *et al.* (2015) 'Characterization of adipose-derived stem cells from subcutaneous and visceral adipose tissues and their function in breast cancer cells', *Oncotarget*, 6(33). doi: 10.18632/oncotarget.5922.

Yuan, X., Larsson, C. and Xu, D. (2019) 'Mechanisms underlying the activation of TERT transcription and telomerase activity in human cancer: old actors and new players', *Oncogene*. Springer US, 38(34), pp. 6172–6183. doi: 10.1038/s41388-019-0872-9.

Zhang, C. *et al.* (2013) 'Mesenchymal stem cells derived from breast cancer tissue promote the proliferation and migration of the MCF-7 cell line in vitro', *Oncology Letters*, 6(6), pp. 1577–1582. doi: 10.3892/ol.2013.1619.

Zhang, J. *et al.* (2012) 'Measuring energy metabolism in cultured cells, including human pluripotent stem cells and differentiated cells', *Nature Protocols*, 7(6), pp. 1068–1085. doi: 10.1038/nprot.2012.048.

Zhong, T. *et al.* (2021) 'Identifying the top research priorities in

postmastectomy breast cancer reconstruction: A James Lind Alliance priority setting partnership', *BMJ Open*, 11(8). doi: 10.1136/bmjopen-2020-047589.

Ziegler, E. *et al.* (2014) 'Generation of MCF-7 cells with aggressive metastatic potential in vitro and in vivo', *Breast Cancer Research and Treatment*, 148(2), pp. 269–277. doi: 10.1007/s10549-014-3159-4.

Zimmerlin, L. *et al.* (2011) 'Regenerative therapy and cancer: In vitro and in vivo studies of the interaction between adipose-derived stem cells and breast cancer cells from clinical isolates', *Tissue Engineering - Part A*, 17(1–2), pp. 93–106. doi: 10.1089/ten.tea.2010.0248.

Zuk, P. A. *et al.* (2001) 'Multilineage Cells from Human Adipose Tissue : Implications for Cell-Based Therapies', 7(2), pp. 211–229.

Zuk, P. A. *et al.* (2002) 'Human Adipose Tissue Is a Source of Multipotent Stem Cells', *Molecular Biology of the Cell*, 13(October), pp. 4279–4295. doi: 10.1091/mbc.E02.